UNIVERSITÀ
DEGLI STUDI
FIRENZE

PhD in

TUSCAN PhD COURSE in EARTH SCIENCE

CYCLE XXXIII

COORDINATOR Prof. Lorella Francalanci

Late Quaternary paleoceanographic variations in the eastern Greenland Sea, Barents Sea and Spitsbergen fjords inferred by the foraminiferal assemblages and sedimentological records

Doctoral Candidate
Dr. Viviana Maria Gamboa Sojo

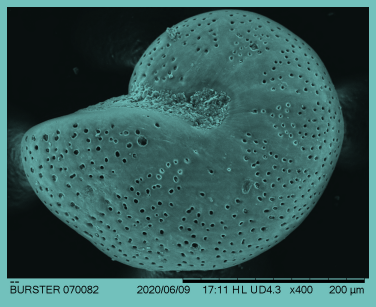
Supervisor
Prof. Caterina Morigi

Co-supervisor
Prof. Katrine Husum

Coordinator
Prof. Lorella Francalanci

Years 2017/2020

Academic Discipline (SSD) GEO /01 and GEO /02



UNIVERSITÀ DEGLI STUDI FIRENZE

PhD in
TUSCAN PhD COURSE in EARTH SCIENCE

CYCLE XXXIII

COORDINATOR Prof. Lorella Francalanci

Late Quaternary paleoceanographic variations in the eastern Greenland Sea, Barents Sea and Spitsbergen fjords inferred by the foraminiferal assemblages and sedimentological records

Academic Discipline (SSD) GEO/01 and GEO/02

Doctoral Candidate
Dr. Viviana Maria Gamboa Sojo

(signature)

Supervisor
Prof. Caterina Morigi

(signature)

Co-supervisor
Prof. Katrine Husum

(signature)

Coordinator
Prof. Lorella Francalanci

(signature)

Years 2017/2020

To my father, because we never said goodbye…

Abstract

The Arctic area is responding more rapidly to global warming than most other areas on our planet. The identification of sedimentary systems and processes in the Arctic area allows the reconstruction of its palaeoclimatic and palaeoenvironmental evolution during the Quaternary period. This work consists of the study of three sites located in the Fram Strait (eastern Greenland Sea), in the western Spitsbergen Fjords and in the northwestern edge of Barents Sea, corresponding with diverse geographical, morphological and oceanographical settings. These sites are all located along the main incoming pathway of the Atlantic Water (AW) into the Arctic area, allowing to reconstruct the oceanographical changes during the last 12 kyr BP, with a special focus on the last centuries. Thus, the overall aim of this PhD Thesis is to improve the knowledge of the centennial and decadal climatic variations and ocean circulation and to trace the AW impact into the Arctic area during the upper Pleistocene and Holocene. A multiproxy (e.g. planktic and benthic foraminifera, sediment lithology) investigation is applied to a long marine sediment core recovered from the Bellsund Drift depocenter and six short cores from Bellsund Drift, a coastal fjord and the Kveithola Trough.

The sedimentary record of the *Calypso* piston core (GS191-01PC, 1647m water depth), records the Upper Pleistocene (12.05 to 11.7 kyr BP), and an expanded Holocene sequence (more than 5 m thick, 11.7 to 0.63 kyr BP). The millennial record of the Bellsund Drift indicates a general progressive increase of the bottom and superficial water temperature, due to the incoming of the warm AW and the decreasing of sea ice extent. In the same area, I also analysed a box-corer (20 cm length, 1647 m water depth), which records the climatic variations of the Modern Period (MP, 1890 A.D. to present). My results indicates a general warm increment during the entire MP, interrupted by short cold events of about *ca.* 5 years.

In the Kongsfjorden-Krossfjorden glacial system, a tidewater glacier fjord, (western margin of Svalbard) I analysed a multi-corer (32 cm at 105.6 m water depth), which records the last 60 years. This ice-covered area shows a decrease of the ice influence not directly related to the AW inflow, but indicated by the dominance of the cold ArW species related to meltwater and the no increment in the AW species.

Four multi-cores collected along the Kveithola Trough are also studied (between 8 and 38 cm of sediment recovered and at water depths ranging from 376 m to 159 m) and correspond with the last part of the Little Ice Age (LIA) and Modern Period (MP). The foraminiferal assemblages indicate the passage from

colder to warmer conditions during the last 350 years, conditioned by the morphology and geographical position of the trough.

The palaeoenvironmental evolution of the bottom and the surface water masses indicate multiyear and decadal variations between warm and cold periods during the last *c.a.* two centuries, related to the interaction between the polar superficial cold-water and the warm bottom AW. The foraminiferal assemblages demonstrate increasing temperatures, but still the dominance of Arctic species, which are related with the continuing retreat of the sea ice, the reduction in the albedo and further favouring heat of the ocean surface; and the increase of the air temperature amplifying the input of heat in the area.

Table of Contents

1. Introduction 4
   1.1. References 8
2. Materials and methodology 12
   2.1. Dataset 12
      2.1.1. *Calypso* Piston core: Holocene record *ca.* 12.0 kyr BP 12
      2.1.2. Multi cores and Box corer: the last *ca.* 100-400 years 12
   2.2. Methodology 14
      2.2.1. Sediment dating and age model 14
      2.2.2. Sedimentology (Grain size analysis) 15
      2.2.3. Micropaleontological analysis 16
      2.2.4. Oceanographic data set 20
   2.3. Thesis organization 21
   2.4. References 22
3. Holocene record from Bellsund Drift, *ca.* 12.0 kyr BP 26
   3.1. Study area 26
   3.2. Material and methodology 29
   3.3. Age model 30
   3.4. Main lithofacies 31
   3.5. Results 32
      3.5.1. Grain Size 32
      3.5.2. Planktic foraminifera 39
      3.5.3. Benthic foraminifera 42
   3.6. Discussion 53
      a. Upper Pleistocene (last *ca.* 900 yr. of the Younger Dryas) 12.0 -11.7 kyr BP. 53
      b. Early Holocene (Greenlandian) 11.7-8.2 kyr BP 53
      c. Mid-Holocene (Northgrippian) 8.2- 4.1 kyr BP 55
      d. Late Holocene (Meghalayan) 4.2 – 0.6 kyr BP 56
   3.7. Conclusions 60
   3.8. References 61

Little Ice Age and Modern Period records 69

4. Modern Period record from Bellsund Drift, the last *ca.* 120 yr 69

4.1. Study area 69
4.2. Temperature and Sea ice record in the Fram Strait, satellite monitoring 70
4.3. Material and methodology 72
4.4. Results 73
4.4.1. Age model 73
4.4.2. Lithological description and grain size analysis 74
4.4.3. Planktic foraminifera 75
4.4.4. Benthic Foraminifera 79
4.5. Discussion 88
a. Period from 1890 to 1957 A.D. 88
b. Period from 1957 to 1990 A.D. 89
c. Period from 1990 to 2014 A.D. 89
4.6. Conclusions 94
4.7. References 95
5. The last half-century record from Krossfjorden (Kongsfjorden-Krossfjorden glacigenic system). 101
5.1. Study area 101
5.2. Age model 104
5.3. Grain Size 105
5.4. Diatom analysis and Sea Surface Temperature (SST) reconstruction 106
5.5. Material and methodology 107
5.6. Results. Benthic foraminiferal analysis 108
5.6.1. General trends 108
5.6.2. Diversity indexes and cluster analysis 110
5.6.3. Benthic foraminiferal pattern 113
5.7. Discussion 117
5.7.1. Benthic foraminiferal events 117
5.7.2. Comparison with another proxy records 120
5.8. Conclusions 123
5.9. References 124
6. The last *ca.* 350 years in the Kveithola Trough 130
I. Palaeoenvironmental reconstructions of the Little Ice Age and Modern Period in Kveithola Trough 130
6.1. Oceanographic settings 130

6.2. Material and methodology 132
6.3. Results 133
6.3.1. Age model 133
6.3.2. Lithological description and grain size analysis 134
6.3.3. Benthic foraminiferal results 136
6.3.4. Benthic foraminiferal pattern along the Kveithola Trough 160
6.4. Discussion 163
6.5. Conclusions 174
II. The last decades in the Kveithola Trough: taphonomic processes to explain the bias between living (CTG-stained) and dead foraminiferal assemblages 175
6.6. Material and methodology 176
6.7. Results 177
6.7.1. Water masses properties and ocean current variability 177
6.7.2. Sea ice extension 181
6.7.3. Sedimentation rate (SR) 182
6.7.4. General faunal distribution and diversity indexes 182
6.7.5. Main foraminiferal species 186
6.8. Discussion 190
6.8.1. Modern situation: Link between the living foraminiferal assemblages and the water masses distribution. 190
6.8.2. Preservation and taphonomic processes 192
6.8.3. Paleoenvironmental variations during the last decades 195
6.9. Conclusions 198
6.10. References 204
7. General considerations and concluding remarks. 213
I. Holocene record 213
II. Little Ice Age and Modern Period, the last *ca.* 350 years 214
Arctic climatic trend 215
Proxies and multidisciplinary work 217
7.1. References 218
8. Supplementary material 219
Micropaleontological analysis 219
Plates 221
Foraminiferal counting sheets 242

1. Introduction

Polar regions are extremely sensitive areas to long-term climatic variations, which include both natural and anthropogenic influences. As indicated in the recently published Intergovernmental Panel on Climate Change report (IPCC 2019), these changes include variations in the Arctic temperature and ice cover, producing alterations in the ocean salinity and primary production, and extreme weather conditions around the world (precipitation, droughts, heat, and cyclones) (Solomon et al., 2007). The sea ice cover and the seasonal/interannual variations of temperature, albedo, productivity, etc., principally influence the Arctic Ocean (Serreze et al., 2007; Screen and Simmonds, 2010a; Comiso and Hall, 2014; Lind et al., 2018).

The three-studied areas are located in different bathymetrical, morphological and oceanographic settings, perfectly located to analyse the changes and the interactions of the two main currents that influence the Arctic area:

I. The Fram Strait area, between Greenland and Svalbard, represents the only deep connection to the Arctic Ocean, allowing the exchange of water masses between the North Atlantic and the Arctic Ocean, with the interaction of two of the main water masses, the warm Atlantic Water (AW) and the cold Arctic water (ArW) (Fig. 1.1). This interaction produces an important heat and mass exchange with the Arctic Ocean, influencing the climate in the entire Arctic region. The inflow of warm AW into the Arctic Ocean throughout the Fram Strait and the Barents Sea is about 5-10 times larger than the inflow of the Pacific water through the Bering Strait (Rudels et al., 1999; Schauer et al., 2004), representing one of the main warm water transporters into the Arctic region. The Bellsund contouritic drift located in the western continental margin of Svalbard, developed by means of the northward moving deep sea North Atlantic currents (here called West Spitsbergen Current, WSC), periodically refilled with across-slope sediment input, conforming an important sedimentary sequence that contains a high resolution depositional record (Rebesco et al., 2013).
II. The Krossfjorden is located in the Kongsfjorden-Krossfjorden system, on the western coast of Spitsbergen (Fig. 1.1). This fjord system corresponds with an open fjord, without sills, and hence, is influenced by the processes on the shelf (Hop et al., 2006). It is a particular site for climatic

studies, because of the connection between the Arctic basin and the Atlantic Ocean. Its position allows the interaction of both ArW and AW into the fjord system (Svendsen et al., 2002; Sundfjord et al., 2017). The influence of two climatic imprints: the end of the fjord opening to the sea, and the inner area limited by the glaciers, become this fjord a sensitive climatic change indicator (Svendsen et al., 2002). (Fig. 1.1). The increasing heat in the Arctic area (Nilsen et al., 2016), affects the hydrography, the glacial meltwater, sediment input, and the water characteristics into the fjord, affecting all the trophic levels (Wlodarska-Kowalczuk et al., 2005), also increases the calving of tidewater glaciers and accelerates the glacial retreat (Luckman et al., 2015).

III. The Barents Sea in the north most Arctic shelf-sea exhibits many special properties that make it an interesting region for studying interactions between the atmosphere, sea ice and ocean water masses (Smedsrud et al., 2013). Thanks to its easy access, it represents a good historical climatic record that has been intensively studied in the past years, indicating partly ice-free ocean conditions during the winter and in the present climatic conditions (Fig. 1.1). The limited depth (around 200-300 m for the most area) defines the Barents Sea as a confined oceanic basin (Smedsrud et al., 2013). The marginal Barents Sea is located south of this area and is characterised by two main climatic regions, the cold and seasonal sea ice covered area in the north, and the warmer and productive area in the south (Loeng, 1991; Screen and Simmonds, 2010b; Smedsrud et al., 2013; Lind et al., 2018). Quaternary climate studies of the Barents Sea, based on the sedimentary record, indicate a general increase in the sea temperature (Duplessy et al., 2001; Rebesco et al., 2011; Rüther et al., 2012; Groot et al., 2014; Dijkstra et al., 2017). In particular, some papers highlighted the variation in the inflow of the warm AW into the Barents Sea during the Holocene (Duplessy et al., 2001; Sarnthein et al., 2003; Ślubowska-Woldengen et al., 2007; Groot et al., 2014) (Fig. 1.1). The Kveithola glacial trough system in the NW Barents Sea corresponds to a complex geomorphological environment located at the sea ice limit and influenced by the interaction of these two different water masses (AW and ArW) (Aagaard, 1989; Loeng, 1991; Vinje and Kvambekk, 1991; Loeng et al., 1997; Orvik and Niiler, 2002; Maslowski et al., 2004; Smedsrud et al., 2013).

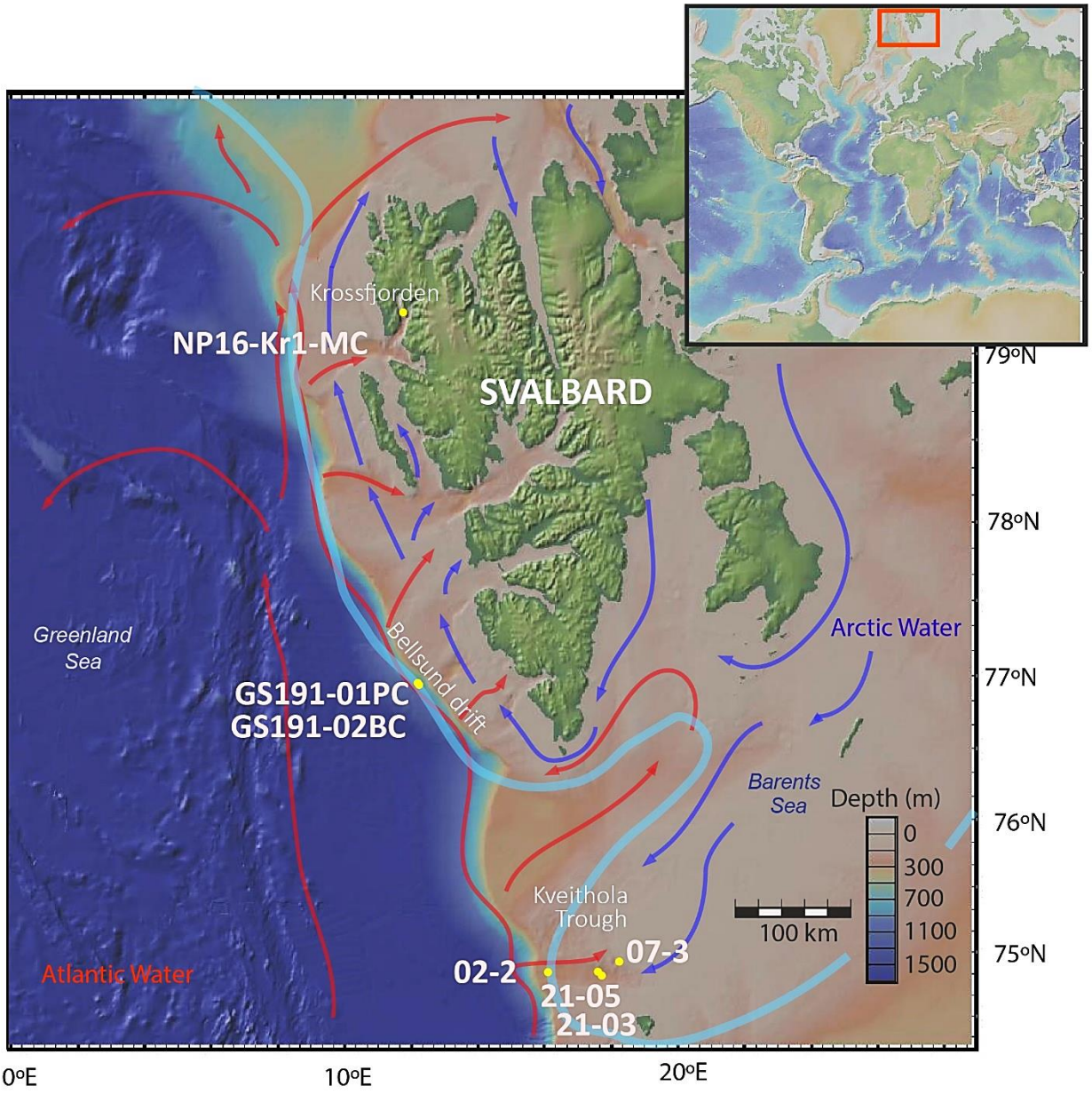


Fig. 1.1. Overview map showing the general location of the study area. The red arrows represent the Atlantic Water; the blue arrows represent the Arctic Water. The yellow dots indicate the sediment cores location. The light-blue line shows the media of the maximum extent of the sea ice in April between the years 1980-2010, using the data from the National Snow and Ice Data Centre (NSIDC), www.nsidc.com, and from Harris et al. (1998) and Faust et al. (2020)

All the chosen study sites are therefore, located under the present complex and quickly changeable interaction between the AW and the ArW, which are expected to be recorded by the sedimentological, the planktic and benthic foraminiferal records.

The overall objective of this study is to gain insight about the general evolution of the foraminiferal assemblages and the sedimentological evidences, under the interaction between the two main water masses forming the northernmost part of the Global Thermohaline Circulation influencing the Earth: the cold ArW and the warm AW. Understanding the potential warming of the Arctic region using as a proxy the temporal variability of the foraminiferal assemblages and the lithological characteristics in three different polar environments is the focus of this work. Furthermore, reconstruct the short-term and the long-term climatic events into the area (events with a duration of a few years to decades and events lasting hundreds of thousands of years, respectively), depicted from the down-core distribution of the foraminiferal fauna and grain size record at each site, will help to define the possible causes that occurred during the Holocene with particular focus to the last *ca.* 400 years. A secondary goal is to compare the living and dead benthic foraminiferal assemblages with the oceanographic data set, of the Kveithola Trough, which is the AW entry area within the Arctic system. The principal aim is to improve the knowledge of the short-term changes that benthic foraminiferal assemblages may suffer under rapid climatic variations.

1.1. References

Aagaard, K. 1989. A synthesis of the Arctic Ocean circulation. Le Conseil. Rapp. P. V. Reun. Cons. Int. Explor. Mer., 188, 11 – 22.

Comiso, J. C., Hall, D. K. 2014. Climate trends in the Arctic as observed from space. Wiley Interdisciplinary Reviews: Climate Change, 5(3), 389-409.

Dijkstra, N., Junttila, J., Skirbekk, K., Carroll, J., Husum, K., Hald, M. 2017. Benthic foraminifera as bio-indicators of chemical and physical stressors in Hammerfest harbor (Northern Norway). Marine Pollution bulletin, 114(1), 384-396.

Duplessy, J. C., Ivanova, E., Murdmaa, I., Paterne, M., Labeyrie, L. 2001. Holocene paleoceanography of the northern Barents Sea and variations of the northward heat transport by the Atlantic Ocean. Boreas, 30(1), 2-16.

Faust, J.C., Tessin, A., Fisher, B.J., Zindorf, M., Papadaki, S., Hendry, K.R., Doyle, K.A., März, C. 2021. Millennial scale persistence of organic carbon bound to iron in Arctic marine sediments. Nature communications, 12(1), 1-9.

Groot, D. E., Aagaard-Sørensen, S., Husum, K. 2014. Reconstruction of Atlantic water variability during the Holocene in the western Barents Sea. Climate of the Past, 10(1), 51-62.

Harris, C. L., Plueddemann, A. J., Gawarkiewicz, G. G. 1998. Water mass distribution and polar front structure in the western Barents Sea. Journal of Geophysical Research: Oceans, 103(C2), 2905- 2917.

Hop, H., Falk-Petersen, S., Svendsen, H., Kwasniewski, S., Pavlov, V., Pavlova, O., Søreide, J. E. 2006. Physical and biological characteristics of the pelagic system across Fram Strait to Kongsfjorden. Progress in Oceanography, 71(2-4), 182-231.

IPCC, 2019: IPCC Special Report on the Ocean and Cryosphere in a Changing Climate [H.-O. Pörtner, D.C. Roberts, V. Masson-Delmotte, P. Zhai, M. Tignor, E. Poloczanska, K. Mintenbeck, A. Alegría, M. Nicolai, A. Okem, J. Petzold, B. Rama, N.M. Weyer (eds.)]. In press.

Lind, S., Ingvaldsen, R. B., Furevik, T. 2018. Arctic warming hotspot in the northern Barents Sea linked to declining sea-ice import. Nature Climate Change, 8(7), 634-639.

Loeng, H. 1991. Features of the physical oceanographic conditions of the Barents Sea. Polar Research, 10(1), 5-18.

Loeng, H., Ozhigin, V., Ådlandsvik, B. 1997. Water fluxes through the Barents Sea. ICES Journal of Marine Science, 54(3), 310-317.

Luckman, A., Benn, D. I., Cottier, F., Bevan, S., Nilsen, F., Inall, M. 2015. Calving rates at tidewater glaciers vary strongly with ocean temperature. Nature Communications, 6(1), 1-7.

Maslowski, W., Marble, D., Walczowski, W., Schauer, U., Clement, J. L., Semtner, A. J. 2004. On climatological mass, heat, and salt transports through the Barents Sea and Fram Strait from a pan-Arctic coupled ice-ocean model simulation. Journal of Geophysical Research: Oceans, 109(C3).

Nilsen, F., Skogseth, R., Vaardal-Lunde, J., Inall, M. 2016. A simple shelf circulation model: intrusion of Atlantic Water on the West Spitsbergen Shelf. Journal of Physical Oceanography, 46(4), 1209-1230.

Orvik, K. A., Niiler, P. 2002. Major pathways of Atlantic water in the northern North Atlantic and Nordic Seas toward Arctic. Geophysical Research Letters, 29(19), 2-1.

Rebesco, M., Liu, Y., Camerlenghi, A., Winsborrow, M., Laberg, J. S., Caburlotto, A., Diviacco, P., Accettella, D., Sauli, C., Wardell, N. Tomini, I. 2011. Deglaciation of the western margin of the Barents Sea Ice Sheet—A swath bathymetric and sub-bottom seismic study from the Kveithola Trough. Marine Geology, 279(1-4), 141-147.

Rebesco, M., Wåhlin, A., Laberg, J.S., Schauer, U., Beszczynska-Möller, A., Lucchi, R.G., Noormets, R., Accettella, D., Zarayskaya, Y., Diviacco, P. 2013. Quaternary contourite drifts of the Western Spitsbergen margin. Deep Sea Research Part I: Oceanographic Research Papers, 79, 156-168.

Rudels, B., Friedrich, H. J., Quadfasel, D. 1999. The Arctic circumpolar boundary current. Deep Sea Research Part II: Topical Studies in Oceanography, 46(6-7), 1023-1062.

Rüther, D. C., Bjarnadóttir, L. R., Junttila, J., Husum, K., Rasmussen, T. L., Lucchi, R. G., Andreassen, K. 2012. Pattern and timing of the northwestern Barents Sea Ice Sheet deglaciation and indications of episodic Holocene deposition. Boreas, 41(3), 494-512.

Sarnthein, M., Van Kreveld, S., Erlenkeuser, H., Grootes, P. M., Kucera, M., Pflaumann, U., Schulz, M. 2003. Centennial-to-millennial-scale periodicities of Holocene climate and sediment injections off the western Barents shelf, 75° N. Boreas, 32(3), 447-461.

Schauer, U., Fahrbach, E., Osterhus, S., Rohardt, G. 2004. Arctic warming through the Fram Strait: Oceanic heat transport from 3 years of measurements. Journal of Geophysical Research: Oceans, 109(C6).

Screen, J. A., Simmonds, I. 2010a. The central role of diminishing sea ice in recent Arctic temperature amplification. Nature, 464(7293), 1334-1337.

Screen, J. A., Simmonds, I. 2010b. Increasing fall-winter energy loss from the Arctic Ocean and its role in Arctic temperature amplification. Geophysical Research Letters, 37(16). L16707, doi:10.1029/2010GL044136.

Serreze, M. C., Holland, M. M., Stroeve, J. 2007. Perspectives on the Arctic's shrinking sea-ice cover. Science, 315(5818), 1533-1536.

Ślubowska-Woldengen, M., Rasmussen, T. L., Koç, N., Klitgaard-Kristensen, D., Nilsen, F., Solheim, A. 2007. Advection of Atlantic Water to the western and northern Svalbard shelf since 17,500 cal yr BP. Quaternary Science Reviews, 26(3-4), 463-478.

Smedsrud, L. H., Esau, I., Ingvaldsen, R. B., Eldevik, T., Haugan, P. M., Li, C., Lien, V.S., Olsen, A., Omar, A.M., Otterå, O.H., Risebrobakken, B. 2013. The role of the Barents Sea in the Arctic climate system. Reviews of Geophysics, 51(3), 415-449.

Solomon, S., Manning, M., Marquis, M., Qin, D. 2007. Climate change 2007-the physical science basis: Working group I contribution to the fourth assessment report of the IPCC (Vol. 4). Cambridge University Press.

Sundfjord, A., Albretsen, J., Kasajima, Y., Skogseth, R., Kohler, J., Nuth, C., Skarðhamar, J., Cottier, F., Nilsen, F., Asplin, L. Gerland, S. 2017. Effects of glacier runoff and wind on surface layer dynamics

and Atlantic Water exchange in Kongsfjorden, Svalbard; a model study. Estuarine, Coastal and Shelf Science, 187, 260-272.

Svendsen, H., Beszczynska-Møller, A., Hagen, J. O., Lefauconnier, B., Tverberg, V., Gerland, S., Børre Ørbæk, J., Bischof, K., Papucci, C., Zajaczkowski, M. Azzolini, R. 2002. The physical environment of Kongsfjorden–Krossfjorden, an Arctic fjord system in Svalbard. Polar research, 21(1), 133-166.

Vinje, T., Kvambekk, Å. S. 1991. Barents Sea drift ice characteristics. Polar Research, 10(1), 59-68.

Wlodarska-Kowalczuk, M., Pearson, T.H., Kendall, M.A. 2005. Benthic response to chronic natural physical disturbance by glacial sedimentation in an Arctic fjord. Marine Ecology Progress Series, 303, 31- 41.

2. Materials and methodology.

2.1. Dataset

The dataset presented in this work was collected during three different oceanographic expeditions that took place between 2014-2016 in the areas of the Bellsund sediment drift, Krossfjorden located in the Kongsfjorden-Krossfjorden glacigenic system and the Kveithola glacigenic trough. Different multi-disciplinary research groups participated in each research cruise, supported by different international projects developed under the direction of diverse leaders and institutions. According to the purpose of each research project, different techniques of analysis were carried out and diverse instruments were used (Tab. 2.1).

2.1.1. *Calypso* Piston core: Holocene record *ca.* 12.0 kyr BP

The core GS191-01PC was collected at the crest of Bellsund sediment drift during the EUROFLEETS-2 Cruise PREPARED on board of the R/V G.O. Sars, June 2014. The core was collected at 1647 m water depth, using a *Calypso* piston corer. The preliminary results on board indicated that the sedimentary record contained the past 20 kyr with an expanded Holocene sequence (more than 5 m-thick) (Lucchi et al., 2014) (Tab. 2.1).

2.1.2. Multi cores and Box corer: the last *ca.* 100-400 years

For the high-resolution paleoclimatic and palaeoenvironmental reconstruction of the last *ca*. 100-400 years, short cores (box-corer and multi-corer) were collected.

a. Box corer: Bellsund drift

The box core GS191-02BC was collected at the crest of the Bellsund Drift, during the EUROFLEETS-2 Cruise PREPARED on board of the R/V G.O. Sars, June 2014. The recovery of the sediment was at the same site of the *Calypso* piston core GS19-01PC (see section 2.1.1.), using a box corer with a 30x3x50 cm steel box, to ensure the recovery of the uppermost part of the sedimentary record that can be compressed and/or disturbed during piston coring (Lucchi et al., 2014) (Tab. 2.1).

b. *Multi cores: Krossfjorden*

A short multi-core NP16-Kr1-MC was collected at the inner part of Krossfjorden during the NPI MOSJ-ICE 2016 cruise on board of the R/V Lance, July 2016. The sediment was recovered at a water deep of 105.6 m (Guruvayoorappan et al., 2019) (Tab. 2.1).

c. *Multi cores: Kveithola Trough*

Four multicores PS99.1/02-2, PS99.1/21-05, PS99.1/21-03 and PS99.1/07-3 (hereafter indicated as cores 02-2, 21-05, 21-03, and 07-3), were collected along the Kveithola glacial Trough, during the EUROFLEETS - 2 Cruise BURSTER on board of the R/V Polarstern, between 19th and 20th June 2016, in the framework of the AXED-PNRA project. The cores were collected using a video-guided multi corer (TV-MUC), at water depths ranging from 376 m to 159 m (Lucchi et al., 2016) (Tab. 2.1).

Location/Cruise	Core code	Type of core	Coordinates	Water depth (m)	Sediment recovered (cm)	Institutions involved in the multidisciplinary work
Bellsund Drift EUROFLEETS-2 Cruise PREPARED 2014	GS191-01PC	*Calypso* piston core	76° 31.30'N 12° 44.29'E	1647	1967	INOGS UniBCN UniPi CNR Bologna INGV Rome NPI
	GS191-02BC	Box-core	76° 31.30'N 12° 44.29'E	1647	25	
Krossfjorden NPI MOSJ-ICE 2016 cruise	NP16-Kr1-MC	Multi-core	79° 17.76'N 11° 36.48'E	105.6	32	NPI UniPi
Kveithola Trough EUROFLEETS - 2 Cruise BURSTER 2016	PS99.1/02-2 (02-2)	Multi-core	74° 51.49'N 16° 05.84'E	376.1	30	INOGS UniPi DiSVA UnivPM UniBCN UAM ISP-CNR Bologna
	PS99.1/21-03 (21-03)	Multi-core	74° 52.40'N 17° 21.57'E	305.7	8	
	PS99.1/21-05 (21-05)	Multi-core	74° 52.40'N 17° 21.60'E	305.4	25	
	PS99.1/07-3 (07-3)	Multi-core	74° 59.69'N 17° 59.72'E	159.1	38	

Tab. 2.1. General information of the sediment cores used for the study. Acronyms: INOGS= National Institute of Oceanography and Applied Geophysics; NPI= Norwegian Polar Institute; UniPi= Earth Science Department, University of Pisa; DiSVA UnivPM= Department of Life and Environmental Sciences, Polytechnic University of Marche; CNR Bologna= National Research Council; INGV Rome (headquarter) = National Institute of Geophysics and Volcanology; UAM= Adam Mickiewicz University, Poznam, Poland; UniBCN= University of Barcelona, Spain. ISP-CNR Bologna = Institute of Polar Sciences, Italian National Research Council.

2.2. Methodology

The *Calypso* piston-core was analysed with X-radiographs at ENI G&P laboratories using a CAT-scan instrument working on the full, unsplit sections. The sections were then transported to the UniBCN where they were split, visually logged, and analysed with an Avaatech XRF (X-ray fluorescence) for sediment chemical composition and Digital Photographs. The working sections were then, sampled at every 1 cm and treated for micropaleontological and sedimentological analysis. The samples used for this study were collected on the base of the age model, every *ca.* 100 years.

The multi-cores and box-corer were opened and sampled on-board, at each 0.5 cm until 2 cm, and at every 1 cm until core-bottom. The samples were used for sedimentological, chemical, ecological and micropaleontological analysis.

2.2.1. Sediment dating and age model

Sediment dating was performed using AMS (Accelerator Mass Spectrometry) radiocarbon (^{14}C) dating for the *Calypso* and box cores from the Bellsund Drift, and by using ^{210}Pb and ^{137}Cs on the short multi-cores collected in the Kveithola Trough.

a. Radiocarbon Dating

Four samples were collected in the core GS191-01PC for radiocarbon dating performed at NOSAM Laboratory (U.S.A.) on monospecific samples of *N. pachyderma* tests. The raw ^{14}C data were calibrated with the CALIB software version 7.1 (Stuiver and Reimer, 1993); using the Marine13 calibration curve (Reimer, 2013), and applying a global ocean reservoir correction (R) of 400 years, and an average marine regional reservoir effect delta R= 105±24, to accommodate local effects; (Mangerud et al., 2006, and Bondevik et al., 2006). The age model was defined by Caricchi et al. (2019) on the basis of the paleomagnetic parameters supported by the radiocarbon datings.

b. 210Pb and 137Cs Dating

Sedimentation rate (SR) for the cores PS99.1/02-2, PS99.1/21-05, PS99.1/21-03 and PS99.1/07-3, was determined on the basis of short-lived radionuclides (^{210}Pb and ^{137}Cs). Samples of 20 gram of sediment were homogenized, packed in vials of uniform geometry and left for three weeks before they were measured for 24 h with a high-purity germanium detector (Canberra BE3830 at the Institute of Geology,

Adam Mickiewicz University in Poznań, Poland). The ages and SR were reviewed and elaborated at CNR-ISP Bologna, where were calculated based on constant flux-constant sedimentation model (CF-CS) (Robbins and Edgington, 1975), and the results were validated through the identification of the peaks in ^{137}Cs activity (Ritchie and McHenry, 1990; Pittauerová, 2013). For this analysis, the samples were dried, homogenised, packet and sealed, and left over for at least 21 days prior to analysis. For age and SAR calculation constant initial concentration model (CIC) was applied (Kirchner, 2011). In order to avoid the compaction-impact on the age calculation, the sediment mass accumulation rate (MAR) was also calculated using the sediments' dry bulk density.

The age model of the box corer GS191-02BC was developed using ^{210}Pb and ^{14}C dating by the ISP-CNR Bologna. The age model of the core NP16-Kr-1-MC was determined at the NPI and was based on two anthropogenic ^{137}Cs time markers (Guruvayoorappan et al., 2019).

2.2.2. Sedimentology (Grain size analysis)

Grain size analyses were performed using different methods on the different datasets. The classical hierarchical Q-mode clustering analysis was used to analyse the grain size of the sediments (from 0.04 to 2000 µm).

a. Standard wet sieving procedure:

This method was applied for the Krossfjorden samples (NP16-Kr1-MC), performed by the NPI laboratories. This is a manual method where the dried, weighed sediment was separated using a sieves stack with different measures (from 8 µm to 63 µm), using water to wash the sediment through the sieve stack. The sediment remaining on each sieve was then dried and weighed. The sediment samples were grouped into three major fraction groups: sand (>63 µm), silt (8 - 63 µm), and clay (<8 µm) (Guruvayoorappan et al., 2019).

b. Laser diffraction granulometry Coulter-counter laser Beckman LS-230 and Camsizer X2:

This method was applied for the Bellsund drift and Kveithola Trough samples. The sediments were treated with peroxide to eliminate the organic matter, and the sediments were suspended into a 0.1% sodium-hexametaphosphate solution to be disaggregated and to prevent sediment flocculation. The samples were left 3 minutes into an ultrasonic bath before measurement (Tab. 2.2). The results were classified according to Friedman and Sanders (1978) grain-size scale.

Sample		Number of samples		Methodology and Institution on charge of the analysis
Calypso piston core	GS191-01PC	67	(each 10 cm)	Coulter-counter laser Beckman LS-230 (0.04-2000 µm), UniBCN
Box-corer	GS191-02BC	21	(each 0.5 cm until 2 cm and each 1 cm until bottom)	Camsizer X2, UniPi
Multicore	NP16-Kr1-MC	32	(each 1 cm)	Standard wet sieving procedure, NPI
Multi-corer	02-2	32	(each 0.5 cm until 2 cm and each 1 cm until bottom)	Coulter-counter laser Beckman LS-230 (0.04-2000 µm), UniBCN
	21-03	10		
	21-05	27		
	07-3	35		

Tab. 2.2. Grain size analysis: sample, instrument and institution in charge to perform the analysis.

c. Processing data set

The full range of the grain size measurements (0.04-2000 µm) were used to categorize the different kinds of deposits. I considered IRD the clasts with dimension ≥500 µm (Andrews, 2000 and references therein). The sediment size-fraction intervals indicate the differences between the resulting cumulative curves; hence, applying the hierarchical Q-mode cluster analysis of the samples, the similarity groups were marked in terms of the grain-size distribution, each group may be similar in shape of the cumulative curve.

2.2.3. Micropaleontological analysis

a. Preparation of the sediment samples:

For the micropaleontological analysis, the 0.5 or 1 cm thick sediment samples were oven-dried, weighed and wet-sieved with filtered tap water using the mesh size of 63 µm, to eliminate the fine fraction (Tab. 2.3). The last rinse was made using distilled water. If the sediment contained a lot of organic matter, to remove it, the sieved material was left in a 5% of sodium hypochlorite solution for 20 min, and washed again with distilled water. The sandy fraction (> 63 µm) was dried for 24 hours in an oven at 40°C (max.) and weighed again. Then, the sandy fraction was dry-sieved at 100 and 150 µm, while the finer sand fraction (63 µm to 100 - 150 µm) was stored for future studies. For this study, the ≥150 µm sieved fractions were used, except for the NP16-Kr1-MC core, where the sieve fraction of ≥100 µm was used, these different sieve fractions correspond with the protocol of work at each institution that was on charge of the data set.

The *Calypso* piston core GS191-01 PC, required special wash-protocol, in fact, the entire wash procedure was made with distilled water and the fine sediment fraction (< 63 μm) were collected and stored for further analysis (Tab. 2.3).

The Department of Life and Environmental Sciences, Polytechnic University of Marche, Ancona carried out the living foraminiferal analysis (Caridi, 2020). The sediment slices taken on board were incubated in a refrigerator for 12-15 hours in Cell Tracker Green CMFDA (CTG), and then fixed in 10% formalin buffered with sodium borate solution, following the staining procedure as indicated in Pucci et al. (2009). CTG is a non- terminal, non- fluorescent probe that can be cleaved by non-specific esterase common to living cells, producing a fluorescent compound, fluorescein, visible using a fluorescent microscope. The requirement of esterase activity means that a cell must be alive to produce fluorescence (Bernhard et al., 2006).

Sample		**Number of samples**		**Sampling frequency**
Calypso piston core Bellsund drift	GS191-01PC	120 (benthic foraminifera)		*ca.* 100 years
Box-corer Bellsund drift	GS191-02BC	21 (benthic foraminifera) 21 (planktic foraminifera)		0.5 cm until 2 cm and each 1cm until bottom
Multi-core Krossfjorden	NP16-Kr1-MC	25 (benthic foraminifera)		1 cm until the bottom
Multi-corer Kveithola Trough	02-2 21-03 21-05 07-3	32 10 27 26	(benthic foraminifera)	0.5 cm until 2 cm and each 1cm until bottom

Tab. 2.3. Number and sampling frequency of the samples used for micropaleontological analysis.

b. Picking and identification of the foraminifera:

The sieve sediment fraction used for micropaleontological analysis (≥100 μm for Krossfjorden core and ≥150 μm for the Bellsund drift and Kveithola Trough cores), was subdivided into equal amounts by microsplitter until a statistically representative sub-portion was obtained. At least 300 benthic and 300 planktic specimens were picked dry and identified at the species level, following the benthic taxonomy by Ellis and Messina catalogues (1940-1978), Loeblich and Tappan (1953, 1987, 2015), Feyling – Hanssen et al. (1971), Gabel (1971), Knudsen (1998), Wollenburg and Mackensen (1998), Holbourn et al. (2013), and Setoyama and Kaminski (2015). The planktic foraminifera were classified following the taxonomy of Darling et al. (2006), Hemleben et al. (2012) and Altuna et al. (2018). For each sample, foraminifera were

mounted on Plummer cells, and stored at the Micropaleo-Lab of the Earth Sciences Department, University of Pisa.

The main species are the taxa with more than 5% of the total assemblage. The paleoenvironmental significance of each species was established using the literature available for similar geographical areas (e.g. North Seas). This bibliographical information was included at the end of each chapter.

The counting of the planktic foraminifera from the *Calypso* piston core was realised at the INOGS laboratories, and I performed the data set analysis.

Taxonomic notes: In this study, I picked, identified and counted separately *Buccella frigida* and *Buccella inusitata,* grouped later as *Buccella* spp. Also, *Islandiella norcrossi* and *Islandiella helenae,* grouped later as *Islandiella* spp. The species *Reophax scorpiurus* and *Reophax fusiformis,* grouped later as *Reophax* spp. The species *Elphidium clavatum* includes the species *Elphidium excavatum* and the subspecies *Elphidium excavatum* var*. clavatum* (Murray, 2006, p. 118). Rotaliida spp. comprises the genera *Rosalina* spp., and a group of species belonging to the same genus difficult to be identified, since they constantly present a preferential breakage in the aperture area (see Chapter 6, Plate 2).

The living foraminiferal taxa have been studied at DiSVA UnivPM, where the sediment samples were sieved through 63 and 150 µm mesh, and kept wet while the total amount of living specimens were hand-sorted using a fluorescence binocular microscope. For this study, the data obtained from the coarse fraction (>150 µm) were used, and the soft-shelled foraminifera were not consider because these taxa are not preserved in the thanatocoenosis, as their organic tests degrade and disappear as soon as they die.

c. Data elaboration, diversity indexes and statistical analysis

Data elaboration

The foraminiferal data were expressed as: relative abundance (%), concentration (specimens per gram of dry sediment, spec./g), and flux (spec./cm^2/yr).

Relative abundance is the proportion of a specimen (taxa) that belongs to the assemblage, and expressed in percentage (Webb, 1974). It was calculated using the number of specimens of one species divided by the total number of the specimens into the assemblage in the sample.

(S1 / ΣS) x 100% = S1% where S1 is the number of specimens of one species and ΣS is the total number of specimens into the assemblage in the sample.

The concentration of the specimens is the number of specimens per gram of dry sediment in one sample.

spec./ sed. (g.) = concentration where spec. is the number of specimens in the sample and sed. (g.) is the weight of the dry sediment in gram.

Foraminiferal flux was calculated using the method of Ehrmann and Thiede (1985).

Flux (spec./cm^2/yr)= concentration (spec./g) x bulk density (g/cm^3) x SAR (cm/yr) where SAR is the Sediment Accumulation Rate at each site (see section 2.3.2) (SR in cm/yr can be also used instead of SAR). Bulk density was calculated from the sediment water content and porosity.

For the Kveithola Trough multi-corer in which the living benthic foraminiferal assemblages were counted, to compare living to dead foraminiferal data, we normalised the values of the living foraminifera for volume of sediment, in gram of sediment, using the following formula:

$m=\rho V$ where: m is the mass of the sediment in gram; ρ is the density in g/c.c. and V the volume in c.c.

The living and dead ratios were calculated against total fauna as follows:

L/(L+D) where: L=% of living foraminifera and D=% of dead foraminifera, according to Jorissen and Wittling (1999).

Diversity indexes and statistical analysis

Using the free software Paleontological Statistics PAST (Hammer et al., 2001), the diversity indexes were calculated. Diversity indexes provide important information about rarity and commonness of species in a community. These indexes aim to describe general properties of communities that allow us to compare different regions, taxa, and trophic levels. The possibility to quantify diversity in this way is an important tool to understand community structure. Diversity indices are statistically used to summarize the diversity of a population in which each member belongs to a unique group (Hammer et al., 2001).

Number of taxa S corresponds to the number of species at each sample (Hammer et al., 2001).

Dominance D, corresponds with a relative abundance index, where the dominance represents the degree to which taxon is more or less numerous than its competitors in an ecological community, or like a part of the biomass indicates the presence of the taxa into the assemblage. Ranges between 0 that indicate that all taxa are equally present to 1 one taxon dominates the assemblage (Hammer et al., 2001).

Shannon index H, it is a diversity index, used to characterize species values into the assemblage taking into account both the number of species (S) and the number of specimens. It varies from 0 indicating an assemblage with only one taxon, to a value of 3 or 4 when the number of species and equitability increases (Hammer et al., 2001).

The classical hierarchical Q-mode clustering analyses were performed to define the periods in which changes occur within the foraminiferal assemblages. All the species identified for the paleo-communities were used for the classical hierarchical Q-mode cluster analyses, based on a similarity measure, in this case, the relative percentage of the species into the assemblages, in vertical distribution (grouping samples by similarities into the assemblage).

2.2.4. Oceanographic data set

The oceanographic analyses were carried out by the scientific party of the INOGS, Trieste.

a. Thermohaline data

In the study area, temperature (T, °C), salinity (SAL, PSU), dissolved oxygen (DO, ml l^{-1}), and light beam transmission (BT, %) were recorded throughout the water column by means of a SeaBird 911-plus CTD (Conductivity-Temperature-Depth) mounted on the SBE 32 Carousel Water Sampler (Rosette) equipped with 24 Niskin Bottles (12-liter capacity). The DO concentration was also determined in parallel on water samples taken at discrete depths from the Niskin bottles using the Winkler method (Carpenter, 1965).

Potential temperature (θ, °C) and potential density anomaly (σ_θ, kg m^{-3}, referred to 0 dbar) were calculated from each original in-situ data set using the toolbox TEOS-10 (http://www.teos-10.org/software.htm). Some data are plotted using Ocean Data View (ODV; Schlitzer, 2018).

b. Horizontal currents

The vertical distributions of horizontal currents were obtained from a vessel mounted Acoustic Doppler Current Profiler (vmADCP, Teledyne RDI 150 kHz Ocean Surveyor configured in 'Narrowband' mode). The water column was divided into 80 cells with 4 m size obtaining data in the range from approximately 10 m to 320 m depth. However, the vmADCP cannot sample more than 80–90 % of the water column within its operating range, so it does not allow for measuring currents close to the seafloor. In our study area, the blanking distance amounts to about 40-50 m above the seafloor.

c. Satellite images

To identify the southern limit of the sea ice extent during winter, I used satellite images that are freely available from the NASA Worldview application (https://worldview.earthdata.nasa.gov), part of the NASA Earth Observing System Data, and Information System (EOSDIS). The imagery resolution is 250 m, and the temporal resolution is daily.

2.3. Thesis organization

The following chapters were organised according to the stratigraphical and geographical location of the studied cores. Starting with the deepest area and the record that includes the entire Holocene, which corresponds to the *Calypso* piston core from Bellsund Drift, followed by the records that comprise the last 400 years: the box corer collected at the Bellsund Drift, the multicore from the northernmost area Krossfjorden, and the multicores from the southernmost area Kveithola Trough. In the Kveithola Trough, additional multidisciplinary analyses were carried out, using a set of biological, oceanographic and paleontological data obtained during the EUROFLEETS - 2 Cruise BURSTER, where the living and dead foraminiferal assemblages were compared, thus closing the thesis with the most recent data of the studied areas.

2.4. References

Altuna, N. E. B., Pieńkowski, A. J., Eynaud, F., Thiessen, R. 2018. The morphotypes of *Neogloboquadrina pachyderma*: Isotopic signature and distribution patterns in the Canadian Arctic Archipelago and adjacent regions. Marine Micropaleontology, 142, 13-24.

Andrews, J. T. 2000. Icebergs and iceberg rafted detritus (IRD) in the North Atlantic: facts and assumptions. Oceanography, 100-10

Bernhard, J. M., Ostermann, D. R., Williams, D. S., Blanks, J. K. 2006. Comparison of two methods to identify live benthic foraminifera: A test between Rose Bengal and CellTracker Green with implications for stable isotope paleoreconstructions. Paleoceanography, 21(4).

Bondevik, S., Mangerud, J., Birks, H. H., Gulliksen, S., Reimer, P. 2006. Changes in North Atlantic radiocarbon reservoir ages during the Allerød and Younger Dryas. Science, 312(5779), 1514–1517. https://doi.org/10.1126/science.1123300

Caricchi, C., Lucchi, R.G., Sagnotti, L., Macrì, P., Di Roberto, A., Del Carlo, P., Husum, K., Laberg, J.S., Morigi, C. 2019. A high-resolution geomagnetic relative paleointensity record from the Arctic Ocean deep-water gateway deposits during the last 60 kyr. Geochemistry, Geophysics, Geosystems, 20(5), 2355-2377.

Caridi, F. 2020. Influence of environmental patterns on the benthic faunal structure in the Kveithola Trough, NW Barents Sea. PhD thesis. Department of Life and Environmental Sciences, Polytechnic University of Marche. 172

Carpenter, J.H. 1965. The Chesapeake Bay Institute technique for the Winkler dissolved oxygen method. Limnology and Oceanography 101, 141-143.

Darling, K. F., Kucera, M., Kroon, D., Wade, C. M. 2006. A resolution for the coiling direction paradox in *Neogloboquadrina pachyderma*. Paleoceanography, 21(2).

Ehrmann, W. U., Thiede, J. 1985. History of mesozoic and cenozoic sediment fluxes to the-North Atlantic Ocean. Contributions to Sedimentary Geology. 15, 119

Ellis, B.E., Messina, A.R. 1940–1978. Catalogue of Foraminifera American Museum of Natural History. (New York).

Feyling-Hanssen, R. W., Jørgensen, J. A., Knudsen, K. L., Lykke-Andersen, A. L. 1971. Late Quaternary Foraminifera from Vendsyssel, Denmark and Sandnes, Norway. Copenhagen: Geological Society of Denmark.

Friedman, G. M., Sanders, J. E. 1978. Principles of sedimentology. Wiley.

Gabel, B. 1971. Die Foraminiferen der Nordsee. Helgoländer wissenschaftliche Meeresuntersuchungen, 22(1), 1-65.

Guruvayoorappan, H., Miettinen, A., Divine, D. V., Moros, M., Orme, L. C., Mohan, R. 2019. Ocean surface warming in Krossfjorden, Svalbard, during the last 60 years. Arktos, 1-13.

Hammer, Ø., Harper, D.A.T., Ryan, P.D. 2001. PAST: Paleontological statistics software package for education and data analysis. Palaeontologia Electronica 4(1): 9 http://palaeo-electronica.org/2001_1/past/issue1_01.htm

Hemleben, C., Spindler, M., Anderson, O. R. 2012. Modern planktonic foraminifera. Springer Science Business Media.

Holbourn, A., Henderson, A. S., MacLeod, N. 2013. Atlas of benthic foraminifera. John Wiley Sons.

Jorissen, F. J., Wittling, I. 1999. Ecological evidence from live–dead comparisons of benthic foraminiferal faunas off Cape Blanc (Northwest Africa). Palaeogeography, Palaeoclimatology, Palaeoecology, 149(1-4), 151-170.

Kirchner, G. 2011. ^{210}Pb as a tool for establishing sediment chronologies: examples of potentials and limitations of conventional dating models. Journal of Environmental Radioactivity, 102(5), 490-494

Knudsen, K. L. 1998. Foraminiferer i Kvartær stratigrafi: Laboratorie-og fremstillingsteknik samt udvalgte eksempler. Geologisk Tidsskrift, 3(125), 1-25.

Loeblich, A. R., Tappan, H. N. 1953. Studies of Arctic foraminifera. Smithsonian Miscellaneous Collections.

Loeblich, A.R., Tappan, H. 1987. Foraminiferal Genera and Their Classification. Van Nostrand Reinhold Co, New York.

Loeblich Jr, A. R., Tappan, H. 2015. Foraminiferal genera and their classification. Springer.

Lucchi R.G., Kovacevic V., Aliani S., Caburlotto A., Celussi M., Corgnati L., Cosoli S., Deponte D., Ersdal E.A., Fredriksson S., Goszczko I., Husum K., Ingrosso G., Laberg J.S., Lacka M., Langone L., Mansutti P., Mezgec K., Morigi C., Ponomarenko E., Realdon G., Relitti F., Robijn A., Skogseth R., Tirelli V. 2014. PREPARED: Present and past flow regime on contourite drifts west of Spitsbergen. EUROFLEETS-2 Cruise Summary Report, R/V G.O. Sars Cruise No. 191, 05/06/2014 – 15/06/2014, Tromsø – Tromsø (Norway), 89. DOI: 10.13140/RG.2.1.1975.3769.

Lucchi, R.G., Bazzaro, M., Biebow, N., Carbonara, K., Caridi, F., De Vittor, C., Dominiczak, A., Gamboa Sojo, V.M., Graziani, S., Kovacevic, V., Krueger, M., Le Gall, C., Mazzini, A., Morigi, C., Musco, M.E., Povea, P., Relitti, F., Ruggiero, L., Rui, L., Sabbatini, A., Sánchez Guillamón, O., Tagliaferro, M., Topchiy, M., Wiberg, D., Zoch, D., with the collaboration of the scientific party of the Italian PNRA project DEFROST: Bensi, M., Deponte, D., Langone, L., Laterza, R. 2016. BURSTER - Bottom Currents in a Stagnant Environment, EUROFLEETS-2 Cruise Summary Report. 106. DOI: 10.13140/RG.2.2.24223.36004.

Mangerud, J., Bondevik, S., Gulliksen S., Hufthammerd A.K., Høisætere, T. 2006. Marine ^{14}C reservoir ages for 19th century whales and molluscs from the North Atlantic. Quaternary Science Reviews, 25, 23-24, 3228-3245

Murray, J. W. 2006. Ecology and applications of benthic foraminifera. Cambridge University Press.

Pittauerová, D., 2013. Gamma spectrometry for chronology of recent sediments. PhD thesis, Bremen University, 213.

Pucci, F., Geslin, E., Barras, C., Morigi, C., Sabbatini, A., Negri, A., Jorissen, F. J. 2009. Survival of benthic foraminifera under hypoxic conditions: Results of an experimental study using the CellTracker Green method. Marine Pollution Bulletin, 59(8-12), 336-351.

Reimer, P. 2013. IntCal13 and Marine13 radiocarbon age calibration curves 0–50,000 years cal BP. Radiocarbon. 55, 1869–1887.

Ritchie, J.C., McHenry, J.R. 1990. Application of radioactive fallout cesium-137 for measuring soil erosion and sediment accumulation rates and patterns: A review. J. Env. Quality 192, 215-233.

Robbins, J.A., Edgington, D.N., 1975. Determination of recent sedimentation rates in Lake Michigan using Pb-210 and Cs-137. Geochim. et Cosmochim. Acta,393, 285-304.

Setoyama, E., Kaminski, M. A. 2015. Neogene benthic foraminifera from the southern Bering Sea (IODP Expedition 323). Palaeontologia Electronica, 18(38A), 1-30.

Stuiver, M., Reimer, P.J. 1993. Extended ^{14}C data base and revised CALIB 3.0 14C age calibration program. Radiocarbon. 35, 215–230

Webb, D. J. 1974. The statistics of relative abundance and diversity. Journal of Theoretical Biology, 43(2), 277–291.

Wollenburg, J. E., Mackensen, A. 1998. Living benthic foraminifers from the central Arctic Ocean: faunal composition, standing stock and diversity. Marine Micropaleontology, 34(3-4), 153-185.

3. Holocene record from Bellsund Drift, *ca.* 12.0 kyr BP

3.1. Study area

The eastern side of the Fram Strait represents an important gateway for the flux of warm water from the middle latitudes to the Arctic Ocean (Schauer et al., 2004). The West Spitsbergen Current (WSC) is the northern branch of the North Atlantic Currents (NAC). The WSC is responsible for the ice-free conditions in the west, and north Svalbard area during the winter; hence, it strongly influences the climate in the Arctic region (IPCC, 2019). In the Fram Strait, the WSC consists of three branches: the Return Atlantic Current (RAC western current), the Svalbard Branch (SB) and the Yermak Branch (YB) (Nilsen et al., 2016) (Fig. 3.1). Other local currents are the Spitsbergen Polar Current (SPC), is a surface coastal current associated with the West Spitsbergen Polar Front; it transports cold, fresh Arctic Water (Nilsen et al., 2016). The Spitsbergen Trough Current (STC) consists of Atlantic Water (AW) forced to circulate in the troughs (Nilsen et al., 2016) (Fig. 3.1). The deep marine environment hosts the northward moving Norwegian Deep Sea Water representing the deep branch of the WSC, which periodically refills with sediments transported by dense shelf waters masses (cold, saline, and sediment-laden). These water masses are formed on the shelf during wintertime by freezing and salt rejection and move to the shelf break to cascade along the slope (Hopkins, 1991). Along the western side of the Fram Strait, instead, it descends the cold Arctic waters forming the East Greenland Current (EGC); this oceanic current contributes to the maintenance of the Greenland ice cap (Hopkins, 1991; Aagaard et al., 1987) (Fig. 3.1).

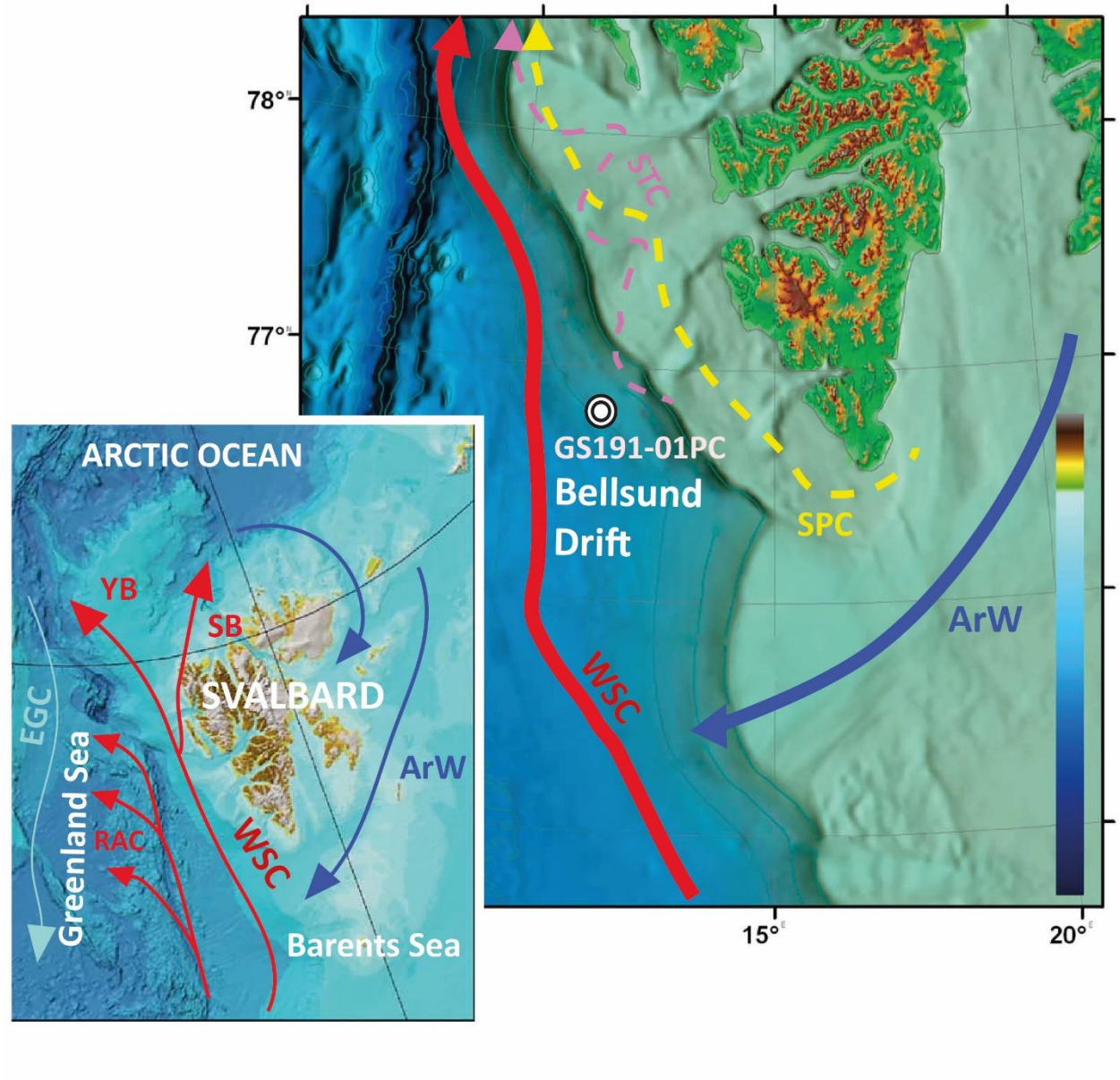


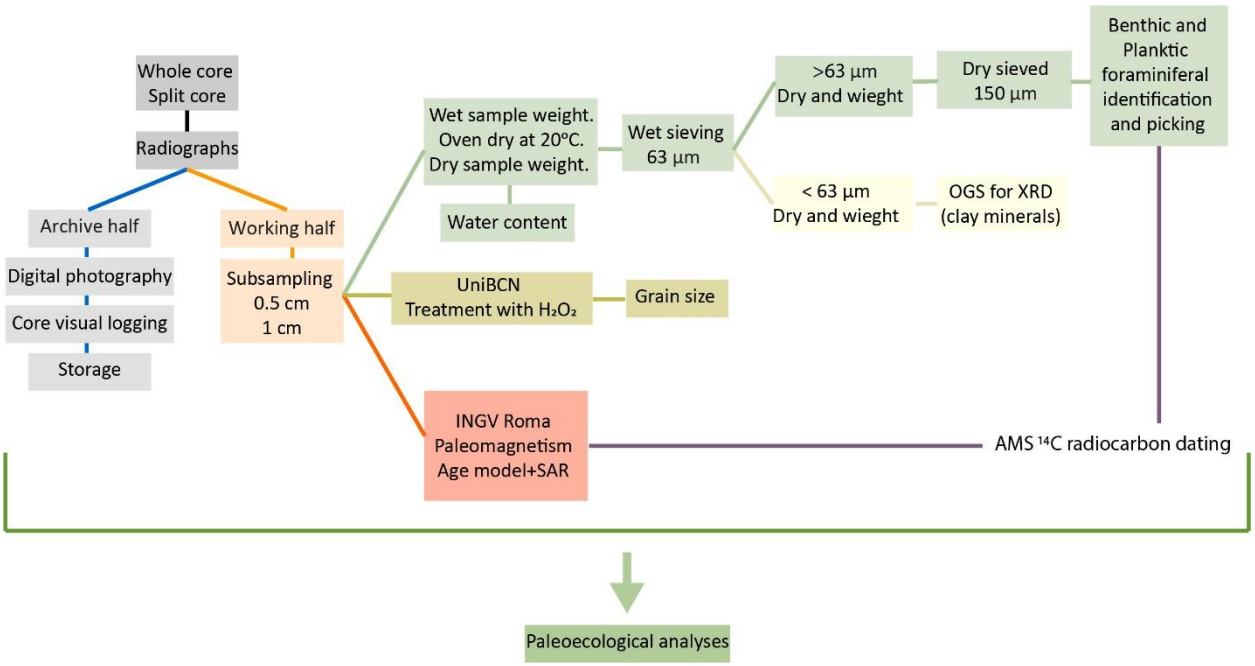
Fig. 3.1. Study area showing the main oceanographic setting. The red arrow indicates the West Spitsbergen Current (WSC) and the correspondent branches: Return Atlantic Current (western RAC), Yermak Branch (YB) and Svalbard Branch (SB). The yellow arrow indicates the Spitsbergen Polar current (SPC) and the pink arrow indicates the Spitsbergen Trough Current (STC). The blue arrow indicates the Arctic Water (ArW). The light-blue arrow indicates the East Greenland Current (EGC) Right the black/white dot shows the point of the *Calypso* piston core GS191-01PC. (After Caricchi et al., 2019; Nilsen et al., 2016).

The sedimentation in the Fram Strait area is mainly controlled by the bottom currents since the Late Miocene (Eiken and Hinz, 1993). The West shelf of Spitsbergen located at the eastern side of the Fram Strait represents an important sediment depocenter (Rebesco et al., 2013). It is characterised by a trough-shaped morphology, resulting from several advances and retreats of the grounded ice as part of the Svalbard-Barents Sea ice sheet, during the Late Quaternary climatic changes (e.g. Elverhøi et al., 1998; Patton et al., 2017). Glacigenic processes influenced this area since the onset of shelf edge glaciations occurred since 1.3 Myr BP (Rebesco et al., 2013), with building of the Trough Mouth Fans (TMF) representing fan-shaped piles of detritus. Contemporaneously with glacigenic deposition occurring during glacials, bottom currents moving along the slope (contour currents) contribute with sediment transport and accumulation forming sediment drifts. Contouritic deposition is the main depositional process occurring during interglacial (Eiken and Hinz, 1993; Lucchi et al., 2013).

The Bellsund drift is a contourite drift, identified on the seismic profiles collected along the western continental margin of Svalbard (76°-78°N), in the north area of the Storfjorden glacial Trough (Rebesco et al., 2013) (Fig. 3.1). Sedimentation by contour currents began in this area during the Early Pleistocene with sediment transport increase during glacials by abundant input of detritus (Rebesco et al., 2013). The sediment accumulation during the millennial activity of bottom currents is responsible for deposition of the contouritic drifts, which are mounded bathymetric features (Rebesco et al., 2014). Contouritic drifts are characterised by relatively high and continuous accumulation rates, in contrast to adjacent condensed hemipelagic/pelagic sequences (Rebesco et al., 2008; 2014). The contourite drifts are, therefore, ideal for the study of oceanographic and climate history (Laberg et al., 2005; Knutz, 2008; Rebesco et al., 2008). The Holocene sedimentary sequences recovered from the Bellsund Drift contain a high-resolution depositional record, which including structural and textural characteristics, indicating persistent bottom currents and sediment transport in nutrient and oxygen-rich depositional environments (Lucchi et al., 2013). The Bellsund sediment drift record is associated with the past climate changes that can contribute significantly to the reconstruction of the Svalbard-Barents Sea ice sheet history and the related palaeoceanographic configuration (Caricchi et al., 2019).

3.2. Material and methodology

The workflow 3.1 shows the scheme of the materials and methods (Chapter 2) followed for the study of the *Calypso* piston core collected in Bellsund Drift.



Workflow 3.1. Summary scheme of the materials and methods used for the *Calypso* piston core GS191-01PC. For more details, see chapter 2. Materials and methodology.

3.3. Age model

Caricchi et al. (2019) developed the age model for the *Calypso* piston core GS191-01PC (Fig. 3.2). The age model is defined on the paleomagnetic record, supported by radiocarbon dates and by using lithostratigraphic information for the identification of key intervals (Caricchi et al., 2019). All ages are calibrated to the calendar year using the Calib 7.1 software and are reported in kyr BP (Tab. 3.1).

The age model indicates that core GS191-01PC contains an expanded stratigraphic sequence for the Holocene (with almost 6 m of sediments) (Caricchi et al., 2019) (Fig. 3.2).

Proxies	Sample code and depth	^{14}C BP radiometric dating
Accelerator mass spectrometry ^{14}C dating	GS191-01PC 45 cm bsf	1212
	GS191-01PC 231 cm bsf	5017
	GS191-01PC 360 cm bsf	7718
	GS191-01PC 552 cm bsf	10472

Tab. 3.1. Accelerator mass spectrometry ^{14}C dating (from Caricchi et al., 2019)

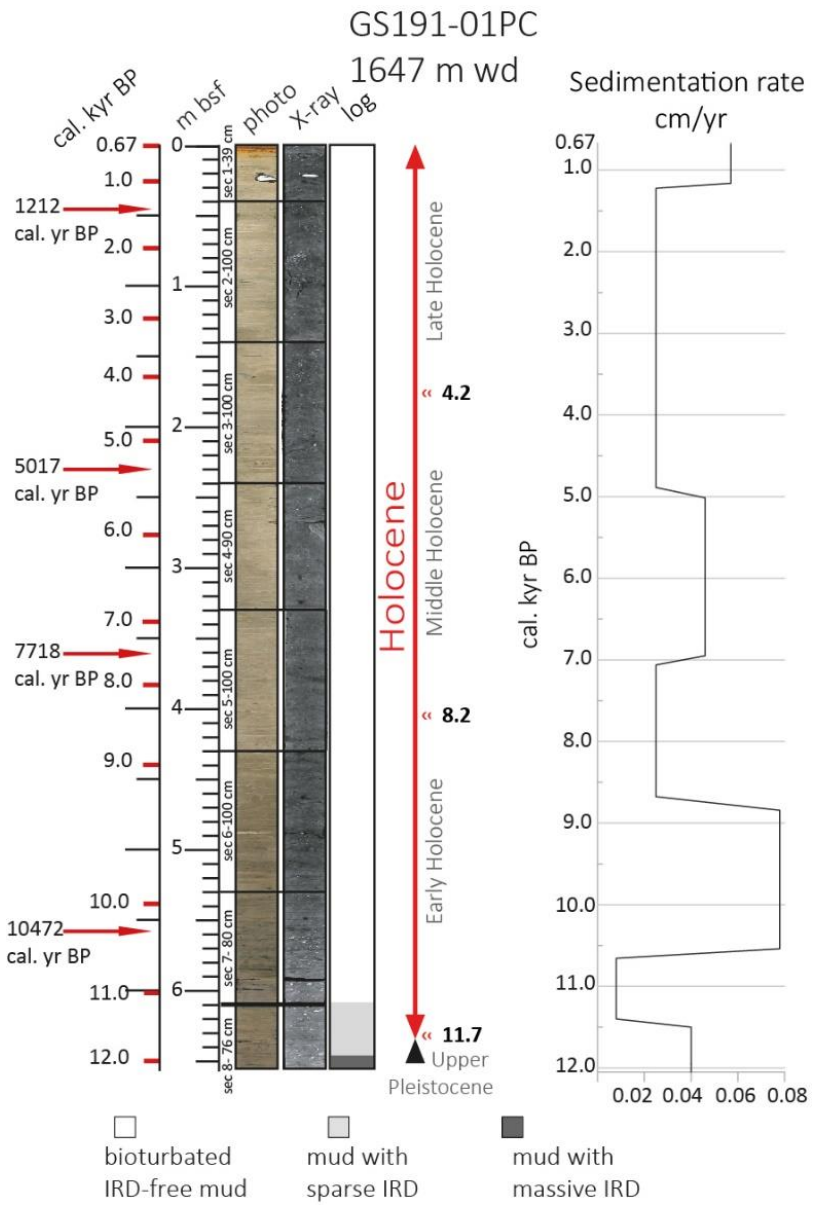


Fig. 3.2. Core data: photo, x-ray and lithological log. Sedimentation rates are calculated using calibrated radiometric ages, and the tie points identified by paleomagnetic and rock magnetic parameters correlations. Ages from the age model are also indicated (after Caricchi et al., 2019).

3.4. Main lithofacies

This study focuses on the last 12.0 kyr BP corresponding to the upper 6.5 m of core GS191-01-PC (Fig. 3.2). The Holocene is formed mud with abundant microfossils, bioturbation marks and very rare ice rafted debris (IRD), whereas very fine-grained sediments (mud) with abundant IRD and rare presence of microfossils forms the older sedimentary records (below 6.2 m bsf).

3.5. Results

3.5.1. Grain Size

The grain size of the entire core is mainly composed of silt (Fig. 3.3). The deeper interval with fine-grained sediments occasionally laminated with IRD levels (picture and X-ray Fig. 3.2), indicates typical glaciomarine sedimentation.

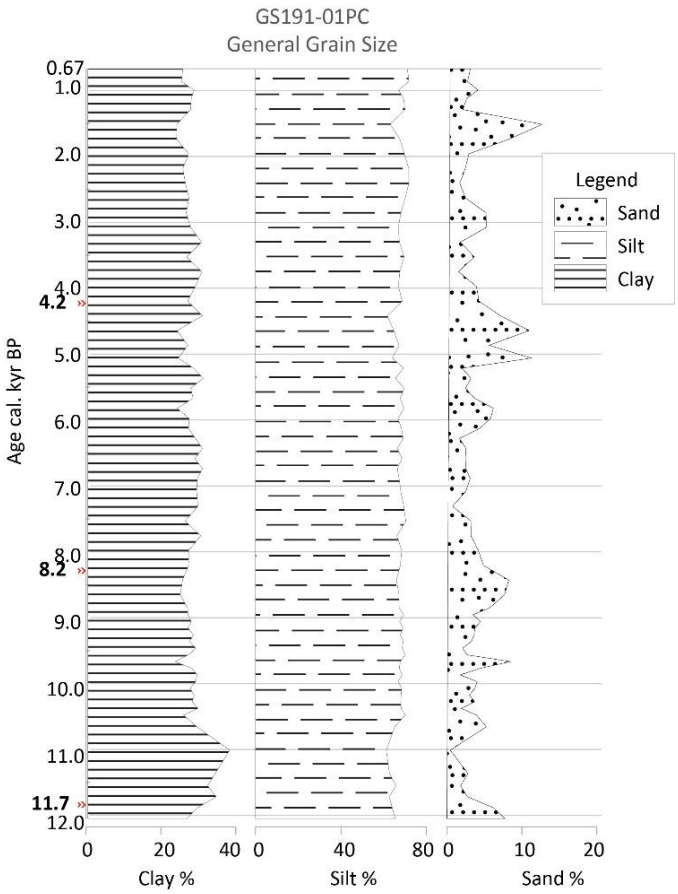


Fig. 3.3. Grain size: relative percentage of sand silt and clay. The x-axes are different.

A Q-mode cluster analysis is applied to the whole dataset of the grain size results, with cluster grouping samples having similar characteristics of the cumulative curve (Fig. 3.4 a). Three cluster analyses are performed, the first cluster allowed us to identify the main granulometric groups. A few samples that could not fit within any group are considered as “outliers” (Fig. 3.4 a). The second cluster is performed by removing the outliers (Fig. 3.4 b), whereas the third cluster is run without the clay fraction 0.04 -2 µm, in order to remove the bias created by the colloidal behaviour of this material, which measurement is at the limit of the instrumental resolution.

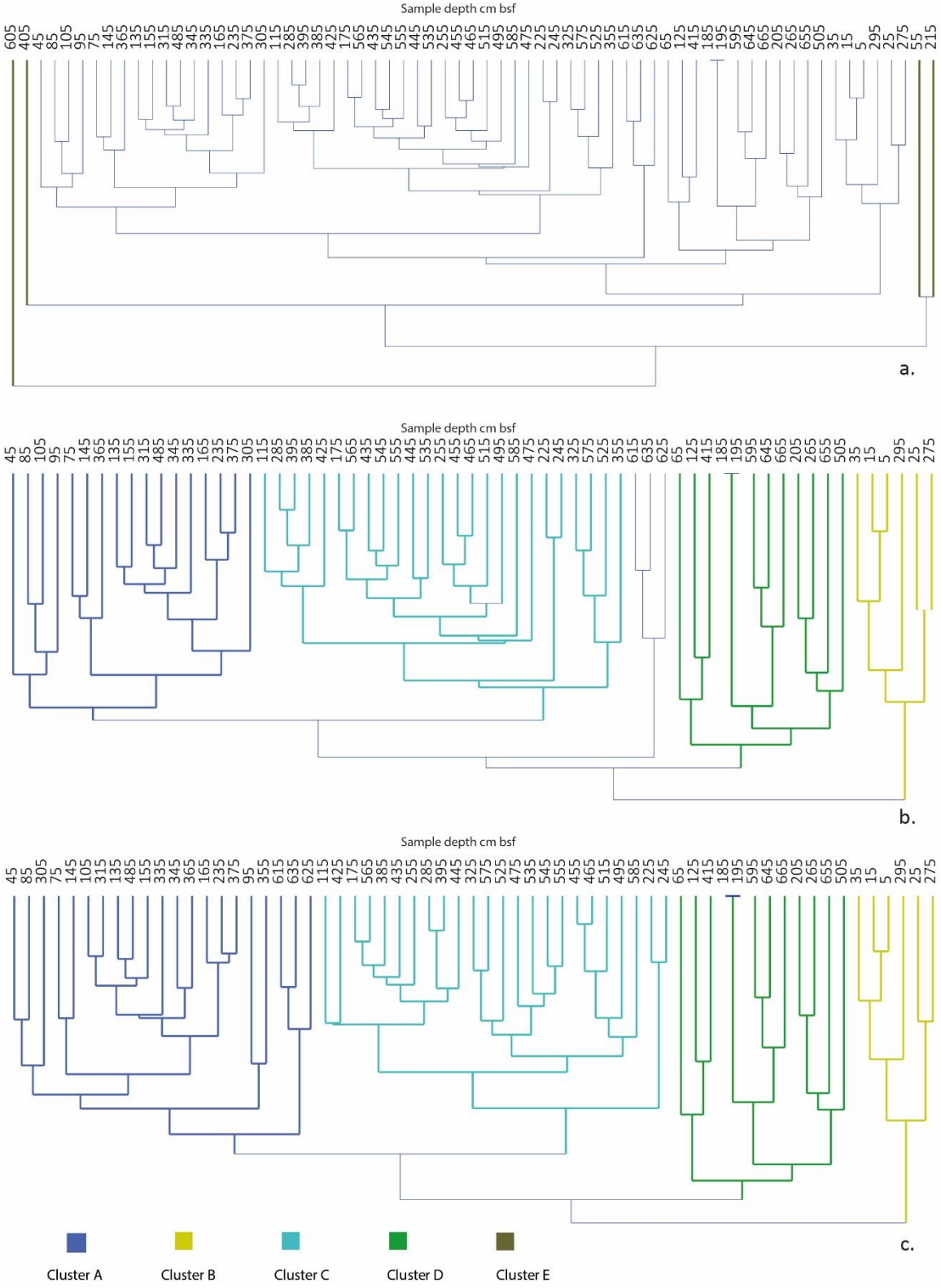


Fig. 3.4. Grain size Q-mode clustering analysis: a. Dendrogram of the grain size distribution showing the outliers (olive-green lines). b. Dendrogram performed without outliers, colours represent each group. c. Dendrogram without the fine fraction with the final division.

The Q-mode cluster analysis allowed dividing the samples in five groups called Cluster A, B, C, D and E (Fig. 3.4 and 3.5). The different clusters are reported on the sedimentary record of Figs. 3.5 and 3.6, and are describes in the following:

Cluster A: group samples containing very fine-grained sediments having mode 5.1 μm (very fine-fine silt). Cluster B: group samples containing fine-grained sediments with a prominent mode at 63 μm (fine silt). Cluster C and D: group sediments having mode at 10 μm (medium silt) corresponding to the sortable silt of McCave et al. (1995). Differently from Cluster C, the samples grouped in Cluster D contain a higher percentage of IRD. Cluster E: group sediments characterised by abundant IRD deposits.

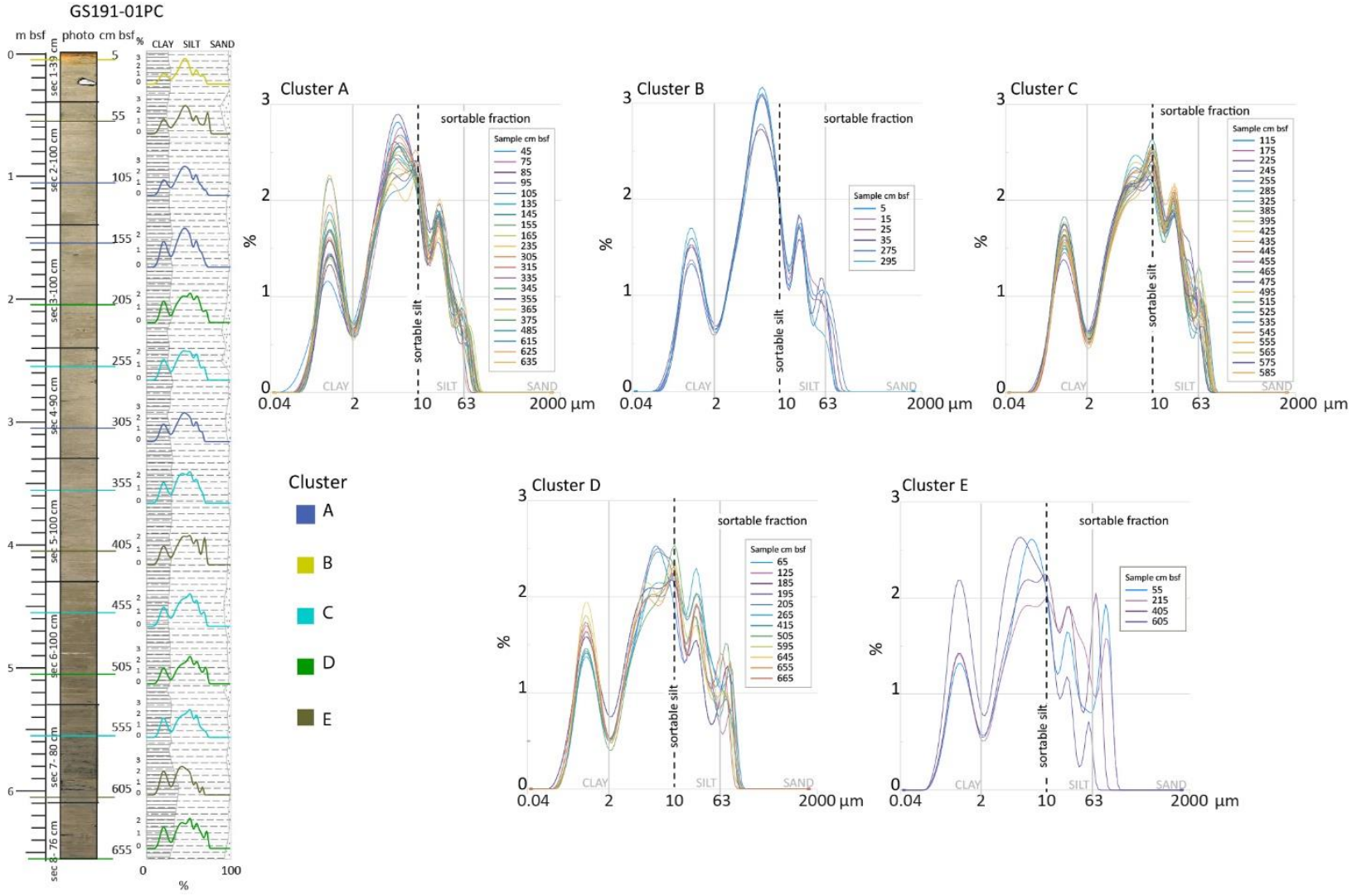


Fig. 3.5. Grain size: frequency curves. a. Distribution on depth on the core (each 50 cm) and b. Grain size spectra per each group based on the Q-mode cluster analysis (Fig. 3.4). The sortable silt fraction corresponds with the fraction superior at 10 µm, defined by Lucchi et al. (2002, 2007) includes the sortable silt fraction (10-36 µm) and the fine fraction of the sand (63-250 µm) (Friedman and Sanders, 1978).

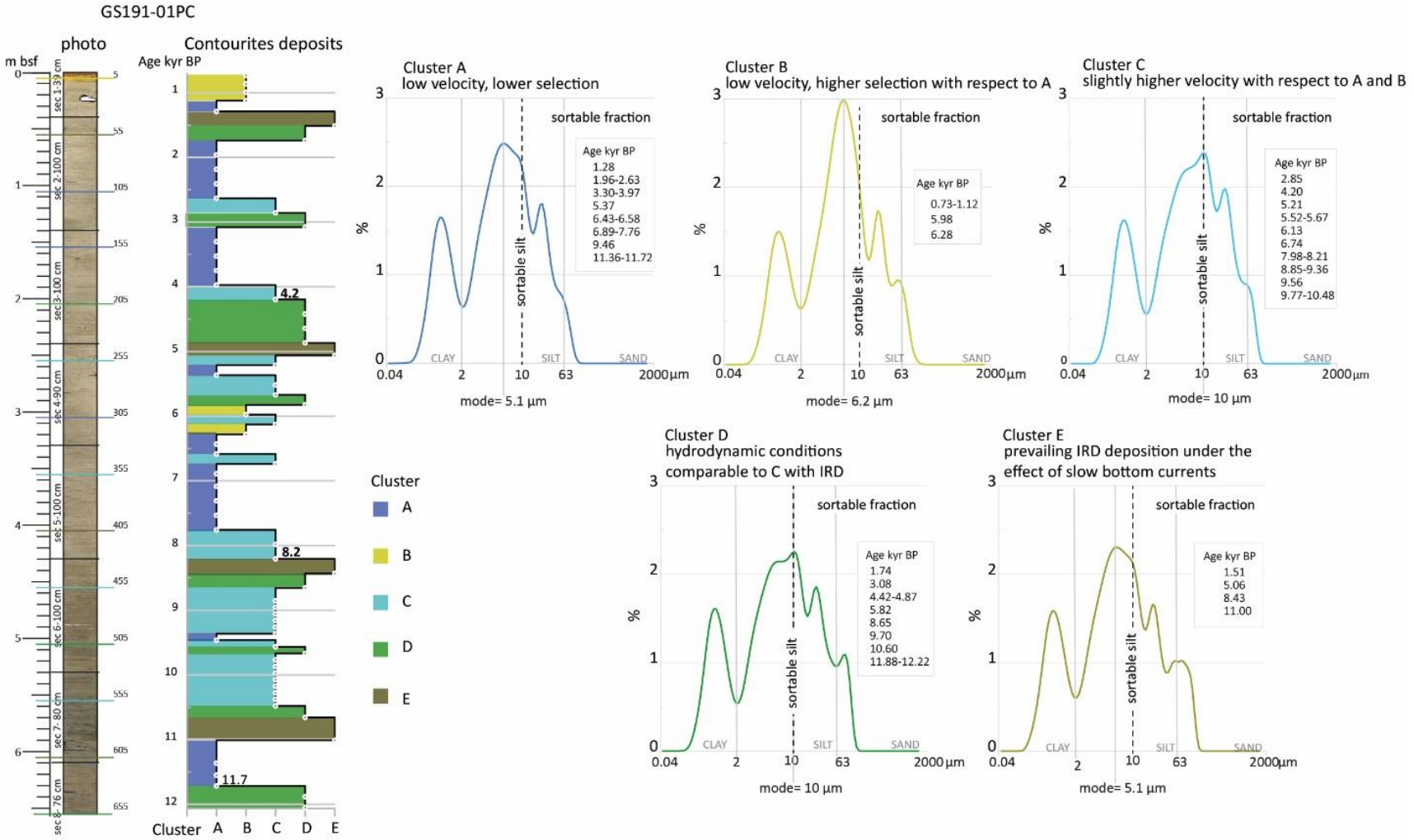


Fig 3.6. Distribution and average value of the grain size spectra.

All the grain size spectra are incorporated in the clusters, therefore, support the interpretation of bottom current related deposition described by Lucchi et al. (2013), with poorly sorted, multimodal grain size spectra. According to the classification by Shanmungam (2006, 2012), and Stow and Faugères (2008), these contourites are classified as muddy contourites characterised by predominant clay and silt, over 20% of biogenic components, and highly bioturbated sediments. The characteristics of each Cluster can also give some additional information about the energy of the bottom current responsible for the deposition of the sediments.

According to the diagram made by (Hjulström 1935, 1939) and modified by McCave (1984) for the deep sea environment (Fig. 3.7), Cluster A indicates a quiet, very low energy environment with limited/null sediment transport and deposition from a suspended nepheloid layer; Cluster B indicates a very low velocity current allowing depositions of the fine grained silt; Cluster C and D indicate low velocity currents with sedimentation at the limit of the sortable silt (10 µm), with higher IRD input for Cluster D samples; Cluster E indicate deposition from a suspended nepheloid layer (mode at 5.1 µm like for Cluster A), with abundant IRD input.

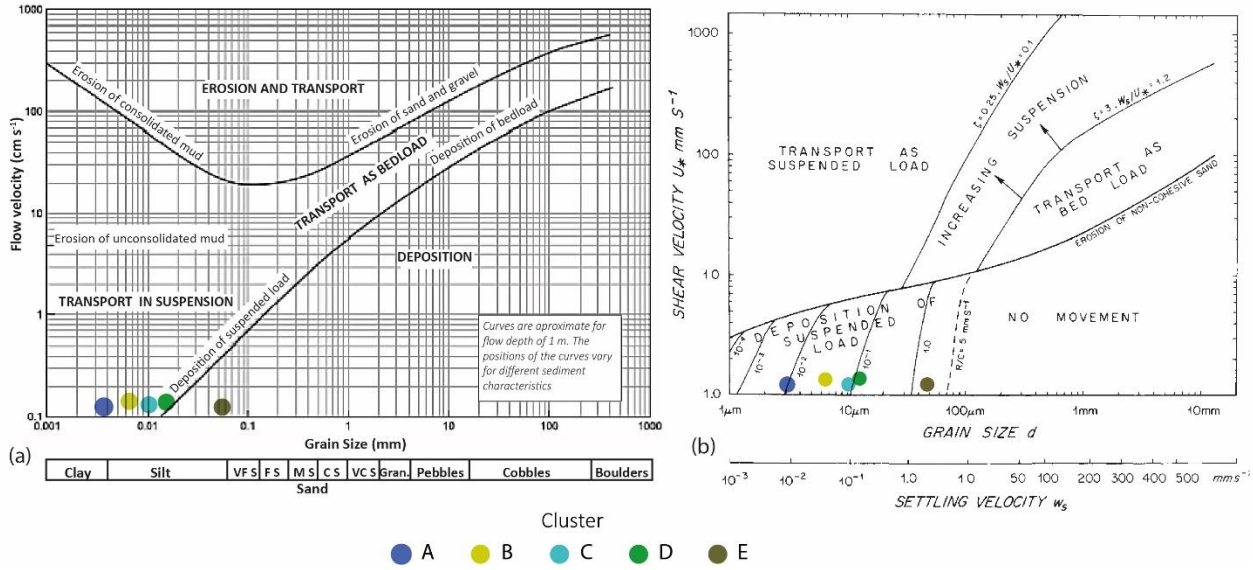


Fig.3.7. Erosion, transport and deposition diagrams according to Hjulström (1935, 1939). (a). General Hjulström (1935, 1939) diagram and (b). McCave (1984) diagram proposed for transport and deposition of sediments in marine environments. According to both diagrams, most of the studied fine-grained sediments are transported in the area as suspended load by weak bottom currents (diagram b) with little/any remobilization after their deposition (too weak currents), whereas the IRD fraction deposited directly after fall-out.

According to the diagram of Hjulström modified by McCave (1984) (Fig. 3.7 a), the velocity of the currents responsible for the deposition of the Holocene sediments in core GS191-01PC, is less than 0.2 cm/ sec. This velocity in relation to the mean grain size of the sediments indicates a depositional environment, with no potential to transport material superior at 20 μm. The diagrams shown in Fig. 3.7, indicates the low possibility of movement of the sediments after their deposition since the current is too weak (the sediments could be transported by the current only as suspended load after their delivery to the system though other processes). IRD (Cluster E) instead deposited immediately with almost no transport.

Deposit with high IRD content, (Cluster D), characterised the Upper Pleistocene (Younger Dryas). The beginning of the Early Holocene corresponds with Cluster A, from *ca*. 11.7 to 11.3 kyr BP, with a diminution of the velocity of the currents leading to lower selection of the sediments. At 11.0 kyr BP an IRD deposit event is recorded (Cluster E) (Fig. 3.6). From 10.6 until 7.9 kyr BP (Early Holocene until the beginning of the Mid Holocene), an increased in the hydrodynamic conditions is shown by diffuse presence of Cluster C, with a periodically input of IRD at 10.6, 9.7 and 8.6 kyr BP (Cluster D), and a decrease in the current velocity at 9.4 kyr BP (Cluster A).

During the Mid-Holocene from 7.7 until 6.4 kyr BP, a period with a low velocity currents and low selection deposits occurred (Cluster A), interrupted at 6.7 kyr BP by an increased in the velocity of the currents and more selected deposits (Cluster C) (Fig. 3.6).

From 6.2 to 4.2 kyr BP (last part of the Mid-Holocene), the sedimentation indicates a period with several hydrodynamic changes, separated by events of IRD input (Fig. 3.6).

The Late Holocene deposits are characterised by intervals with low velocity contour currents and deposits with lower selection, interrupted by events with higher velocity and IRD input between 3.0 and 2.8 kyr BP and between 1.7 and 1.5 kyr BP (Fig. 3.6). The most recent part of the studied record (1.1-0.7 kyr BP) shows deposits with a slightly higher selection (Cluster B) (Fig. 3.6).

3.5.2. Planktic foraminifera

a. General trends

In the planktic foraminiferal assemblages, 6 species are identified, with 3 main species (more than 5%) (Tab. 3.2).

	Planktic species		
Main species (>5%)	*Neogloboquadrina pachyderma*	*Turborotalita quinqueloba*	*Neogloboquadrina incompta*
Secondary species (<5%)	*Globigerina bulloides*	*Globigerinita glutinata*	*Globigerinita uvula*

Tab. 3.2: Planktic foraminiferal species.

The Upper Pleistocene and the beginning of the Early Holocene, from 12.0 to 11.7 kyr BP, the planktic foraminiferal concentration ranged between 297 and 565 spec./g, the flux values ranged between 11 to 67 spec./cm^2/yr. The concentration fluctuates with values between 14 and 5187 spec./g, while the flux increased during the Early Holocene, with a peak at 9.5 kyr BP and 278 spec./cm^2/yr (Fig. 3.8). During the Mid-Holocene, the concentration increased between 6.2 and 4.8 kyr BP reaching 3326 spec./g. The flux showed an increase between 6.7 and 5.0 kyr BP reached 280 spec./cm^2/yr, both peaks at 6.1 kyr BP. During the Late Holocene the concentration surpassed the 1800 spec./g, and the flux of planktic foraminifera is relatively constant, varying between 97 and 236 spec./cm^2/yr (Fig. 3.8).

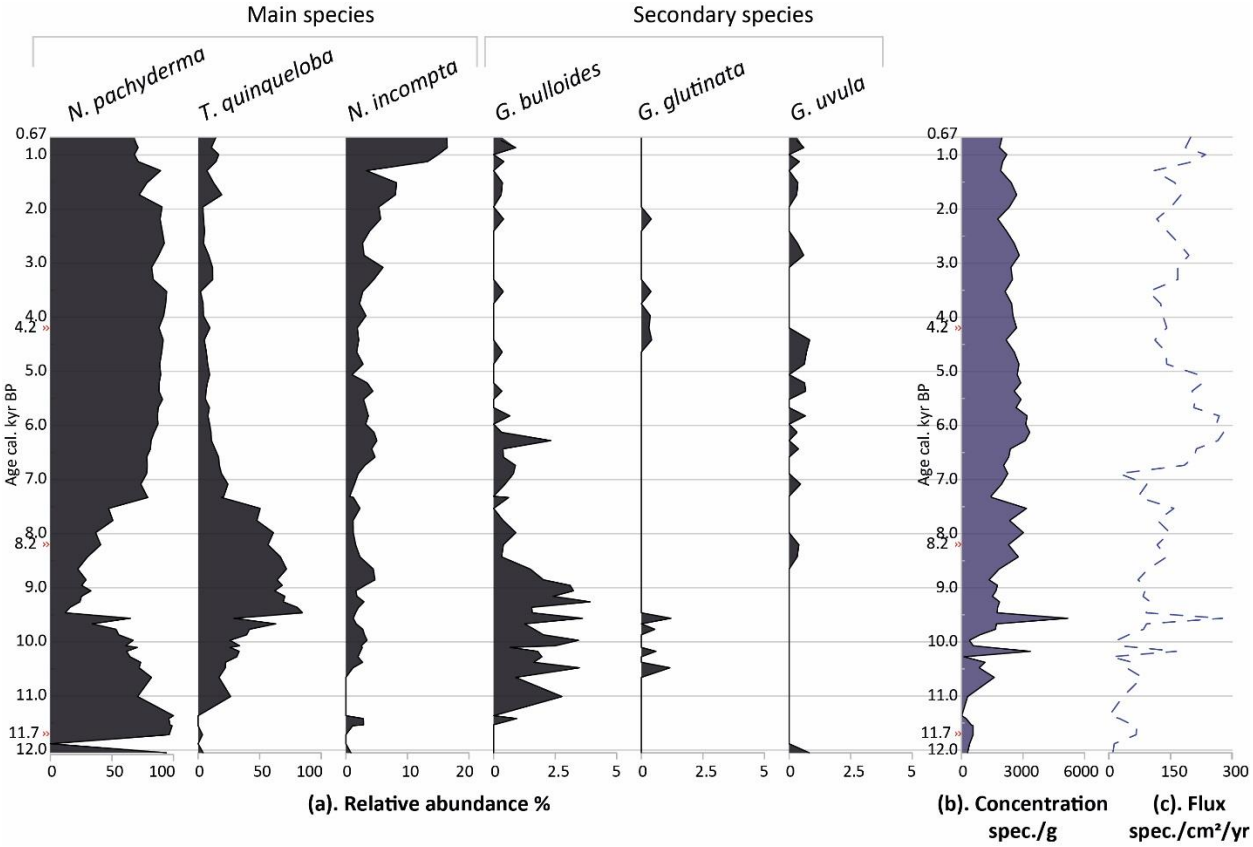


Fig. 3.8. Planktic foraminifera: (a). Relative abundance (%) of the main and secondary species versus age. (b). Concentration: species per gram of dry sediment (spec./g). (c). Foraminiferal flux (spec./cm^2/yr). The x-axes are different.

b. Planktic diversity indexes

The number of the planktic foraminiferal taxa (S) and Shannon (H) are the lowest of the record during the Younger Dryas and the beginning of the Early Holocene (Fig. 3.9). From c.a. 11.7 kyr BP the number of taxa and Shannon index shows an increase (reached a maximum of 5 and 0.9 respectively), while the dominance decreases, reaching the values of 0.4 (Fig. 3.9).

During the Mid-Holocene, the S values fluctuates between 3 and 5. The D presents an increase from *ca.* 7.4 kyr BP arriving until 0.8, and the H values decreases until 0.3 during the same period (Fig. 3.9).

During the Late Holocene, the S values varied from 3 to 5 (Fig. 3.9). Towards the top of the record, the values of D decreases, while the values of H increases, ranging between a minimum of 0.5 for D and 0.3 for H and a maximum of 0.9 for both diversity indexes (Fig. 3.9).

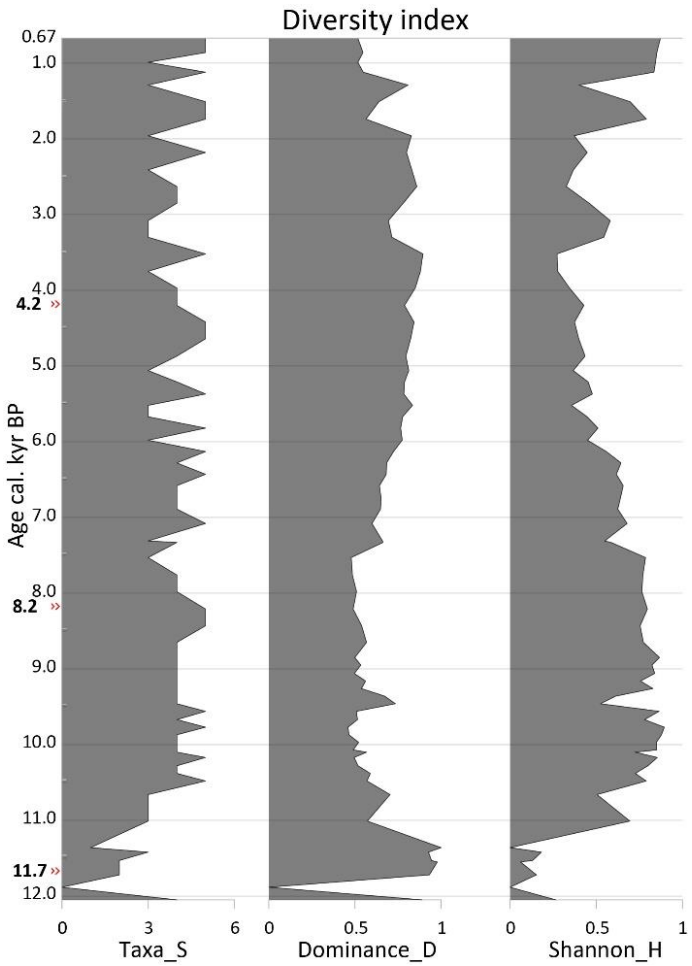


Fig. 3.9. Planktic foraminifera: diversity indexes. The x-axes are different.

c. Main planktic foraminiferal species pattern

Upper Pleistocene (last *ca.* 900 yr of the Younger Dryas) (12.0 – 11.7 kyr BP)

The main species is *N. pachyderma* with 94% at 12.0 kyr BP, while *T. quinqueloba* is present with 4%, and *N. incompta* together with the secondary species *G. uvula* are present with 0.8% (Fig. 3.8).

Early Holocene (11.7 – 8.2 kyr BP)

N. pachyderma is the main species between 11.7 and 11.3 kyr BP, reaching the maximum of 100% at 11.3 kyr BP. While, *T. quinqueloba* and *N. incompta* are present with less than 5% (Fig. 3.8).

A decreased of *N. pachyderma* is shown between 9.5 and 8.6 kyr BP, arriving until 2%, while *T. quinqueloba* reaches 85% at 9.4 kyr BP and *N. incompta* increases until 5% at 8.8 kyr BP (Fig. 3.8).

Mid-Holocene (8.2 – 4.2 kyr BP)

The *T. quinqueloba* declines, reaching less than 20% and does not retrieve during the entire Mid-Holocene. *Neogloboquadrina pachyderma* is more successful during the Mid-Holocene, increasing in relative abundance and arriving at a percentage higher than 80% from 6.4 kyr BP. *Neogloboquadrina incompta* increases during this period, reaching 5% at 6.2 kyr BP (Fig. 3.8).

Late Holocene (4.2 – 0.6 kyr BP)

Neogloboquadrina pachyderma occurs with high percentage during all the Late Holocene, decreasing until 68% between 1.7 and 0.6 kyr BP, while *T. quinqueloba* continues with a stable trend, with percentage less than 20%. *Neogloboquadrina incompta* slowly increases, reaching about 10% between 1.1 and 0.6 kyr BP (Fig. 3.8).

The secondary species *G. bulloides, G. glutinata* and *G. uvula* are present with less than 5% throughout the sedimentary record (Fig. 3.8).

3.5.3. Benthic foraminifera

a. General trends

A total of 84 species are identified at a species level in the size fraction >150 µm along the sediment core GS191-01PC (Tab. 3.3 and 3.4). The entire record is dominated by calcareous imperforate species with 58 species corresponding to 94% of the total relative percentage, the calcareous imperforate group has 13 species and represents 3.5%, and the agglutinated group with 13 species representing 2.5% (Fig. 3.10 a).

Main Benthic foraminiferal species (>5%)				
Calcareous perforate	*Cassidulina neoteretis*	*Cassidulina reniforme*	*Cibicidoides lobatulus*	*Cibicidoides wuellerstorfi*
	Elphidium clavatum	*Epistominella exigua*	*Haynesina orbiculare*	**Lagena* spp.
	Melonis barleeanus	*Oridorsalis tener*	*Parrelloides* cf. *healdi*	
Calcareous imperforate	*Miliolinella* cf. *enoplostoma*	*Triloculina tricarinata*		
Agglutinated	*Adercotryma* cf. *glomeratum*	*Labrospira subglobosa*	*Recurvoides trochamminiforme*	*Reophax scorpiurus*

Tab. 3.3: Main benthic foraminiferal species.**Lagena* spp., includes *L. curvilineata, L. distoma, L. elongata, L. gracilis, L. hispidula, L. mollis, L. nebulosa, L. stelligera, L. substriata* and *Lagena* spp.

Secondary Benthic foraminiferal species (<5%)				
Calcareous perforate	*Astrononion gallowayi*	*Bolivinellina pseudopunctata*	*Buccella* spp.	*Cassidulina laevigata*
	**Dentalina* spp.	*Elphidium albiumbilicatum*	*Elphidium hallandense*	*Fissurina danica*
	Globocassidulina subglobosa	*Globulina landesi*	*Haynesina depressula*	*Lenticulina gibba*
	Haynesina germanica	*Hoeglundina elegans*	*Ioanella tumidula*	*Islandiella norcrossi*
	Lagenosolenia lagenoides	*Marginulina obesa*	*Nonionella auricula*	***Oolina* spp.
	Patellina corrugata	*Pseudopolymorphina novangliae*	*Pullenia bulloides*	*Pullenia* cf. *catalinaensis*
	Pullenia osloensis	*Robertinoides pumilum*	*Rosalina villardeboana*	*Stainforthia concava*
	Stainforthia feylingi	*Stainforthia fusiformis*	*Trifarina fluens*	*Valvulineria minuta*
	Other indeterminated species			
Calcareous imperforate	*Cornuspira* spp.	*Miliolinella* spp.	*Pyrgo lucernula*	*Pyrgo subglobulus*
	Pyrgo williamsoni	*Pyrgoella globula*	*Pyrgoella sphaera*	*Triloculina oblonga*
	Quinqueloculina annectens		*Triloculina rotunda*	*Quinqueloculina* spp.
Agglutinated	*Adercotryma glomeratum*	*Eggerella scabra*	*Hyperammina subnodosa*	
	Psammosphaera fusca	*Trochammina* cf. *rotaliformis*	*Reophax guttifer*	
	Reophax micaceus	*Rhabdammina scabra*	*Trochammina globigeriniformis*	

Tab. 3.4 Secondary benthic foraminiferal species. **Dentalina* spp. includes *Dentalina drammenensis* and *Dentalina* spp. ***Oolina* spp. includes *Oolina costata*, *Oolina elegantissima, Oolina globosa, Oolina hexagona.*

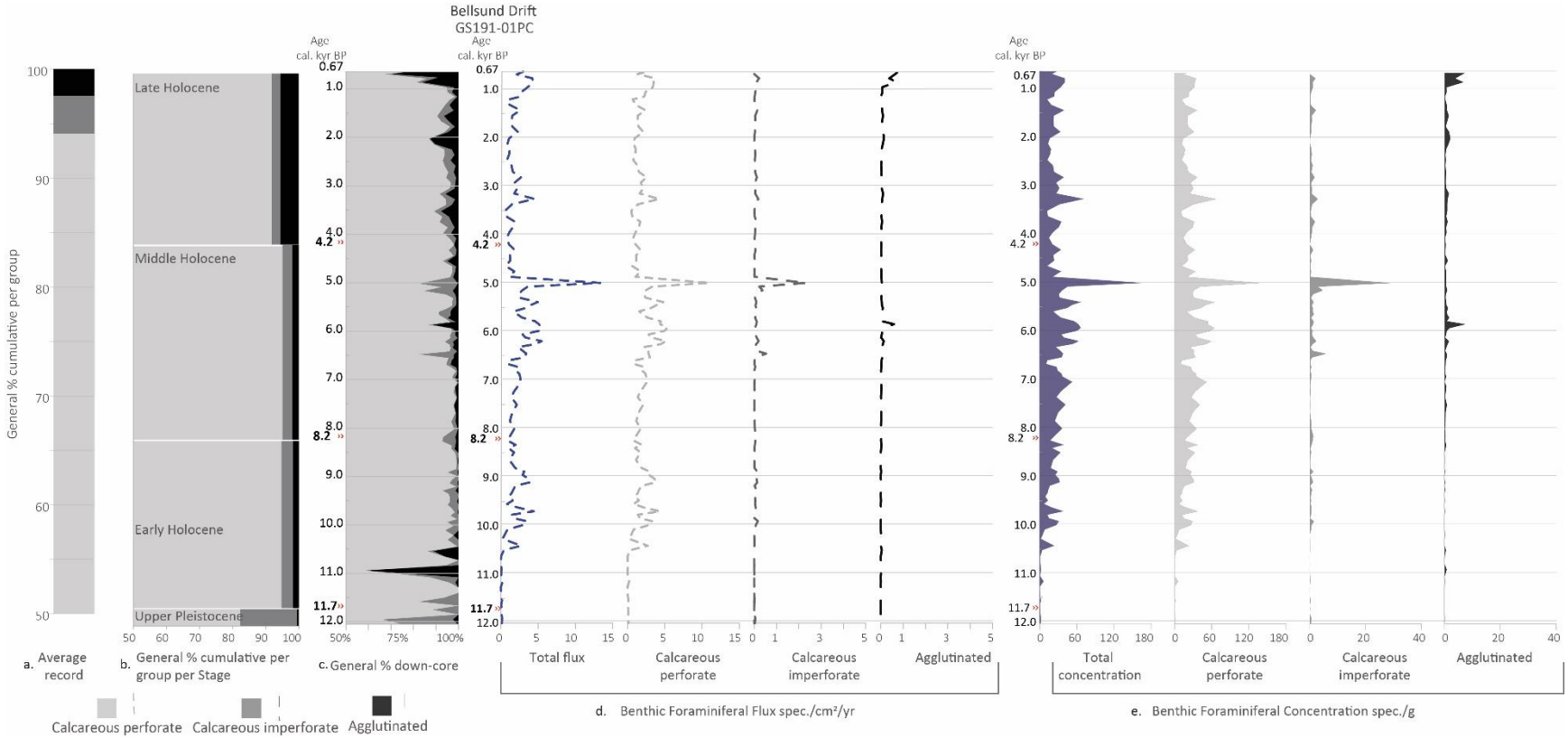


Fig. 3.10. Benthic foraminiferal a. General average percentage per group in the entire record. b. Average percentage group per age. c. General relative abundance per group down-core. d. Benthic foraminiferal Flux: total and flux of the taxonomic groups. e. Benthic foraminiferal concentration: total and concentration of the taxonomic groups. The x-axes are different.

During the passage from Upper Pleistocene to Early Holocene, the calcareous perforate group presents an average percentage of 82%, 17% the calcareous imperforate group, and 1% the agglutinated group. Calcareous imperforate and agglutinated groups reaches their maximum relative percentage at 11.9 kyr BP, with 32 and 2%, respectively (Fig. 3.10 a-b-c). At 11.8 kyr BP calcareous perforate is the only group present in the assemblage. During this period, the foraminiferal flux is less than 0.2 spec./cm^2/yr (Fig. 3.10 d).

The dominance of the calcareous perforate group continues during the entire Early Holocene, with an average of 95%, reaching 100% at different intervals and dropping to a minimum of 58% at 10.9 kyr BP. The calcareous imperforate group is present with an average of 3%, their maximum is 18% at 11.5 kyr BP, and it appears occasionally during the Early Holocene with less than 10%. During the Early Holocene the agglutinated group has an average percentage of 2%, reaching the maximum of 42% at 10.9 kyr BP. In the upper part of the record, they occur sporadically with percentages less than 10% (Fig. 3.10 c). The foraminiferal flux has a change during the Early Holocene, where it starts to increase from 10.4 kyr BP, reaching the maximum of 4 spec./cm^2/yr at 9.7 kyr BP (Fig. 3.10 d).

During the Mid-Holocene the benthic foraminiferal situations are similar to the Early Holocene. The calcareous perforate group is still dominant with more than 80% down core. The calcareous imperforate group is present continuously during this period, with less than 10% (maximum of 17% at 5.0 kyr BP). The agglutinated group is present with less than 5% (maximum of 11% at 5.8 kyr BP) (Fig. 3.10 c). The maximum of the foraminiferal flux is at 5.0 kyr BP (13 spec./cm^2/yr), with the maximum input of calcareous foraminifera group (Fig. 3.10 d).

During the Late Holocene, the average percentage of the calcareous perforate foraminifera lightly decreases till 92%, allowing an increase of the agglutinated group to 5%, while the calcareous imperforate group remains with an average of 3%. The calcareous perforate group occurs with more than 90% until 0.9 kyr BP; between 0.9 and 0.6 kyr BP the relative percentage decreases till 67%. The agglutinated group increases to percentages higher than 10%, with the maximum values of 33% and 25% between 0.6 and 0.6 kyr BP (Fig. 3.10 c). The calcareous imperforate group shows no significant increase during the Late Holocene, occurring with less than 5% during this period. The foraminiferal flux shows values between 0.5 and 4 spec./cm^2/yr (Fig. 3.10 d).

The foraminifera per gram of dry sediment (spec./g) has a similar trend of the benthic foraminiferal flux (Fig. 3.10 e). From 12.0 until 10.6 kyr BP, the spec./g shows the minimum values, ranging between 0.2 and 2 spec./g (Fig. 3.10 e). From 10.6 until 5.0 kyr BP the trend increases, with a maximum peak of 164 spec./g. Between 4.8 and 0.6 kyr BP, the values range between 12 and 39 spec./g, with a maximum at 3.2 kyr BP with 71 spec./gram (Fig. 3.10 e). The maximum concentrations for the calcareous perforate and calcareous imperforate groups are at 5.0 kyr BP with 136 spec./g, and with 29 spec./g respectively (Fig. 3.10 e). While the agglutinated group shows two peaks of maximum concentration: at 5.8 and at 0.6 kyr BP, both with 7 spec./g (Fig. 3.10 e).

b. Benthic diversity indexes

The lowest number of taxa (S) occurs during the Younger Dryas and the beginning of the Early Holocene. The S is less than 10 between 12.0 and 10.2 kyr BP, arriving at a maximum of 17 at 11.1 kyr BP (Fig 3.11). Between 10.1 and 8.2 kyr BP, S increases with values higher than 15, with a maximum of 26, at 8.4 kyr BP (Fig. 3.11). The dominance (D) ranges from 0.1 and 0.3 between 12.0 kyr BP and 11.7 kyr BP, then increases during the Early Holocene arriving to 0.7 at 10.2 kyr BP. Between 12.0 kyr BP and 11.7 kyr BP, Shannon (H) index values varies between 1.5 and 2.3, and during the Early Holocene it ranges between 0.6 to 2.2 (Fig. 3.11).

During the Mid-Holocene, the number of taxa (S) increases, with a maximum value of 29 at 6.8 kyr BP and the lowest values, 10 at 6.7 kyr BP. The dominance (D) decreases, while Shannon (H) increases, with a range of D between 0.2 and 0.5, and H between 1.1 and 2.2 (Fig. 3.11).

The number of taxa (S) reaches the maximum values during the Late Holocene, with a maximum of 35 at 1.5 kyr BP. The dominance (D) shows a decreasing trend reaching the value of 0.1 at 2.0 kyr BP, and then it increases until 0.6 kyr BP with a maximum of 0.4 at 0.9 kyr BP. The Shannon index (H) increases during this period, with values between 1.4 and 2.7 (Fig. 3.11).

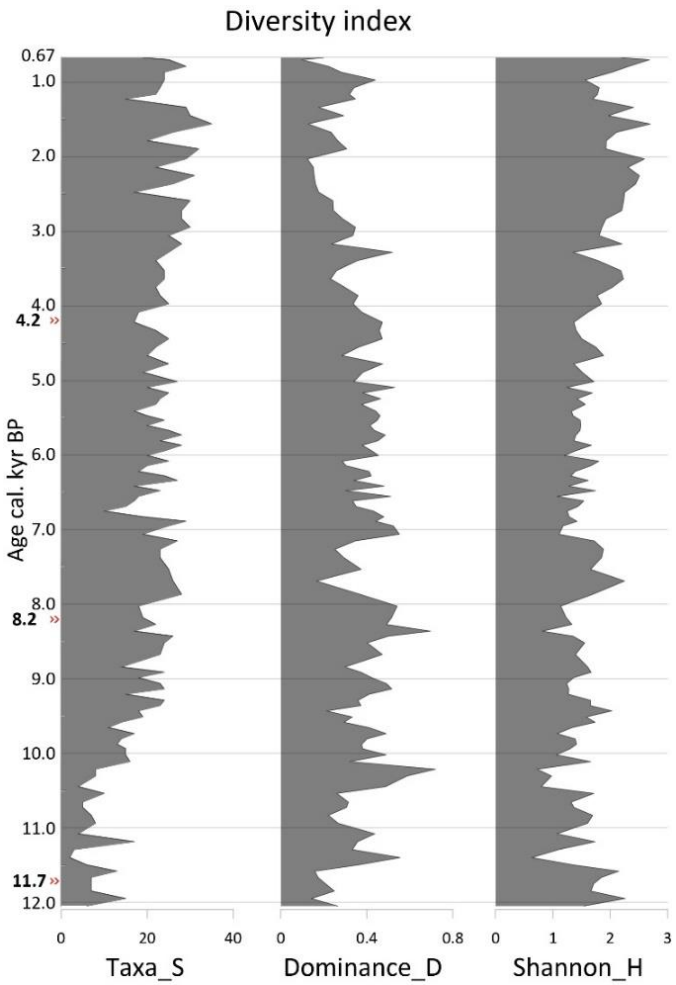


Fig. 3.11. Benthic foraminifera: diversity indexes. The x-axes are different.

c. Main benthic foraminiferal species pattern

The main foraminiferal species are 17 (Tab. 3), of which 11 are calcareous perforate, 2 calcareous imperforate and 4 agglutinated (Fig. 3.12).

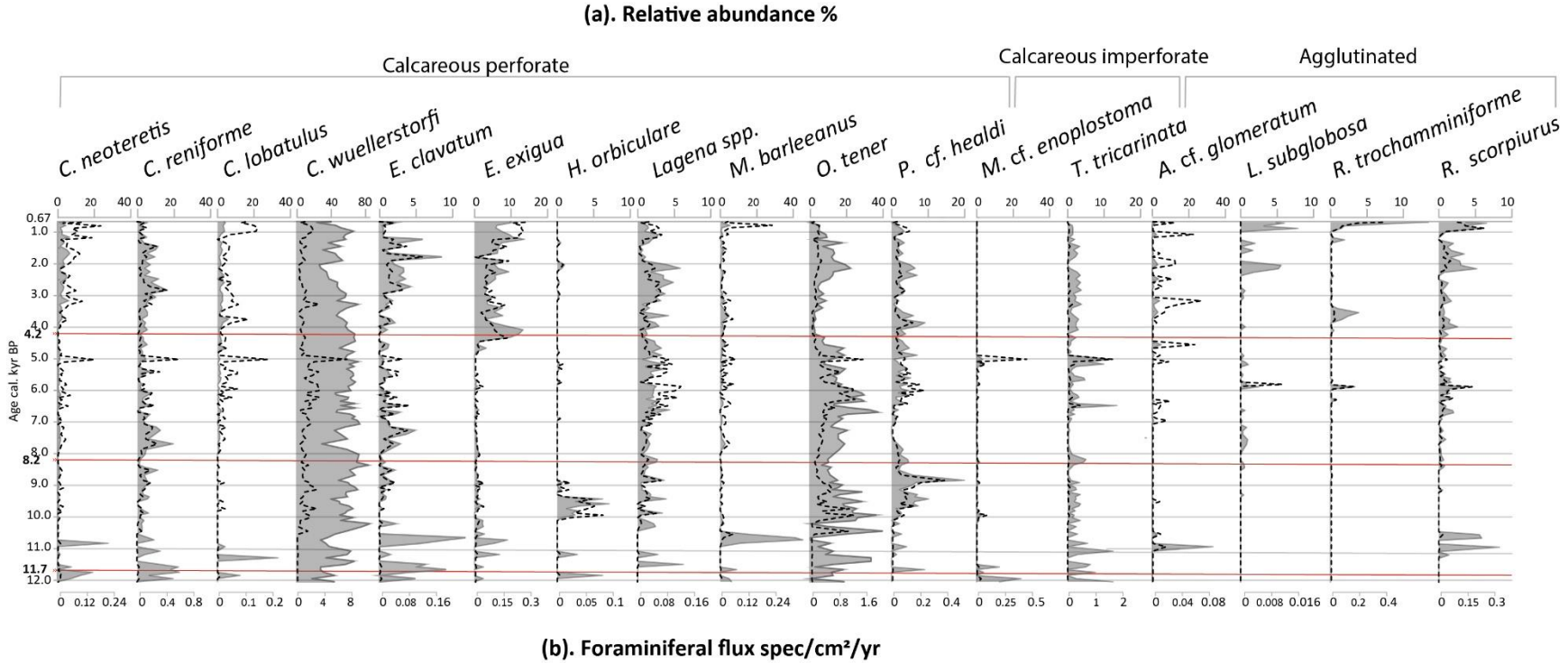


Fig. 3.12. Benthic foraminifera: (grey area) relative abundance and (black dashed line) foraminiferal flux of the main species. The red lines indicate the age limit Younger Dryas, Early Holocene, Mid-Holocene and Late Holocene. The x-axes are different.

Upper Pleistocene (last *ca.* 900 yr of the Younger Dryas) (12.0 – 11.7 kyr BP)

During this age, the dominant calcareous perforate species are *C. wuellerstorfi* with a maximum of 48% at 12.0 and 11.8 kyr BP, *C. reniforme* with a maximum of 23% at 11.7 kyr BP, *O. tener* with 19% at 12.0 and *C. neoteretis* at 17.5 kyr BP with 19%. *Cibicidoides lobatulus* and *H. orbiculare* are present only at 11.8 kyr BP with 13% and 6% respectively. *Elphidium clavatum* and *E. exigua* are present with less than 5% (Fig. 3.12).

The calcareous imperforate *M.* cf. *enoplostoma* is present with a maximum of 24% at 11.9 kyr BP and *T. tricarinata* with 13% at 12.0 kyr BP (Fig. 3.12).

In general, the benthic foraminiferal flux is low during this period (Fig. 3.12).

Early Holocene (11.7 – 8.2 kyr BP)

Cibicidoides wuellerstorfi is still the main species during this period, increasing constantly with a minimum of 27%, and with two maxima at 10.2 kyr BP (85%), and at 8.2 kyr BP (83%) (Fig. 3.12). *Oridorsalis tener* shows an irregular increase between 11.7 and 10.2 kyr BP, reaching the maximum at 10.4 kyr BP, with 40%; from 10.1 kyr BP it becomes constantly present, ranging between 36% and 20%, decreasing again to 6% during the last part of this period (Fig. 3.12). *Cassidulina reniforme* is mainly present between 11.7 and 11.5 kyr BP with a maximum of 23%: then it decreases between 11.4 and 8.5 kyr BP, reaching a percentage of only 1% at the end of the Early Holocene (Fig. 3.12).

Some species appear randomly. *Cassidulina neoteretis* ha peaks at 11.7kyr BP (19%) and 10.8 kyr BP (28%) (Fig. 3.12); *C. lobatulus* has its maximum at 11.2 kyr BP (33%) (Fig. 3.12); *E. clavatum* is present at 10.6 kyr BP with a maximum of 12%. *Melonis barleeanus* reaches it maxima abundance (45%) between 10.8 and 10.5 kyr BP (Fig. 3.12). *Parrelloides* cf. *healdi* increases at 8.8 kyr BP with a peak of 20% (Fig. 3.12). *Epistominella exigua, H. orbiculare* and *Lagena* spp (Fig. 3.12).

Calcareous imperforate, *M.* cf. *enoplostoma* and *T. tricarinata* are present respectively, with a peak of 13%, 11.5 kyr BP and at 11.0 kyr BP (Fig. 3.12). Agglutinated group is present with less than 5% whit *L. subglobosa* and *A.* cf. *glomeratum* (with a peak of 33% at 10.9 kyr BP); while *R. scorpiurus* shows a peak between 10.9 and 10.5 kyr BP with values ranging between 6 and 8% (Fig. 3.12).

In general, the foraminiferal flux shows an increase from the *ca.* 10.5 kyr BP. From *ca.* 8.8 and 8.3 8.3 kyr BP, the species *O. tener* and *P*. cf *healdi* (respectively) show a decreasing flux until the finish of this period (Fig. 3.12).

Mid-Holocene (8.2 – 4.2 kyr BP)

The dominance of *C. wuellerstorfi* is continuous in this period; it reaches the minimum at 7.6 kyr BP (29%) and the maximum at 7.0 kyr BP (73%), remaining stable until the end of this period (Fig. 3.12). *Oridorsalis tener* is still present, increasing in percentage from the 8.2 kyr BP (10%) until 6.69 kyr BP (37%), and later decreasing between 6.6 kyr BP (33%) until 4.2 kyr BP (3%) (Fig. 3.12).

Cassidulina reniforme is concentrated between 8.2 kyr (1%) BP until 6.8 kyr BP (8%), reaching the maximum relative percentage at 7.6 kyr BP with 20%; from 6 to 4.2 kyr BP, and the relative percentage of *C. reniforme* is less than 5% (Fig. 3.12).

Epistominella exigua is present with a relative percentage less than 5%, reaching 10% at 4.3 kyr BP (Fig. 3.12). The calcareous perforate species occurring with less than 5% are *C. neoteretis, C. lobatulus, E. clavatum, Lagena* spp., and *P.* cf. *healdi* (Fig. 3.12).

The calcareous imperforate *T. tricarinata* remains with a constant percentage between 6.7 and 4.7 kyr BP, reaching 14% at 6.4 kyr BP (Fig. 3.12). *Miliolinella* cf. *enoplostoma* occurs with less than 5%. The four main agglutinated species occur occasionally with less than 5% (Fig. 3.12 a).

The foraminiferal flux increases during the Mid-Holocene, since 5.0 kyr BP, when a general decrease is showed until the end of the period (Fig. 3.12).

Late Holocene (4.2 – 0.6 kyr BP)

Cibicidoides wuellerstorfi presents high percentage (between 71 to 23%), with a decreasing trend during this period (Fig. 3.12). In this period *O. tener* occur with low relative percentage (less than 3%) until 3.5 kyr BP, then it increases between 3.3 and 1.3 kyr BP, reaching the maximum (22%)at 2.1 kyr BP, and finally decreases (0-2%) until 0.6 kyr BP (Fig. 3.12).

Cassidulina reniforme shows a general increase, with highest values between 3.0 and 1.4 kyr BP, reaching the maximum percentage at 2.8 kyr BP with 16% (Fig. 3.12). *Epistominella exigua* increases during this

period (mainly present with more than 5%), with high percentage between 1.2 and 0.6 kyr BP, with values ranging between 6 and 14% (Fig. 3.12). *Cassidulina neoteretis* relative abundance increases from 3.9 kyr BP, it is usually present with less than 7% (Fig. 3.12).

The species *E. clavatum* and *P.* cf. *healdi* are present with a maximum of 9% at 3.8 kyr BP (Fig. 3.12). *Cibicidoides lobatulus, H. orbiculare, Lagena* spp. and *M. barleeanus* are the calcareous perforate species occurring with less than 5% (Fig. 3.12).

The calcareous imperforate taxa decreases during the Late Holocene. *Triloculina tricarinata* only reaches the maximum of 4% (Fig. 3.12). The agglutinated *L. subglobosa* and *R. scorpiurus* increases until the top of the sequence (0.6 kyr BP), while *A.* cf. *glomeratum* shows a percentage less than 5% (Fig. 3.12).

During this period, the foraminiferal flux fluctuates, with the increase of the species *C. neoteretis, C. lobatulus, C. wuellerstorfi, E. exigua, Lagena* spp., *M. barleeanus,* and the agglutinated main species *A.* cf. *glomeratum, L. subglobosa, R. trochamminiforme* and *R. scorpiurus.* The species *C. reniforme, O. tener and P.* cf. *healdi;* show a stable flux throughout this period (Fig. 3.12).

The secondary group of species represent species with less than 5% in the entire record (Tab. 4; Fig. 3.13).

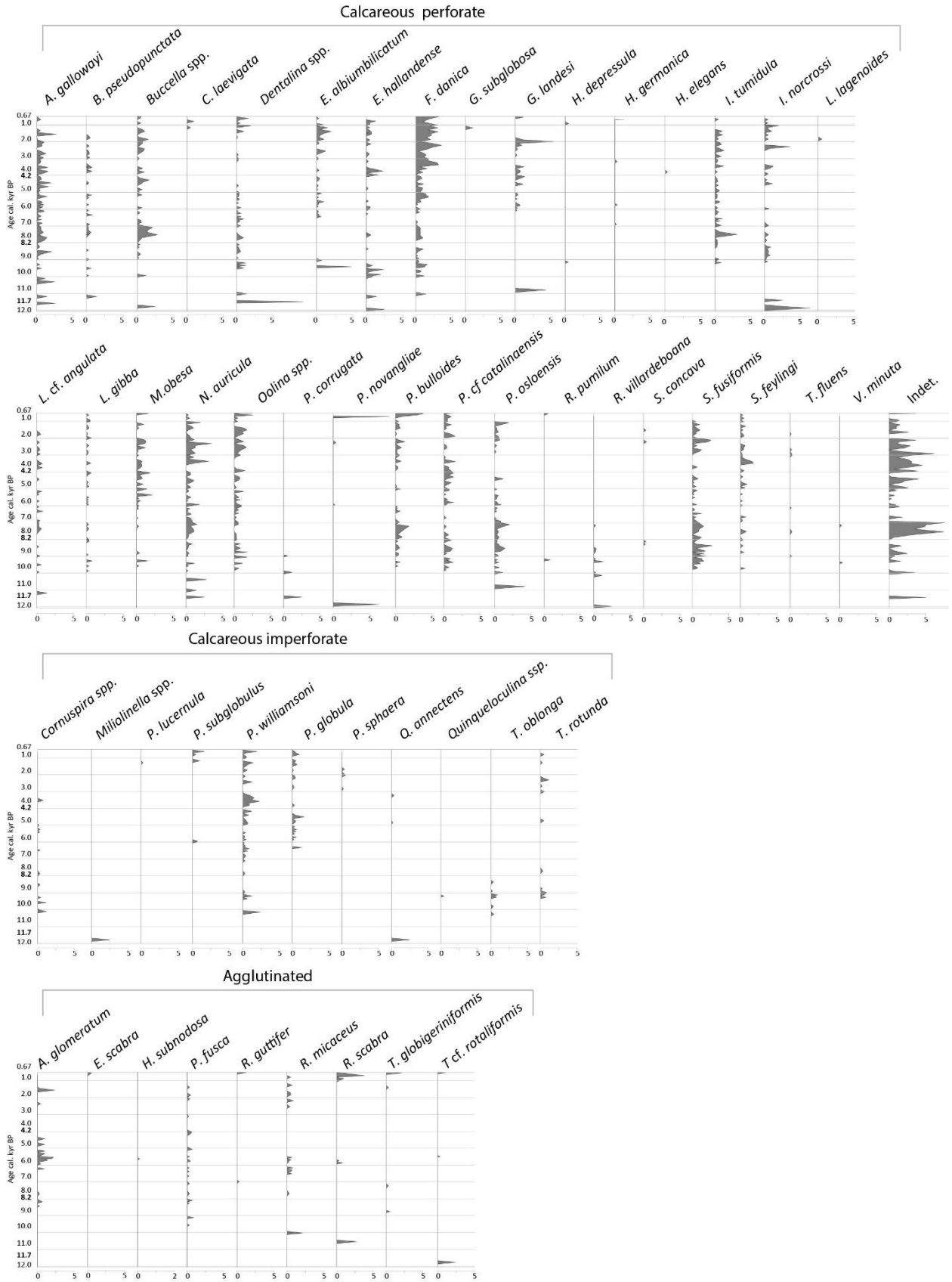


Fig. 3.13. Benthic foraminifera: secondary species relative abundance. The x-axes are different.

3.6. Discussion

The studied record contains the Upper Pleistocene (12.0-11.7 kyr BP) and the Holocene (11.7-0.6 kyr BP) periods.

a. Upper Pleistocene (last *ca.* 900 yr. of the Younger Dryas) 12.0 -11.7 kyr BP.

The beginning of the record corresponds with the end of the Upper Pleistocene, which in the Northern Hemisphere is well recognised as the cold spell event Younger Dryas. The end of the Upper Pleistocene represents an episode of low productivity indicated by the low flux of benthic and planktic foraminifera, dominated by the cold taxa *N. pachyderma* (Fig.3.14). Ebbesen et al. (2007) described the low-productivity conditions in the Fram Strait, using planktic foraminifera as proxy, and they explained this phenomenon due to the increasing sea ice cover during this age (Fig. 3.14 and 3.15; Tab. 3.5).

The cold sea bottom conditions are supported by the presence of *E. clavatum* and *C. reniforme*. This condition is also reported by Rasmussen et al. (2007 b) and Ślubowska-Woldengen et al. (2008), the latter suggesting that the environmental conditions are similar to the late glacial period (polar conditions and cooling of the bottom waters). A dynamic environment is indicated by the presence of the coarse sediment species *C. wuellerstorfi* and *C. lobatulus* and the low productivity conditions are suggested by the occurrence of *O. tener* (Fig. 3.14 and 3.15; Tab. 3.5). The IRD deposits and the high sedimentation rates suggest the melting of the sea ice or icebergs. The instability of the sea ice is reported also in the Fram Strait (and nearby area) by several authors (e.g. Ebbesen et al., 2007; Ślubowska-Woldengen et al., 2007; Aagaard-Sørensen et al., 2014a; Jessen et al., 2010; Melis et al., 2018) using as proxies the relative abundances of benthic and planktic foraminiferal assemblages.

b. Early Holocene (Greenlandian) 11.7-8.2 kyr BP

During the onset of this period until the *ca.* 11.0 kyr BP, cold surface conditions are prevalent; this evidence is supported by the high percentage of *N. pachyderma* (Fig. 3.14). Superficial warm water conditions started at 10.1 kyr BP, indicated by the increase of the planktic foraminiferal flux, following to a rapid increment of percentage and flux of *T. quinqueloba* and the drop of percentage of *N. pachyderma* (Fig. 3.14 and 3.15; Tab. 3.5). This warmer period is correlated with the transition between the Late Glacial Termination into the warm sea-surface conditions during the Holocene (Aagaard-Sørensen et al., 2014a); this transition is indicated by Hald et al (2007) occurring at *ca.* 10.5 kyr BP at 77°N.

The establishment of interglacial conditions at 10.1 kyr BP, due to warm superficial water masses (AW related), is associated with the presence of *N. incompta;* this event can be considered synchronous with that reported in the south-western margin of Svalbard (Rasmussen et al., 2007b; Ślubowska-Woldengen et al., 2007). The increase in productivity indicated by the abundance of *T. quinqueloba* between *ca.* 9.9 until *ca.* 9.1 kyr BP, might correspond to the beginning of the Holocene Thermal Maximum (HTM). This warm interval is also recorded in nearby sedimentary records indicated by a temperate planktic foraminiferal fauna *T. quinqueloba* (e.g. Rasmussen et al., 2007b; Aagaard-Sørensen et al., 2014a; Werner et al., 2016; Melis et al., 2018; Consolaro et al., 2018). The ameliorate conditions during the passage between Early to Mid-Holocene continued until *ca.* 7.2 kyr BP, as shown by the high relative abundance of *T. quinqueloba.* These conditions are reported in the eastern Fram Strait and in the Barents Sea, extended till the 8.8 kyr BP indicated by the increasing of the *T. quinqueloba* (Ebbesen et al., 2007; Rasmussen et al., 2007 b; Aagaard-Sørensen et al., 2014a; Werner et al., 2016).

During this warmer phase, the bottom environment is characterised by cold conditions indicated by the increase in the relative percentage of *C. wuellerstorfi* and *O. tener*, and by the presence of *E. clavatum*. The record of benthic foraminifera is characterised by unstable conditions from *ca.* 11.0 to 10.5 kyr BP, as indicated by the increase of opportunistic taxa *E. exigua* (Fig. 3.14 and 3.15; Tab. 3.5). These fluctuations, associated with the Preboreal oscillations, are observed in the areas located south and north of the Bellsund Drift, by Rasmussen et al. (2007 a).

The ice sheet and sea ice melting during this interval deliver coarse sediment that feed the contourite deposits with IRD (eg. Aagaard-Sørensen et al., 2014a) (Fig. 3.14 and 3.6). A peak of IRD is recorded at 11.0 kyr BP, coeval to what observed in Fram Strait by Aagaard-Sørensen et al. (2014 a), and is correlated with the rapid ice-sheet retreat in the Svalbard and Barents Sea (Landvik et al., 1998).

The influence of warm AW between *ca.* 10.8 and 10.2 kyr BP, is shown by the abundance of *M. barleeanus* indicating the arrival of relatively warm water, and *C. neoteretis* suggesting the ice free conditions (Fig. 3.14 and 3.15; Tab. 3.5). Knudsen et al. (2008), in the study carried out in Baffin Bay, suggest that the presence of *C. neoteretis* related to nutrients brought by the AW. This AW influx is recorded by Rasmussen et al. (2007b) and Melis et al. (2018) in the Storfjorden area, by Ebbesen et al. (2007) and Consolaro et al. (2018) in the Fram Strait, and by Ślubowska-Woldengen et al. (2008) in the Svalbard shelf and the Barents Sea. This event is considered the first indicator of warming of the bottom water during the Early Holocene (Melis et al., 2018).

From 10.5 kyr BP the sedimentation rate increased, and the benthic foraminiferal flux became more stable (Fig. 3.14). At 10.5 kyr BP the input of IRD decreased, due to the increased of AW influx and the decreasing of ice melting (e.g. Aagaard-Sørensen et al., 2014a), the same condition is reported along the West Spitsbergen Slope by several authors (e.g. Ebbesen et al., 2007; Rasmussen et al., 2007 b; Jessen et al., 2010).

High-energy conditions occurred at the end of this period (8.3 – 8.2 kyr BP) indicated by the increase of *C. wuellerstorfi*, and the increased of the IRD deposits (Fig. 3.6 and 3.15).

c. Mid-Holocene (Northgrippian) 8.2- 4.1 kyr BP

The cool surface water masses are still dominant during this period. However, the inflow of warm AW continues until *ca.* 7.3 kyr BP, as shown by the abundance of *T. quinqueloba* and by the presence of temperate taxa *N. incompta* (Fig. 3.14 and 3.15; Tab. 3.5). This climatic period starts with a decrease of the input of coarse, IRD-rich sediment, and fine-grained contouritic depositions associated with low velocity currents (Fig. 3.6).

The cooler surface water conditions is evidenced by the abrupt decrease in the relative abundance of *T. quinqueloba* and the increasing percentages of *N. pachyderma* at 7.2 kyr BP. These colder conditions are prevalent during the rest of the Mid-Holocene until 4.2 kyr BP (Fig. 3.14).

Between *ca.* 7.7 and 6.4 kyr BP, the bottom conditions are characterised by low-velocity contouritic deposits (Fig. 3.14), low-productivity and low-salinity (associated with the presence of *O. tener* and *E. clavatum*), and low-energy conditions related with the low relative abundance of *C. wuellerstorfi* (Fig. 3.14; Tab. 3.5).

A colder event is registered from *ca.* 6.5 kyr BP until 4.2 kyr BP, in concordance with the increase of IRD content, associated with melting of the ice (sea ice and icebergs) in the area (Fig. 3.14 and 3.15). In the area of West Spitsbergen, Jessen et al. (2010) and Slubowska-Woldengen et al. (2007) mentioned these colder conditions; also, Müller et al. (2012) identified a cooling event between 7.0 and 3.0 kyr BP. Moreover, Werner et al. (2013), Ebbesen et al. (2007) and Werner et al. (2016) recognised a maximum peak in the cold conditions at *ca.* 5.0 kyr BP, registered in Bellsund Drift between *ca.* 6.2 and 5.2 kyr BP with the input of IRD-rich sediment and the maximum values of *N. pachyderma* (Fig. 3.14).

After the 5.0 kyr BP cold event, the flux of benthic foraminifera decreases, and the increase of the opportunistic species (*E. exigua*) is constant until the end of the Mid-Holocene (Fig. 3.14; Tab. 3.5).

d. Late Holocene (Meghalayan) 4.2 – 0.6 kyr BP

From 4.2 kyr BP until 1.7 kyr BP, the cold superficial conditions are maintained, as evidenced by the consistent presence of the cold indicator *N. pachyderma* prevailing into the planktic assemblage (Fig. 3.14 and 3.15; Tab. 3.5). These cold conditions are related with the Neoglacial period, started at 4.0 kyr BP, as indicated by Sarnthein et al. (2003) in the western Barents shelf (75°N); Hald et al. (2004) along western area of Spitsbergen; and in the Isfjorden by Rasmussen et al. (2012). During the same time, a slight increase of *N. incompta* and *T. quinqueloba* indicates a switch to warmer conditions. The co-presence of *N. pachyderma* and *T. quinqueloba* may indicate a strong seasonality that allowed the increase of both species, respectively during the cold seasons and during the warm seasons. Moreover, some studies explained the increase in the percentage of both planktic cold and warm water species by strong stratification during the last period of the Late Holocene, during which the cold surface water is separate from the bottom warm water (AW) by a marked pycnocline (Werner et al., 2013, 2016; Aagaard-Sørensen et al., 2014 b). Deposition during this period is predominantly characterised by well-sorted sedimentation suggesting slightly stronger bottom currents (Fig. 3.6); while the influence of cooling surface water between 3.0 and 1.4 kyr BP, is evidenced by the sporadic depositions of IRD (eg. Slubowska-Woldengen et al., 2008) that can be associated with increased ice melting.

The cooling period is also evidenced in the bottom environment by the proliferation of the cold-water indicators *C. reniforme* at 3.0 - 2.4 kyr BP and *E. clavatum* at *ca.* 2.7 kyr BP (Fig. 3.14; Tab. 3.5). Slubowska-Woldengen et al. (2008) and Consolaro et al. (2018), reported during this period the increase of *E. excavatum* (for this study called *E. clavatum*) and *C. lobatulus*, indicating cold bottom conditions and stronger currents.

The period between 1.7 kyr BP until 1.2 kyr BP is marked by the increase of the bottom-current activity, testifies by the coarser sediment input and by the presence of *C. wuellerstorfi.* The occurrence of IRD-rich deposits, linked to the melting of the ice, can be related to freshwater supply in the area (Fig. 3.14; Tab. 3.5). These conditions are also indicated by Müller et al. (2012) and Werner et al. (2013; 2016) in the Fram Strait area.

The general settings during this period indicate an unstable environment, with predominantly cold conditions indicated by the presence of *E. clavatum*; changes in salinity (increased in the *C. reniforme* abundance), and fluctuations in the productivity flux to the sea bottom (showed by alternate presence of *E. exigua* and *O. tener*) (Fig. 3.14; Tab. 3.5).

	Main species	Environmental conditions	References
Planktic species	*Neogloboquadrina incompta*	Sub-polar species. Warm Atlantic surface water. Seasonal peak abundances in late summer.	Bé and Tolderlund (1971); Carstens et al. (1997); Volkmann (2000); Schiebel et al. (2001); Simstich et al. (2003).
	Neogloboquadrina pachyderma	Polar species. Related to Arctic and Polar surface waters.	Bé and Tolderlund (1971); Kohfeld et al. (1996); Carstens et al. (1997); Simstich et al. (2003).
	Turborotalita quinqueloba	Sub-polar species. Arctic water and related to the Arctic and Polar fronts. Near surface dweller. In areas influenced by warm Atlantic Water.	Bé and Tolderlund (1971); Carstens et al. (1997); Volkmann (2000); Simstich et al. (2003); Husum and Hald (2012).
Benthic species	*Cassidulina neoteretis*	Cool transformed surface Atlantic Water. Seasonal ice-free conditions. Stable salinity. High seasonal productivity. Epifaunal- shallow infaunal species. Warm bottom conditions.	Lagoe (1979); Mackensen and Hald (1988); Jennings and Weiner (1996); Wollenburg and Mackensen (1998); Lubinski et al. (2001); Wollenburg et al. (2004); Jennings et al. (2004).
	Cassidulina reniforme	Arctic-Polar species. Cold and salty. Locally related to glaciomarine environments. Associated to E. clavatum. Epifaunal-Shallow infaunal.	Serjup et al. (1981); Macckensen et al. (1985); Hald and Korsun (1997); Korsun and Hald (2000); Polyak et al. (2002); Steinsund (1994).
	Cibicidoides lobatulus	High-energy environments. Epifaunal species, in coarser sediment, attached to hard substrates.	Macckensen et al. (1985); Hald and Steinsund (1992); Hald and Korsun (1997); Murray (2006).
	Cibicidoides wuellerstorfi	Associated to Arctic waters and Arctic/Polar fronts. High-energy environments. Epifaunal in coarser sediments and attached to hard substrates.	Belanger and Streeter (1980); Serjup et al. (1981); Mackensen et al. (1985); Wollenburg and Mackensen (1998); Bauch et al. (2001).
	Elphidium clavatum	Arctic-Polar species prefer cold bottom waters (glacier front and ice margin). Highly adaptable, resists low salinity, low temperatures and high turbidity.	Hald and Korsun (1997); Korsun and Hald (2000); Polyak et al. (2002); Sejrup et al. (2004).
	Epistominella exigua	Opportunistic species. Able to feed on fresh phytodetritus. Epifaunal.	Gooday (1993); Thomas et al. (1995); Wollenburg and Mackensen (1998).
	Melonis barleeanus	Arctic- Boreal. Related to cooled Atlantic water with supply of degraded organic matter. High salinities. Fine sediments and high sedimentation rates with constant food supply. Infaunal.	Caralp (1989); Hald and Steinsund (1992); Korsun and Hald (1998); Polyak et al. (2002); Jennings et al. (2004).
	Oridorsalis tener	Related with low productivity. Deep water species 2000-3000 m. Epifaunal.	Osterman et al. (1999). Wollenburg and Mackensen, (1998).

Tab. 3.5. Foraminiferal main ecological indicators.

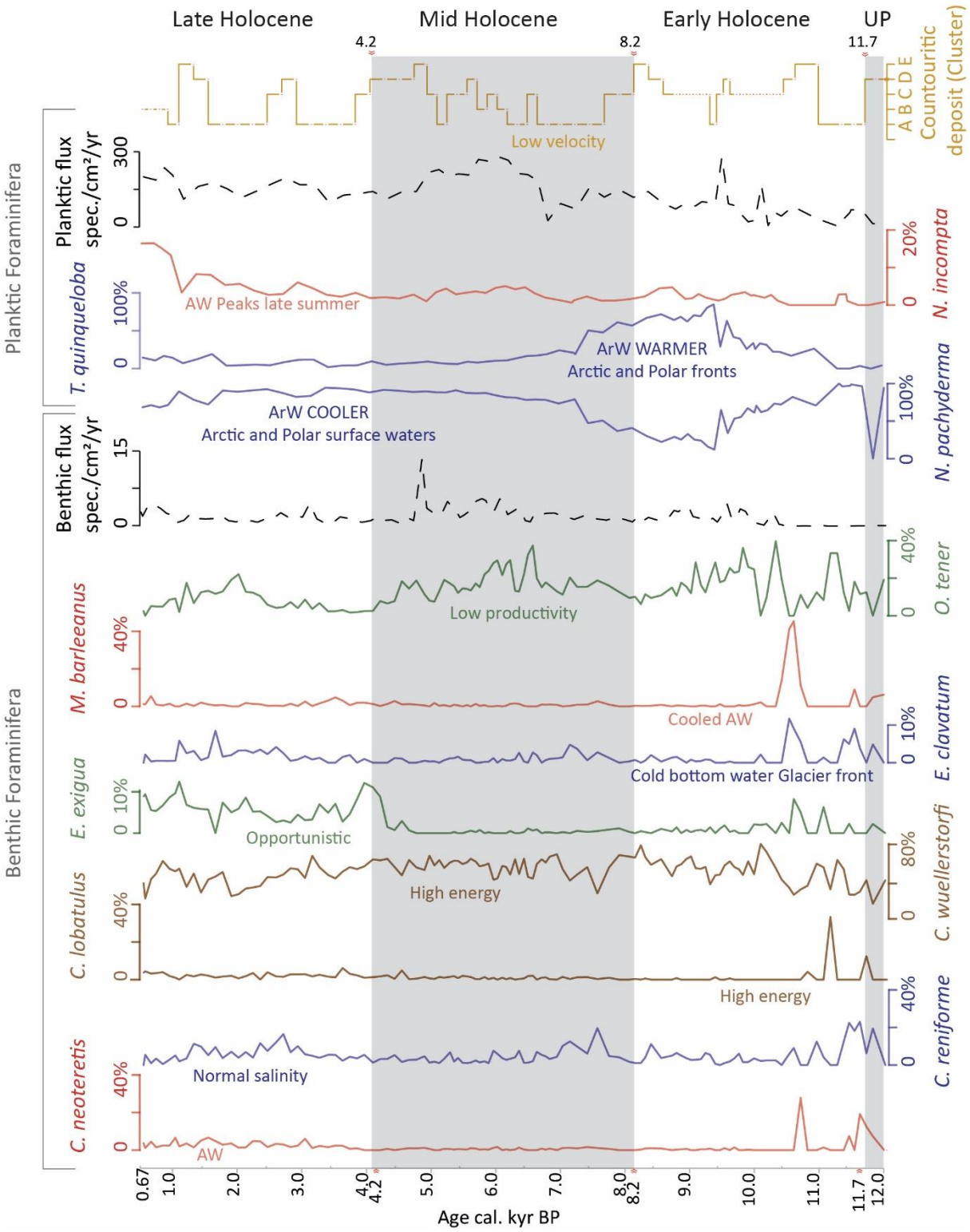


Fig. 3.14. Key proxies, presenting: Q-mode cluster division of the contouritic deposits. Benthic foraminiferal flux. Planktic foraminiferal flux (dashed graphic). Relative abundance of the main planktic and benthic foraminiferal species divided by colours: red the warm water related species, blue the cold-water related species, green opportunistic or productivity indicators, brown energy indicators. The gold graphic represents the contouritic deposits. The x-axes are different.

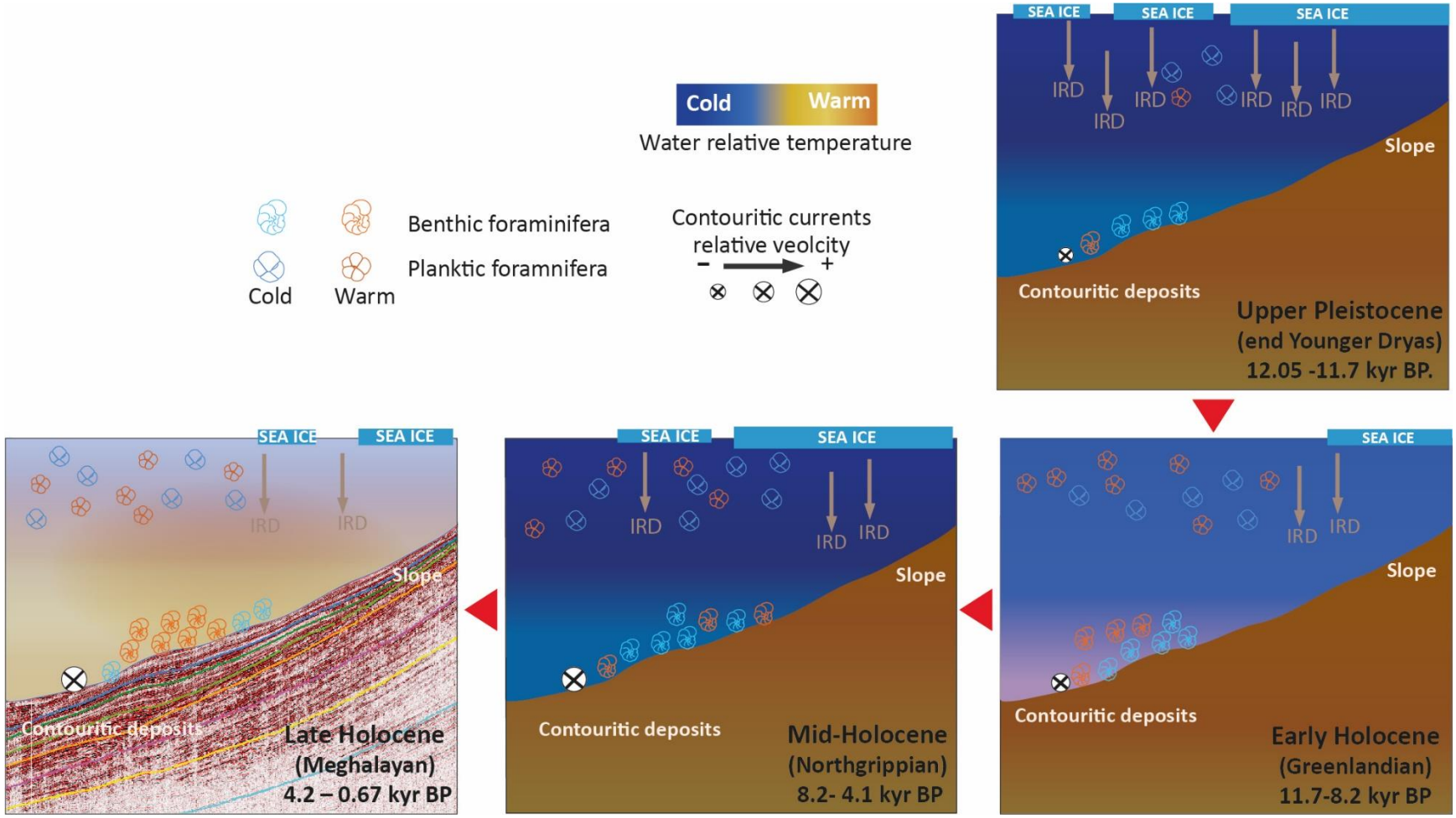


Fig. 3.15. Sketch showed the conditions at each stratigraphic stage. The seismic profile of Bellsund Drift is after Rebesco et al. (2013). The relative velocity contouritic currents varied between 0.1 and 0.2 cm/s. The red arrows indicate the progressive order of figures.

3.7. Conclusions

The main regional climatic and environmental events, identified in the Arctic area during the Holocene are also recorded in our sediment core, although with some chronological and/or different intensity. This time-lapse between records could be due to local conditions, also signed by other authors (e.g. Consolaro et al., 2018).

During the Upper Pleistocene-Holocene, important variations between the superficial and sea bottom waters are mostly related to the presence of the sea ice and the variable influx of the AW. The last 1000 yr of the Upper Pleistocene are relatively cold, with high input of IRD into the sediments indicating melting of the sea ice and a progressive shift to warmer conditions as supported by the presence of the warm AW input occurred at the sea bottom. These conditions continued since *ca.* 10.7 kyr BP when a stronger influence of the AW in the entire water column is recorded. A consistent warming period started at 10.1 kyr BP until the 9.4 kyr BP, with the establishment of firmly warm conditions corresponding to the Holocene Thermal Maximum (HTM).

During the Mid-Holocene the warmer conditions are re-stablished, with strong fluctuations in primary productivity and bottom current strength that increased during the end of the Mid-Holocene.

The Late Holocene is dominated by cold superficial water conditions; with the progressive intrusion of the AW into the entire water column. At the end of the Late Holocene, the sea bottom environmental conditions indicate the influx of warm water and changes in productivity, related to the occurrence of opportunistic species. The warmer conditions increased during the last *ca.* 3.0 kyr BP with the increase of AW influx into the entire water column.

In general the sub-superficial water environment is dominated by Polar and Sub Polar species (*N. pachyderma* and *T. quinqueloba*, respectively), indicating the continuous influence of the ArW during the entire record. Instead, the increase of the AW influence is recorded by the increase of *N. incompta*, mainly during the Late Holocene. The sea bottom environment suggests high energy conditions (*C. wuellerstorfi*), with the interaction of the warm and cold-water masses, conditioning the productivity, the salinity, and the food-influx to the bottom.

3.8. References

Aagaard, K., Foldvik, A., Hillman, S.R. 1987. The West Spitsbergen Current: disposition and water mass transformation. Journal of Geophysical Research 92, 3778–3784.

Aagaard-Sørensen, S., Husum, K., Werner, K., Spielhagen, R. F., Hald, M., Marchitto, T. M. 2014 a. A Late Glacial–Early Holocene multiproxy record from the eastern Fram Strait, Polar North Atlantic. Marine Geology, 355, 15-26.

Aagaard-Sørensen, S., Husum, K., Hald, M., Marchitto, T., Godtliebsen, F. 2014 b. Sub sea surface temperatures in the Polar North Atlantic during the Holocene: Planktonic foraminiferal Mg/Ca temperature reconstructions. The Holocene, 24(1), 93-103.

Bauch, H. A., Erlenkeuser, H., Spielhagen, R. F., Struck, U., Matthiessen, J., Thiede, J., Heinemeier, J. 2001. A multiproxy reconstruction of the evolution of deep and surface waters in the subarctic Nordic seas over the last 30,000 yr. Quaternary Science Reviews, 20(4), 659-678.

Bé, A.W.H., Tolderlund, D.S. 1971. Distribution and ecology of living planktonic foraminifera in surface waters of the Atlantic and Indian Oceans. In: Funnell, B.M., Riedel, W.R. (Eds.), The Micropaleontology of the Oceans. Cambridge University Press, 105–149.

Belanger, P. E., Streeter, S. S. 1980. Distribution and ecology of benthic foraminifera in the Norwegian-Greenland Sea. Marine Micropaleontology, 5, 401-428.

Caralp, M. H. 1989. Abundance of *Bulimina exilis* and *Melonis barleeanum*: Relationship to the quality of marine organic matter. Geo-Marine Letters, 9(1), 37-43.

Caricchi, C., Lucchi, R.G., Sagnotti, L., Macrì, P., Di Roberto, A., Del Carlo, P., Husum, K., Laberg, J.S. Morigi, C. 2019. A high-resolution geomagnetic relative paleointensity record from the Arctic Ocean deep-water gateway deposits during the last 60 kyr. Geochemistry, Geophysics, Geosystems, 20(5), 2355-2377.

Carstens, J., Hebbeln, D., Wefer, G. 1997. Distribution of planktonic foraminifera at the ice margin in the Arctic (Fram Strait). Marine Micropaleontology, 29(3-4), 257-269.

Consolaro, C., Rasmussen, T. L., Panieri, G. 2018. Palaeoceanographic and environmental changes in the eastern Fram Strait during the last 14,000 years based on benthic and planktonic foraminifera. Marine Micropaleontology, 139, 84-101.

Ebbesen, H., Hald, M., Eplet, T. H. 2007. Late glacial and early Holocene climatic oscillations on the western Svalbard margin, European Arctic. Quaternary Science Reviews, 26(15-16), 1999-2011.

Eiken, O., Hinz, K. 1993. Contourites in the Fram Strait. Sedimentary Geology, 82(1-4), 15-32.

Gooday, A. J. 1993. Deep-sea benthic foraminiferal species which exploit phytodetritus: characteristic features and controls on distribution. Marine Micropaleontology, 22(3), 187-205.

Hald, M., Andersson, C., Ebbesen, H., Jansen, E., Klitgaard-Kristensen, D., Risebrobakken, B., Salomonsen, G.R., Sarnthein, M., Sejrup, H.P. Telford, R.J. 2007. Variations in temperature and extent of Atlantic Water in the northern North Atlantic during the Holocene. Quaternary Science Reviews, 26(25-28), 3423-3440.

Hald, M., Ebbesen, H., Forwick, M., Godtliebsen, F., Khomenko, L., Korsun, S., Olsen, L.R., Vorren, T.O. 2004. Holocene paleoceanography and glacial history of the West Spitsbergen area, Euro-Arctic margin. Quaternary Science Reviews, 23(20-22), 2075-2088.

Hald, M., Korsun, S. 1997. Distribution of modern benthic foraminifera from fjords of Svalbard, European Arctic. The Journal of Foraminiferal Research, 27(2), 101-122.

Hald, M., Steinsund, P. I. 1992. Distribution of surface sediment benthic foraminifera in the southwestern Barents Sea. The Journal of Foraminiferal Research, 22(4), 347-362.

Hopkins, T. S. 1991. The GIN Sea—A synthesis of its physical oceanography and literature review 1972–1985. Earth-Science Reviews, 30(3-4), 175-318.

Husum, K., Hald, M. (2012). Arctic planktic foraminiferal assemblages: Implications for subsurface temperature reconstructions. Marine Micropaleontology, 96, 38-47.

IPCC, 2019: IPCC Special Report on the Ocean and Cryosphere in a Changing Climate [H.-O. Pörtner, D.C. Roberts, V. Masson-Delmotte, P. Zhai, M. Tignor, E. Poloczanska, K. Mintenbeck, A. Alegría, M. Nicolai, A. Okem, J. Petzold, B. Rama, N.M. Weyer (eds.)]. In press.

Jennings, A. E., Weiner, N. J. 1996. Environmental change in eastern Greenland during the last 1300 years: evidence from foraminifera and lithofacies in Nansen Fjord, 68 N. The Holocene, 6(2), 179-191.

Jennings, A. E., Weiner, N. J., Helgadottir, G., Andrews, J. T. 2004. Modern foraminiferal faunas of the southwestern to northern Iceland shelf: oceanographic and environmental controls. The Journal of Foraminiferal Research, 34(3), 180-207.

Jessen, S. P., Rasmussen, T. L., Nielsen, T., Solheim, A. 2010. A new Late Weichselian and Holocene marine chronology for the western Svalbard slope 30,000–0 cal years BP. Quaternary Science Reviews, 29(9-10), 1301-1312.

Knudsen, K. L., Stabell, B., Seidenkrantz, M. S., Eiriksson, J., & Blake Jr, W. 2008. Deglacial and Holocene conditions in northernmost Baffin Bay: sediments, foraminifera, diatoms and stable isotopes. Boreas, 37(3), 346-376.

Knutz, P. C. 2008. Palaeoceanographic significance of contourite drifts. Developments in Sedimentology, 60, 511-535.

Kohfeld, K. E., Fairbanks, R. G., Smith, S. L., Walsh, I. D. 1996. Neogloboquadrina pachyderma (sinistral coiling) as paleoceanographic tracers in polar oceans: Evidence from Northeast Water Polynya plankton tows, sediment traps, and surface sediments. Paleoceanography, 11(6), 679-699.

Korsun, S., Hald, M. 1998. Modern benthic foraminifera off Novaya Zemlya tidewater glaciers, Russian Arctic. Arctic and Alpine Research, 30(1), 61-77.

Korsun, S., Hald, M. 2000. Seasonal dynamics of benthic foraminifera in a glacially fed fjord of Svalbard, European Arctic. The Journal of Foraminiferal Research, 30(4), 251-271.

Laberg, J.S., Stoker, M.S., Dahlgren, K.T., de Haas, H., Haflidason, H., Hjelstuen, B.O., Nielsen, T., Shannon, P.M., Vorren, T.O., van Weering, T.C., Ceramicola, S. 2005. Cenozoic along slope processes and

sedimentation on the NW European Atlantic margin. Marine and Petroleum Geology, 22(9-10), 1069-1088.

Lagoe, M. B. 1979. Recent benthonic foraminiferal biofacies in the Arctic Ocean. Micropaleontology, 25(2), 214-224.

Landvik, J. Y., Bondebik, S., Elyerhoi, A., Fjeldskaar, W. I. L. L. Y., Mangerud, J. A. N., Siegert, S., Salvigsen, O., Svendsen, J.I. Vorren, T. O. 1998. The last glacial maximum of Svalbard and the Barents Sea area: ice sheet extent and configuration. Quaternary Science Reviews, 17(1), 43-76.

Lubinski, D. J., Polyak, L., Forman, S. L. 2001. Freshwater and Atlantic water inflows to the deep northern Barents and Kara seas since ca 13 ^{14}C ka: foraminifera and stable isotopes. Quaternary Science Reviews, 20(18), 1851-1879.

Lucchi, R. G., Camerlenghi, A., Rebesco, M., Colmenero-Hidalgo, E., Sierro, F. J., Sagnotti, L., Giorgetti, G. 2013. Postglacial sedimentary processes on the Storfjorden and Kveithola trough mouth fans: Significance of extreme glacimarine sedimentation. Global and Planetary Change, 111, 309-326.

Lucchi, R. G., Rebesco, M. 2007. Glacial contourites on the Antarctic Peninsula margin: insight for palaeoenvironmental and palaeoclimatic conditions. Geological Society, London, Special Publications, 276(1), 111-127.

McCave, I. N. 1984. Erosion, transport and deposition of fine-grained marine sediments. Geological Society, London, Special Publications, 15(1), 35-69.

Mackensen, A., Hald, M. 1988. *Cassidulina teretis* Tappan and *C. laevigata* d'Orbigny; their modern and late Quaternary distribution in northern seas. The Journal of Foraminiferal Research, 18(1), 16-24.

Mackensen, A., Sejrup, H. P., Jansen, E. 1985. The distribution of living benthic foraminifera on the continental slope and rise off southwest Norway. Marine Micropaleontology, 9(4), 275-306.

Melis, R., Carbonara, K., Villa, G., Morigi, C., Bárcena, M. A., Giorgetti, G., Caburlotto, A., Rebesco, M., Lucchi, R. G. 2018. A new multi-proxy investigation of Late Quaternary palaeoenvironments along

the north-western Barents Sea (Storfjorden Trough Mouth Fan). Journal of Quaternary Science, 33(6), 662-676.

Müller, J., Werner, K., Stein, R., Fahl, K., Moros, M., Jansen, E. 2012. Holocene cooling culminates in sea ice oscillations in Fram Strait. Quaternary Science Reviews, 47, 1-14.

Murray, J. W. 2006. Ecology and applications of benthic foraminifera. Cambridge University Press.

Nilsen, F., Skogseth, R., Vaardal-Lunde, J., Inall, M. 2016. A simple shelf circulation model: intrusion of Atlantic Water on the West Spitsbergen Shelf. Journal of Physical Oceanography, 46(4), 1209-1230.

Osterman, L. E., Poore, R. Z., Foley, K. M. 1999. Distribution of Benthic Foraminifers (> 125 μm) in the Surface Sediments of the Arctic Ocean (Vol. 2164). US Government Printing Office.

Polyak, L., Korsun, S., Febo, L. A., Stanovoy, V., Khusid, T., Hald, M., Paulsen, B.E., Lubinski, D. J. 2002. Benthic foraminiferal assemblages from the southern Kara Sea, a river-influenced Arctic marine environment. The Journal of Foraminiferal Research, 32(3), 252-273.

Rasmussen, S. O., Vinther, B. M., Clausen, H. B., Andersen, K. K. 2007 a. Early Holocene climate oscillations recorded in three Greenland ice cores. Quaternary Science Reviews, 26(15-16), 1907-1914.

Rasmussen, T. L., Thomsen, E., Ślubowska, M. A., Jessen, S., Solheim, A., Koç, N. 2007 b. Paleoceanographic evolution of the SW Svalbard margin (76 N) since 20,000 ^{14}C yr BP. Quaternary Research, 67(1), 100-114.

Rasmussen, T. L., Forwick, M., Mackensen, A. 2012. Reconstruction of inflow of Atlantic Water to Isfjorden, Svalbard during the Holocene: Correlation to climate and seasonality. Marine Micropaleontology, 94, 80-90.

Rebesco, M., Camerlenghi, A., Van Loon, A. J. 2008. Contourite research: A field in full development. In M. Rebesco, & A. Camerlenghi (Eds.), Contourites. Developments in sedimentology (Vol. 60, 1–10).

Rebesco, M., Wåhlin, A., Laberg, J.S., Schauer, U., Beszczynska-Möller, A., Lucchi, R.G., Noormets, R., Accettella, D., Zarayskaya, Y., Diviacco, P. 2013. Quaternary contourite drifts of the Western Spitsbergen margin. Deep Sea Research Part I: Oceanographic Research Papers, 79, 156-168.

Rebesco, M., Hernández-Molina, F. J., Van Rooij, D., Wåhlin, A. 2014. Contourites and associated sediments controlled by deep-water circulation processes: state-of-the-art and future considerations. Marine Geology, 352, 111-154.

Sarnthein, M., Van Kreveld, S., Erlenkeuser, H., Grootes, P. M., Kucera, M., Pflaumann, U., Schulz, M. 2003 Centennial-to-millennial-scale periodicities of Holocene climate and sediment injections off the western Barents shelf, 75° N. Boreas, 32(3), 447-461.

Schauer, U., Fahrbach, E., Osterhus, S., Rohardt, G. 2004. Arctic warming through the Fram Strait: Oceanic heat transport from 3 years of measurements. Journal of Geophysical Research: Oceans, 109(C6).

Sejrup, H.P., Fjaeran, T., Hald, M., Beck, L., Hagen, J., Miljeteig, I., Morvik, I., Norvik, O. 1981. Benthonic foraminifera in surface samples from the Norwegian continental margin between 62 degrees N and 65 degrees N. The Journal of Foraminiferal Research, 11(4), 277-295.

Sejrup, H. P., Birks, H. J. B., Kristensen, D. K., Madsen, H. 2004. Benthonic foraminiferal distributions and quantitative transfer functions for the northwest European continental margin. Marine Micropaleontology, 53(1-2), 197-226.

Simstich, J., Sarnthein, M., Erlenkeuser, H. 2003. Paired $\delta^{18}O$ signals of *Neogloboquadrina pachyderma* (s) and *Turborotalita quinqueloba* show thermal stratification structure in Nordic Seas. Marine Micropaleontology, 48(1-2), 107-125.

Shanmugam, G. 2006. Deep-water processes and facies models: Implications for sandstone petroleum reservoirs. Elsevier.

Ślubowska-Woldengen, M., Rasmussen, T. L., Koç, N., Klitgaard-Kristensen, D., Nilsen, F., Solheim, A. 2007. Advection of Atlantic Water to the western and northern Svalbard shelf since 17,500 cal yr BP. Quaternary Science Reviews, 26(3-4), 463-478.

Ślubowska-Woldengen, M., Koç, N., Rasmussen, T. L., Klitgaard-Kristensen, D., Hald, M., Jennings, A. E. 2008. Time-slice reconstructions of ocean circulation changes on the continental shelf in the Nordic and Barents Seas during the last 16,000 cal yr BP. Quaternary Science Reviews, 27(15-16), 1476-1492.

Steinsund, P. I., Polyak, L., Hald, M., Mikhailov, V., Korsun, S. 1994. Distribution of calcareous benthic foraminifera in recent sediments of the Barents and Kara Sea. Benthic Foraminifera in Surface Sediments of the Barents and Kara Seas: Modern and Late Quaternary Application. Ph. D. Thesis, Department of Geology, Institute of Biology and Geology, University of Tromsø, Norway.

Stow, D. A. V., & Faugères, J. C. 2008. Contourite facies and the facies model. Developments in Sedimentology, 60, 223-256.

Stow, D. A., Hernández-Molina, F. J., Llave, E., Sayago-Gil, M., Díaz del Río, V., & Branson, A. 2009. Bedform-velocity matrix: the estimation of bottom current velocity from bedform observations. Geology, 37(4), 327-330.

Svendsen, J. I., Mangerud, J. 1997. Holocene glacial and climatic variations on Spitsbergen, Svalbard. The Holocene, 7(1), 45-57.

Thomas, E., Booth, L., Maslin, M., Shackleton, N. J. 1995. Northeastern Atlantic benthic foraminifera during the last 45,000 years: changes in productivity seen from the bottom up. Paleoceanography, 10(3), 545-562.

Volkmann, R. 2000. Planktonic foraminifers in the outer Laptev Sea and the Fram Strait—Modern distribution and ecology. The Journal of Foraminiferal Research, 30(3), 157-176.

Werner, K., Spielhagen, R. F., Bauch, D., Hass, H. C., Kandiano, E. 2013. Atlantic Water advection versus sea-ice advances in the eastern Fram Strait during the last 9 ka: Multiproxy evidence for a two-phase Holocene. Paleoceanography, 28(2), 283-295.

Werner, K., Müller, J., Husum, K., Spielhagen, R. F., Kandiano, E. S., Polyak, L. 2016. Holocene sea subsurface and surface water masses in the Fram Strait–Comparisons of temperature and sea-ice reconstructions. Quaternary Science Reviews, 147, 194-209.

Wollenburg, J. E., Mackensen, A. 1998. Living benthic foraminifers from the central Arctic Ocean: faunal composition, standing stock and diversity. Marine Micropaleontology, 34(3-4), 153-185.

Wollenburg, J. E., Knies, J., Mackensen, A. 2004. High-resolution paleoproductivity fluctuations during the past 24 kyr as indicated by benthic foraminifera in the marginal Arctic Ocean. Palaeogeography, Palaeoclimatology, Palaeoecology, 204(3-4), 209-238.

4. Modern Period record from Bellsund Drift, the last *ca.* 120 yr

A short sediment-core, GS191-02BC was obtained at the same site as the long sediment core *Calypso* piston core GS191-01PC at the western Svalbard margin (see chapter 3).

4.1. Study area

The western Svalbard sediments recovered multidecadal information about climatic variability during the last centuries. The main interaction between cold and warm waters starts at the eastern area of the Fram Strait where the main Atlantic Water (AW) input occurs; in this area, the AW receives the name of West Spitsbergen Current (WSC) (Fig. 4.1). Several studies are performed to understand the influence of the warm AW into the Nordic Seas during the last millennia, centuries or decades throughout the Fram Strait (e.g. Quadfasel et al., 1988; Karcher et al., 2003; Schauer et al, 2004; Werner et al, 2011; Kinnard et al., 2011; Langehaug and Falck, 2012; Müller et al., 2012, Nilsen et al., 2016).

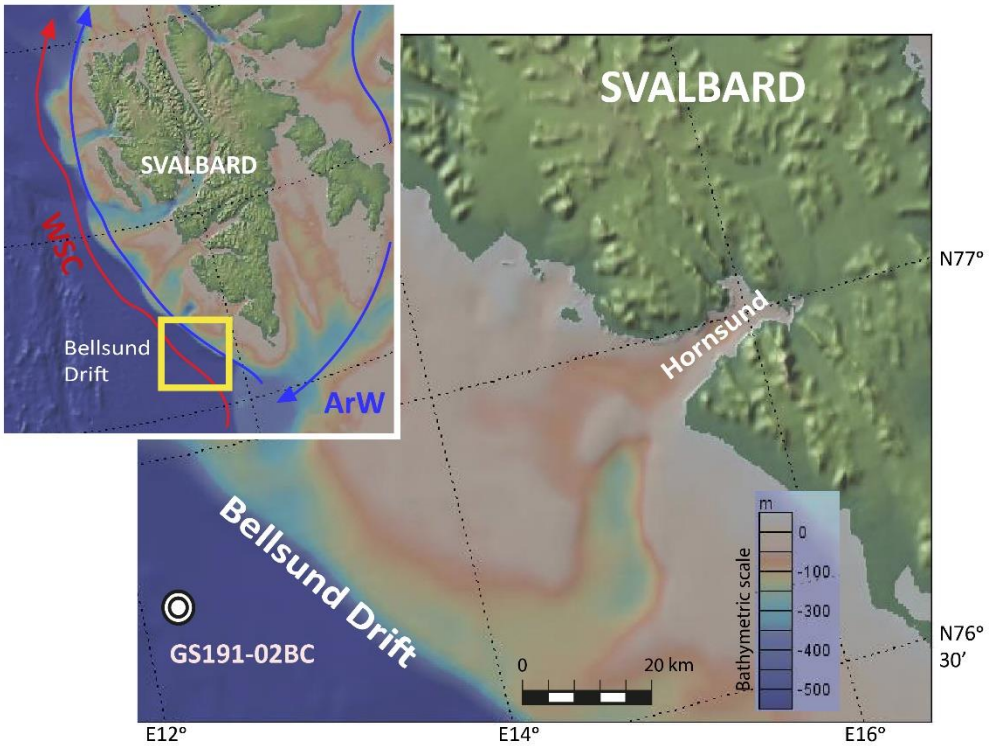


Fig. 4.1. Study area showing the location of the box-corer GS191-02BC. The left figure shows the WSC (West Spitsbergen Current, red arrow) and the location of the study area (yellow square).

The climate variability across the Fram Strait is recorded by the glacier history in the area, the last greatest extension of sea ice during the Late Holocene is documented during the Little Ice Age (1500 to 1890 A.D.) (Werner, 1993; Svendsen and Mangerud, 1997). Many of these studies concluded that it is necessary to perform more studies focussed on the decennial climatic changes during the Late Holocene, to understand the climate variation in the Svalbard area (Werner et al., 2011).

The eastern area of the Fram Strait is characterised by the AW input as a bottom current beneath the cold and less saline Arctic Water (ArW) (Ślubowska et al., 2005), this is the hydrographic situation which controls the presence and extension of the seasonal sea ice at western Svalbard (Werner et al., 2011). Studies performed in this area reported during the last *ca.* 150 years alternating positions of the sea ice margin during the winter, with evidence of persistent ice-retreat (Vinje, 2001), and no presence of the sea ice in the western Svalbard area during the last 200 years (Divine and Dick, 2006). Spielhagen et al. (2011), indicate an increasing trend of the ocean temperatures, showing an unprecedented warming of the AW in the past 200 years.

4.2. Temperature and Sea ice record in the Fram Strait, satellite monitoring

The ocean temperature, the sea ice extent, and the sea ice thickness represent important climate indicators, linked to dynamic and thermodynamic processes. The extent of the sea ice is strongly affected by the thermal effect of the currents since 1860 (Vinje, 2001). Among the main factors that affect the sea ice extent there is the sea and air temperatures; their inter-annual changes can affect the growth and recover of the sea ice, and high temperatures during the winter season can inhibit the extent whereas high temperatures during the summer can accelerate the melt of the ice cover (Comiso et al., 2008). Spielhagen et al. (2011) indicate that the mean temperature values for the Modern Period (since 1890), exceeded the temperature of the last 2000 years, and the superficial water became warmer, which is in accordance to the consistent retreat of the sea ice in the area (Divine and Dick, 2006).

The hydrographic survey in the Fram Strait started in 1910 in order to redact a record of the WSC temperature (with diverse gaps into the record at 1926 to 1962 and at 1964 to 1973) (www.mosj.no). The satellite data monitoring the ice extent in Fram Strait started from 1979, and showed the maximum extension in the northernmost area of the Fram Strait, leaving the southern area free of sea ice (including

the area of the Bellsund Drift) (www.mosj.no). Historically, the maximum extension of the sea ice occurs usually during March-April (Fig. 4.2 a). The data set showed a decreasing trend of the sea ice extent, with some peaks of recovery of the sea ice extent-covered area (Fig. 4.2 b). The uninterrupted dataset from 1963 showed an increased in the WSC temperature from 4.4 °C in 1963 to 5.8 °C in 2016 (Fig. 4.2 b).

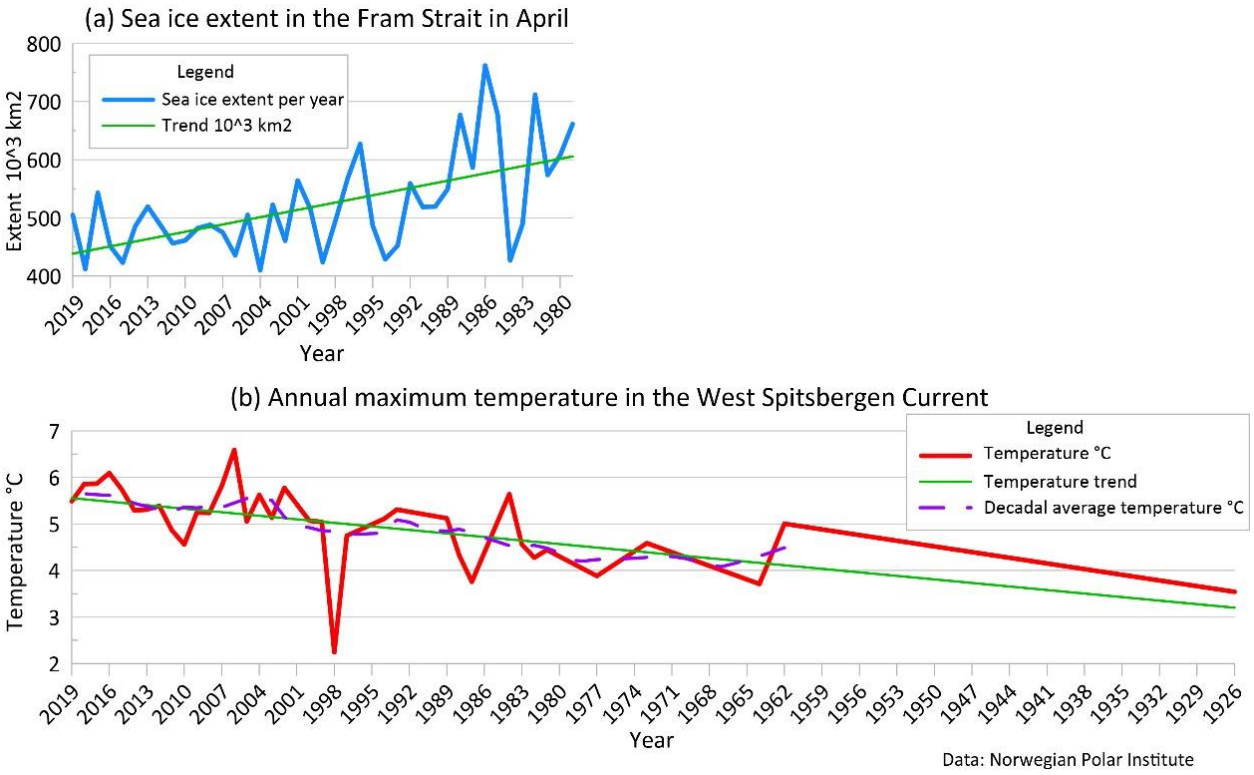
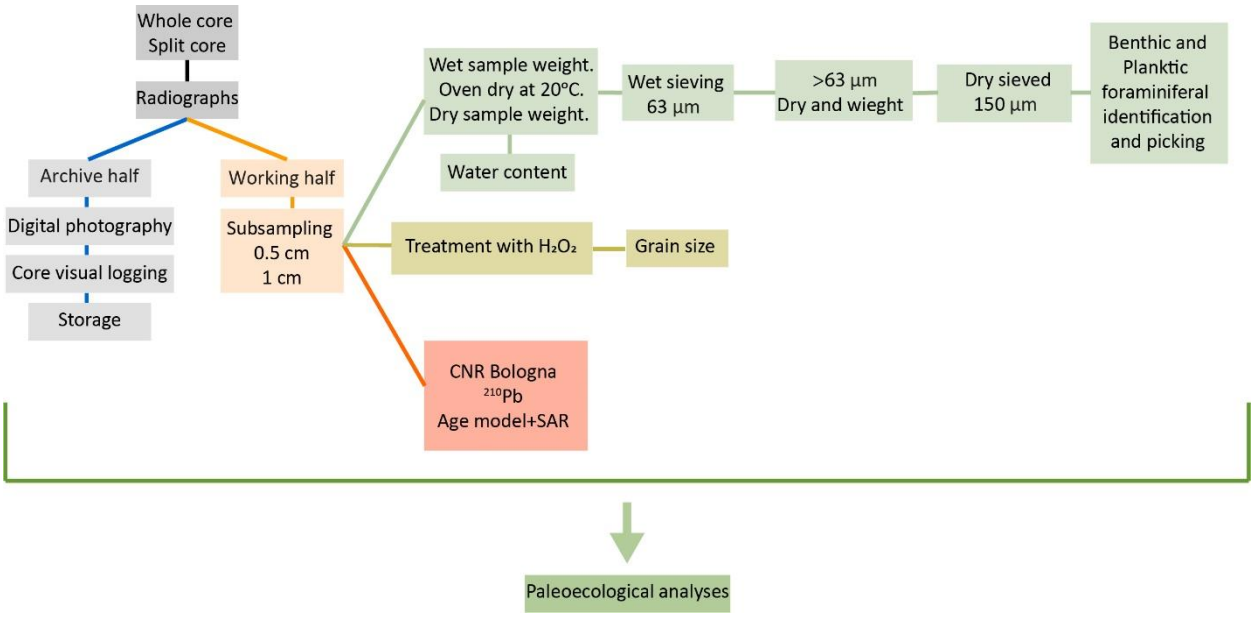


Fig. 4.2. (a) Sea ice extent of the sea ice in the Fram Strait area. The graphic shows the record of the last 50 years during the month of maximum extent (April) (blue line). (b) Annual maximum temperature in the WSC. The graphic shows the annual temperature from 1926 (red line), the decadal average temperature from 1962 (dashed purple-line), and the general trend of the sea ice extent and the temperature (green line). Database Norwegian Polar Institute (2020 a & b).

4.3. Material and methodology

The workflow 4.1 shows the scheme of the materials and methods (Chapter 2) followed for this chapter for the study of the box-corer collected in Bellsund Drift.



Workflow 4.1. Summary scheme of the materials and methods used for the Box corer core GS191-02BC. For more details, see chapter 2. Materials and methodology

4.4. Results

4.4.1. Age model

The age model is developed using ^{210}Pb and ^{14}C dating by Dr. Leonardo Langone, ISP-CNR Bologna (National Research Council, Bologna) (Tab. 4.1). ^{14}C dating at the bottom of the core (22 cm) resulted in a calibrated age of 1866 A.D., in accordance with the estimated age derived by ^{210}Pb method.

Depth (cm)	^{210} Pb Excess (Bq/kg)	SAR (cm/yr)	Estimated date A.D.
0-0.5	380.6		2013
1-1.5	465.3		2006
2-3	354.4		1998
4-5	438.7		1984
5-6	266.9		1977
6-7	375.8		1971
7-8	194.3		1964
8-9	136.7	0.148	1957
9-10	176.2		1950
10-11	113.1		1944
12-13	247.7		1930
13-14	9.4		1923
14-15	192.2		1917
15-16	3.6		1910
16-17	54.0		1903
18-19	27.0		1890

Tab. 4.1. Age model: lead measurements, sedimentation rate and date A.D.

4.4.2. Lithological description and grain size analysis

Lucchi et al. (2014) carried out the lithological description on-board during the oceanographic campaign. The core is constituted by silt-clay sediments slightly bioturbated from the bottom to 5 cm and the surface sediment is made of soft brown silt and silty-clay with abundant bioclasts (Fig. 4.3) (Lucchi et al., 2014).

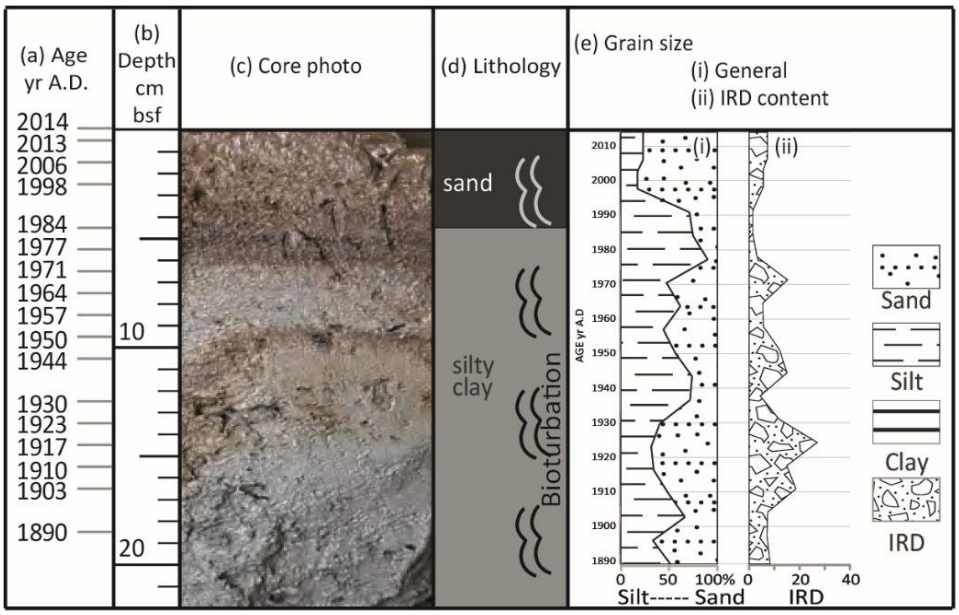


Fig. 4.3. Box-core data description: (a) Age yr A.D. (see Tab. 4.1); (b) Depth cm bsf; (c) Core photo; (d) log description (Lucchi et al., 2014); (e) Grain size, with the relation between silt and sand (see chapter 2) and (ii) IRD content (≥500 µm).

4.4.3. Planktic foraminifera

a. General trends

Six planktic foraminiferal species are recognised (Tab. 4.2), five of them present with more than 5% in the record (Fig. 4.4).

	Planktic species		
Main species (>5%)	*Neogloboquadrina pachyderma* *Globigerina bulloides*	*Turborotalita quinqueloba* *Globigerinita glutinata*	*Neogloboquadrina incompta*
Secondary species (<5%)	*Globigerinita uvula*		

Tab. 4.2. Planktic foraminiferal species

The total planktic foraminiferal flux and the total concentration show an upward general decreasing trend in the sequence (Fig. 4.4 d). The planktic foraminiferal flux varies from *ca.* 200 to 75 spec./cm^2/yr between 1903 and 1971 A.D. From 1977 until 2014 A.D., the flux of planktic foraminifera varies from the maximum of 98 spec./cm^2/yr at 1991 A.D., and reaches the minimum at the top of the sequence with 25 spec./cm^2/yr (Fig. 4.4 d). The total concentration shows a similar trend of the flux, ranging between a maximum of 1515 spec./g at 1903 A.D., and 190 spec./g at 2014 A.D (Fig. 4.4 c).

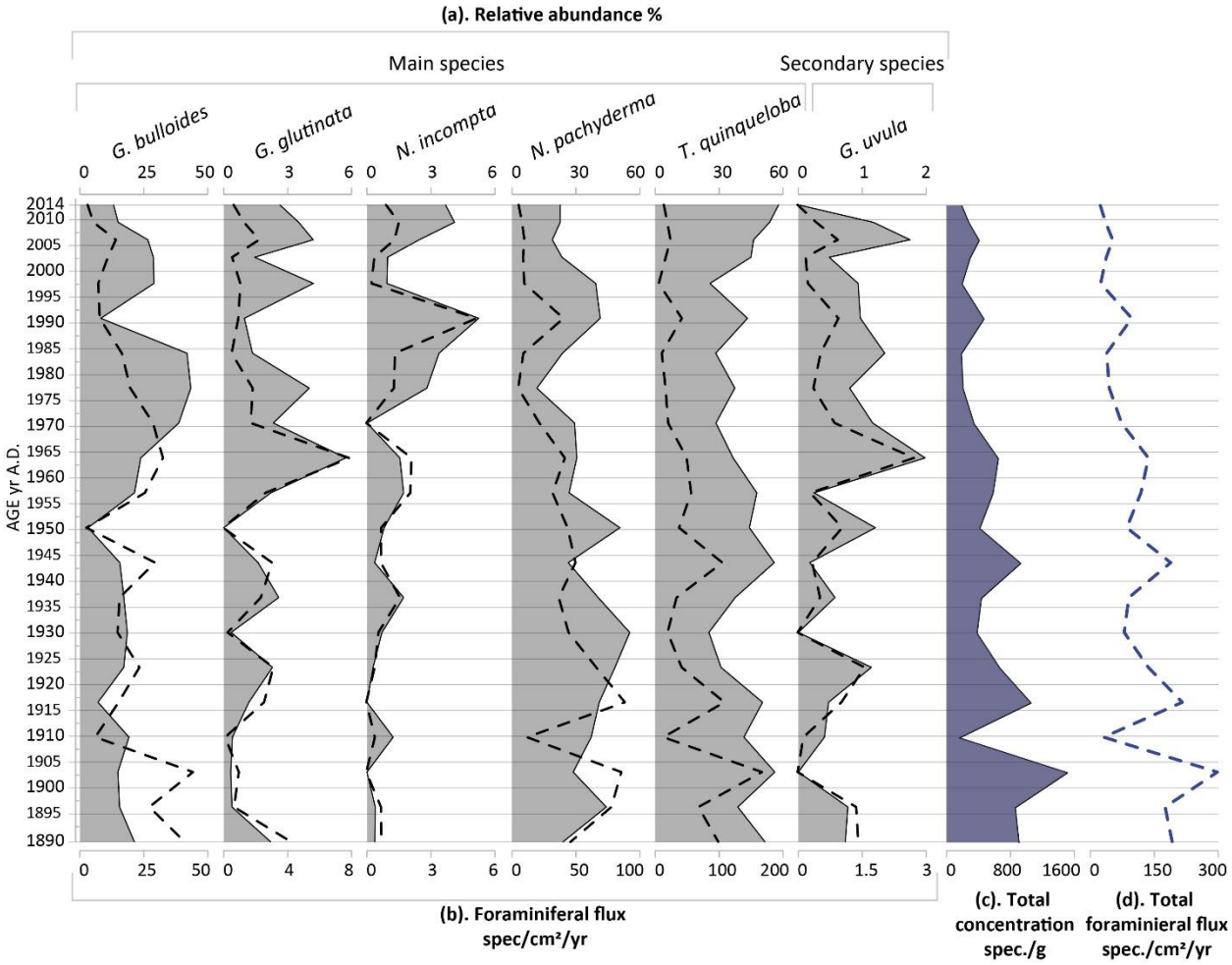


Fig. 4.4. Main and secondary planktic foraminiferal species by age: (a). grey area: percentage of relative abundance. (b). Dashed black line: Foraminiferal flux. (c). Total foraminiferal concentration per gram of dry sediment. (d). General foraminiferal flux. The x-axes are different.

b. Diversity indexes and cluster analysis

The diversity indexes show a fluctuating trends. From 1890 to1970 A.D. the number of taxa (S) arrives until 4 at 1903 A.D., then from 1975 until 2009 A.D., reaches the maximum of 6 (Fig. 4.5). The dominance values never exceed 0.5, which indicates the presence of almost all species in the record (Fig. 4.5). From 1890 to 1950 A.D., the H index shows values lower than 1.2, after 1950 A.D. the values surpass the 1.2 that indicates the increase in the number of species (Fig. 4.5).

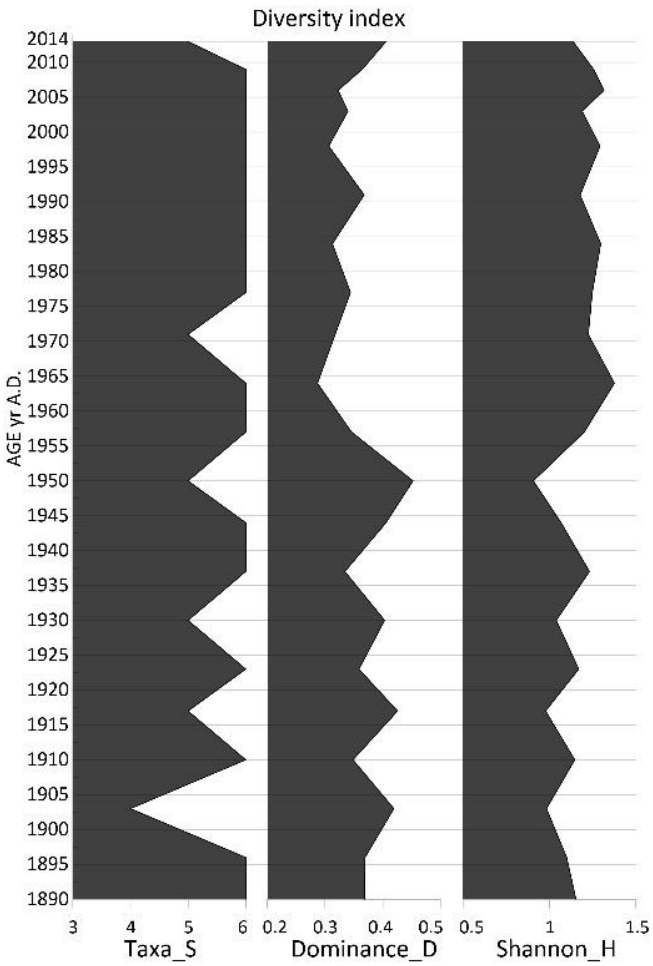


Fig. 4.5. Planktic foraminifera: diversity indexes. The x-axes are different.

The classical hierarchical Q-mode cluster analysis, indicates three cluster groups within the planktic foraminiferal assemblage A, B and C (Fig. 4.6 a). Time-wise, the clusters have some few overlaps, but in general, they are separated in three main periods: 1890 - 1957 A.D; 1957 - 1998 A.D.; and 1998 - 2014 A.D. (Fig. 4.6-b). Cluster A is dominated by *N. pachyderma* and with relatively high abundance of *T. quinqueloba* and *N. incompta* (Fig. 4.6). Cluster B shows an increase of *N. pachyderma* compared to the Cluster A and a reduced frequency of *T. quinqueloba*, *G. bulloides* and *N. incompta* (Fig. 4.6). Cluster C indicates a reduction of *N. pachyderma* and *T. quinqueloba* compared to the clusters A and B and in addition an increased frequency of *G. bulloides* (Fig. 4.6).

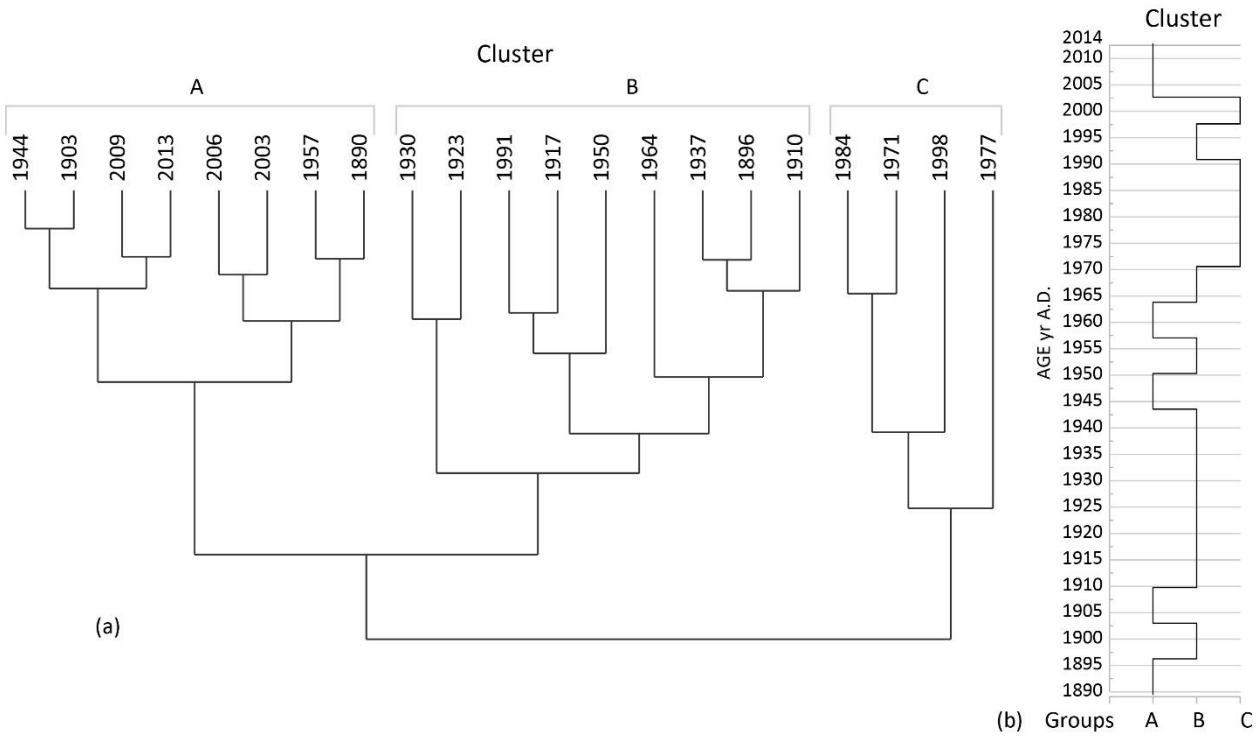


Fig. 4.6. Q-mode cluster analysis of the planktic foraminifera. (a). Cluster analysis dendrogram in Q-mode. (b). Cluster groups by age distribution down-core.

c. Planktic foraminiferal pattern

Period 1890 - 1957 A.D.

High fluxes and high relative abundances of *N. pachyderma* and *T. quinqueloba* occur from 1890 to 1957 A.D. (Fig. 4.4). *Neogloboquadrina pachyderma* reaches its maximum percentage at 1930 A.D. with 55%, while *T. quinqueloba* arrives at 56% at 1903 A.D. (Fig. 4.4). *Globigerina bulloides* occurs with maximum percentage (21%) at 1890 A.D., *G. glutinata* and *N. incompta* show a maximum value of 2% along the record (Fig. 4.4).

Period 1957 - 1990 A.D.

Neogloboquadrina pachyderma and *T. quinqueloba* fluxes and percentages decrease between 1957 and 1990 A.D. with a maximum of 41% and 48%, respectively (Fig. 4.4). *Neogloboquadrina pachyderma* reaches the minimum (12%) at 1977 A.D. G*lobigerina bulloides*, *G. glutinata* and *N. incompta* increase

during this period. The maximum percentage of *G. bulloides* at 1977 A.D. is 43% and *G. glutinata* at 1964 A.D., reached 6% (Fig. 4.4).

Period 1990 - 2014 A.D.

Finally, from 1990 to 2014 A.D, *N. pachyderma* shows a strong decrease in arriving at 19% (Fig. 4.4). *Turborotalita quinqueloba* increases with a maximum of 58% at 2014 A.D.; *G. bulloides* declines until 13% at 2014 A.D.; *G. glutinata* has a peak at 2006 A.D. with 4%, to continue to decrease until 2014 A.D.; *N. incompta* shows fluctuating record, reaching the maximum of 5% at 1991 A.D (Fig. 4.4).

4.4.4. Benthic Foraminifera

a. General trends

Into the sedimentary record of the box-corer GS191-02BC, 79 benthic foraminiferal species are identified, with 14 main species (Tabs. 4.1.3 and 4.1.4). In general, the main group (68%) is the calcareous perforate, with 36 species The calcareous imperforate group has 11 species and represents 2% of the assemblage and the agglutinated group has 24 species corresponding to the 31% of the assemblage (Fig.4.1.7 a).

Main Benthic foraminiferal species (>5%)				
Calcareous perforate	*Cassidulina laevigata*	*Cassidulina neoteretis*	*Cassidulina reniforme*	*Cibicidoides wuellerstorfi*
	Epistominella exigua	*Oridorsalis tener*	*Parrelloides* cf. *healdi*	
Agglutinated	*Adercotryma* cf. *glomeratum*	*Hyperammina subnodosa*	*Labrospira crassimargo*	*Labrospira subglobosa*
	Recurvoides trochamminiforme	*Reophax scorpiurus*	*Trochammina globigeriniformis*	

Tab. 4.3. Main benthic foraminiferal species.

Secondary Benthic foraminiferal species (<5%)				
Calcareous perforate	*Astrononion gallowayi*	*Bolivinellina pseudopunctata*	*Buccella* spp.	*Cibicides refulgens*
	Cibicidoides lobatulus	*Dentalina drammenensis.*	*Elphidium albiumbilicatum*	*Elphidium clavatum*
	Elphidium hallandense	*Elphidium macellum*	*Fissurina* spp.	*Globulina landesi*
	Haynesina orbiculare	*Ioanella tumidula*	*Islandiella norcrossi*	*Lagena* spp.
	Lenticulina gibba	*Marginulina obesa*	*Melonis barleeanus*	*Nonionella auricula*
	Oolina spp.	*Pullenia bulloides*	*Pullenia* cf. *catalinaensis*	*Pullenia elegans*
	Pullenia osloensis	*Robertinoides pumilum*	*Stainforthia feylingi*	*Stainforthia fusiformis*
	Trifarina fluens	Indeterminate		
Calcareous imperforate	*Cornuspira* spp.	*Miliolinella* cf. *enoplostoma*	*Miliolinella subrotunda*	*Pyrgo lucernula*
	Pyrgo subglobulus	*Pyrgo williamsoni*	*Pyrgoella globula*	*Quinqueloculina arctica*
	Triloculina oblonga	*Triloculina rotunda*	*Triloculina tricarinata*	
Agglutinated	*Ammobaculites aggutinans*	*Ammodiscus minimus*	*Armorella sphaera*	
	Adercotryma glomeratum	*Bathysiphon* spp.	*Eggerella arctica*	
	Lagenammina difflugiformis	*Psammosphaera fusca*	*Recurvoides contorta*	
	Reophax difflugiformis	*Reophax guttifer*	*Reophax micaceus*	
	Rhabdammina discrete	*Rhabdammina scabra*	*Rhizammina* spp.	
	Spiroplectammina biformis	*Trochammina rotaliformis*		

Tab. 4.4. Secondary benthic foraminiferal species.

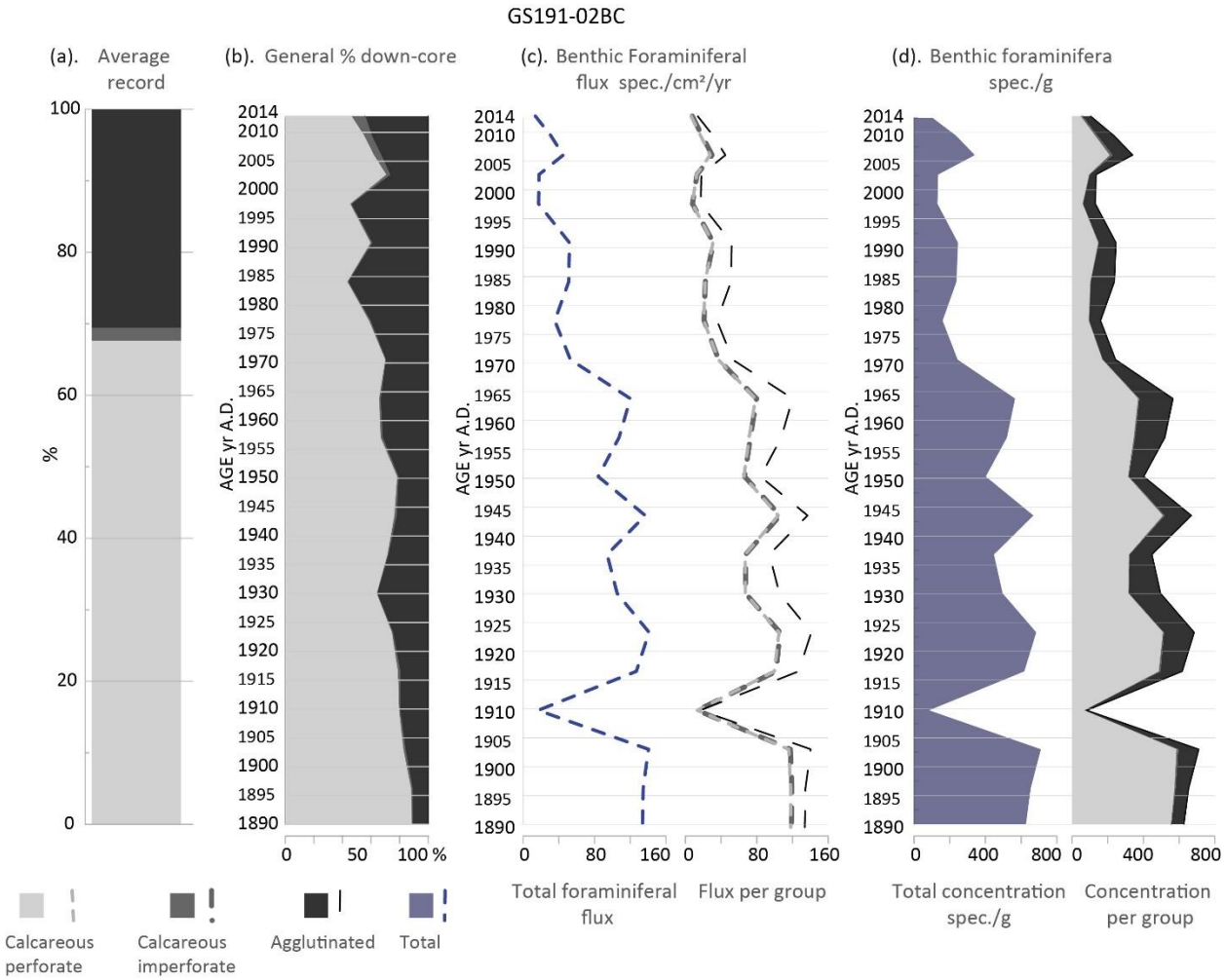


Fig.4.7. Benthic foraminifera (a). General average percentage per group in the entire record. (b). General relative abundance per group down-core. (c). Benthic foraminiferal flux (spec./cm^2/yr). (d). Benthic foraminifera concentration per gram of dry sediment (spec./g). The x-axes are different.

Between 1890 and 1970 A.D., the relative abundance of the calcareous perforate group is about 75%, arriving until the maximum of 88% (interval between 1890 and 1896 A.D.) (Fig. 4.7 b). The calcareous imperforate group are present with less than 1%, reaching 2% at 1917 A.D (Fig. 4.7 b). The average value of the agglutinated group is 24%, showing a general increase toward the top, with a maximum of 36% at 1930 A.D. (Fig. 4.7 b). The foraminiferal flux reached more than 100 spec./cm^2/yr in several levels, with the maximum of 141 spec./cm^2/yr at 1923 A.D. (Fig. 4.7 c) The spec./g reached 710 spec./g at 1903 A.D. (Fig. 4.7 d). Both, foraminiferal flux and spec./g, reach their minimum value at 1910 A.D., with 17 spec./cm^2/yr and 84 spec./g, respectively (Fig. 4.7 c and d).

From 1970 to 2014 A.D., the relative abundance indicates a decrease in the calcareous perforate group and an increase in the agglutinated group, with average values of 55% and 42%, respectively. The calcareous imperforate group increased toward the top, with an average value of 3%, and a maximum value of 10%, at 2013 A.D (Fig. 4.7 a). A decrease in the flux and the spec./g occurred, with maximum values of 52 spec./cm^{2}yr at 1991 A. D., and 340 spec./g at 2006 A.D. (Fig. 4.7 c and d).

b. Diversity indexes and cluster analysis

The diversity indexes indicate an increased number of taxa (S) from 1890 until 1950 A.D., and shows a maximum peak at 1944 A.D. with 40 taxa (Fig.4.1.8). During this period, dominance (D) reaches a maximum value of 0.225 at 1950 A.D. The Shannon index (H) reaches a maximum of 2.73 at 1937 A.D. (Fig. 4.8).

From 1950 to 2014 A.D., the number of taxa (S) is relatively stable, arriving at the minimum of 20 taxa at 1998 A.D. (Fig. 4.8). The D record varies, ranging between 0.197 at 2003 A.D. and 0.112 at 1984 A.D. (Fig. 4.8). The Shannon (H) index shows a shifted trend with a maximum of 2.48 at 1977 A.D., and a minimum of 2.13 at 1971 A.D. (Fig. 4.8).

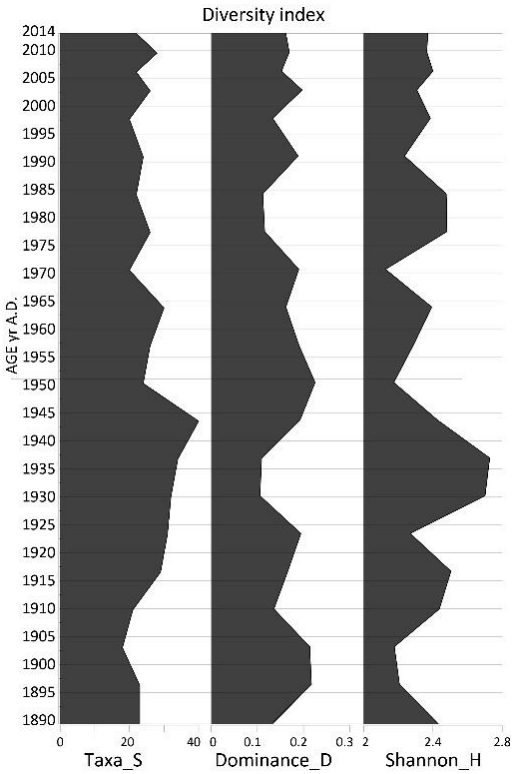


Fig. 4.8. Benthic foraminifera: diversity indexes. The x-axes are different.

The classical hierarchical Q-mode cluster analysis is performed in two steps. The first analysis recognised the main groups and the outliers. A second cluster analysis is performed without the outliers, allowing to identify the cluster groups (Fig. 4.9). Two main cluster groups are identified, plus an outlier.

Three periods are define from the distribution of the cluster analysis, the first period from 1890 to 1957 A.D., the second period from 1957 to 1990 A.D. and the third period from 1990 to 2014 A.D. (Fig. 4.9).

Cluster A is characterised by the high abundance of *C. neoteretis* and *C. wuellerstorfi.* The subgroups into the cluster A are characterised by: I. high relative abundance of *C. neoteretis;* II. high relative abundance of *C. wuellerstorfi*; and III. by the high abundance of *C. reniforme* and *O. tener*. Cluster B (subgroup IV) is characterised by high abundance of *E. exigua*. Cluster C (outlier) is characterised by high relative abundance of the agglutinated species *L. crassimargo* and *R. scorpiurus.*

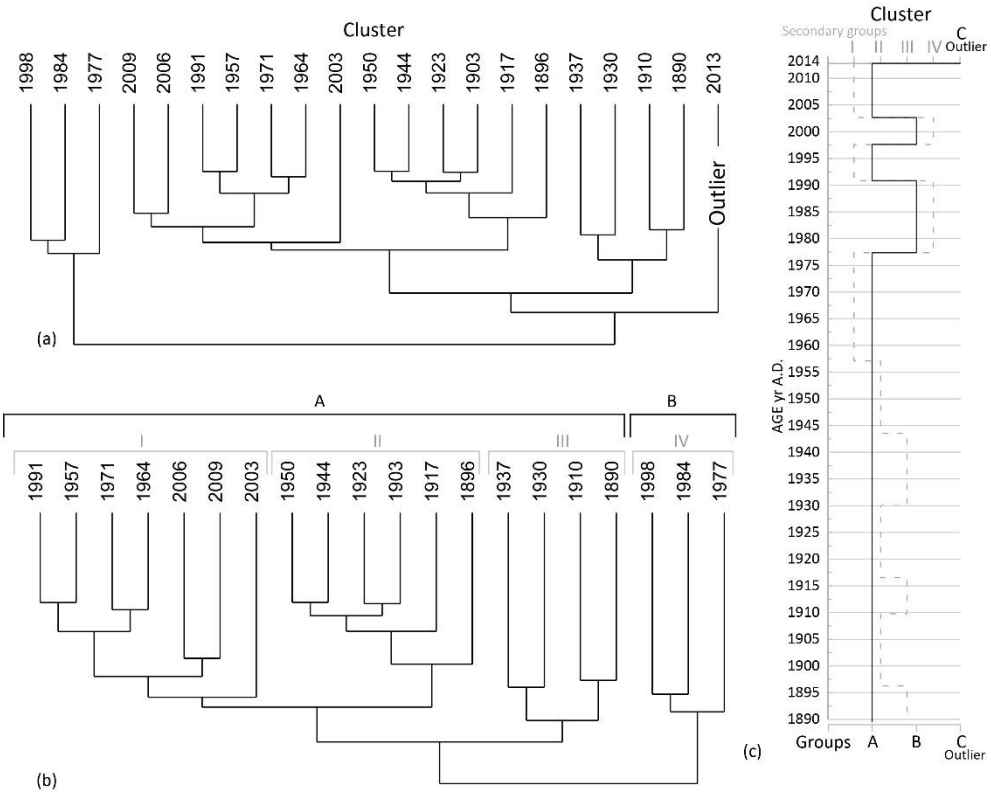


Fig. 4.9. Q-mode cluster analysis of the benthic foraminifera. (a). Cluster analysis dendrogram in Q-mode with outliers. (b). Cluster analysis dendrogram in Q-mode without outliers. (c). Cluster groups by age distribution down-core.

c. Benthic foraminiferal pattern

Period 1890 - 1957 A.D.

The dominant species is *C. wuellerstorfi* with a fluctuating record, ranging between 24 to 44%. *Cassidulina reniforme* increased until a maximum of 11% at 1937 A.D., *E. exigua* and *O. tener* show a similar fluctuating trend, both with a maximum of 11% at 1890 and at 1896 A.D. respectively (Fig. 4.10). *Cassidulina neoteretis* shows a decrease from 8% at 1890 A.D, arriving to 2% at 1910 A.D. (Fig. 4.10). *Parrelloides* cf. *healdi* reaches the maximum of 7% at 1910 A.D. (Fig. 4.10). *Cassidulina laevigata* is only present with 2% at 1917 A.D. The calcareous perforate foraminiferal flux shows a decline towards the topmost centimetres (Fig. 4.10).

The main agglutinated species is *A.* cf*. glomeratum*, with a maximum of 8% at 1890 A.D., decreasing on top arriving until 1% at 1955 A.D. (Fig. 4.10). *Reophax scorpiurus* increases during this period and reaches 15% at 1930 A.D. The species *L. subglobosa* ranges from 1 to 9%, and *R. trochamminiforme* ranges from 0.8 until 11% (Fig. 4.10). Less than 5% are present *H. subnodosa*, *L. crassimargo* and *T. globigeriformis*. The flux of the agglutinated foraminifera increases on top, except for *A.* cf*. glomeratum* that decline towards the topmost centimetres (Fig. 4.10).

Period 1957 - 1990 A.D.

A high concentration of *C. wuellerstorfi* occurred at the beginning of this period, and then decreased up to 10% at 1984 A.D. (Fig. 4.10). *Epistominella exigua* shows a high concentration between 1965 and 1985 A.D, arriving until 14% at 1971 A.D. The relative abundance of *O. tener* register a peak of 9% at 1977 A.D. (Fig. 4.10). *Cassidulina neoteretis* and *C. reniforme* remain stable during this period, showing an increase from 1980 to 1990 A.D. (Fig. 4.10). Between 1957 and 1970 A.D., the foraminiferal flux increases; then to finish this period (until 1990 A.D.) with a decreasing flux (Fig. 4.10).

Adercotryma cf. *glomeratum* dropped to 0.4% at 1971 A.D. (Fig. 4.10). *Labrospira subglobosa*, *R. trochamminiforme* and *R. scorpiurus* show an increase reaching *ca.* 10% during this period. The foraminiferal flux for *L. subglobosa*, *R. trochamminiforme* and *R. scorpiurus* increased, while for *A.* cf. *glomeratum* decreases (Fig. 4.10).

Period 1990 - 2014 A.D.

Cibicidoides wuellerstorfi increases until 41% at 2003 A.D. (Fig. 4.10). *Cassidulina laevigata* record a peak at 2003 A.D. (Fig. 4.10). High concentration of *C. neoteretis* and *E. exigua* occur during this period, reaching 8 and 10% respectively. *Cassidulina reniforme*, *O. tener* and *P.* cf. *healdi* show a decrease. *Parrelloides* cf. *healdi* disappeared in 1998 A.D. (Fig. 4.10). The calcareous perforate flux reaches their minimum at the top of the core (Fig. 4.10).

The relative abundance of the agglutinated group increases toward the top, becoming more abundant, following the trend of the flux.

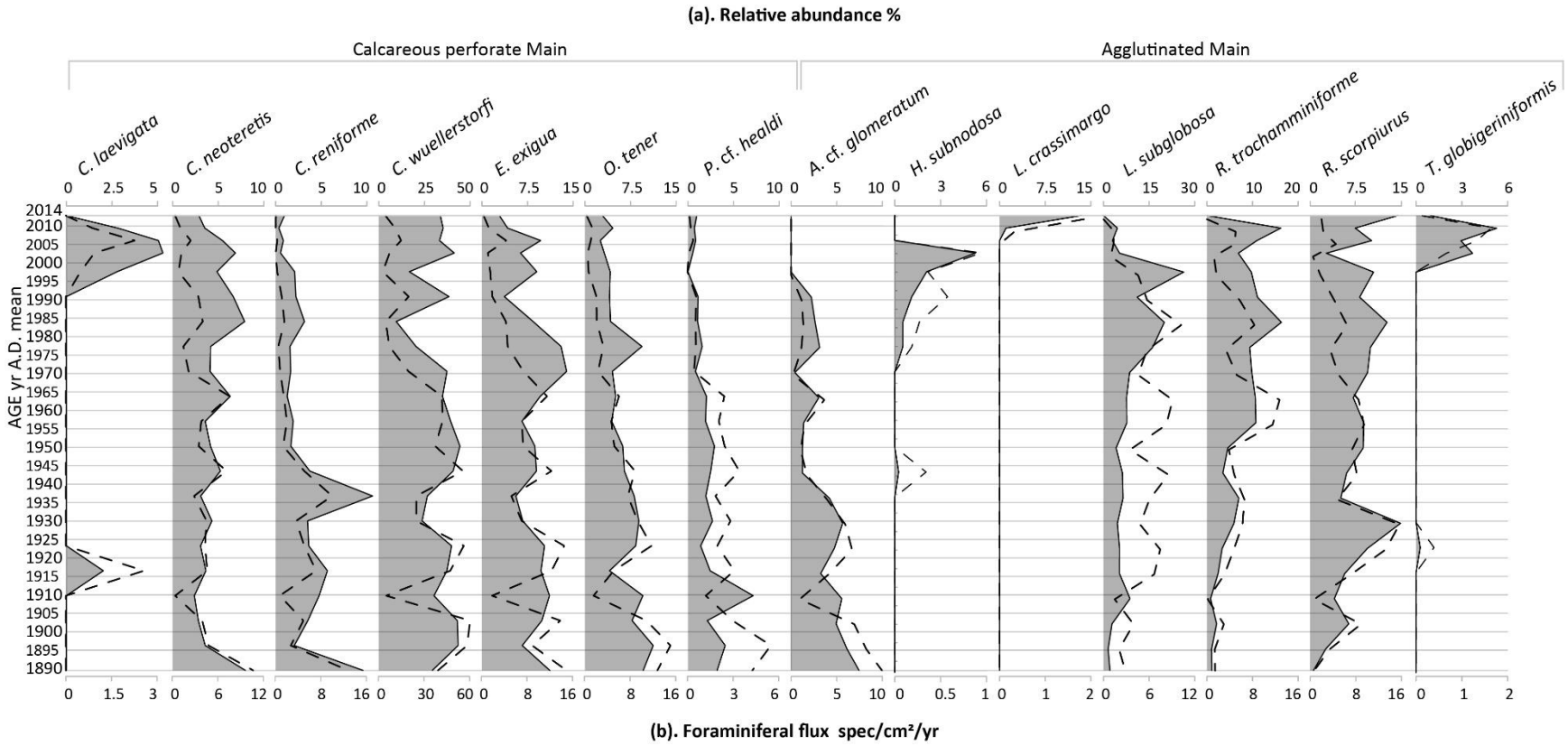


Fig. 4.10. Benthic foraminifera: (a). Relative abundance (grey) and (b). Foraminiferal flux (black dashed line) of the main species. The x-axes are different.

The secondary species are present in less than 5% in the record (Fig. 4.11).

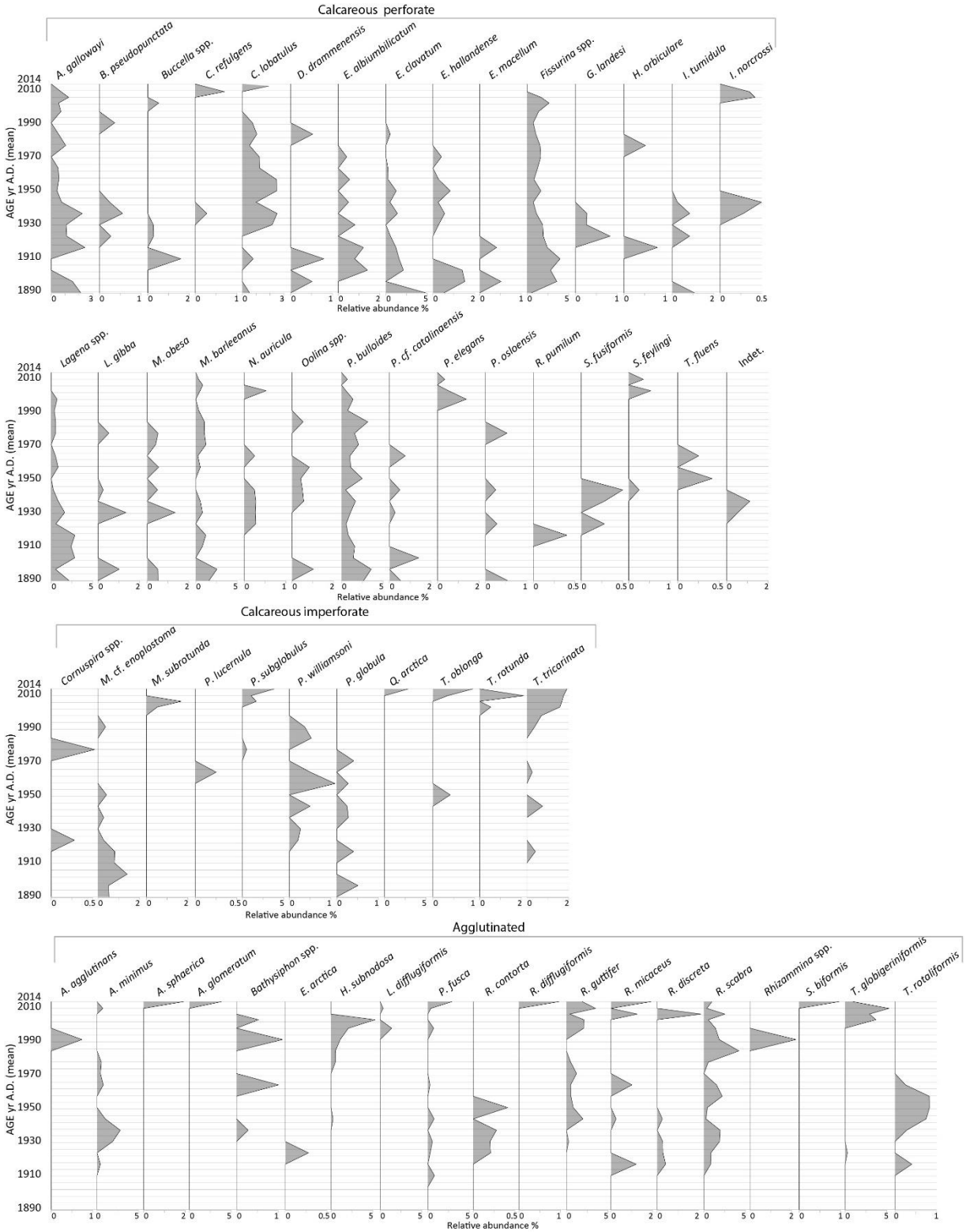


Fig. 4.11. Secondary species

4.5. Discussion

The analysis of the planktic and benthic foraminiferal assemblages of the last 120 years together with the knowledge of their ecological requirements allow to reconstruct the main hydrological changes linked to the superficial and bottom water masses. Using the Q-mode cluster analysis, three main periods are identify and discussed in the following paragraphs.

a. Period from 1890 to 1957 A.D.

During this first period, warmer conditions are registered, indicated by the increase of *G. bulloides*, reaching the maximum between 1905 and 1945 A.D. Nevertheless, the cold conditions are dominant, indicated by the presence of *N. pachyderma*, showing maxima at 1896 A.D., 1930 A.D. (the last long cold period from 1910 to 1940 A.D.) and 1950 A.D. (Tab. 4.5; Fig. 4.12). This cold period must be related to that report by Divine and Dick (2006) during the 1940s, and mention by Chylek et al. (2009) from 1940 until 1970 A.D., where the influx of cold ArW is strong. Vinje (2001) and Divine and Dick (2006), indicate the last cold event in the Arctic during the period from 1949 until 1966 A.D., recorded in our study by the peak in abundance of the cold species *N. pachyderma* at 1950 A.D. and by the low abundance of warm species *N. incompta*, *G. bulloides* and *G. glutinata* (Tab. 4.5; Fig. 4.12).

The presence and increase of subpolar species as *N. incompta*, *G. bulloides, G. glutinata* and *T. quinqueloba,* are recorded in other studies, related with the influx of AW coming from the Norwegian Sea (Carstens et al., 1997; Volkmann, 2000; Spielhagen et al., 2011; Werner et al., 2011). The warmer conditions and the increase of primary productivity is associated with the high flux of planktic foraminifera in the Arctic region (Carstens et al., 1997; Pados and Spielhagen, 2014).

The occurrence of *C. reniforme* suggests cold sea-bottom conditions and an environment with high-energy and low productivity, indicated by the predominance of the species *C. wuellerstorfi* (Altenbach and Sarnthein, 1989) together with *O. tener* (Tab. 4.5; Figs. 4.12-4.13). The high energy is indicate by a high influx of coarse sediment occurring between 1920 and 1930 A.D., suggesting an increase of the bottom speed currents (Fig. 4.3). The presence of *C. neoteretis* indicates events of interaction with warmer and seasonal ice-free conditions during this period (Tab. 4.5). These warmer events improved the seasonal productivity, increasing the occurrence of the opportunistic species as the *E. exigua* (Fig. 4.12; Tab. 4.5), and the increase in the number of taxa (S) (Fig.4.8).

b. Period from 1957 to 1990 A.D.

Increasing of the warmer conditions during this period are shown by the increase of AW indicators *T. quinqueloba*, *G. bulloides*, *G. glutinata* and *N. incompta* (Tab. 4.5; Figs. 4.12-4.13). The last three species reached their maximum percentages (and flux) during this period. (Tab. 4.5; Figs. 4.12-4.13). This increase in the water temperature is agree to conditions reported between 1966 and 1992 by several authors using planktic foraminifera (Vinje, 2001; Polyakov et al., 2004; Screen and Simmonds, 2010 a; Comiso and Hall, 2014), and by the trend shown by the instrumental dataset of the temperature of the WSC during the same period (Fig.4.1.2 b). Dickson et al. (2000) and (Spielhagen et al. (2011) report that since 1980 A.D., the increased of the warm water species confirmed the spreading of AW into the Arctic Ocean, determining warmer conditions (Figs. 4.12-4.13). In our record, an event of colder conditions is indicated after 1985 A.D. and the beginning of the 1990s, with the increase of *N. pachyderma* (Fig. 4.12), Divine and Dick, (2006) indicate this cold event during the late 1980s.

During this period, the sea-bottom indicates warmer conditions; intensified from 1984 A.D. with the increase of the AW related *C. neoteretis* (Tab. 4.5; Fig. 4.12). The increased of the opportunistic taxon *E. exigua*, indicates the increase of the seasonal food supply, also associated with the high abundance of *C. neoteretis* and with the low abundance of *C. reniforme*. In general, this period is characterised by high productivity (Tab. 4.5; Fig. 4.12).

c. Period from 1990 to 2014 A.D.

During this last period, a warmer trend amplified, confirmed by the rise of the warm-water indicators *T. quinqueloba*, *N. incompta*, *G. bulloides* and *G. glutinata* (Tab. 4.5; Figs. 4.12 - 4.13), and agreed with the annual maximum temperature in the WSC (Fig. 4.2 b). A general downward trend, of the cool-water indicator *N. pachyderma*, confirmed the diminution in the influx of cold water (Tab. 4.5; Fig. 4.12). This trend is in accordance to the warming event that occurred at 1991 A.D. in the Arctic area (Nansen Basin) and documented by Quadfasel et al. (1991). Kinnard et al. (2011), indicate a warm-water inflow event in the Arctic Ocean, started during the 1990s, which produced heat conditions that invade the entire water column (Steele and Boyd, 1998; Dickson et al., 2000; Karcher et al., 2003). This increase of the heat influx into the water column is related to the decrease of the sea ice extent (e.g. Comiso et al., 2008). According to Kaufman et al. (2009), the period between 1999 and 2008 is the warmest of the last 200 years.

A high-productivity event from 1991 to 2002 A.D. is testified by the high relative abundance of *N. pachyderma* and *T. quinqueloba* (Carstens et al., 1997). The satellite monitoring indicates a warmer trending of the WSC and continuing retreat of the sea ice in the northern area, producing over time the shortness of the cold periods and seasonal sea ice decrease (Fig. 4.2). The planktic foraminiferal assemblages reflect these conditions, in the sea-surface water, with the increasing abundance of the warmer indicator species as *T. quinqueloba, N. incompta, G. glutinata* and *G. bulloides* (Fig 4.12).

The bottom warming conditions continuing during this period, indicated by the increase of *C. laevigata* and *C. neoteretis*, both reached a maximum peak between 2003 and 2009 A.D. (Tab. 4.5; Fig. 4.12), and agreed with an increase in the annual maximum temperature, in the WSC between 2000 and 2009 A.D. (Fig. 4.2). *Cassidulina reniforme* reaches the minimum values during the end of this period, suggesting the increasing of warmer sea-bottom temperatures (Tab. 4.5; Fig. 4.12). The sea-bottom show the high-energy conditions, linked to the increase of *C. wuellerstorfi*, associated with the input of sandy sediment (Tab. 4.5; Figs.4.3-4.12 and 4.13).

In general, this record shown a predominance of cold superficial water conditions iindicated by the dominance of the cold ArW indicator *N. pachyderma*, associated with the AW inflow indicator *T. quinqueloba* (Husum and Hald, 2012) (Tab. 4.5; Figs. 4.12 and 4.13). Instead, the increased in the warm superficial water conditions are indicated by the presence of *G. bulloides*, together with the occurrence of the accessory-species *G. glutinata* and *N. incompta* (Tab. 4.5; Fig. 4.12). Werner et al. (2011) indicate that the high abundance of both, ArW and AW indicator species (at the same time) that associated with the ameliorate water-column temperature, related with the inflow of AW, and the surface-water conditions predominantly cold, the same authors indicate that this difference into the water column is prevailing during the 20th century (Fig. 4.13). While the bottom warming conditions are prevalent during the entire record demonstrated by the abundance of AW indicators *C. laevigata* and *C. neoteretis.* These conditions suggest a well-stratified water column from 1890 A.D.

	Main species	Environmental conditions	References
Planktic species	*Neogloboquadrina pachyderma*	Polar species. Related to Arctic and Polar surface waters.	Bé and Tolderlund (1971); Kohfeld et al. (1996); Carstens et al. (1997); Simstich et al.(2003); Schiebel and Hemleben (2005).
	Neogloboquadrina incompta, Globigerina bulloides, Globigerinita glutinata	Sub-polar species. Warm Atlantic surface water. Seasonal peak abundances in late summer.	Bé and Tolderlund (1971); Carstens et al. (1997); Volkmann (2000); Schiebel et al. (2001); Simstich et al.(2003); Schiebel and Hemleben (2005).
	Turborotalita quinqueloba	Sub-polar species. Arctic water and related to the Arctic and Polar fronts. Near surface dweller. In areas influenced by warm Atlantic Water.	Bé and Tolderlund (1971); Carstens et al. (1997); Volkmann (2000); Simstich et al.(2003); Schiebel and Hemleben (2005); Husum and Hald (2012).
Benthic species	*Cassidulina laevigata*	Warm, high-salinity bottom water of Atlantic origin and to sandy substrates.	Lagoe (1977); Mackensen and Hald (1988);
	Cassidulina neoteretis	Cool transformed surface Atlantic water. Stable salinity. Seasonal ice-free conditions. High seasonal productivity. Warm bottom conditions. Epifaunal- shallow infaunal species.	Lagoe (1979); Mackensen and Hald (1988); Jennings and Weiner (1996); Wollenburg and Mackensen (1998); Lubinski et al. (2001); Wollenburg et al. (2004); Jennings et al. (2004).
	Cassidulina reniforme	Arctic-Polar species. Cold and salty. Locally related to glaciomarine environments. Associated to E. clavatum. Epifaunal-shallow infaunal.	Serjup et al. (1981); Mackensen et al. (1985); Hald and Korsun (1997); Korsun and Hald (2000); Polyak et al. (2002); Steinsund et al.(1994)
	Cibicidoides wuellerstorfi	Associated to Arctic waters and Arctic/Polar fronts. High-energy environments. Bottom current activity. Epifaunal in coarser sediments and attached to hard substrates.	Belanger and Streeter (1980); Sejrup et al. (1981); Mackensen et al. (1985); Wollenburg and Mackensen (1998); Bauch et al. (2001)
	Epistominella exigua	Opportunistic species. Able to feed fresh phytodetritus. Epifaunal.	Gooday (1993); Thomas et al. (1995); Wollenburg and Mackensen (1998)
	Oridorsalis tener	Related with low productivity. Deep water species 2000-3000 m	Osterman et al. (1999). Wollenburg and Mackensen, (1998)

Tab. 4.5. Main ecology indicators

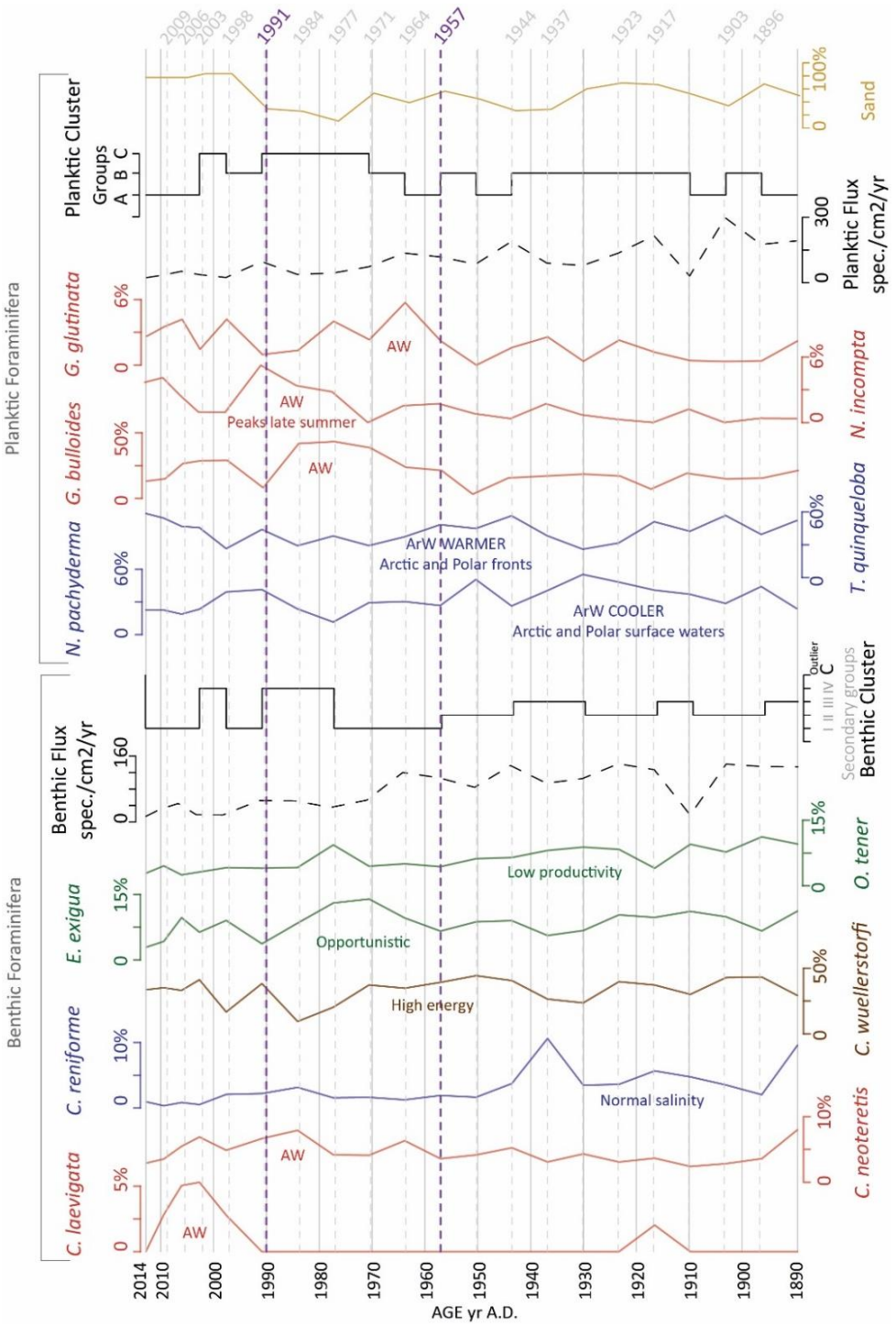


Fig. 4.12. Key proxy correlation: Q-mode cluster division of benthic and planktic foraminifera; benthic and planktic foraminiferal flux (dashed graphic). Relative abundance of the main planktic and benthic foraminiferal species divided by colours: red the warm water related species, blue the cold-water related species, green opportunistic or productivity indicators, brown energy indicators. The gold graphic represents the sand content. The x-axes are different. The vertical divisions purple dashed lines indicate the periods established with the Q-mode clustering analyses; grey line age each 10 years, and the grey-dashed line the years according to the age model.

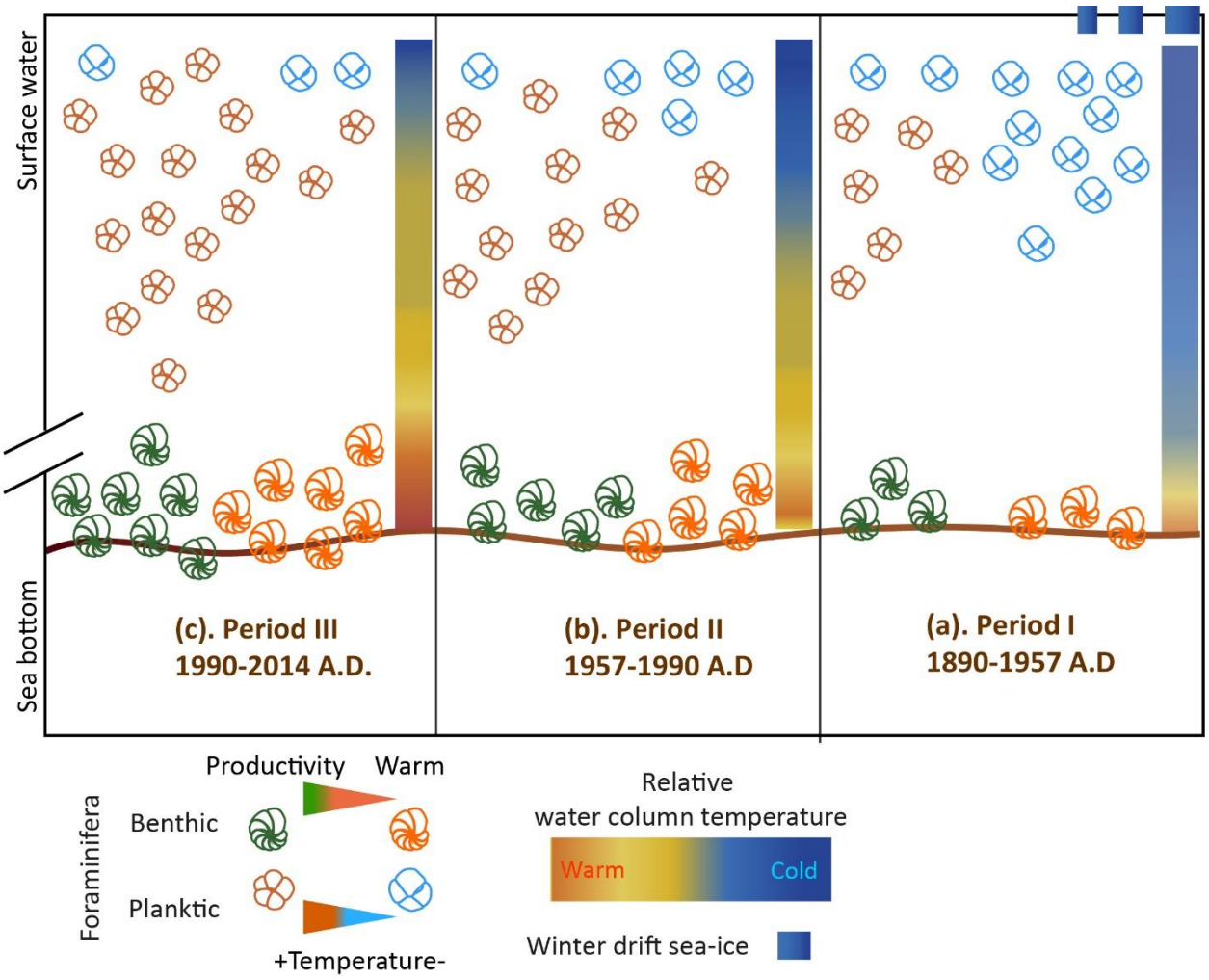


Fig. 4.13. Palaeoenvironmental reconstruction of the record from Bellsund Drift. (a). Period I. (b). Period II. (c). Period III. The sketch indicates the relative temperature of the surface and sub-surface water and the productivity at the sea bottom. The colour-bar scale shows the relative temperature of the water at each period.

4.6. Conclusions

The sedimentary record of the box-core GS191-02BC covers the last 120 years of the oceanographic and sedimentological history of the Bellsund Drift south of the Fram Strait area. High-resolution analysis of the benthic and planktic foraminiferal assemblages are performed to understand the recent (paleo) climatic events. The main species are five planktic taxa, with the dominance of the Arctic species *N. pachyderma* and *T. quinqueloba*, and six benthic species with the dominance of *C. wuellerstorfi*, *E. exigua* and *O. tener*. The grain-size analyses and the satellite monitoring of the sea ice extent and the record of annual temperature of the WSC from the last 50 years, are used to sustain the interpretations of the foraminiferal record.

Three periods are defined in the Bellsund Drift sedimentary record of the last 120 years. The first period from 1890 to 1957 A.D. is characterise by cold superficial water conditions with duration of about 5 to 35 years, alternated to shorter warmer periods (about 5 years). The productivity is possibly related to the input of the AW. The second period (1957 to 1990 A.D.) indicates increasing warmer conditions. The superficial water showed increasing in the temperature and high productivity, with the continuing but less intense input of cold water. At the sea-bottom, the increase of flux of organic matter and the warmer conditions are testified by the presence of more opportunistic species. The third period from 1990 until 2014 A.D., an increment of the warmer conditions related to the AW invading the entire water column, with the occasional input of cold-water. The benthic environment showed warmer conditions and increased productivity.

This environmental reconstruction of the last 120 years points out the increase of the heat influx into the Arctic Ocean, due to the AW increasing inflow suggested also by the satellite monitoring that indicates the progressive diminution of the sea ice and the increasing temperature of the WSC.

4.7. References

Altenbach, A. V., Sarnthein, M. 1989. Productivity Record in Benthic foraminifera. Productivity of the ocean: present and past, 8, 255.

Bauch, H. A., Erlenkeuser, H., Spielhagen, R. F., Struck, U., Matthiessen, J., Thiede, J., Heinemeier, J. 2001. A multiproxy reconstruction of the evolution of deep and surface waters in the subarctic Nordic seas over the last 30,000 yr. Quaternary Science Reviews, 20(4), 659-678.

Bé, A.W.H., Tolderlund, D.S. 1971. Distribution and ecology of living planktonic foraminifera in surface waters of the Atlantic and Indian Oceans. In: Funnell, B.M., Riedel, W.R. (Eds.), The Micropaleontology of the Oceans. Cambridge University Press, pp. 105–149.

Belanger, P. E., Streeter, S. S. 1980. Distribution and ecology of benthic foraminifera in the Norwegian-Greenland Sea. Marine Micropaleontology, 5, 401-428.

Carstens, J., Hebbeln, D., Wefer, G. 1997. Distribution of planktic foraminifera at the ice margin in the Arctic (Fram Strait). Marine Micropaleontology, 29(3-4), 257-269.

Chylek, P., Folland, C. K., Lesins, G., Dubey, M. K., Wang, M. 2009. Arctic air temperature change amplification and the Atlantic Multidecadal Oscillation. Geophysical Research Letters, 36(14).

Comiso, J. C., Hall, D. K. 2014. Climate trends in the Arctic as observed from space. Wiley Interdisciplinary Reviews: Climate Change, 5(3), 389-409.

Comiso, J. C., Parkinson, C. L., Gersten, R., Stock, L. 2008. Accelerated decline in the Arctic sea ice cover. Geophysical research letters, 35(1).

Dickson, R.R., Osborn, T.J., Hurrell, J.W., Meincke, J., Blindheim, J., Adlandsvik, B., Vinje, T., Alekseev, G. and Maslowski, W. 2000. The Arctic ocean response to the North Atlantic oscillation. Journal of Climate, 13(15), pp.2671-2696.

Divine, D. V., Dick, C. 2006. Historical variability of sea ice edge position in the Nordic Seas. Journal of Geophysical Research: Oceans, 111(C1).

Friedman, G. M., Sanders, J. E. 1978. Principles of sedimentology. Wiley.

Gooday, A. J. 1993. Deep-sea benthic foraminiferal species which exploit phytodetritus: characteristic features and controls on distribution. Marine Micropaleontology, 22(3), 187-205.

Hald, M., Korsun, S. 1997. Distribution of modern benthic foraminifera from fjords of Svalbard, European Arctic. The Journal of Foraminiferal Research, 27(2), 101-122.

Husum, K., Hald, M. 2012. Arctic planktic foraminiferal assemblages: Implications for subsurface temperature reconstructions. Marine Micropaleontology, 96, 38-47.

Jennings, A. E., Weiner, N. J. 1996. Environmental change in eastern Greenland during the last 1300 years: evidence from foraminifera and lithofacies in Nansen Fjord, 68 N. The Holocene, 6(2), 179-191.

Jennings, A. E., Weiner, N. J., Helgadottir, G., Andrews, J. T. 2004. Modern foraminiferal faunas of the southwestern to northern Iceland shelf: oceanographic and environmental controls. The Journal of Foraminiferal Research, 34(3), 180-207.

Johannessen, T., Jansen, E., Flatøy, A., Ravelo, A. C. 1994. The relationship between surface water masses, oceanographic fronts and paleoclimatic proxies in surface sediments of the Greenland, Iceland, Norwegian Seas. In Carbon cycling in the glacial ocean: constraints on the ocean's role in global change (61-85). Springer, Berlin, Heidelberg.

Karcher, M. J., Gerdes, R., Kauker, F., Köberle, C. 2003. Arctic warming: Evolution and spreading of the 1990s warm event in the Nordic seas and the Arctic Ocean. Journal of Geophysical Research: Oceans, 108(C2).

Kaufman, D.S., Schneider, D.P., McKay, N.P., Ammann, C.M., Bradley, R.S., Briffa, K.R., Miller, G.H., Otto-Bliesner, B.L., Overpeck, J.T., Vinther, B.M. and Lakes, A. 2009. Recent warming reverses long-term Arctic cooling. Science, 325(5945), 1236-1239.

Kinnard, C., Zdanowicz, C. M., Fisher, D. A., Isaksson, E., de Vernal, A., Thompson, L. G. 2011. Reconstructed changes in Arctic sea ice over the past 1,450 years. Nature, 479(7374), 509-512.

Kohfeld, K. E., Fairbanks, R. G., Smith, S. L., Walsh, I. D. 1996. *Neogloboquadrina pachyderma* (sinistral coiling) as paleoceanographic tracers in polar oceans: Evidence from Northeast Water Polynya plankton tows, sediment traps, and surface sediments. Paleoceanography, 11(6), 679-699.

Korsun, S., Hald, M. 2000. Seasonal dynamics of benthic foraminifera in a glacially fed fjord of Svalbard, European Arctic. The Journal of Foraminiferal Research, 30(4), 251-271.

Lagoe, M. B. 1977. Recent benthic foraminifera from the central Arctic Ocean. The Journal of Foraminiferal Research, 7(2), 106-129.

Lagoe, M. B. 1979. Recent benthonic foraminiferal biofacies in the Arctic Ocean. Micropaleontology, 25(2), 214-224.

Langehaug, H. R., Falck, E. 2012. Changes in the properties and distribution of the intermediate and deep waters in the Fram Strait. Progress in Oceanography, 96(1), 57-76.

Lubinski, D. J., Polyak, L., Forman, S. L. 2001. Freshwater and Atlantic water inflows to the deep northern Barents and Kara seas since ca 13 14C ka: foraminifera and stable isotopes. Quaternary Science Reviews, 20(18), 1851-1879.

Lucchi R.G., Kovacevic V., Aliani S., Caburlotto A., Celussi M., Corgnati L., Cosoli S., Deponte D., Ersdal E.A., Fredriksson S., Goszczko I., Husum K., Ingrosso G., Laberg J.S., Lacka M., Langone L., Mansutti P., Mezgec K., Morigi C., Ponomarenko E., Realdon G., Relitti F., Robijn A., Skogseth R., Tirelli V. 2014. PREPARED: Present and past flow regime on contourite drifts west of Spitsbergen. EUROFLEETS-2 Cruise Summary Report, R/V G.O. Sars Cruise No. 191, 05/06/2014 – 15/06/2014, Tromsø – Tromsø (Norway), 89. DOI: 10.13140/RG.2.1.1975.3769.

Mackensen, A., Hald, M. 1988. *Cassidulina teretis* Tappan and *C. laevigata* d'Orbigny; their modern and late Quaternary distribution in northern seas. The Journal of Foraminiferal Research, 18(1), 16-24.

Mackensen, A., Sejrup, H. P., Jansen, E. 1985. The distribution of living benthic foraminifera on the continental slope and rise off southwest Norway. Marine Micropaleontology, 9(4), 275-306.

Müller, J., Werner, K., Stein, R., Fahl, K., Moros, M., Jansen, E. 2012. Holocene cooling culminates in sea ice oscillations in Fram Strait. Quaternary Science Reviews, 47, 1-14.

Nilsen, F., Skogseth, R., Vaardal-Lunde, J., Inall, M. 2016. A simple shelf circulation model: intrusion of Atlantic Water on the West Spitsbergen Shelf. Journal of Physical Oceanography, 46(4), 1209-1230.

Norwegian Polar Institute 2020 a. Annual maximum temperature in the West Spitsbergen Current. Environmental monitoring of Svalbard and Jan Mayen (MOSJ). URL: http://www.mosj.no/en/climate/ocean/temperature-salinity-fram-strait.html

Norwegian Polar Institute. 2020 b. Sea ice extent in the Fram Strait in September. Environmental monitoring of Svalbard and Jan Mayen (MOSJ). URL: http://www.mosj.no/en/climate/ocean/sea ice-extent-barents-sea-fram-strait.html

Osterman, L. E., Poore, R. Z., Foley, K. M. 1999. Distribution of Benthic Foraminifers (> 125 Um) in the Surface Sediments of the Arctic Ocean (Vol. 2164). US Government Printing Office.

Pados, T., Spielhagen, R. F. 2014. Species distribution and depth habitat of recent planktic foraminifera in Fram Strait, Arctic Ocean. Polar Research, 33(1), 22483.

Polyak, L., Korsun, S., Febo, L. A., Stanovoy, V., Khusid, T., Hald, M., Paulsen, B.E. Lubinski, D. J. 2002. Benthic foraminiferal assemblages from the southern Kara Sea, a river-influenced Arctic marine environment. The Journal of Foraminiferal Research, 32(3), 252-273.

Polyakov, I.V., Alekseev, G.V., Timokhov, L.A., Bhatt, U.S., Colony, R.L., Simmons, H.L., Walsh, D., Walsh, J.E. and Zakharov, V.F. 2004. Variability of the intermediate Atlantic water of the Arctic Ocean over the last 100 years. Journal of climate, 17(23), 4485-4497.

Quadfasel, D., Rudels, B., Kurz, K. 1988. Outflow of dense water from a Svalbard fjord into the Fram Strait. Deep Sea Research Part A. Oceanographic Research Papers, 35(7), 1143-1150.

Quadfasel, D., SY, A., Wells, D., Tunik, A. 1991. Warming in the Arctic. Nature, 350(6317), 385-385.

Schauer, U., Fahrbach, E., Osterhus, S., Rohardt, G. 2004. Arctic warming through the Fram Strait: Oceanic heat transport from 3 years of measurements. Journal of Geophysical Research: Oceans, 109(C6).

Schiebel, R., Hemleben, C. 2005. Modern planktic foraminifera. Paläontologische Zeitschrift, 79(1), 135-148.

Schiebel, R., Waniek, J., Bork, M., Hemleben, C. 2001. Planktic foraminiferal production stimulated by chlorophyll redistribution and entrainment of nutrients. Deep Sea Research Part I: Oceanographic Research Papers, 48(3), 721-740.

Screen, J. A., Simmonds, I. 2010. The central role of diminishing sea ice in recent Arctic temperature amplification. Nature, 464(7293), 1334-1337.

Sejrup, H.P., Fjaeran, T., Hald, M., Beck, L., Hagen, J., Miljeteig, I., Morvik, I., Norvik, O. 1981. Benthonic foraminifera in surface samples from the Norwegian continental margin between 62 degrees N and 65 degrees N. The Journal of Foraminiferal Research, 11(4), 277-295.

Simstich, J., Sarnthein, M., Erlenkeuser, H. 2003. Paired $\delta^{18}O$ signals of *Neogloboquadrina pachyderma* (s) and *Turborotalita quinqueloba* show thermal stratification structure in Nordic Seas. Marine Micropaleontology, 48(1-2), 107-125.

Ślubowska, M. A., Koç, N., Rasmussen, T. L., Klitgaard-Kristensen, D. 2005. Changes in the flow of Atlantic water into the Arctic Ocean since the last deglaciation: evidence from the northern Svalbard continental margin, 80 N. Paleoceanography, 20(4).

Spielhagen, R. F., Werner, K., Sørensen, S. A., Zamelczyk, K., Kandiano, E., Budeus, G., Husum, K., Marchitto, T. M., Hald, M. 2011. Enhanced modern heat transfer to the Arctic by warm Atlantic water. Science, 331(6016), 450-453.

Steele, M., Boyd, T. 1998. Retreat of the cold halocline layer in the Arctic Ocean. Journal of Geophysical Research: Oceans, 103(C5), 10419-10435.

Steinsund, P. I., Polyak, L., Hald, M., Mikhailov, V., Korsun, S. 1994. Distribution of calcareous benthic foraminifera in recent sediments of the Barents and Kara Sea. Benthic Foraminifera in Surface

Sediments of the Barents and Kara Seas: Modern and Late Quaternary Application. Ph. D. Thesis, Department of Geology, Institute of Biology and Geology, University of Tromsø, Norway.

Svendsen, J. I., Mangerud, J. 1997. Holocene glacial and climatic variations on Spitsbergen, Svalbard. The Holocene, 7(1), 45-57.

Thomas, E., Booth, L., Maslin, M., Shackleton, N. J. 1995. Northeastern Atlantic benthic foraminifera during the last 45,000 years: changes in productivity seen from the bottom up. Paleoceanography, 10(3), 545-562.

Vinje, T. 2001. Anomalies and trends of sea-ice extent and atmospheric circulation in the Nordic Seas during the period 1864–1998. Journal of Climate, 14(3), 255-267.

Volkmann, R. 2000. Planktic foraminifers in the outer Laptev Sea and the Fram Strait—Modern distribution and ecology. The Journal of Foraminiferal Research, 30(3), 157-176.

Werner, A. 1993. Holocene moraine chronology, Spitsbergen, Svalbard: lichenometric evidence for multiple Neoglacial advances in the Arctic. The Holocene, 3(2), 128-137.

Werner, K., Spielhagen, R. F., Bauch, D., Hass, H. C., Kandiano, E., Zamelczyk, K. 2011. Atlantic Water advection to the eastern Fram Strait—Multiproxy evidence for late Holocene variability. Palaeogeography, Palaeoclimatology, Palaeoecology, 308(3-4), 264-276.

Wollenburg, J. E., Mackensen, A. 1998. Living benthic foraminifers from the central Arctic Ocean: faunal composition, standing stock and diversity. Marine Micropaleontology, 34(3-4), 153-185.

Wollenburg, J. E., Knies, J., Mackensen, A. 2004. High-resolution paleoproductivity fluctuations during the past 24 kyr as indicated by benthic foraminifera in the marginal Arctic Ocean. Palaeogeography, Palaeoclimatology, Palaeoecology, 204(3-4), 209-238.

5. The last half-century record from Krossfjorden (Kongsfjorden-Krossfjorden glacigenic system).

5.1. Study area

Kongsfjorden-Krossfjorden system is located at west margin of Spitsbergen continental margin (Est of Fram Strait), it continues across the continental shelf as a cross-shelf trough, Kongsfjordrenna (Howe et al., 2003; Ottesen et al., 2007; Dowdeswell et al., 2016) (Fig. 5.1). The Krossfjorden side corresponds with a 30 km length and 3 to 6 km wide area. The outer part of Krossfjorden is up to 374 m deep (Maclachlan et al., 2010). The inner part corresponds with Lillehöökfjorden and Mollerfjorden by Cape Kong Haakons Halvøya. The Lillehöökbreen tidewater glaciers confine the innermost of the fjords, together with five glaciers along the east coast (Svendsen et al., 2002).

This area is under the prevalent Atlantic Water (AW) influence with the arriving of the West Spitsbergen Current (WSC) (northern branch of the North Atlantic Current NAC) and the East Spitsbergen Current (ESC) (Fig. 5.1). The ESC current surrounds Svalbard passing from the Arctic Ocean, the East coast of Svalbard and enters as a coastal current into the fjord (Svendsen et al., 2002; Ebbesen et al., 2007; Sundfjord et al., 2017; Jernas et al., 2018). ESC flows onto the shelf as two branches Spitsbergen Polar Current (parallel to WSC) and Spitsbergen Trough Current (closer to the coast), both transport colder and less saline ArW from the Barents Sea and Storfjorden area (Nilsen et al., 2016) (Fig. 5.1). The water masses inside the fjord are defined by temperature and salinity, and correspond to three main water masses: External, Internal and Mixed. The External water masses includes AW and ArW, both converging in the shelf area and becomes a mixed water masses (includes Transformed Atlantic Water (TAW) and Intermediate Water. The Internal water masses includes the Winter Cooled Water (WCW, originated during sea ice formation), the Local Water (LW also formed during sea ice formation) and the Surface Water (SW, formed during the late spring to early summer) (Svendsen et al., 2002; Cottier et al., 2007).

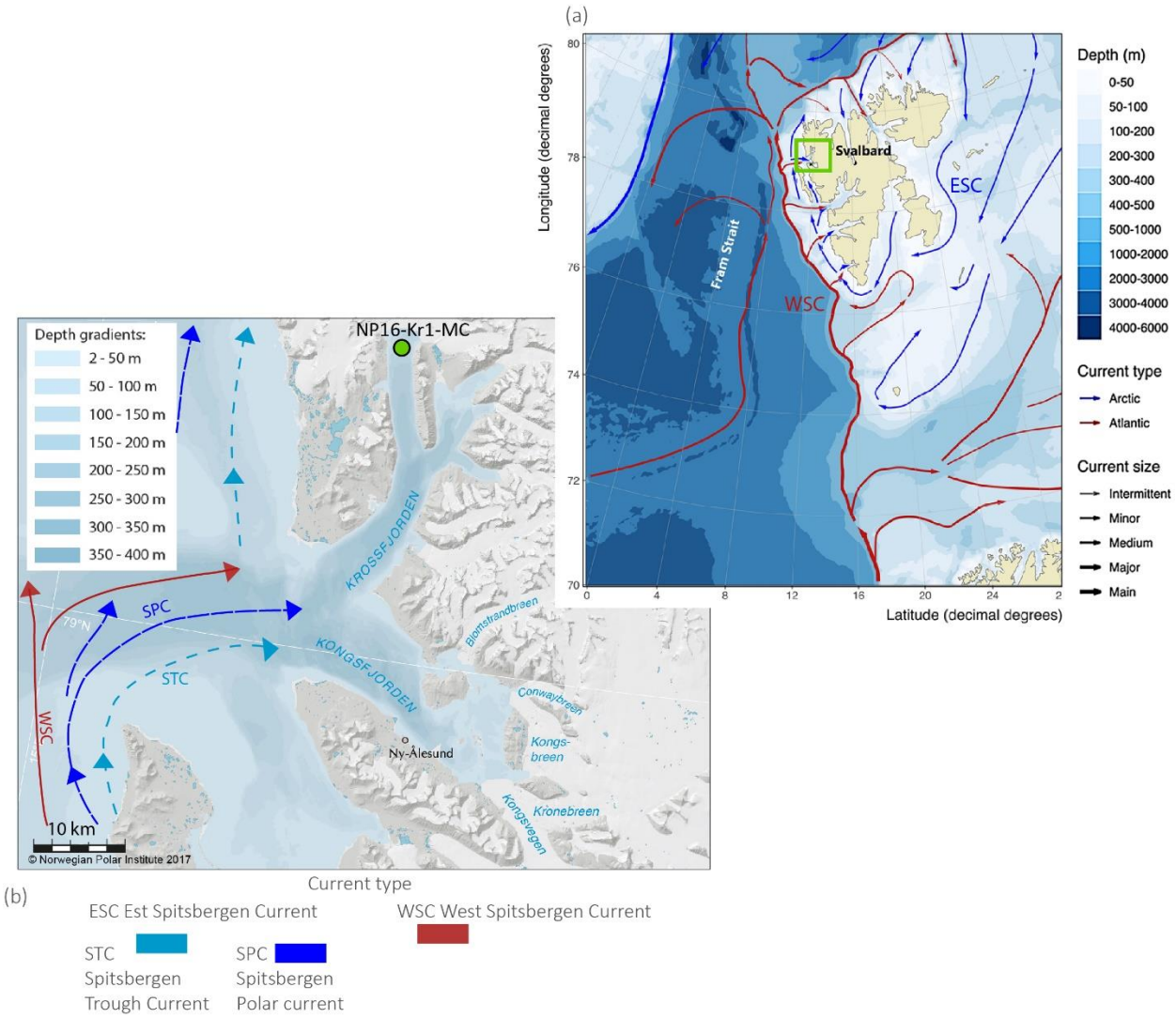


Fig. 5.1. Study area and oceanographic setting. (a). Overall map showing the location of the study area (green square) and major surface circulation features (Data base Vihtakari, 2019). (b). Kongsfjorden-Krossfjorden system showing the core location (green-dot).

The inflow of AW into the fjord influences the tidewater glaciers and accelerates the glacial melting (Luckman et al., 2015). The increase in the sediment input into the fjord is a consequence of ice-melting, these glacigenic sediments produce changes in the light penetration, temperature and salinity into the water column (Husum et al., 2019). This glacier activity also influences the mixing processes affecting the surface waters, e.g. the freshwater runoff from the glacier. The sea ice melting favouring that the surface water remains fresh, helping the stratification especially close to the glacier, where the influence of the AW decreases (Piquet et al., 2014). The seasonality shows different pattern into the fjord; during the

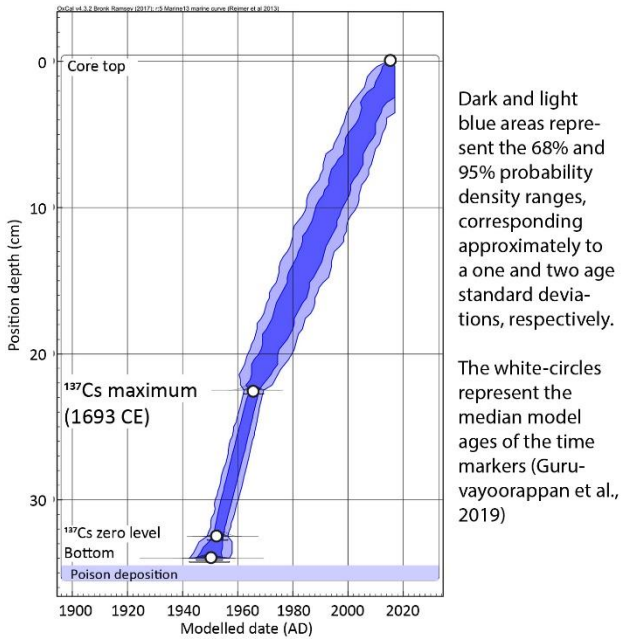
winter the young ice is mainly present, during the early spring, the fast ice becomes dominant, and during the late spring and early summer the combination of fast ice and drift ice along with icebergs, growlers and bergy bits of fresh ice are common (Svendsen et al., 2002). During the winter, the removal of the freshwater from the surface waters occurs with the freezing, and during the summer, the supply of freshwater arises with the ice melting.

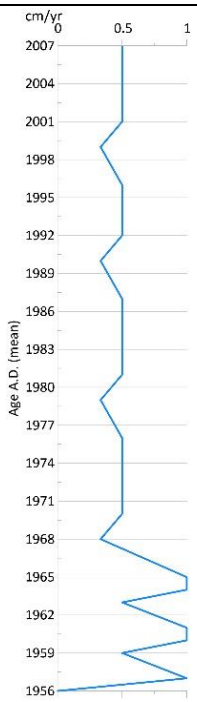
The productivity into the fjord is limited by the glacier proximity where the phytoplankton blooms occur during May (Hegseth and Tverberg, 2013; Piquet et al., 2014). All the hydrography, glacial meltwater flux and sedimentation influence the benthic ecosystem, affecting all trophic levels (Wlodarska-Kowalczuk et al., 2005).

Paleoenvironmental studies in the Arctic fjords focus on the paleoceanographic changes, using the benthic foraminiferal fauna and their ecological significance (e.g. Jennings and Helgadottir, 1994; Korsun et al., 1995; Hald and Korsun, 1997; Korsun and Hald, 1998-2000; Wlodarska-Kowalczuk et al., 2005; Majewski and Zajaczkowski, 2007; Kubischta et al., 2011; Jernas et al., 2013; Włodarska-Kowalczuk et al., 2013; Alve et al., 2016; Jernas et al., 2018), because they are excellent paleoenvironmental indicators, due to their abundance, diversity and sensitivity to the rapid environmental changes.

5.2. Age model

Guruvayoorappan et al. (2019) presented the age model based on two anthropogenic ^{137}Cs time markers from depths of 22.5 cm and 32.5 cm, and the age recorded at the top of the core (Tab. 5.1). The average accumulation rate (SAR) corresponds with 0.5 cm/year (Tab. 5.1) (Guruvayoorappan et al., 2019).

Age model. (after Guruvayoorappan et al., 2019)	Depth (cm)	SAR (cm/yr)	Estimated date A.D.
 Dark and light blue areas represent the 68% and 95% probability density ranges, corresponding approximately to a one and two age standard deviations, respectively. The white-circles represent the median model ages of the time markers (Guruvayoorappan et al., 2019)	3-4	0.50	2007
	4-5	0.50	2005
	5-6	0.50	2003
	6-7	0.50	2001
	7-8	0.50	1999
	8-9	0.33	1996
	9-10	0.50	1994
	11-12	0.50	1990
	12-13	0.50	1987
	13-14	0.33	1985
	14-15	0.50	1983
	15-16	0.50	1981
	16-17	0.50	1979
	17-18	0.50	1976
	18-19	0.33	1974
	19-20	0.50	1972
	21-22	0.50	1968
	22-23	0.50	1965
	23-24	0.50	1964
	24-25	0.33	1963
	25-26	1.00	1961
	26-27	1.00	1960
	27-28	0.50	1959
	28-29	1.00	1957
	29-30	1.00	1956



Tab. 5.1. Age model measurements (after Guruvayoorappan et al., 2019), Sediment accumulation rate (with the graphic) and date A.D.

5.3. Grain Size

The sedimentation into the fjord is characterised by fine-grained sediment from the meltwater plumes and ice rafting (Elverhøi et al., 1980-1983; Howe et al., 2003; Streuff et al., 2015; Meslard et al., 2018; Husum et al., 2019). This sediment distribution is distinguished by bi-modal or tri-modal grain size distribution (Kumar et al., 2018), including the deposits of IRD (≥500 µm) as a secondary component (Husum et al., 2019) (Fig. 5.2 a).

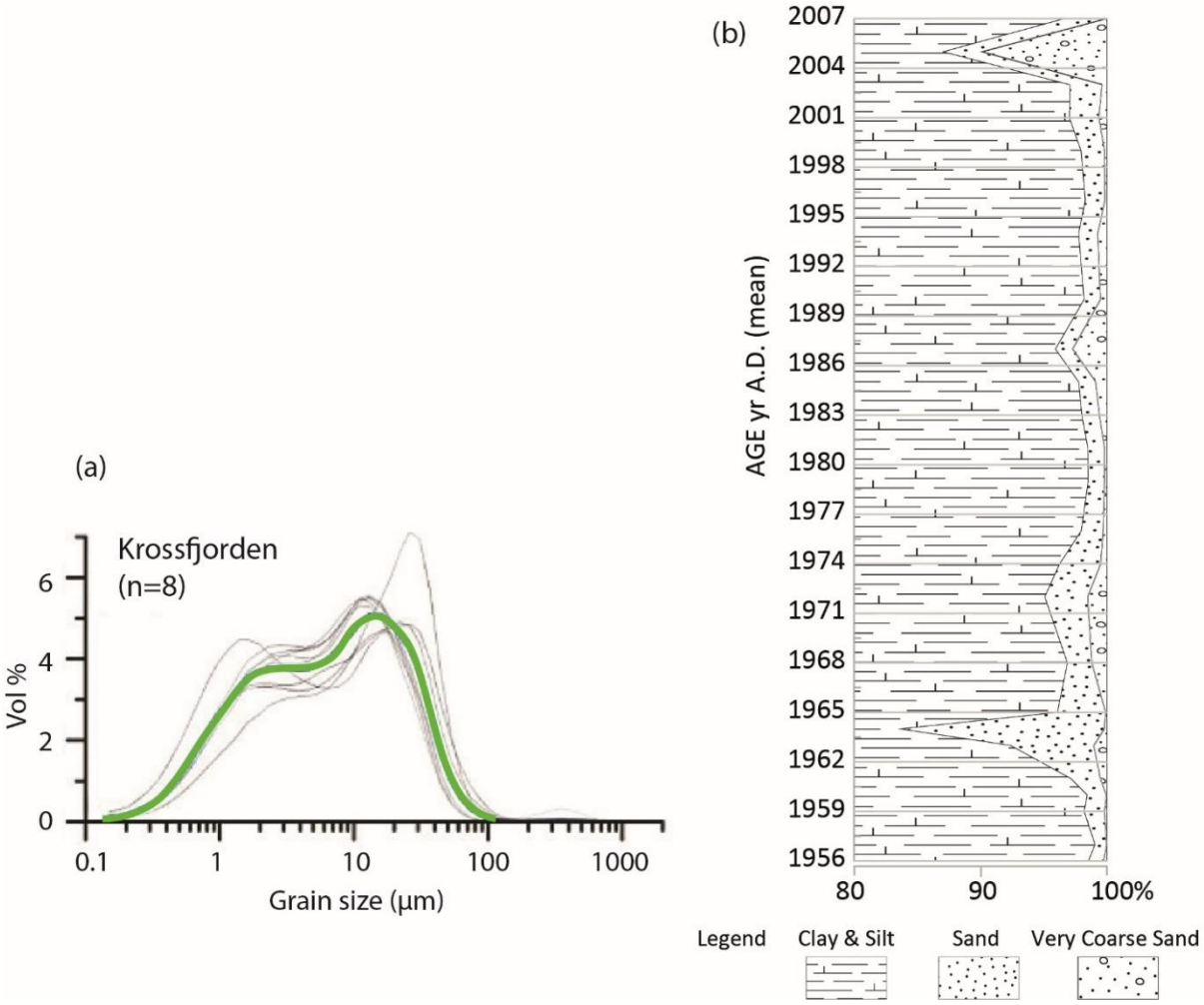


Fig. 5.2. Krossfjorden (a). Grain size distribution (grey lines) and mean grain size (green line) (after Husum et al., 2019). (b). Grain size relative percentage.

The mean grain size in Krossfjorden consists of silt-clay *ca.* 90%, sand 5% and very-coarse sand 0-2%, indicating a stable depositional environment with the input of coarse material (including IRD) from 1959 to 1963 A.D., from 1986 to 1991 A.D. and from 2003 to 2007 A.D (Fig. 5.2 b).

5.4. Diatom analysis and Sea Surface Temperature (SST) reconstruction

Guruvayoorappan et al. (2019) indicate that the diatom assemblage is dominated by ArW indicators together with the sea ice related groups, also shows the low-presence of AW indicators. The qualitative sea ice reconstruction based on diatoms indicates a low seasonal sea ice cover during the periods between 1981-1987 A.D. and 2007-2014 A.D. (Guruvayoorappan et al., 2019).

The August SST (aSST) quantitative reconstruction indicates an increasing trend of 0.6°C (Guruvayoorappan et al., 2019) (Fig. 5.3 a). The marginal ice zone (MIZ) calculated for the same time registers a general decrease, indicating the continuing reduction of the sea ice in Krossfjorden from 1950 A.D. The warming trend of the ocean surface indicated by Guruvayoorappan et al. (2019), for Krossfjorden, suggests a warming pattern agreed with the warming record in Fram Strait (Guruvayoorappan et al., 2019) (Fig. 5.3 b).

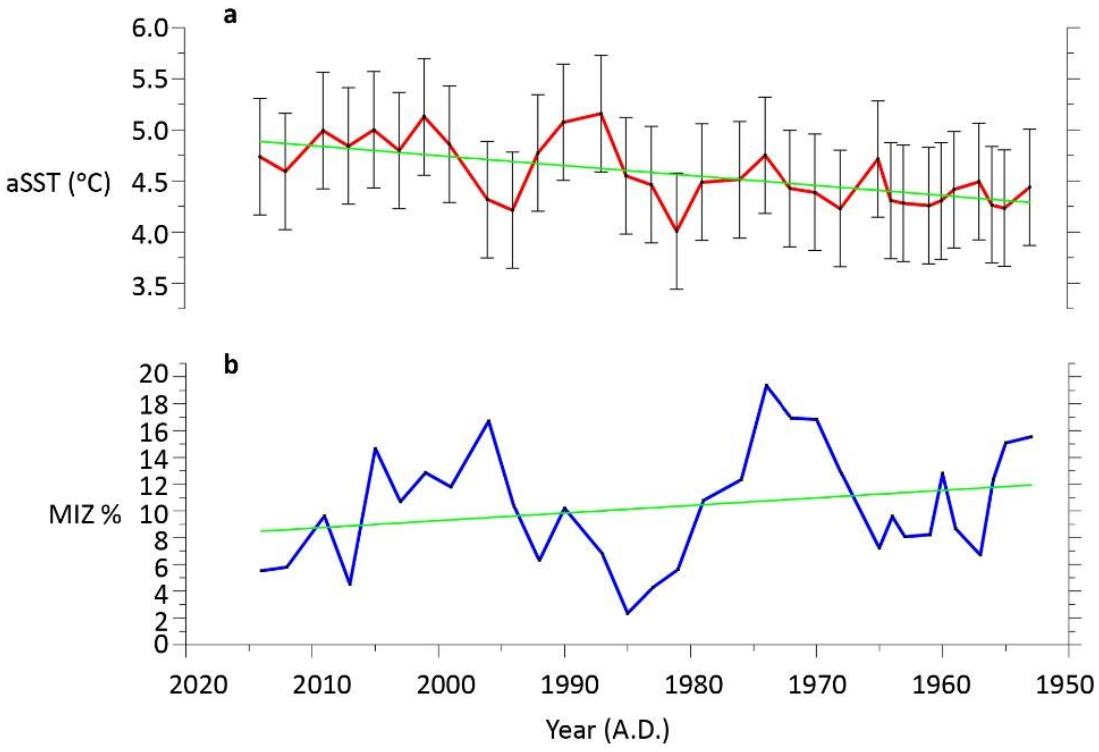
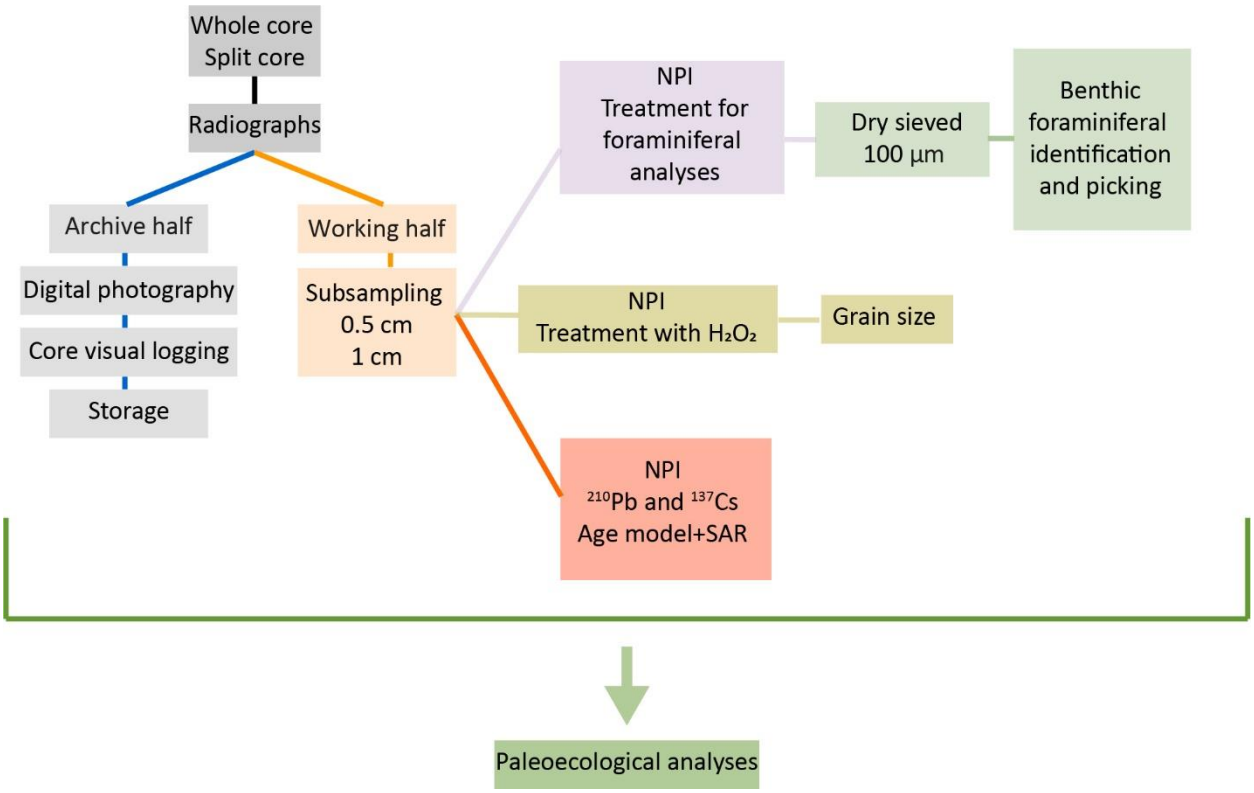


Fig. 5.3. (a). Reconstructed summer sea-surface temperatures using diatom based transfer functions (aSST), the black-bars indicate the confidence interval (b). Relative frequency (%) of diatoms characteristic of the marginal ice zone (MIZ) for the period 1953-2014 A.D. (after Guruvayoorappan et al., 2019). The green lines in (a) and (b) indicate the statistical linear fits for the data.

5.5. Material and methodology

The workflow 5.1 shows the scheme of the materials and methods followed for the analysis of the multicore NP16-Kr1 MC.



Workflow 5.1. Summary scheme of the materials and methods used for the Multi-core NP16 Kr1- MC. For more details, see chapter 2: Materials and methodology

5.6. Results. Benthic foraminiferal analysis

5.6.1. General trends

A total of 57 species are identified at a species level in the Krossfjorden multi-corer, where 13 species are recognised as main species (Tab. 5.2 and 5.3). The calcareous perforate group corresponds with 37 species, representing more than 76% in the entire record. The calcareous imperforate group is represented by 4 species, with less than 1% and the agglutinated group with 16 species, is present in 23% (Fig. 5.4).

Main Benthic foraminiferal species (>5%)				
Calcareous perforate	*Cassidulina reniforme*	*Elphidium clavatum*	*Islandiella norcrossi*	*Nonionella auricula*
	Nonionellina labradorica	*Nonionoides turgidus*	*Stainforthia concava*	*Stainforthia fusiformis*
Agglutinated	*Adercotryma glomeratum*	*Haplophragmoides fragile*	*Labrospira crassimargo*	
	Quinqueloculina agglutinans	*Spiroplectammina biformis*		

Tab. 5.2. Main benthic foraminiferal species.

Secondary Benthic foraminiferal species (<5%)				
Calcareous perforate	*Astrononion gallowayi*	*Bolivinellina pseudopunctata*	*Buccella* spp.*	*Cassidulina laevigata*
	Cassidulina neoteretis	*Cibicidoides lobatulus*	*Dentalina* spp.	*Elphidium albiumbilicatum*
	Elphidium hallandense	*Epistominella exigua*	*Globobulimina arctica*	*Globobulimina auriculata*
	Globocassidulina subglobosa	*Haynesina depressula*	*Haynesina germanica*	*Haynesina orbiculare*
	Islandiella helenae	*Islandiella norcrossi*	*Lagena* spp	*Melonis barleeanus*
	Nodosaria lagenifera	*Nonionella iridea*	*Nonionella stella*	*Procerolagena mollis*
	Pullenia bulloides	*Pullenia osloensis*	*Rosalina* spp.	*Stainforthia feylingi*
	Stainforthia loeblichi	Indeterminate		
Calcareous imperforate	*Cornuspira* spp.	*Miliolinella inflate*	*Pyrgo subglobulus*	*Triloculina tricarinata*
Agglutinated	*Cribrostomoides kosterensis*	*Haplophragmoides membranaceum*	*Lagenammina* spp.	
	Liebusella göesi	*Psammosphaera fusca*	*Quinqueloculina stalkeri*	
	Recurvoides trochamminiformis	*Reophax catenatus*	*Reophax scorpiurus*	
	Reophax subfusiformis	*Textularia earlandi*		

Tab. 5.3. Secondary benthic foraminiferal species. **Buccella* spp. also includes *Buccella frigida.*

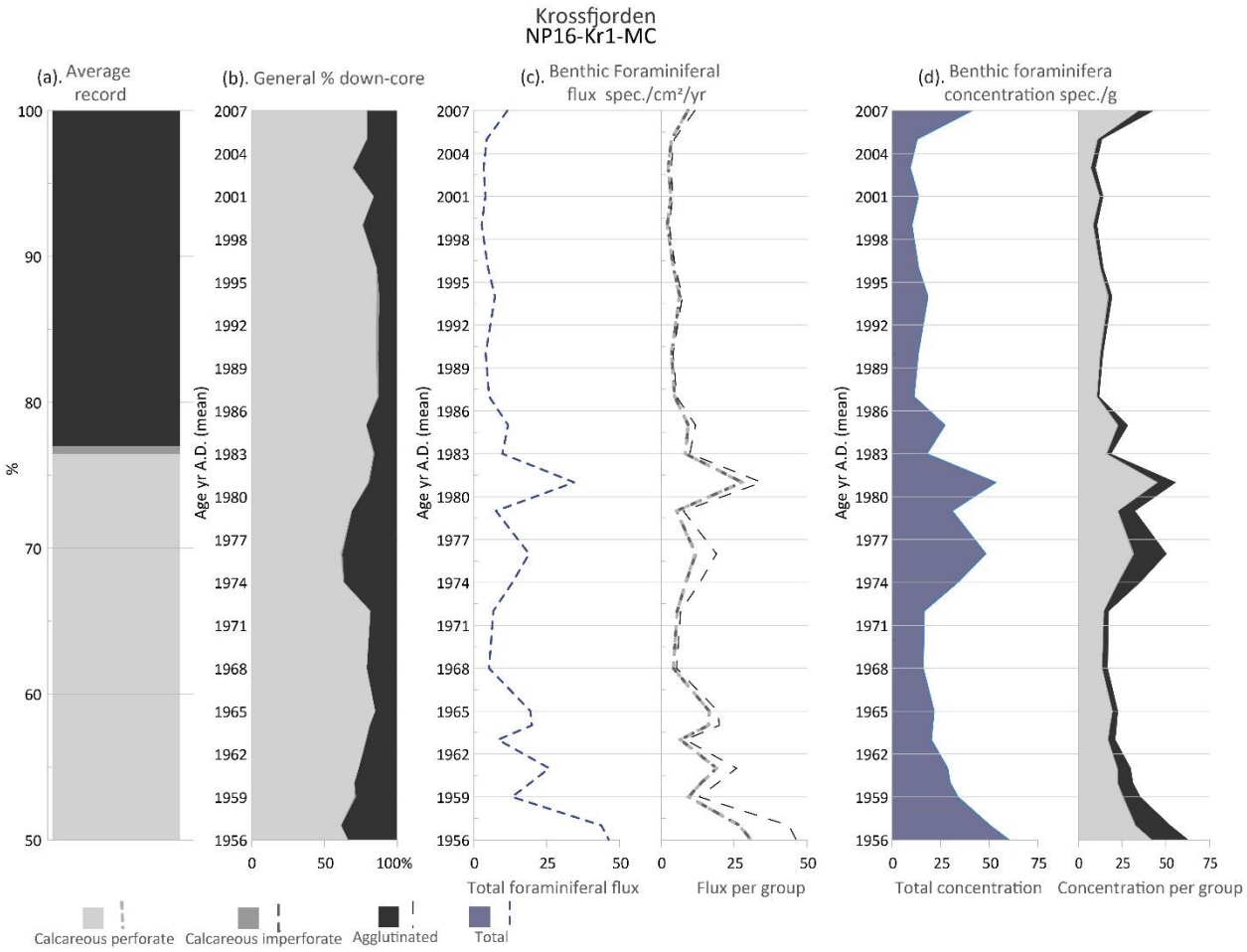


Fig. 5.4. Benthic foraminifera (a). General average percentage per group in the entire record. (b). General relative abundance per group down-core. (c). Flux of benthic foraminifera down-core. (d). Benthic foraminifera concentration (note that the concentration of the calcareous imperforate group is less than 1 spec./g). The x-axes are different.

The calcareous perforate group from 1956 to 1974 A.D. is dominant with more than 60%, reaching 85% at 1965 A.D. (Fig. 5.4). The agglutinated group is present with more than 15%; reaching 39% at 1957 A.D. Calcareous imperforate group is present with a maximum of 1%. The benthic foraminiferal flux and the concentration show a general decrease (Fig. 5.4). The calcareous perforate flux started with 31 spec./cm^2/yr at 1956 A.D., and arriving until 8 spec./cm^2/yr at 1975 A.D.; a similar trend is observed with the concentration, varying from 40 spec./g to 21 spec./g, in the same years. The agglutinated group followed a decreasing trend during this period, with the flux changing from 16 to 5 spec./cm^2/yr, and the concentration from 20 to 12 spec./gram. The calcareous imperforate group shows low values of foraminiferal flux and concentration, with less than 0.5 spec./cm^2/yr and 0.5 spec./gram (Fig. 5.4).

Between 1974 and 1987 A.D., the calcareous perforate group is dominant, while the calcareous imperforate group continues with less than 1%. An increase in the agglutinated group from 1973 to 1980 A.D. is shown, with a maximum of 38% (Fig. 5.4.). The foraminiferal flux and concentration increase between 1980 and 1982 A.D., where calcareous perforate reached 28 spec./cm2/yr and 43 spec./g; the agglutinated group reaches 7 spec./cm2/yr and 10 spec./g; and the calcareous imperforate continues with less than 0.5 spec./cm2/yr and 0.5 spec./g (Fig. 5.4).

From 1987 to 1997 A.D., the calcareous perforate relative abundance increased, arriving to 85%. The agglutinated group relative abundance ranges between 12 and 14% (Fig. 5.4). The calcareous imperforate group raises until 2% (Fig. 5.4). The values of the flux and concentration are low; the calcareous perforate group register a maximum of 6 spec./cm^2/yr and 16 spec./g, while the calcareous imperforate and agglutinated groups show values less than 1 spec./cm^2/yr and 2 spec./gram (Fig. 5.4).

From 1997 and 2007 A.D. the record of the calcareous perforate ranges between 70 and 84%. The agglutinated group increases, arriving until 30% at 2003 A.D (Fig. 5.4). The relative abundance of the calcareous imperforate group is low, with less than 1%. In 2007 A.D., the flux and concentration increase, with the maximum of the calcareous perforate of 9 spec./cm^2/yr and 32 spec./g, and for the agglutinated group of 2 spec./cm^2/yr and 9 spec./g. The calcareous imperforate group disappeared on top (Fig. 5.4).

5.6.2. Diversity indexes and cluster analysis

From 1956 to 1968 A.D., the taxa index (S) presented the lowest values between 28 and 18. During this period, Dominance (D) reaches a maximum value of 0.3, Shannon (H) shows an opposite trend with a minimum of 1.7 and a maximum of 2.6 (Fig. 5.5).

Between 1968 and 1986 A.D., the number of taxa (S) increased with 32 taxa at 1979 A.D. The dominance (D) decreases, showing the minimum values of the record ranging between 0.1 and 0.2 (Fig. 5.5). Shannon (H) index increases between 2.2 and 2.4. From 1986 to 1992 A.D., an increase of S and D are shown, arriving to 28 and 0.3, respectively. Whereas, H decreases until 1.9 from 1992 to 2007 A.D., and S increases to 33. The dominance (D) trend decreases arriving until 0.1. Shannon (H) index increases until 2.6 at 2007 A.D. (Fig. 5.5).

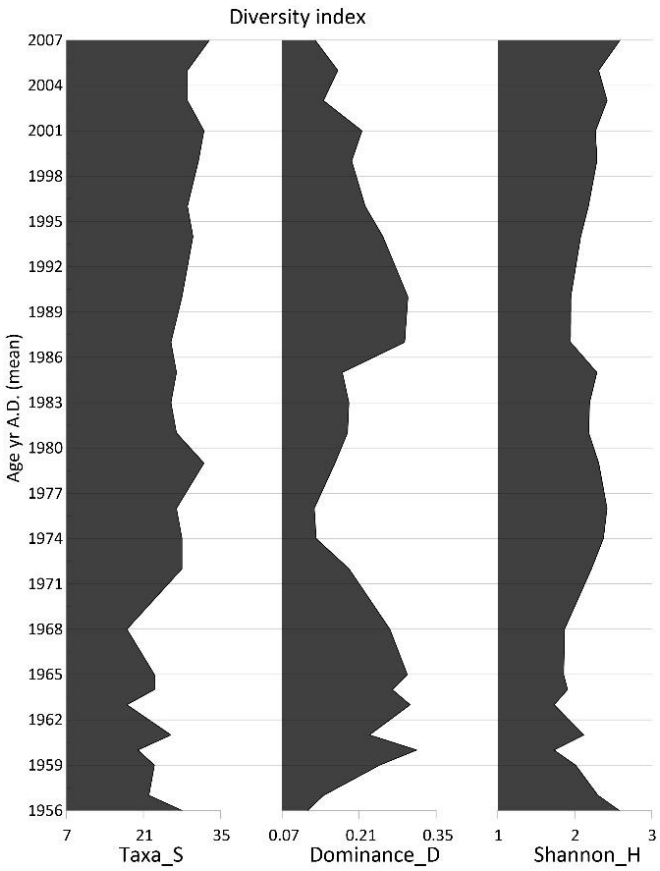


Fig. 5.5. Benthic foraminifera: diversity indexes. The x-axes are different.

The classical hierarchical Q-mode cluster analysis is performed in two steps. The first results include the outliers values corresponding at 1972 A.D. (Cluster C or secondary group V). The second cluster analysis shows two main clusters A and B, which in turn can be subdivided into two secondary groups each one, resulting in Cluster A including subgroups I and II and Cluster B including subgroups III and IV (Fig. 5.6).

Cluster A is marked by the abundance of *E. clavatum*. The subgroup I corresponds with the assemblage of the agglutinant *H. fragile*, *Q. agglutinans* and *S. biformis*. The subgroup II corresponds with the abundance of *N. labradorica* and *I. norcrossi* (Fig. 5.6 and 5.7).

Cluster B is characterised by the abundance of *C. reniforme*. The subgroup III presents *I. norcrossi* and *S. concava* contemporaneously. The group IV indicates the association of *S. fusiformis* and *L. crassimargo*. The outlier C is marked by a peak of *S. concava* (Fig. 5.6 and 5.7).

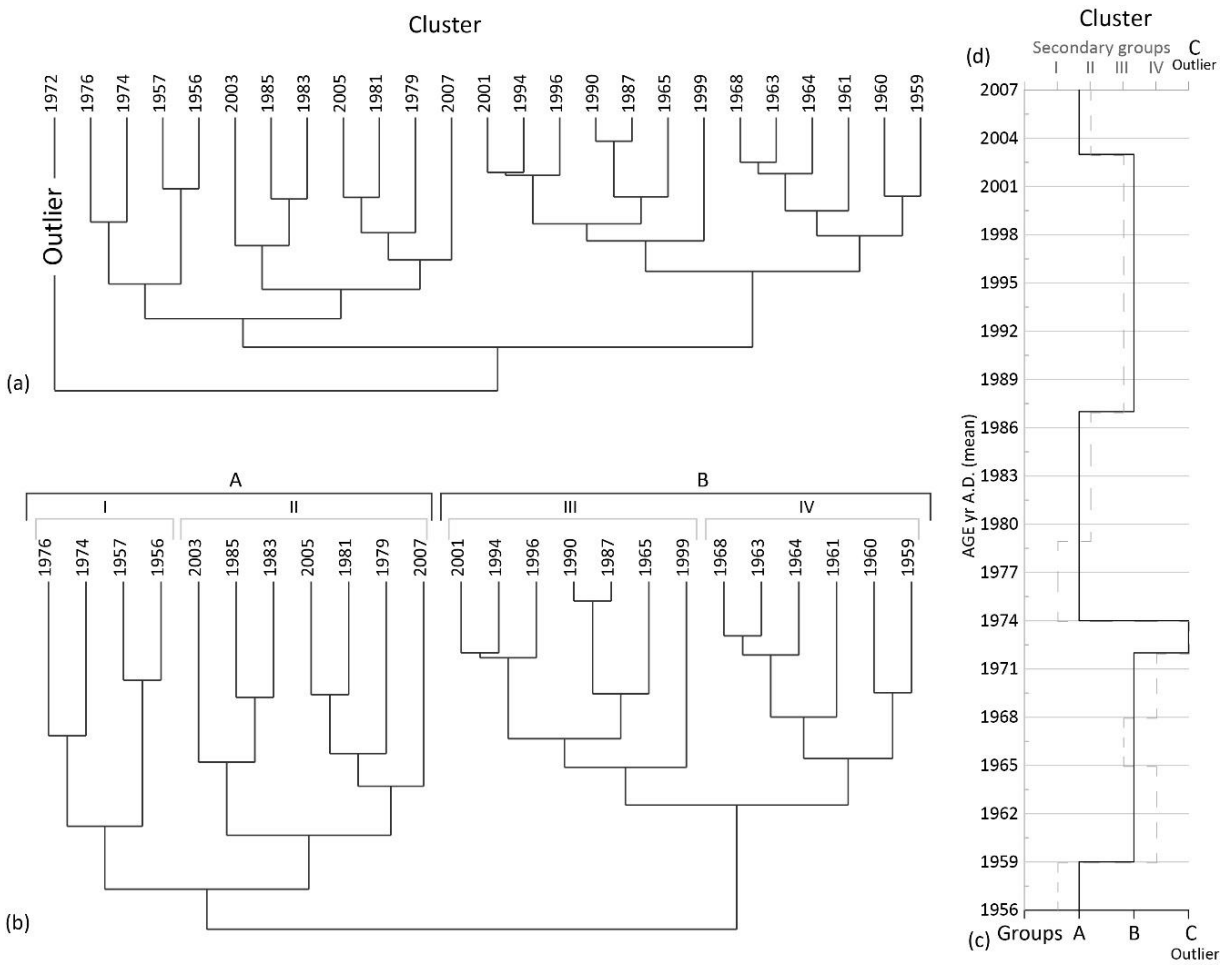


Fig. 5.6. Q-mode cluster analysis of the benthic foraminifera. (a). Dendrogram in Q-mode with outliers. (b). Dendrogram in Q-mode without outliers. (c). Cluster groups by age distribution down-core (black-line) (d). Secondary groups (grey-dashed line) correspond with the subdivision of the main groups (c).

5.6.3. Benthic foraminiferal pattern

On the base of the classical hierarchical Q-mode cluster analysis using the record of the foraminiferal assemblages, four periods are recognised: 1956-1972 A.D., 1972-1986 A.D., 1986-2003 A.D. and 2003-2007 A.D. (Fig. 5.6 and 5.7).

Period 1956-1972 A.D.

The main species present during this period is *C. reniforme,* reaching 52% at 1965 A.D. An opposite trend is shown by *E. clavatum* with low abundance during this period, with less than 10% from 1956 to 1960 A.D., it reached a maximum of 14% at 1965 A.D. (Fig. 5.7). The species *I. norcrossi* reaches the maximum of 8% at 1965 A.D*., S. concava* reaches 37% at 1972 A.D., and at 1960 A.D. *L. crassimargo* with 20%. Sporadically are present *S. fusiformis* with a maximum of 6% at 1964 A.D., *H. fragile* with 7% at 1961 A.D., *Q. agglutinans* with 9% and *S. biformis* with 8% at 1957 A.D. (Fig. 5.7).

The flux of *C. reniforme, I. norcrossi, S. concava, S. fusiformis, L. crassimargo, Q. agglutinans* and *S. biformis* is high at the beginning of this period, and it showed a decrease after 1965 A.D. (Fig. 5.7).

Period 1972-1986 A.D.

Cassidulina reniforme continues to dominate the assemblage, but decreases respect to the preceding period, while *E. clavatum* increases, arriving until 33% at 1981 A.D. (Fig. 5.7). *Islandiella norcrossi* and *S. concava* decrease until 1981 A.D., when their relative percentage becomes more stable. *Nonionoides turgidus* reaches the maximum abundance at 1983 A.D. with 6%. *Quinqueloculina agglutinans* and *S. biformis* increase, reaching their maximum between 1974 and 1979 A.D. *Labrospira crassimargo* is present mainly from 1974 and 1981 A.D., ranging between 15 and 5% (Fig. 5.7).

In general, the fluxes decrease during this period. Between 1979 and 1983 A.D., a peak of the species *C. reniforme, E. clavatum, I. norcrossi, N. labradorica, N. turgidus, S. concava, H. fragile, L. crassimargo* and *Q. agglutinans* is recorded (Fig. 5.7).

Period 1986-2003 A.D.

An increase in *C. reniforme* and decrease of *E. clavatum* ranging between 52 and 28% and 20 and 15% respectively. *Islandiella norcrossi* increased reaching 5% at 1994 A.D. *Stanforthia concava* and the agglutinated *S. biformis* registered an abundance between 1999 and 2003 A.D. (Fig. 5.7). The species *A. glomeratum* and *Q. agglutinans* increased to 9% and 4% in that order (Fig. 5.7).

The foraminiferal fluxes mostly decreases, except for the agglutinate species *A. glomeratum* (Fig. 5.7).

Period 2003-2007 A.D.

A decrease of *C. reniforme* (until 13%) and the increase of *E. clavatum* (reached 32%), are shown during this period, and *N. auricula* and *N. labradorica* reach the abundance of 5 and 11%, respectively. *Stainforthia concava* is also present with a maximum of 7% (Fig. 5.7). The agglutinated species show a reduction in the diversity, only present with more than 5% *L. crassimargo* and *S. biformis* (Fig. 5.7).

In general, the foraminiferal fluxes decrease, except for *E. clavatum, N. auricula* and *N. labradorica* (Fig. 5.7).

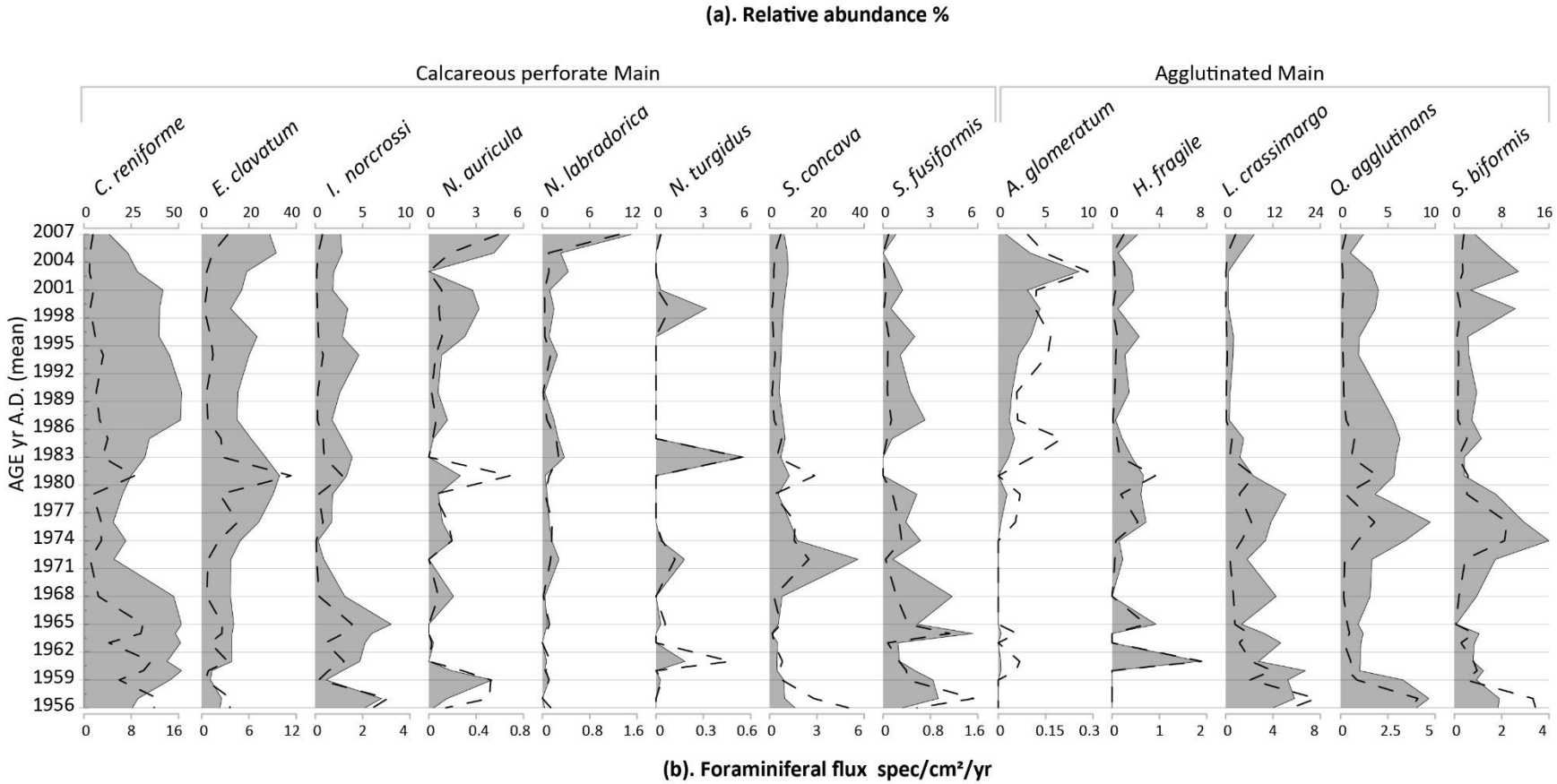


Fig. 5.7. Benthic foraminifera: (a). Relative abundance (grey) and (b). Foraminiferal flux (black dashed line) of the main species. The x-axes are different

The secondary species are present in less than 5% into the entire record. (Fig. 5.8)

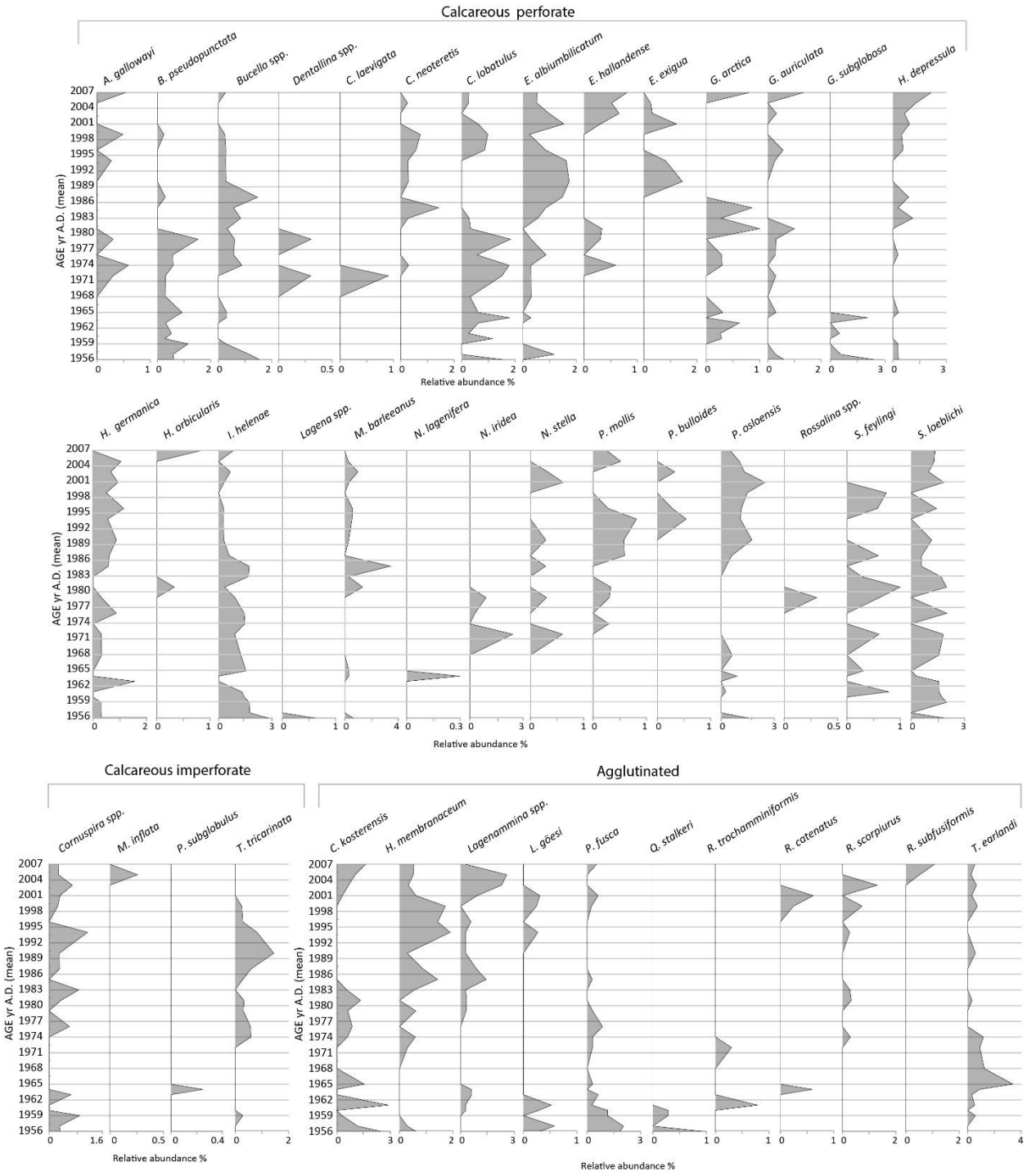


Fig. 5.8. Secondary species. The x-axes are different.

5.7. Discussion

5.7.1. Benthic foraminiferal events

Following the Q-mode cluster analysis (Fig. 5.6) four periods are recognised. During the entire record the common Arctic species *C. reniforme* and *E. clavatum* are dominant in the assemblage (e.g. Polyak and Mikhailov, 1996; Korsun and Hald, 1998) (Fig. 5.9; Tab. 5.4). Both species are associated with the cold bottom waters in the inner fjords (Hald and Korsun, 1997) and glacier proximal environments (Korsun et al., 1995) (Fig. 5.9).

a. Period from 1956 to 1972 A.D.

During this period, cold conditions are indicated by the abundance of the glaciomarine taxon *C. reniforme* (e.g. Hald and Korsun, 1997) and by the low percentages of *E. clavatum* indicate the low influence of meltwater (Tab. 5.4; Fig. 5.9.). The presence of the opportunistic *S. fusiformis* evidences oxygen-depleted conditions, unfavourable for the bloom of many taxa (Fig. 5.5 and 5.9). The agglutinated species *L. crassimargo* and *S. biformis* are abundant during this period (Fig. 5.7), both species are common in high-latitudes associated with cold Arctic waters and glaciomarine conditions (Madsen and Knudsen, 1994; Hald and Korsun, 1997; Korsun and Hald; 1998; Korsun and Hald, 2000; Lloyd, 2006). In addition, *S. biformis* is related to the glaciomarine environment in Svalbard glacial-fed fjords (Korsun and Hald, 2000).

The input of nutrients is fluctuating, probably in relation to the seasonal food supply (Tab. 5.4), showing peaks of *I. norcrossi* at 1965 A.D., and two maxima of *S. concava* between 1956 and 1959 A.D. and at the end of this period, from 1967 to 1972 A.D.

b. Period from 1972 to 1986 A.D.

A shift between the main species *C. reniforme* and the increases in the abundance of *E. clavatum* suggests an increment of the influence of meltwater input into the fjord (Fig. 5.9), reaching the maximum between 1976 and 1981 A.D. (Tab. 5.4). This release of freshwater is also recognise by the increase of *S. biformis* that is related to low salinity (Lloyd, 2006).

The meltwater input enhances the food supply to the sea bottom during this period, providing an important food source for foraminifera, allowing the increase of some species as *S. concava* and

N. turgidus (Tab. 5.4; Fig. 5.9). This increase in the food supply, could be also related to warmer seasonal conditions, suggested by the diminution of the MIZ % of diatom species and the warming aSST during the 80s (Guruvayoorappan et al., 2019). These conditions favouring the diversity and low dominance into the assemblage, indicating favourable conditions at the sea bottom for the benthic microfauna (Fig. 5.5).

c. Period from 1986 to 2003 A.D.

The increase in the abundance of *C. reniforme* indicates a new increased of the occurrence of the seasonal of the ice covering in the area (Fig. 5.9). However, presence of *E. clavatum* indicates the input of meltwater during this period (Fig. 5.9), supported by the presence of *S. biformis* (Fig. 5.7). The difference in relative abundance between *C. reniforme* and *E. clavatum* is smaller than in the previous years when *C. reniforme* dominated the assemblage, which could indicate the longer open-water period.

The lack of a durable sea ice results in the increase of food supply, indicate by the presence of *I. norcrossi*, *S. concava* and phytodetritus species *N. auricula* and *N. turgidus* (Fig. 5.9).

d. Period from 2003 to 2007 A.D.

The increase of the meltwater input is indicated by the abundance of *E. clavatum* and by the decrease of the *C. reniforme*. The difference between these two species reached their maximum at 2007 A.D. when *E. clavatum* surpassed *C. reniforme* in 15% (Fig. 5.7 and 5.9).

The open-water conditions improve the possibility of the bloom of phytodetritus, hence the food supply, indicated by the increase of *N. auricula* and *N. labradorica* (Fig. 5.9).

	Main species	Environmental conditions	References
Main benthic species	*Cassidulina reniforme*	Arctic-Polar species. Cold and salty water. Locally related to glaciomarine environments. Associated to *E. clavatum*. Epifaunal-Shallow infaunal.	Sejrup et al. (1981); Mackensen et al. (1985); Steinsund et al.(1994); Hald and Korsun (1997); Korsun and Hald (1998); Korsun and Hald (2000); Polyak et al. (2002); Forwick et al. (2010).
	Elphidium clavatum	Arctic-Polar species prefers cold bottom waters (glacier front and ice margin). Highly adaptable, resists low salinity, low temperatures and high turbidity.	Hald and Korsun (1997); Korsun and Hald (1998); Korsun and Hald (2000); Polyak et al. (2002); Sejrup et al., 2004
	Islandiella norcrossi	Detritivore, high food supply. Seasonal sea ice cover and productivity. Sea ice edge productivity. High and stable bottom salinities. Mud-silt sediments, infaunal, free	Steinsund et al. (1994); Korsun et al. (1995); Polyak and Mikhailov (1996); Korsun and Hald (1998); Murray, (2006); Saher et al. (2009); Saher et al. (2012); Dijkstra et al. (2017).
	Nonionellina labradorica	Cold water, seasonal sea ice cover, high food supply	Korsun et al. (1995); Korsun and Hald (1998); Sejrup et al. (2004); Murray (2006); Saher et al. (2009); Saher et al. (2012)
	Nonionella auricula *Nonionoides turgidus*	Phytodetritus species, infaunal	Murray (2006).
	Stainforthia concava	High seasonal productivity. Organic-rich sediments	Polyak et al. (2002)
	Stainforthia fusiformis	High seasonal productivity. Opportunistic. Organic-rich sediments and oxygen depleted muddy sediments	Murray (1992); Alve (1994);Gooday and Alve (2001); Polyak et al. (2002)

Tab. 5.4. Main ecology indicators.

5.7.2. Comparison with another proxy records

Investigations of the surface water conditions based on diatoms from the same sediment core show an increasing summer surface temperature (aSST) from 1956 to 2007 A.D., together with an increasing frequency of diatom species related to the marginal ice zone (MIZ) indicating a change from sea ice flora to marginal ice zone flora (Fig. 5.3 and 5.9) (Guruvayoorappan et al., 2019). The dominance of the Arctic diatoms, and the low presence of the Atlantic diatoms, suggests that the warming surface water masses and decreasing sea ice extent are not caused by the increasing influence of the AW (Guruvayoorappan et al., 2019).

The benthic foraminiferal record from 1956 until 1972 A.D., indicates the dominance of Arctic glaciomarine species, which main variations into the assemblage are related to the change in the input of meltwater. This evidence agrees with the decrease of the percentage of diatom MIZ species and the increase in aSST related to general warming indicated by Guruvayoorappan et al. (2019). From 1972 to 1986 A.D., a decrease in the percentage of MIZ diatom species and the increase of the aSST, suggesting warmer sub-surface water conditions, which favour the food supply, show by the foraminiferal fauna with the shift between glaciomarine species (*C. reniforme*) to cold open-water conditions (*E. clavatum*), suggesting these warmer conditions are not mainly related to the AW influence. Between 1986 and 2003 A.D., Guruvayoorappan et al. (2019), indicate an increase of the percentage of the MIZ diatom species (colder surface water conditions), which also affect the benthic fauna, shown a new shift between open water species, *E. clavatum*, to glaciomarine related species, *C. reniforme*. Despite this increased of the percentage of the MIZ diatom species, the general trend is towards the decrease, with the ice-cover less strong or less durable, which results in a continuous inflow of meltwater arriving until the sea bottom, supporting the presence of the *E. clavatum*. During the last period, between 2003 and 2007 A.D., the percentage of MIZ diatoms species document a new diminution, traceable in the benthos with a further increase of *E. clavatum* and a decrease of *C. reniforme*.

The low presence of benthic foraminiferal species related to warm AW is also according to the no rise of AW diatoms shown by Guruvayoorappan et al. (2019). This study agrees and reinforces the indicated by Guruvayoorappan et al. (2019), explaining that an increase in temperature is not related to the influx of AW into the fjord, or at least it is not the main factor of increasing temperature in the area. Guruvayoorappan et al. (2019) further suggested the increase in CO_2, together with the ocean-atmosphere interaction, as the cause of the increase in aSST and the low presence of sea ice.

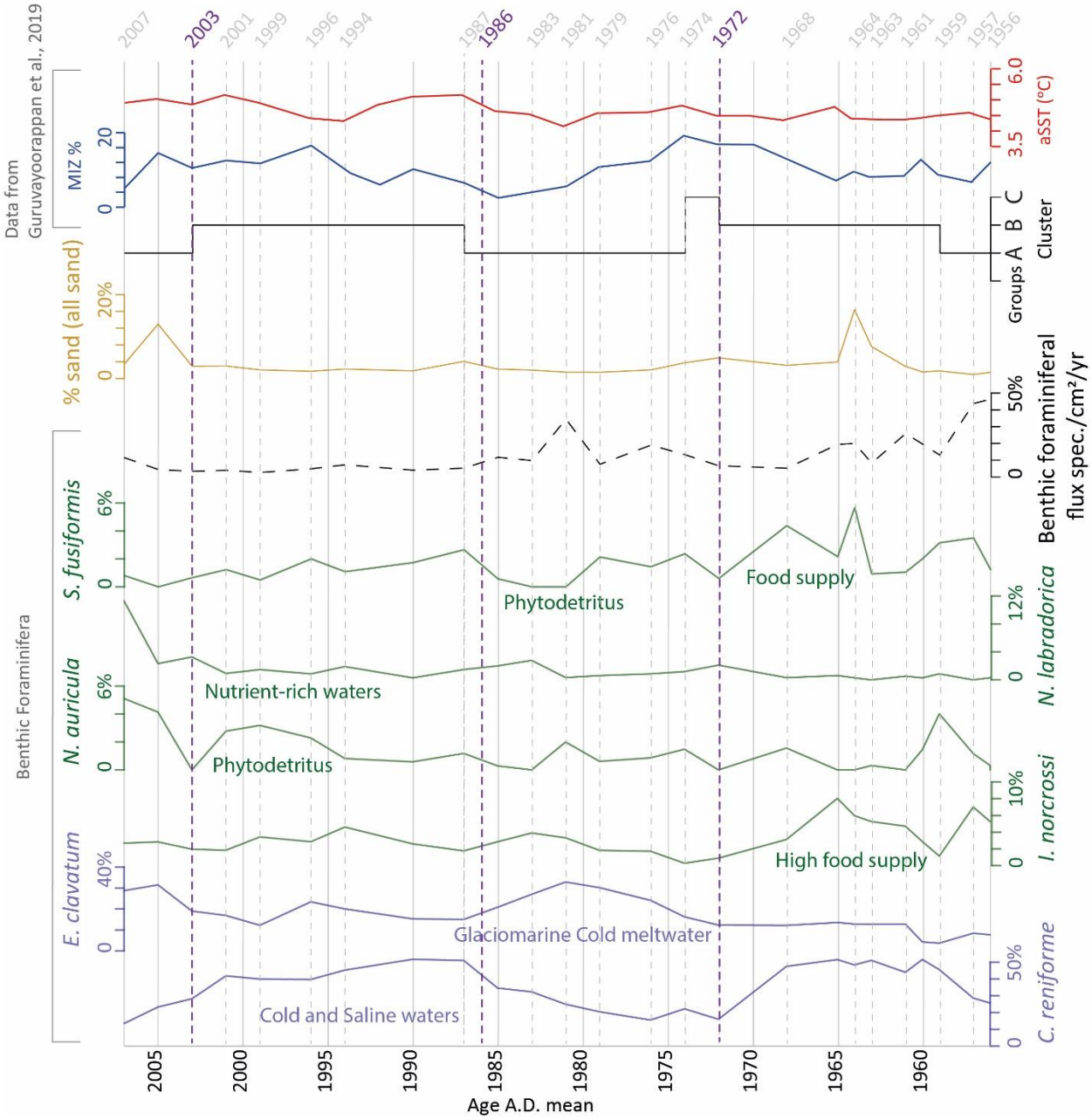


Fig. 5.9. Key proxy correlation. Includes the MIZ (marginal ice zone) in red and aSST (august sea surface temperature) in blue, defined by Guruvayoorappan et al. (2019). Q-mode cluster division of benthic foraminifera. Benthic foraminiferal flux (dashed graphic). Relative abundance of the main benthic foraminiferal species divided by colours: dark-blue the cold-water related species, green productivity indicators. The gold graphic represents the sand content. The x-axes are different. The vertical divisions purple dashed lines indicate the periods established with the Q-mode clustering analyses, grey line the age each 10 years, and the grey-dashed line the years according to the age model.

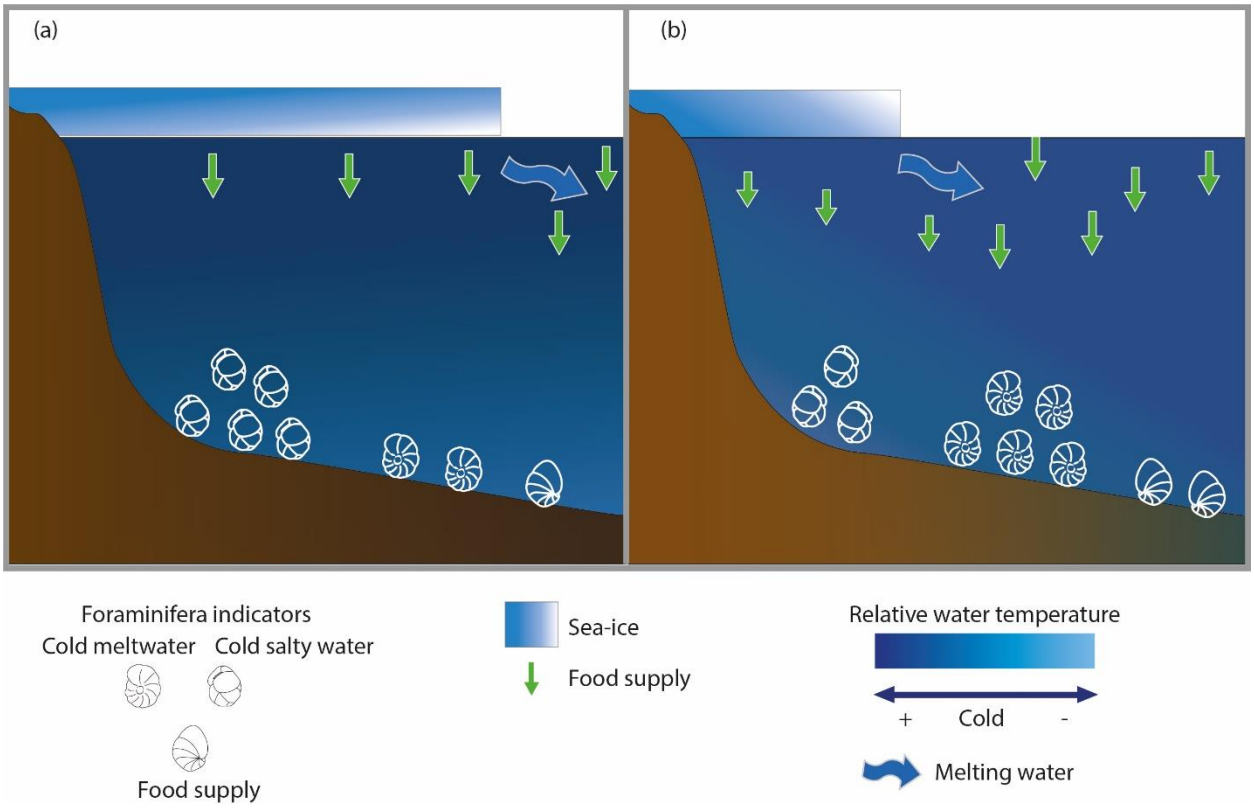


Fig. 5.10. Palaeoenvironmental reconstruction of the record from Krossfjorden from 1956 to 2007 A.D. indicating the two main environmental scenarios. (a) Decrease of meltwater input, corresponding with the periods: a. from 1956 to 1972 A.D. and c. from 1986 to 2003 A.D. (b) Increased of the meltwater input, corresponds with the periods: b. from 1972 to 1986 A.D. and d. from 2003 to 2007 A.D.

5.8. Conclusions

The main benthic foraminiferal species from 1956 to 2007 A.D. recorded in Krossfjorden are the typical Arctic species *C. reniforme* and *E. clavatum*. These two species are related to glacier activity and cold waters. *Elphidium clavatum* is a pioneer species, which appears with the beginning of the ice retreat and is related to the cold meltwater influx. *Cassidulina reniforme* appears when the ice-covered area increases and the bottom water conditions become cold and saltier. The shifting between the dominance of these two species indicates that the Krossfjorden area is characterised by the ice-cover seasons, and periods of open water conditions with the increase influx of the meltwater, influencing the salinity and the food supply settings.

Four main periods are recognised with the Q-mode cluster analysis of the benthic foraminiferal species in Krossfjorden. The first period, from 1956 to 1972 A.D, is characterised by the dominance of *C. reniforme*, which indicates a low influence of meltwater. During the second period from 1972 to 1986 A.D., *E. clavatum* became a dominant species, indicating more influx of the meltwater and open water conditions. From 1986 to 2003 A.D., the dominant species is *C. reniforme* that indicate the strong presence of ice-cover in the fjord; however, the constant increase of *E. clavatum* indicates the constant meltwater input and the retreat of the ice. The last period, from 2003 to 2007 A.D., show an increment of *E. clavatum* become the dominant species, together with the decrease of the *C. reniforme* indicating the increase of the meltwater.

Our data agree with the data presented by Guruvayoorappan et al. (2019), performed on the same sediment record using diatoms assemblage to establish the superficial water conditions, which indicates a general warming trend. The increase of the meltwater input is associated with the retreat of the ice-covered area. The increase of food supply indicate ameliorate conditions, but the Arctic origin of the primary production shown by the diatoms assemblage and the dominance of the benthic foraminifera glaciomarine species indicate that this warming increase is not related with the AW influx into the fjord.

5.9. References

Alve, E. 1994. Opportunistic features of the foraminifer *Stainforthia fusiformis* (Williamson): evidence from Frierfjord, Norway. Journal of Micropalaeontology, 13(1), 24-24.

Alve, E., Korsun, S., Schönfeld, J., Dijkstra, N., Golikova, E., Hess, S., Husum, K., Panieri, G. 2016. Foram-AMBI: A sensitivity index based on benthic foraminiferal faunas from North-East Atlantic and Arctic fjords, continental shelves and slopes. Marine Micropaleontology, 122, 1-12.

Cottier, F. R., Nilsen, F., Inall, M. E., Gerland, S., Tverberg, V., Svendsen, H. 2007. Wintertime warming of an Arctic shelf in response to large-scale atmospheric circulation. Geophysical Research Letters, 34(10).

Dijkstra, N., Junttila, J., Aagaard-Sørensen, S. 2017. Environmental baselines and reconstruction of Atlantic Water inflow in Bjørnøyrenna, SW Barents Sea, since 1800 CE. Marine environmental research, 132, 117-131.

Dowdeswell, J.A., Ottesen, D., Forwick, M. 2016. Grounding-zone wedges on the western Svalbard shelf. Geological Society, London, Memoirs, 46(1), 233-234.

Ebbesen, H., Hald, M., Eplet, T. H. 2007. Lateglacial and early Holocene climatic oscillations on the western Svalbard margin, European Arctic. Quaternary Science Reviews, 26(15-16), 1999-2011.

Elverhøi, A., Liestøl, O. Nagy, J. 1980. Glacial erosion, sedimentation and microfauna in the inner part of Kongsfjorden, Spitsbergen. Norsk Polarinstitutt Skrifter, 172, 33-58.

Elverhøi, A., Lønne, Ø. Seland, R. 1983. Glaciomarine sedimentation in a modern fjord environment, Spitsbergen. Polar Research, 1(2), 127-150.

Forwick, M., Vorren, T. O., Hald, M., Korsun, S., Roh, Y., Vogt, C., Yoo, K. C. 2010. Spatial and temporal influence of glaciers and rivers on the sedimentary environment in Sassenfjorden and Tempelfjorden, Spitsbergen. Geological Society, London, Special Publications, 344(1), 163-193.

Gooday, A. J., Alve, E. 2001. Morphological and ecological parallels between sublittoral and abyssal foraminiferal species in the NE Atlantic: a comparison of *Stainforthia fusiformis* and *Stainforthia* sp. Progress in Oceanography, 50(1-4), 261-283.

Guruvayoorappan, H., Miettinen, A., Divine, D. V., Moros, M., Orme, L. C., Mohan, R. 2019. Ocean surface warming in Krossfjorden, Svalbard, during the last 60 years. Arktos, 1-13.

Hald, M., Korsun, S. 1997. Distribution of modern benthic foraminifera from fjords of Svalbard, European Arctic. The Journal of Foraminiferal Research, 27(2), 101-122.

Hegseth, E.N., Tverberg, V. 2013. Effect of Atlantic water inflow on timing of the phytoplankton spring bloom in a high Arctic fjord (Kongsfjorden, Svalbard). Journal of Marine Systems, 113, 94-105.

Howe, J. A., Moreton, S. G., Morri, C., Morris, P. 2003. Multibeam bathymetry and the depositional environments of Kongsfjorden and Krossfjorden, western Spitsbergen, Svalbard. Polar Research, 22(2), 301-316.

Husum, K., Howe, J. A., Baltzer, A., Forwick, M., Jensen, M., Jernas, P., Korsun, S., Miettinen, A., Mohan, R., Morigi, C. Myhre, P. I. Prins M, Skirbekk K, Sternal B, Boos M, Dijkstra N, Troelstra S. 2019. The marine sedimentary environments of Kongsfjorden, Svalbard: an archive of polar environmental change. Polar Res. https ://doi.org/10.33265 /polar .v38.3380

Jennings, A. E., Helgadottir, G. 1994. Foraminiferal assemblages from the fjords and shelf of eastern Greenland. The Journal of Foraminiferal Research, 24(2), 123-144.

Jernas, P., Klitgaard Kristensen, D., Husum, K., Wilson, L., Koç, N. 2013. Palaeoenvironmental changes of the last two millennia on the western and northern Svalbard shelf. Boreas, 42(1), 236-255.

Jernas, P., Klitgaard-Kristensen, D., Husum, K., Koç, N., Tverberg, V., Loubere, P., Prins, M., Dijkstra, N. Gluchowska, M. 2018. Annual changes in Arctic fjord environment and modern benthic foraminiferal fauna: Evidence from Kongsfjorden, Svalbard. Global and Planetary change, 163, 119-140.

Korsun, S. A., Pogodina, I. A., Forman, S. L., Lubinski, D. J. 1995. Recent foraminifera in glaciomarine sediments from three arctic fjords of Novaja Zemlja and Svalbard. Polar Research, 14(1), 15-32.

Korsun, S., Hald, M. 1998. Modern benthic foraminifera off Novaya Zemlya tidewater glaciers, Russian Arctic. Arctic and Alpine Research, 30(1), 61-77.

Korsun, S., Hald, M. 2000. Seasonal dynamics of benthic foraminifera in a glacially fed fjord of Svalbard, European Arctic. The Journal of Foraminiferal Research, 30(4), 251-271.

Kubischta, F., Knudsen, K.L., Ojala, A.E., Salonen, V.P. 2011. Holocene benthic foraminiferal record from a high-Arctic fjord, Nordaustlandet, Svalbard. Geografiska Annaler: Series A, Physical Geography, 93(4), 227-242.

Kumar, P., Pattanaik, J. K., Khare, N., Balakrishnan, S. 2018. Geochemistry and provenance study of sediments from Krossfjorden and Kongsfjorden, Svalbard (Arctic Ocean). Polar Science, 18, 72-82.

Lloyd, J. M. 2006. Modern distribution of benthic foraminifera from Disko Bugt, West Greenland. The Journal of Foraminiferal Research, 36(4), 315-331.

Luckman, A., Benn, D. I., Cottier, F., Bevan, S., Nilsen, F., Inall, M. 2015. Calving rates at tidewater glaciers vary strongly with ocean temperature. Nature Communications, 6(1), 1-7.

Mackensen, A., Sejrup, H. P., Jansen, E. 1985. The distribution of living benthic foraminifera on the continental slope and rise off southwest Norway. Marine Micropaleontology, 9(4), 275-306.

Maclachlan, S. E., Howe, J. A., Vardy, M. E. 2010. Morphodynamic evolution of Kongsfjorden-Krossfjorden, Svalbard, during the late Weichselian and Holocene. Geological Society, London, Special Publications, 344(1), 195-205.

Madsen, H. B., Knudsen, K. L. 1994. Recent foraminifera in shelf sediments of the Scoresby Sund fjord, East Greenland. Boreas, 23(4), 495-504.

Majewski, W., Zajaczkowski, M. 2007. Benthic foraminifera in Adventfjorden, Svalbard: Last 50 years of local hydrographic changes. The Journal of Foraminiferal Research, 37(2), 107-124.

Meslard, F., Bourrin, F., Many, G., Kerhervé, P. 2018. Suspended particle dynamics and fluxes in an Arctic fjord (Kongsfjorden, Svalbard). Estuarine, Coastal and Shelf Science, 204, 212-224.

Murray, J.W. 1992. Distribution and population dynamics of benthic foraminifera from the southern North Sea. The Journal of Foraminiferal Research, 22(2), 114-128.

Murray, J. W. 2006. Ecology and applications of benthic foraminifera. Cambridge University Press.

Nilsen, F., Skogseth, R., Vaardal-Lunde, J., Inall, M. 2016. A simple shelf circulation model: intrusion of Atlantic Water on the West Spitsbergen Shelf. Journal of Physical Oceanography, 46(4), 1209-1230.

Ottesen, D.A.G., Dowdeswell, J.A., Landvik, J.Y., Mienert, J. 2007. Dynamics of the Late Weichselian ice sheet on Svalbard inferred from high-resolution sea-floor morphology. Boreas, 36(3), 286-306.

Piquet, A. T., Van de Poll, W. H., Visser, R. J. W., Wiencke, C., Bolhuis, H., Buma, A. G. J. 2014. Springtime phytoplankton dynamics in Arctic Krossfjorden and Kongsfjorden (Spitsbergen) as a function of glacier proximity. Biogeosciences, 11(8), 2263-2279.

Polyak, L. Solheim, A. 1994. Late-and postglacial environments in the northern Barents Sea west of Franz Josef Land. Polar Research, 13(2), 197-207.

Polyak, L., Mikhailov, V. 1996. Post-glacial environments of the southeastern Barents Sea: foraminiferal evidence. Geological Society, London, Special Publications, 111(1), 323-337.

Polyak, L., Korsun, S., Febo, L. A., Stanovoy, V., Khusid, T., Hald, M., Paulsen, B.E. Lubinski, D. J. 2002. Benthic foraminiferal assemblages from the southern Kara Sea, a river-influenced Arctic marine environment. The Journal of Foraminiferal Research, 32(3), 252-273.

Saher, M. H., Kristensen, D. K., Hald, M., Korsun, S., Jørgensen, L. L. 2009. Benthic foraminifera assemblages in the Central Barents Sea: an evaluation of combining live and total fauna studies in tracking environmental change. Norwegian Journal of Geology/Norsk Geologisk Forening, 89, 149-161

Saher, M., Kristensen, D. K., Hald, M., Pavlova, O., Jørgensen, L. L. 2012. Changes in distribution of calcareous benthic foraminifera in the central Barents Sea between the periods 1965–1992 and 2005–2006. Global and Planetary Change, 98, 81-96.

Sejrup, H.P., Fjaeran, T., Hald, M., Beck, L., Hagen, J., Miljeteig, I., Morvik, I., Norvik, O. 1981. Benthonic foraminifera in surface samples from the Norwegian continental margin between 62 degrees N and 65 degrees N. The Journal of Foraminiferal Research, 11(4), 277-295.

Sejrup, H. P., Birks, H. J. B., Kristensen, D. K., Madsen, H. 2004. Benthonic foraminiferal distributions and quantitative transfer functions for the northwest European continental margin. Marine Micropaleontology, 53(1-2), 197-226.

Steinsund, P. I., Polyak, L., Hald, M., Mikhailov, V., Korsun, S. 1994. Distribution of calcareous benthic foraminifera in recent sediments of the Barents and Kara Sea. Benthic Foraminifera in Surface Sediments of the Barents and Kara Seas: Modern and Late Quaternary Application. Ph. D. Thesis, Department of Geology, Institute of Biology and Geology, University of Tromsø, Norway.

Streuff, K., Forwick, M., Szczuciński, W., Andreassen, K. Cofaigh, C.Ó. 2015. Submarine landform assemblages and sedimentary processes related to glacier surging in Kongsfjorden, Svalbard. Arktos, 1(1), 1-19.

Sundfjord, A., Albretsen, J., Kasajima, Y., Skogseth, R., Kohler, J., Nuth, C., Skarðhamar, J., Cottier, F., Nilsen, F., Asplin, L. Gerland, S. 2017. Effects of glacier runoff and wind on surface layer dynamics and Atlantic Water exchange in Kongsfjorden, Svalbard; a model study. Estuarine, Coastal and Shelf Science, 187, 260-272.

Svendsen, H., Beszczynska-Møller, A., Hagen, J. O., Lefauconnier, B., Tverberg, V., Gerland, S., Børre Ørbæk, J., Bischof, K., Papucci, C., Zajaczkowski, M. Azzolini, R. 2002. The physical environment of Kongsfjorden–Krossfjorden, an Arctic fjord system in Svalbard. Polar Research, 21(1), 133-166.

Vihtakari M. 2019 PlotSvalbard: PlotSvalbard—plot research data from Svalbard on maps. R package version 0.8.5. https ://githu b.com/Mikko Vihta kari/PlotS valba rd

Włodarska-Kowalczuk, M., Pawłowska, J., Zajączkowski, M. 2013. Do foraminifera mirror diversity and distribution patterns of macrobenthic fauna in an Arctic glacial fjord?. Marine Micropaleontology, 103, 30-39.

Wlodarska-Kowalczuk, M., Pearson, T.H., Kendall, M.A. 2005. Benthic response to chronic natural physical disturbance by glacial sedimentation in an Arctic fjord. Marine Ecology Progress Series, 303, 31-41.

6. The last *ca.* 350 years in the Kveithola Trough

I. Palaeoenvironmental reconstructions of the Little Ice Age and Modern Period in Kveithola Trough

6.1. Oceanographic settings

The Kveithola Trough located in the NW Barents Sea, is an abrupt bathymetric feature about 100 km long and 13 km wide, with a water depth ranging from 100–400 m (Fohrmann et al., 1998; Rüther et al., 2012) (Fig.6.1). The longitudinal profile of the trough is markedly staircase-like, composed of five transverse ridges located about 15 km apart from each other, and interpreted as Grounding Zone Wedges (*sensu* Dowdeswell and Fugelli, 2012) that testify the episodic mode of the retreat of former ice stream(s) after Last Glacial Maximum (Rebesco et al., 2011; Bjarnadóttir et al., 2013). Others seafloor prominent morphological features are mega-scale glacial lineations generated by grounded ice sheet advance (Rebesco et al., 2011), and two mounded depocentres with an associated moat developing along the northern margin of the glacial trough that are interpreted as a sediment drift complex (Rebesco et al., 2016) (Fig. 6.1). The northernmost area is crossed by a pronounced moat, that channelize dense bottom currents crossing the trough from the inner (East) to the outer (West) area delivering sediments to the shelf break and to the drift system (Rebesco et al., 2016; Lantzsch et al., 2017) (Fig. 6.1). Another important element in the area is a system of faults in the inner part of the Kveithola Trough and the northern part of the shelf evidenced by Mau et al. (2017). Along this fault system a local evidence of hydrocarbon seepage activity is detected (station 21) (Lucchi et al., 2016; Mau et al., 2017; Bazzaro et al., 2020), driving macrofaunal diversity and trophic conditions (Caridi et al., 2019).

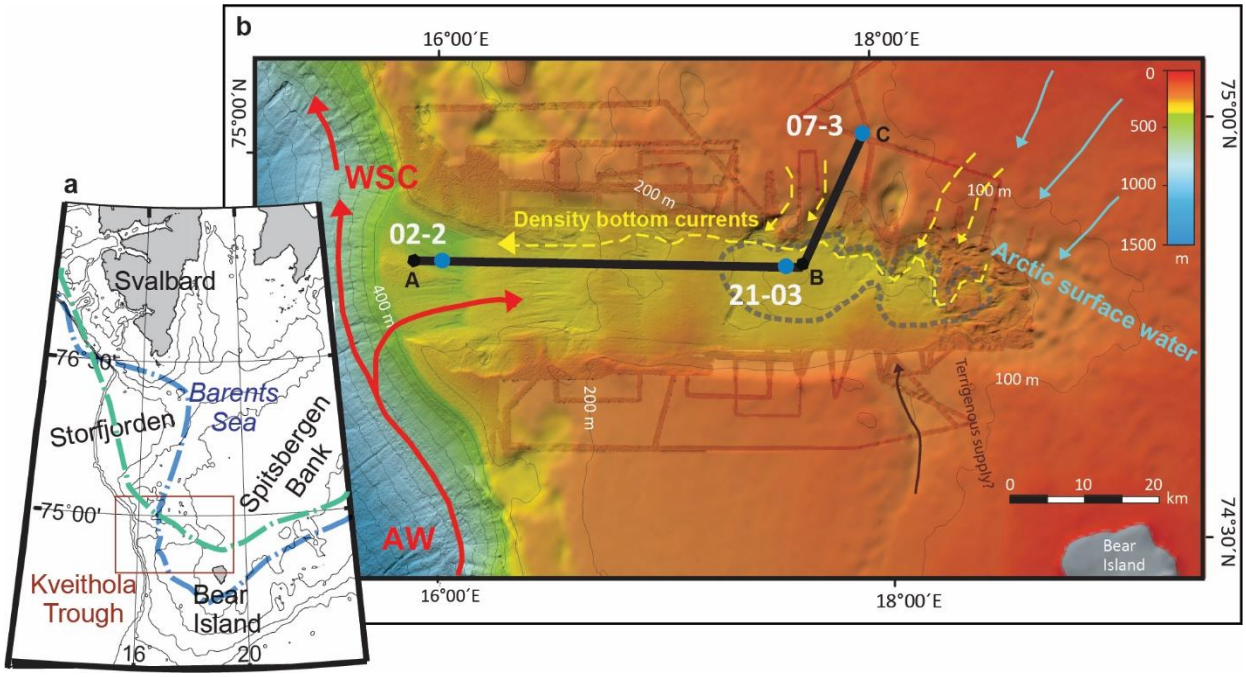


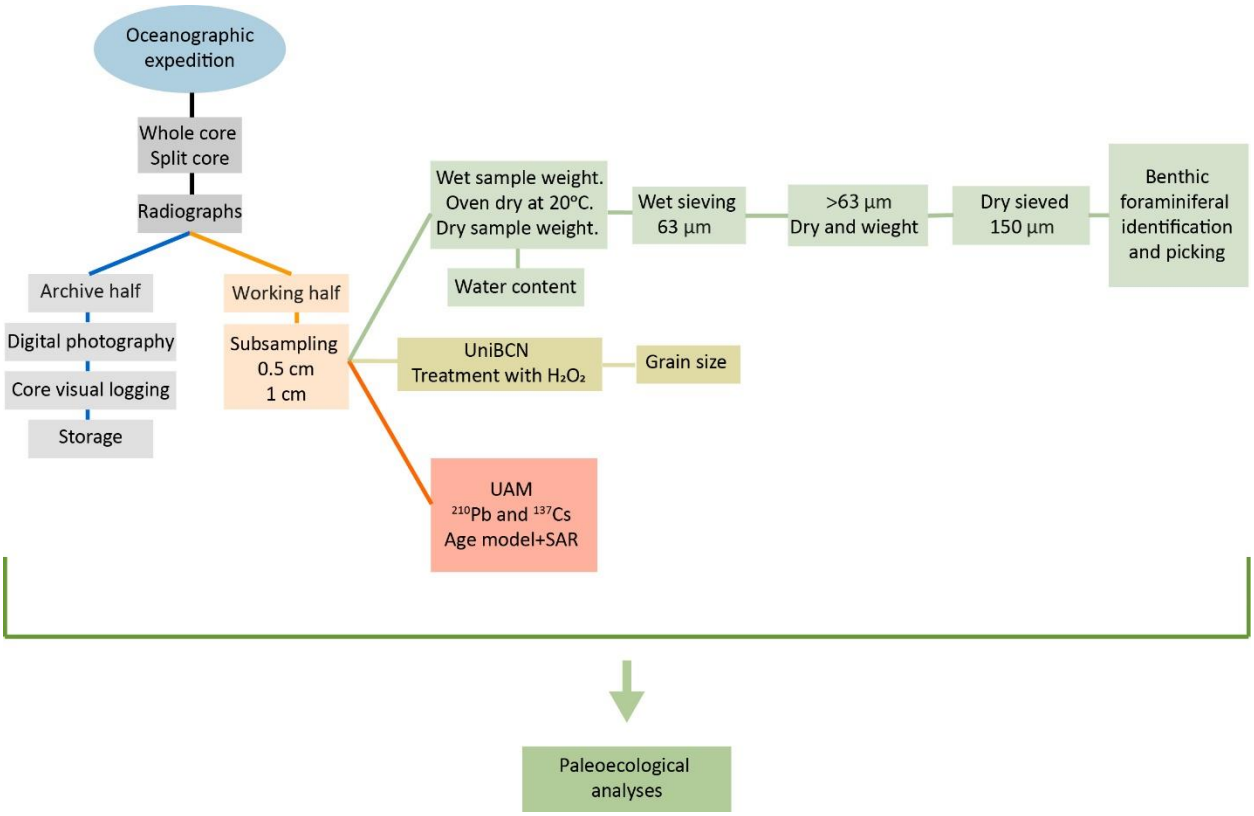
Fig. 6.1. (a) Overview map showing the location of the Kveithola Trough in the NW Barents Sea. The blue dashed line shows the position of the Polar Front; and the green dashed line represents the mean of the maximum sea ice extent from 1980-2010; obtained using the data from the National Snow and Ice Data Centre (NSIDC, https://nsidc.org/), and data from Harris et al. (1998), and Faust et al. (2020). (b) Bathymetric map of Kveithola Trough. The black ABC line shows the location of the bathymetric profile displayed in Fig. 7. The blue dots indicate the cored sites. The red arrows represent the path of the West Spitsbergen Current (WSC) transporting Atlantic Water (AW), whereas the light blue arrows indicate the input of the Arctic surface water. The yellow dashed arrows indicate the direction of density bottom currents. The grey dashed polygon on the inner Kveithola Trough delimits the sediment drift complex, and the dark brown arrow indicates a possible terrigenous supply coming from the south (Lantzsch et al., 2017).

Relatively fresh, cold Arctic waters (ArW) and warm, salty Atlantic waters (AW) constantly interact within the Kveithola Trough (Fig. 6.1). ArW flow from the Arctic Ocean and influence the northern-eastern part of the trough (Aagaard et al., 1985; Aagaard, 1989; Loeng, 1991; Orvik and Niiler, 2002); whereas the warm and saline AW are transported in the area by the West Spitsbergen Current (WSC), representing the northernmost branch of the North Atlantic Current proceeding from south along the bathymetric contour (Aagaard et al., 1973; Aagaard et al., 1981; Aagaard, 1989; Vinje and Kvambekk, 1991; Loeng et al., 1997; Maslowski et al., 2004; Smedsrud et al., 2013). The Kveithola Trough is seasonally influenced by the presence of sea ice during the winter seasons as it is on the southern limit of the maximum ice extent during late winter, around March-April (Fig. 6.1). However, the sea-ice extent in the Barents Sea suffers

from a strong interannual variability as well as a progressive long-term reduction (www.mosj.no). Decadal oscillations of the sea-ice extent in the Arctic and hence in the Barents Sea seem to be linked to large scale climatic patterns such as the Pacific Decadal Oscillation, the North Pacific Gyre Oscillation, and the North Atlantic Oscillation-like atmospheric pressure conditions (see e.g., Koenigk et al., 2009; Yang et al., 2020).

6.2. Material and methodology

The workflow 6.1 shows the scheme of the materials and methods followed for this chapter. Four cores collected in Kveithola Trough are studied for radiogenic analysis, grain size and micropaleontological content.



Workflow 6.1. Summary scheme of the materials and methods used for the multi-cores from Kveithola Trough. For more details, see chapter 2. Materials and methodology.

6.3. Results

6.3.1. Age model

The results of SR determination are summarised in Tab. 6.1. Station 02-2 located at the mouth of the trough, is characterised by the lowest average SR, thus only the first six centimetres are in ^{210}Pb dating applicability range and samples below this depth are thus considered older than 100 years. Stations 21-5, 21-3 and 07-3 are spanning the same time period, from late '60s, both showing presence of ^{137}Cs in the bottom samples, but station 21 that is located in the inner through has a lower SR than core 07-3 located nearby on the shelf. The obtained values of SR are comparable with literature values reported for the Barents Sea (e.g. Zaborska et al., 2008).

Station 02-2			Station 21-5			Station 21-3			Station 07-3		
Age AD	Depth bsf Cm	SR cm/yr	Age AD	Depth bsf cm	SR cm/yr	Age AD	Depth bsf cm	SR cm/yr	Age AD	Depth bsf cm	SR cm/yr
2016	0-0.5		2016	0-0,5		2016	0-0.25		2016	0-0.5	
2010	0.5-1		2014	0,5-1		2014	0.25-0.5		2014	0.5-1	
2001	1-1.5		2009	1-1,5		2008	0.5-1		2011	1-1.5	
1998	1.5-2		2005	1,5-2		2003	1-1.5		2010	1.5-2	
1986	2-3		2000	2-3		1998	1.5-2		2005	2-3	
1974	3-4		1993	3-4		1989	2-3	0.092	2001	3-4	
1962	4-5		1983	4-5		1979	3-4		1996	4-5	
1950	5-6		1974	5-6		1968	4-5		1992	5-6	
1937	6-7		1964	6-7		1957	5-6		1987	6-7	
1925	7-8		1955	7-8		1946	6-7		1983	7-8	
1913	8-9		1945	8-9		1935	7-8		1978	8-9	
1901	9-10		1936	9-10					1973	9-10	
1889	10-11		1927	10-11					1971	10-11	0.220
1883	11-12		1912	11-12	0.106				1967	11-12	
1864	12-13		1898	12-13					1962	12-13	
1858	13-14	0.082	1893	13-14					1958	13-14	
1840	14-15		1884	14-15					1953	14-15	
1834	15-16		1870	15-16					1949	15-16	
1816	16-17		1860	16-17					1944	16-17	
1810	17-18		1855	17-18					1939	17-18	
1791	18-19		1841	18-19					1935	18-19	
1779	19-20		1832	19-20					1930	19-20	
1773	20-21		1827	20-21					1926	20-21	
1755	21-22		1813	21-22					1921	21-22	
1743	22-23		1803	22-23					1917	22-23	
1731	23-24		1794	23-24					1908	23-24	
1724	24-25		1784	24-25							
1706	25-26										
1694	26-27										
1682	27-28										
1676	28-29										
1658	29-30										

Tab. 6.1. Age, depth and sediment accumulation rates based on values of 137Cs and 210Pb.

6.3.2. Lithological description and grain size analysis

During the oceanographic cruise, one of the cores are opened and visually described for the lithological description (Lucchi et al., 2016) (Fig. 6.2). In the core 02-2, the grain size shows a predominance of clay with an average of 56 % from the bottom until 1925 A.D., the increase of the sand fraction until 60%, and a general mean grain size of 31-63 µm (5 phi). The grain size of the other three cores are similar with mean grain size corresponding with medium-coarse silt (8-15 µm - 6 phi). At the core 21-05, the silt fraction is dominant with an average of 58%. The core 21-03 is characterised by silt (average 60%), except at the bottom of the core where the sand fraction reaches 64%. At the station 07-3, the grain size is predominantly silt with an average of 64%, the sand fraction reaches a maximum of 35% at 1958 A.D. (Fig. 6.2).

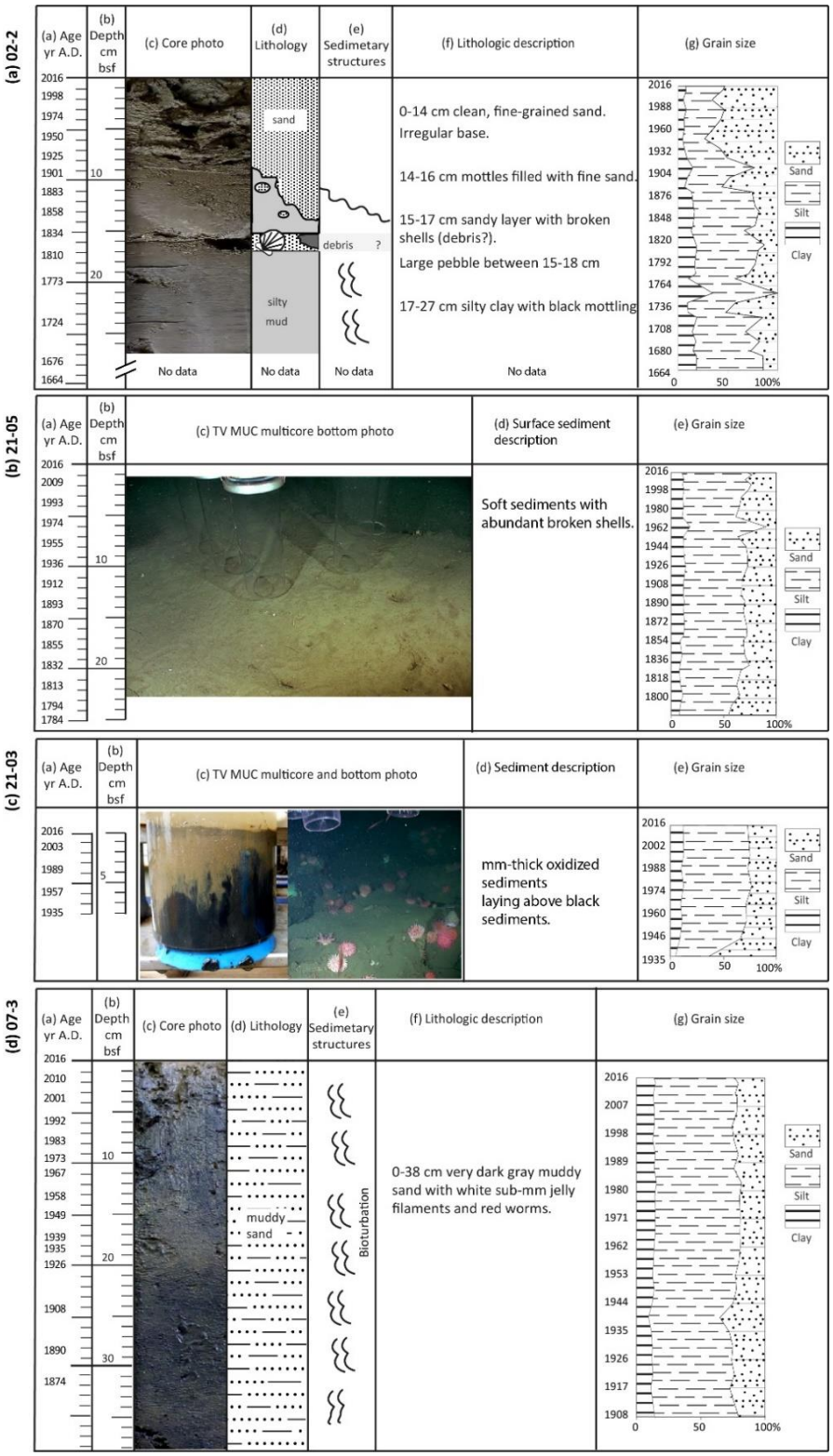


Fig. 6.2. Age, core depth, sediment photo of the core or photo of the sea-surface bottom, lithological description (after Lucchi et al., 2016) and gain size of (a) 02-2, (b) 21-05, (c) 21-03 and (d) 07-3.

6.3.3. Benthic foraminiferal results

a. Station 02-2

The outermost station 02-2 corresponds with the longest-time record, 1658 A.D. at 30 cm bsf (Fig. 6.1, Tab. 6.1., and see chapter 2 for details about the multi-core).

General foraminiferal trend

In the sedimentary record of the station 02-2, 54 species are recognised, of which 15 species are present with more than 5% (main species) (Tab. 6.2 and 6.3, Fig. 6.6). Calcareous perforate group with 40 species occurs with more than 99% of the total assemblage; the calcareous imperforate (4 species) and the agglutinate (10 species) groups are present with 1%, of the total assemblage (Fig. 6.3).

Main Benthic foraminiferal species (>5%)				
Calcareous perforate	*Astrononion gallowayi*	*Buccella* spp.	*Cassidulina laevigata*	*Cassidulina neoteretis*
	Cassidulina reniforme	*Cibicides refulgens*	*Cibicidoides lobatulus*	*Elphidium clavatum*
	Islandiella norcrossi	*Melonis barleeanus*	*Nonionellina labradorica*	*Nonionella iridea*
	Trifarina angulosa	*Trifarina carinata*	*Trifarina fluens*	

Tab. 6.2. Core 02-2. Main benthic foraminiferal species.

Secondary Benthic foraminiferal species (<5%)				
Calcareous perforate	*Bolivinellina pseudopunctata*	*Bolivina* spp.	*Discorbis vilardeboanus*	*Fissurina* spp.
	Globobulimina auriculata	*Globobulimina arctica.*	*Globocassidulina subglobosa*	*Guttulina* spp.
	Haynesina depressula	*Haynesina germanica*	*Haynesina orbiculare*	*Hoeglundina elegans*
	Islandiella helenae	*Lagena* spp.	*Lenticulina* spp.	*Nonionella auricula*
	Nonionella iridea	*Oolina* spp.	*Oridorsalis tener*	*Patellina corrugata*
	Pullenia bulloides	*Pullenia osloensis*	*Pullenia subcarinata*	*Rosalina* spp.
	Stainforthia loeblichi			
Calcareous imperforate	*Planispirinoides bucculentus*	*Pyrgo* spp.	*Quinqueloculina seminula*	*Triloculina tricarinata*
Agglutinated	*Astrorhiza granulosa*	*Eggerelloides scaber*	*Hyperammina elongate*	
	Hyperammina friabilis	*Lagenammina* spp.	*Psammosiphonella crassatina*	
	Reophax guttifer	*Reophax* spp.	*Rhabdammina scabra*	
	Saccorhiza ramose			

Tab. 6.3. Core 02-2. Secondary benthic foraminiferal species.

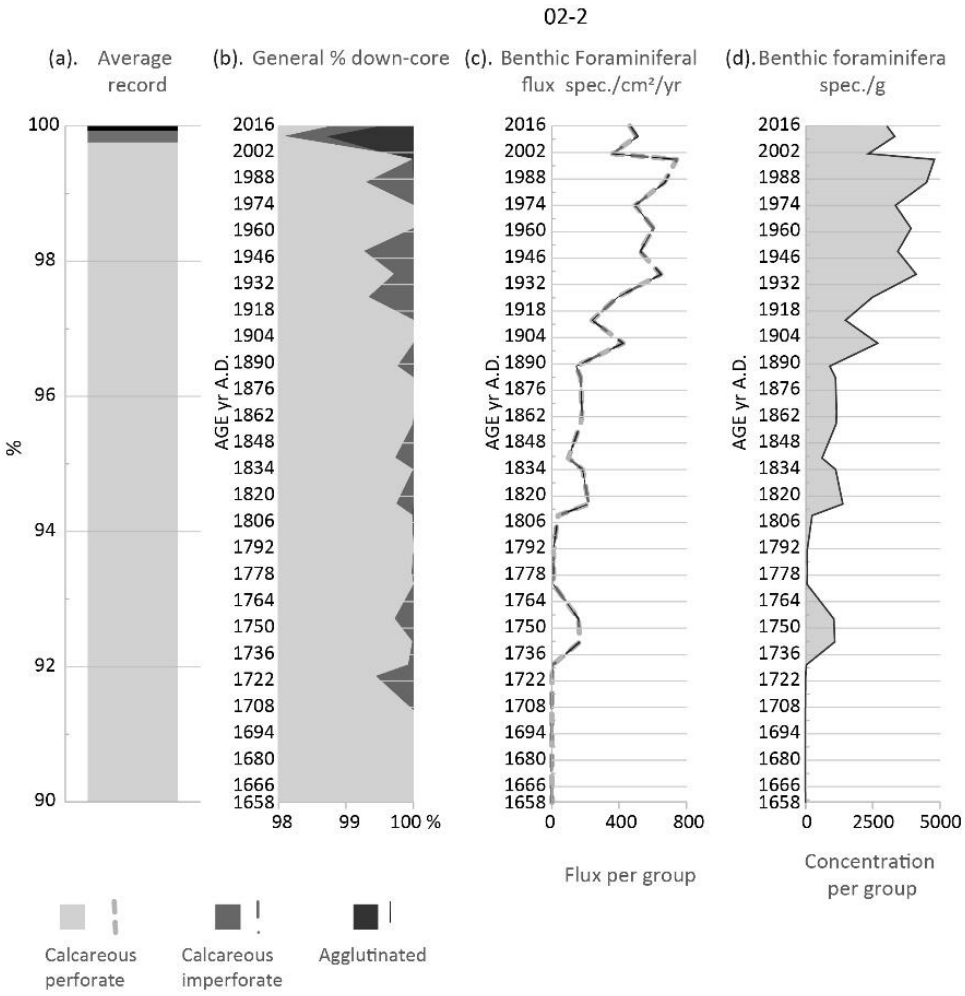


Fig. 6.3. Core 02-2. (a). General average percentage per group in the entire record. (b). General relative abundance per group down-core. (c). Benthic foraminiferal flux. (d). Benthic foraminifera concentration per gram of dry sediment (note that the concentration of the calcareous imperforate and agglutinated groups is less than 1 spec./g). The x-axes are different.

The foraminiferal flux and the concentration of foraminifera increased from 1806 A.D. reaching a maximum between 1932 and 2002 A.D., the foraminiferal flux with more than 740 spec./cm^2/yr, and the foraminiferal concentration with more than 4700 spec./g (Fig. 6.3).

Diversity indexes and cluster analysis

The number of taxa (S) increases on top reaching 34 species at 2016 A.D. (Fig. 6.4). The Dominance (D) shows high values at the bottom of the core reaching 0.24 at 1682 A.D., and the minimum value at 1960 A.D. with 0.1. Shannon index (H) shows high values especially on top reaching 2.6 and the lowest value is 1.8 at 1682 A.D. (Fig. 6.4).

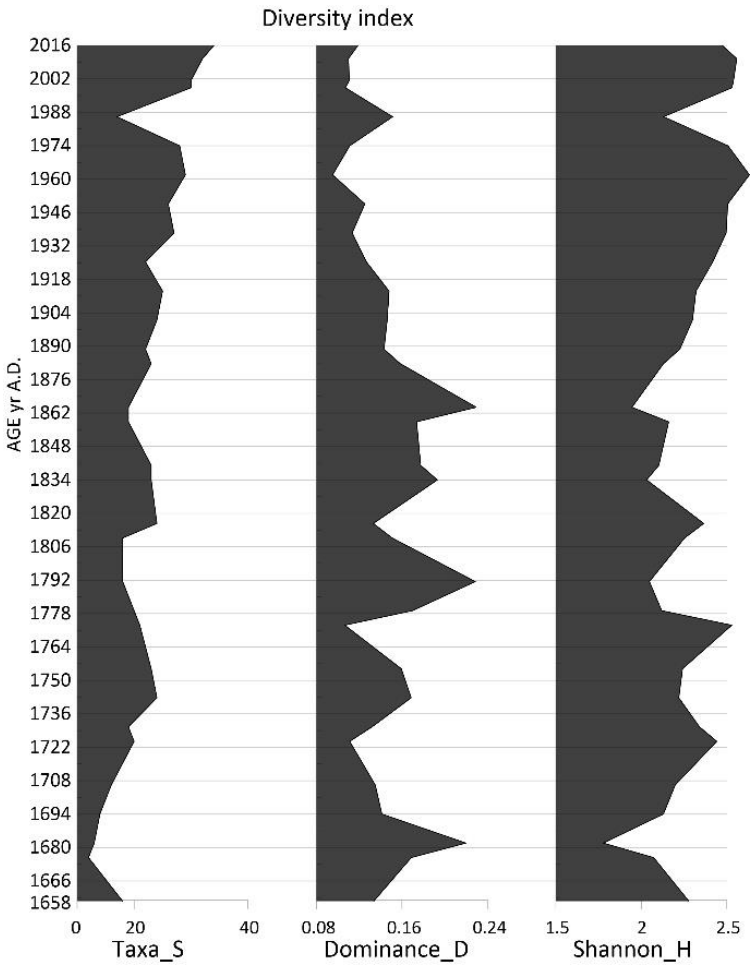


Fig. 6.4. Core 02-2. Diversity indexes. The x-axes are different.

The classical hierarchical Q-mode cluster analysis shows a long-time interval. The cluster C corresponds with an outlier at 1773 A.D., which corresponds with low abundances of *C. neoteretis* and *C. lobatulus*. The second cluster analysis without the outlier indicates two clusters of samples; Cluster A: samples with abundance of *C. laevigata* and *C. neoteretis*, and the Cluster B: samples with a high abundance of *T. fluens* (Fig. 6.5).

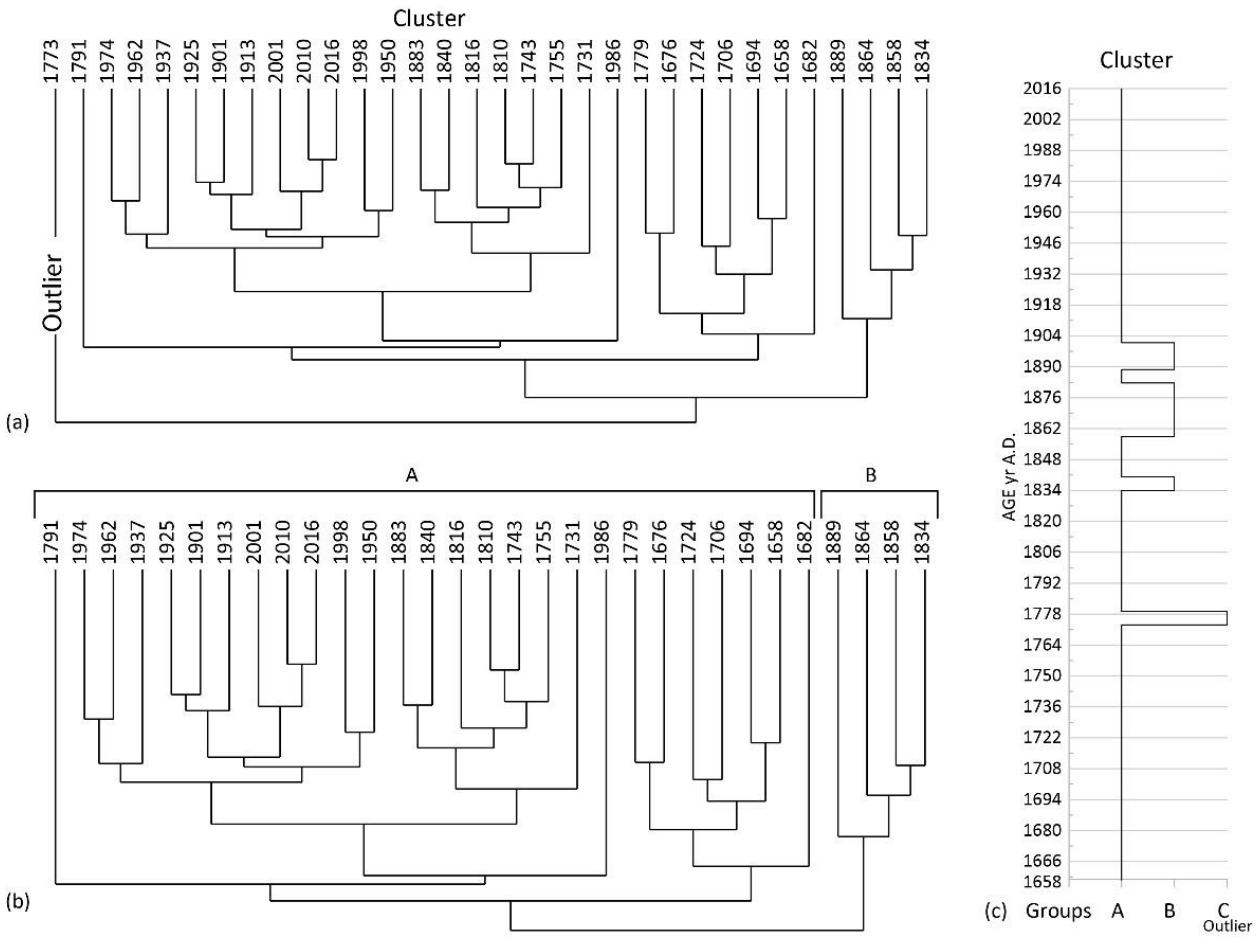


Fig. 6.5. Core 02-2. Q-mode cluster analysis (a). Dendrogram groups with outlier. (b). Dendrogram groups without outliers. (c). Cluster groups by age distribution down-core.

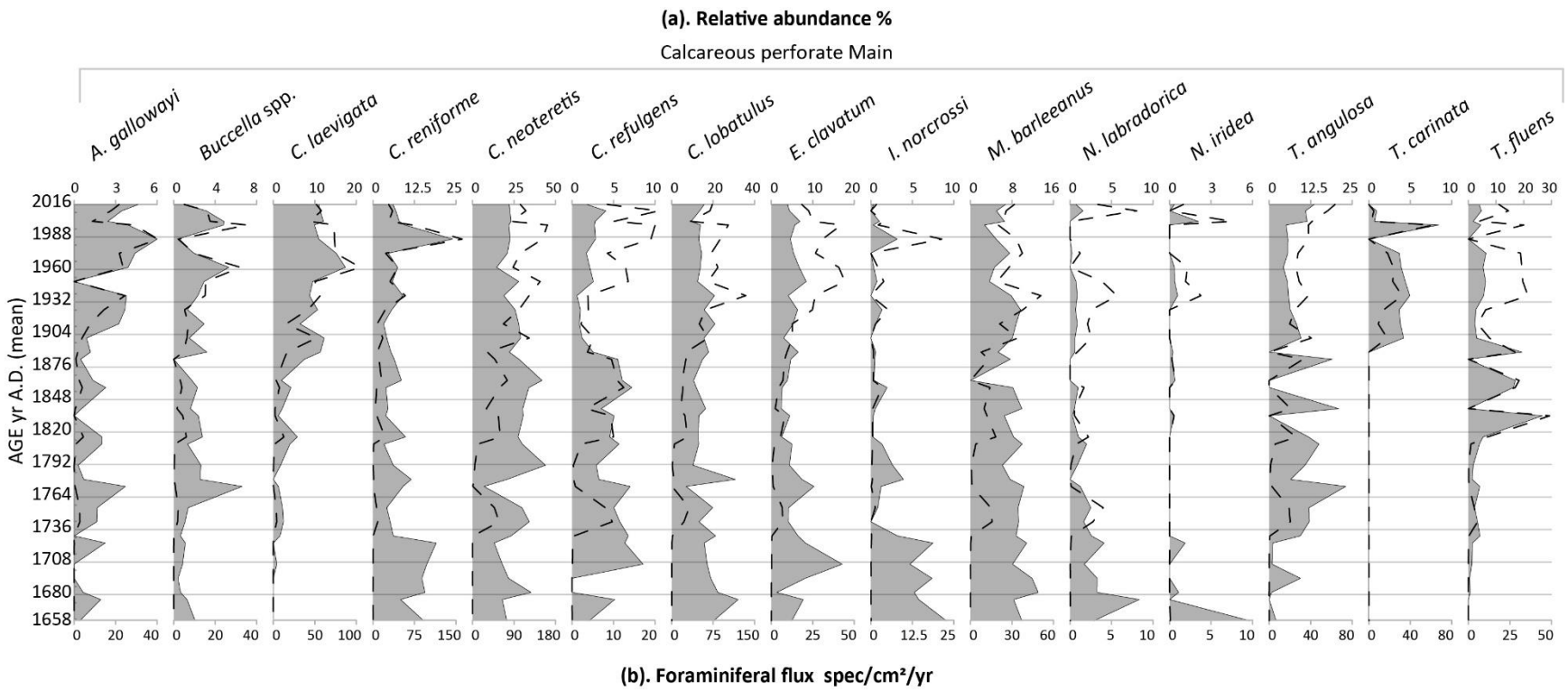


Fig. 6.6. Core 02-2. Benthic foraminifera: (a). Relative abundance (grey) and (b). Foraminiferal flux (black dashed line) of the main species. The x-axes are different.

The secondary species are present in less than 5% in the record (Fig. 6.7).

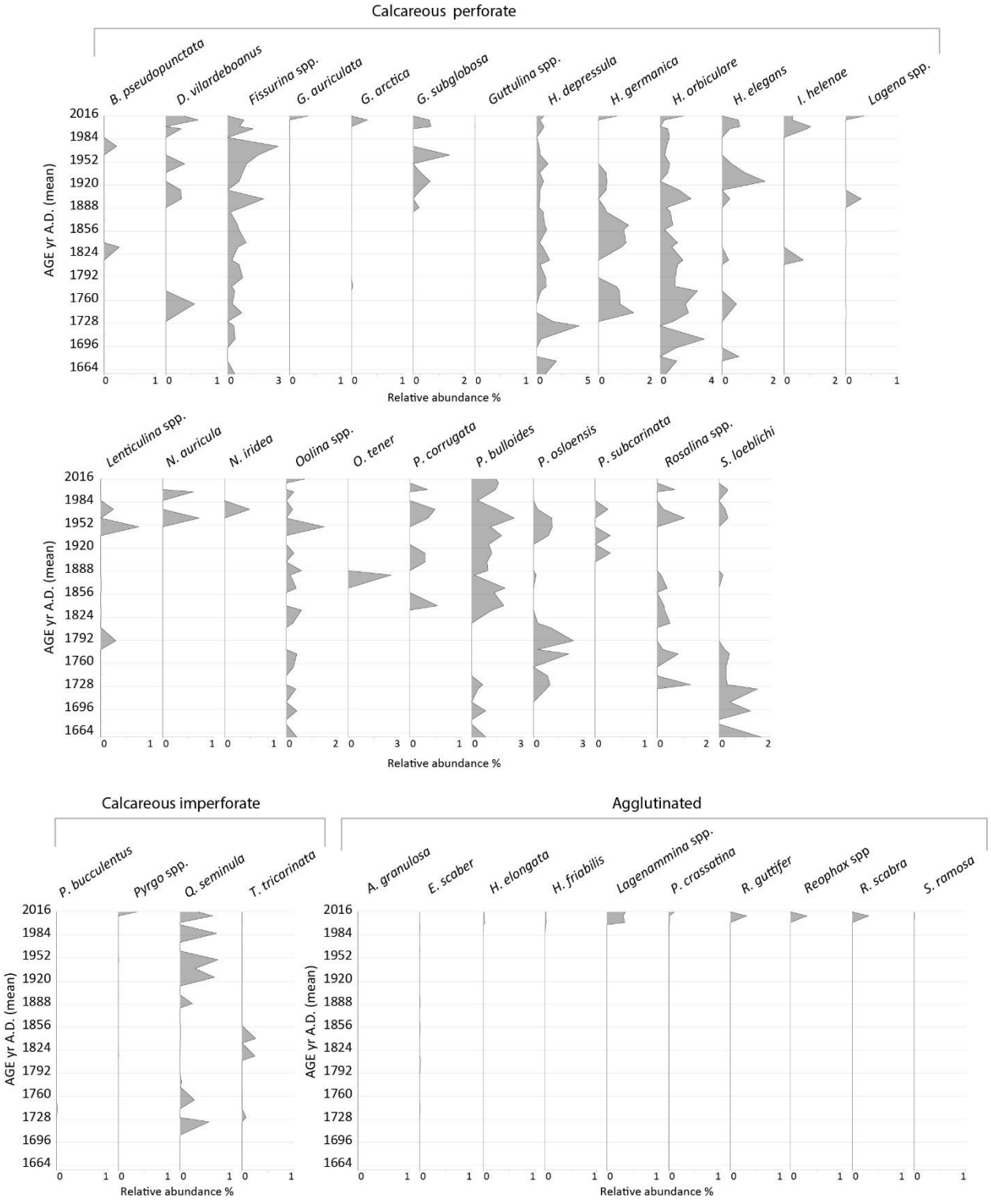


Fig. 6.7. Core 02-2. Secondary species.

b. Station 21-05

Station 21-05 is one of the inner stations located into the main drift; the sedimentary time record arrives until 1784 A.D. at 25 cm bsf (Fig. 6.1, Tab. 6.1., and see chapter 2 for details about the multi-core).

General foraminiferal trend

A total of 43 species are identified at the station 21-05. The 12 main species are present with more than 5% of relative abundance (Tab. 6.4 and 6.5; Fig. 6.11). In general, 33 species of the calcareous perforate group occurred with more than 99%. The calcareous imperforate group (4 species) and the agglutinated group (5 species), with less than 1% of the total assemblage (Fig. 6.8).

Main Benthic foraminiferal species (>5%)				
Calcareous perforate	*Astrononion gallowayi*	*Cassidulina laevigata*	*Cassidulina neoteretis*	*Cassidulina reniforme*
	Cibicides refulgens	*Cibicidoides lobatulus*	*Elphidium clavatum*	*Globocassidulina subglobosa*
	Islandiella helenae	*Islandiella norcrossi*	*Melonis barleeanus*	*Nonionellina labradorica*

Tab. 6.4. Core 21-05. Main benthic foraminiferal species.

Secondary Benthic foraminiferal species (<5%)				
Calcareous perforate	*Bolivinellina pseudopunctata*	*Buccella* spp.	*Dentalina advena*	*Fissurina* spp.
	Globobulimina auriculata	*Globobulimina arctica.*	*Hoeglundina elegans*	*Lagena* spp.
	Lenticulina spp.	*Marginulina obesa*	*Nonionella auricula*	*Oolina* spp.
	Patellina corrugata	*Pullenia bulloides*	*Robertinoides charlottensis*	*Rosalina* spp.
	Stainforthia loeblichi	*Trifarina angulosa*	*Trifarina carinata*	*Trifarina fluens*
	Turrispirillina arctica			
Calcareous imperforate	*Pyrgo* spp. *Pyrgo subglobulus*	*Pyrgo williamsoni*	*Quinqueloculina seminula*	*Triloculina tricarinata*
Agglutinated	*Lagenammina difflugiformis.*	*Lagenammina micacea*	*Psammosphaera* spp.	
	Quinqueloculina agglutinate	*Rhabdammina scabra*		

Tab. 6.5. Core 21-05. Secondary benthic foraminiferal species.

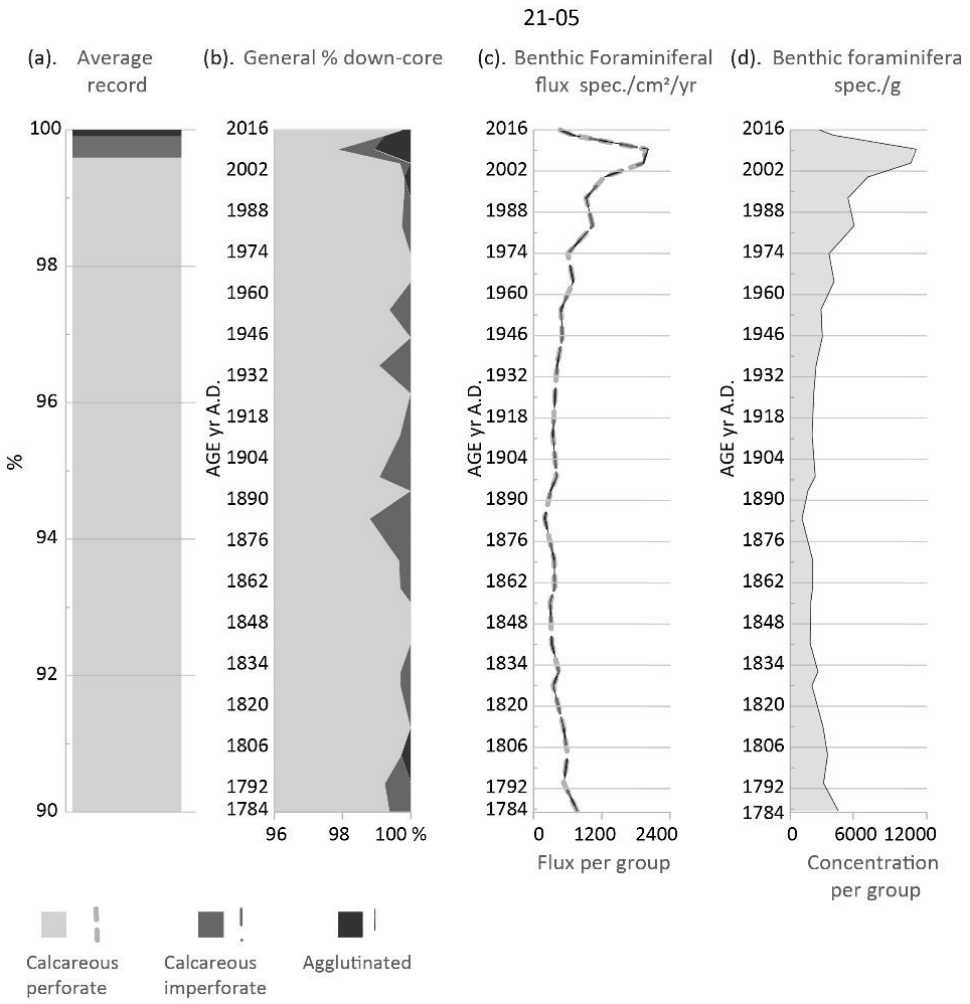


Fig. 6.8. Core 21-05. (a). General average percentage per group in the entire record. (b). General relative abundance per group down-core. (c). Benthic foraminiferal flux. (d). Benthic foraminifera concentration per gram of dry sediment (note that the concentration of the calcareous imperforate and agglutinated groups is less than 1 spec./g). The x-axes are different.

The foraminiferal flux and the foraminiferal concentration show a similar trend. From 1784 until 1884 A.D. decreases from 770 until 196 spec/cm^2/yr, while the concentration from 4222 until 1025 spec./g (Fig. 6.8). An increase from 1884 until 2009 A.D. is shown, both flux and concentration show a peak between 2000 and 2009 A.D., with a maximum of 2018 spec/cm^2/yr and 11701 spec./gram. From 2000 until 2016 A.D. the record decreases until 137 spec/cm^2/yr and 2560 spec./g (Fig. 6.8).

Diversity indexes and cluster analysis

The number of taxa (S) ranged between 25 and 18. The Dominance (D) and Shannon (H) indexes are relatively constant, D with maximum of 0.14 and minimum of 0.10, while H with a maximum value of 2.6 and a minimum of 2.3 (Fig. 6.9).

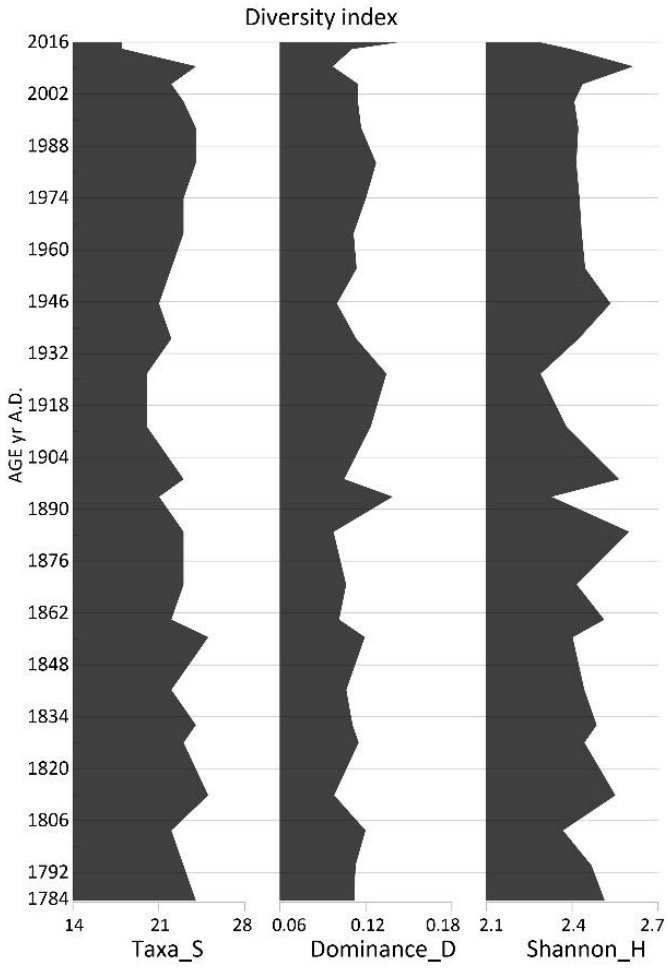


Fig. 6.9. Core 21-05. Diversity indexes. The x-axes are different.

The classical cluster analysis indicates a continuous record with multi-decadal events. Three clusters including one outlier are identified: Cluster A: samples with abundance of *C. neoteretis* and *C. lobatulus;* Cluster B: samples with abundance of *C. laevigata* and *I.* norcrossi, and the outliers Cluster C is a sample with a minimum of *C. laevigata* (Fig. 6.10).

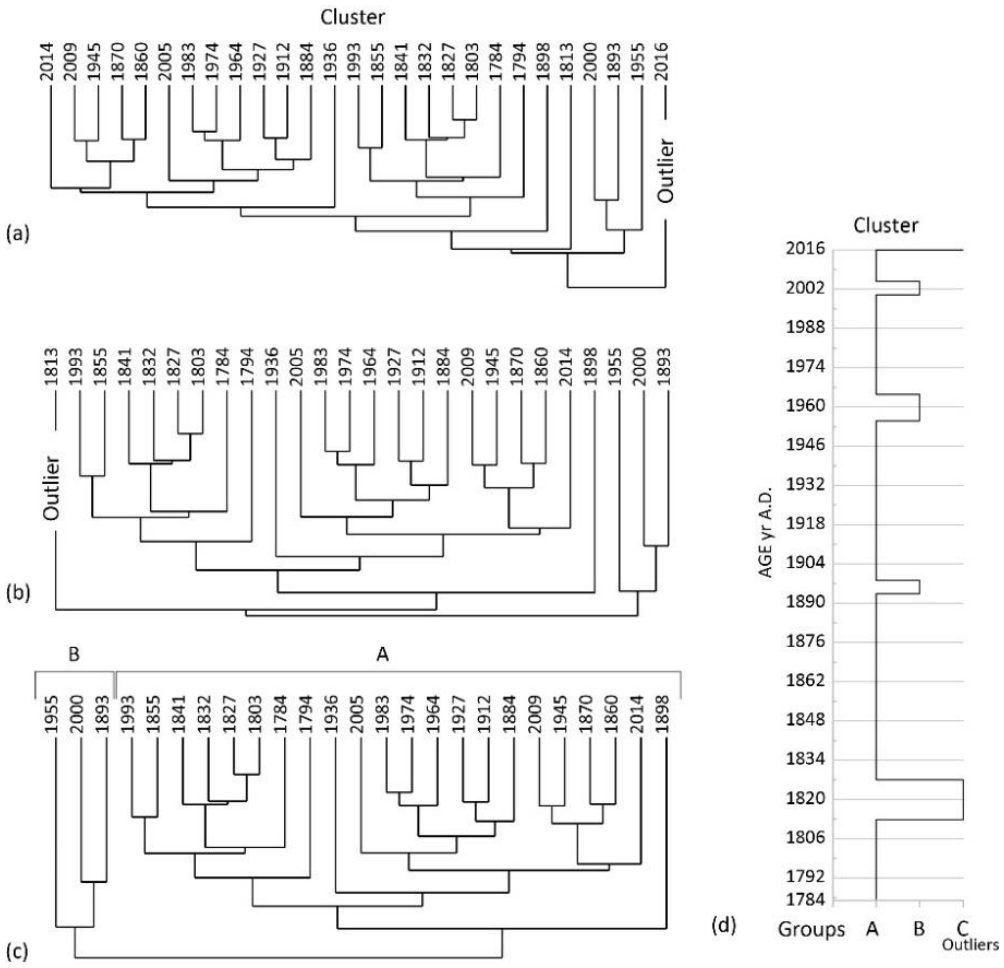


Fig. 6.10. Core 21-05. Q-mode cluster analysis (a) and (b). Dendrogram groups with outliers. (c). Dendrogram groups without outliers. (d). Cluster groups by age distribution down-core.

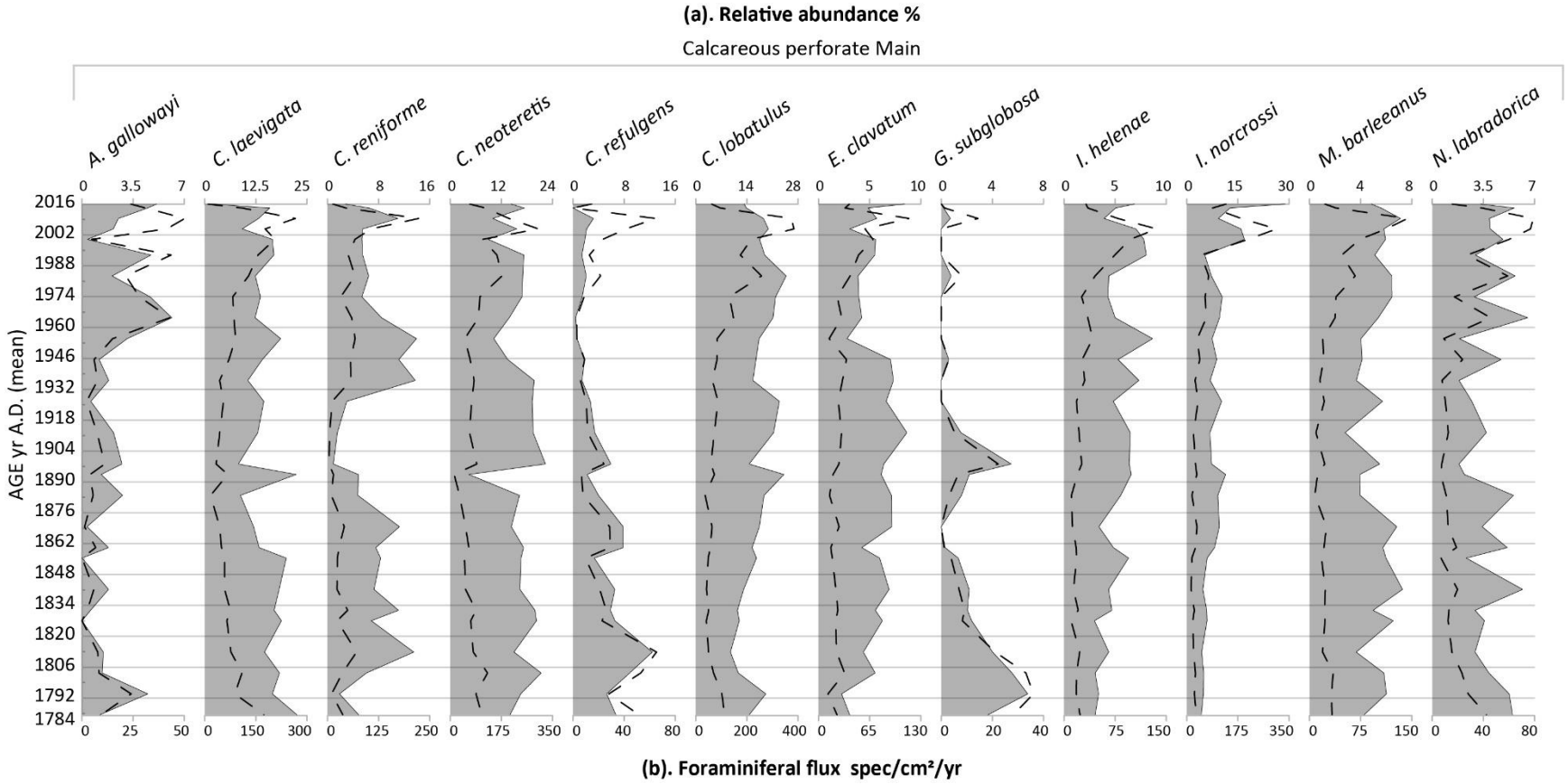


Fig. 6.11. Core 21-05. Benthic foraminifera: (a). Relative abundance (grey) and (b). Foraminiferal flux (black dashed line) of the main species. The x-axes are different.

The secondary species are present in less than 5% in the record (Fig. 6.12).

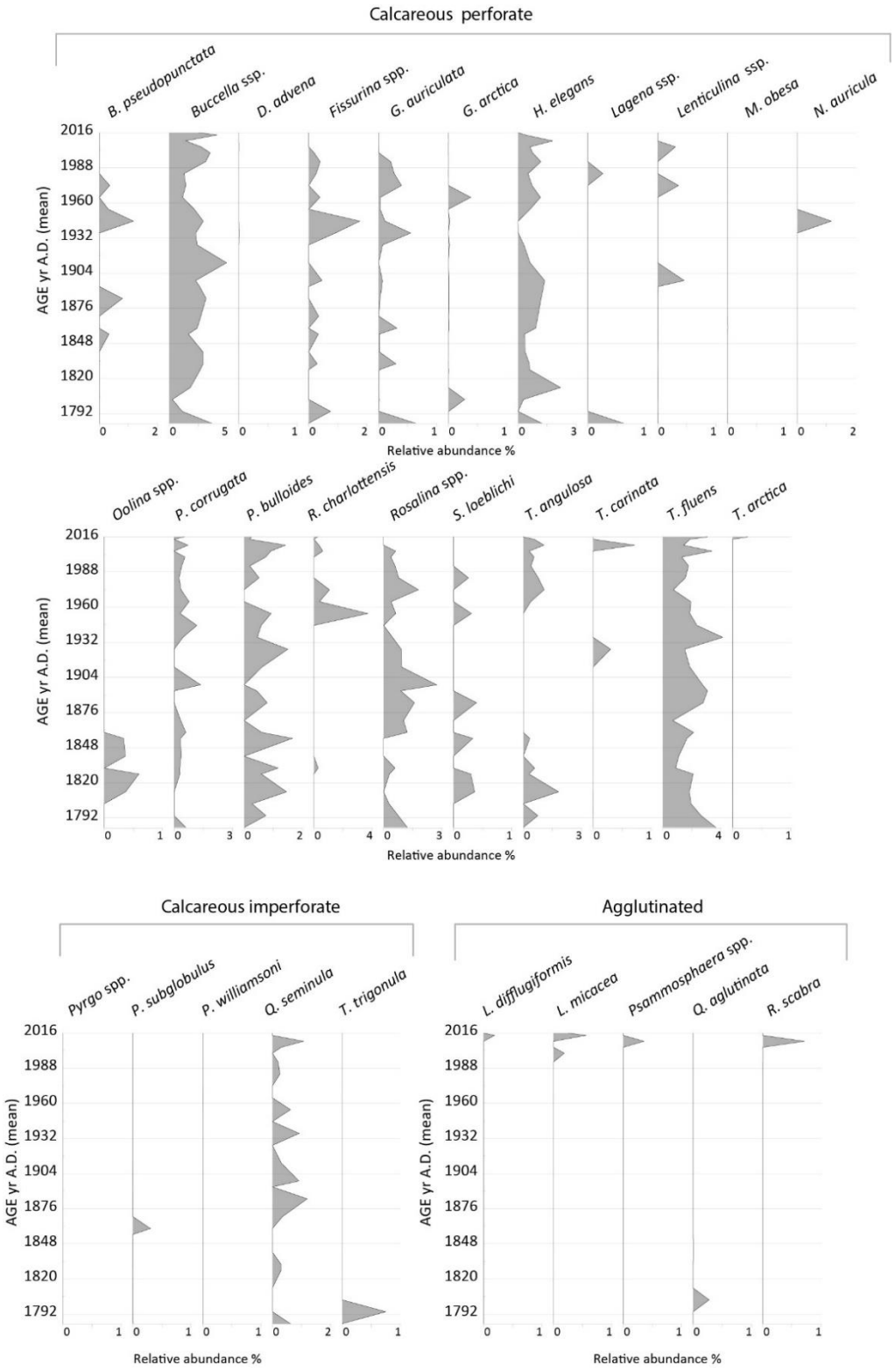


Fig. 6.12. Core 21-05. Secondary species.

c. *Station 21-03*

Station 21-03 is the second inner station located into the main drift; the sedimentary record arrives until 1935 A.D. at 8 cm bsf (Fig. 6.1, Tab. 6.1., and see chapter 2 for details about the multi-core).

General foraminiferal trend

In total, 36 species are recognised. The calcareous perforate group (31 species), represents more than 99% of the total assemblage, 9 of these species are present with more than 5% (main species) (Tab. 6.6 and 6.7, Fig. 6.16). The calcareous imperforate (1 species), and the agglutinated group (4 species) represent less than 1% of the total assemblage (Fig. 6.13).

Main Benthic foraminiferal species (>5%)				
Calcareous perforate	*Cassidulina laevigata*	*Cassidulina neoteretis*	*Cassidulina reniforme*	*Cibicidoides lobatulus*
	Elphidium clavatum	*Islandiella helenae*	*Islandiella norcrossi*	*Melonis barleeanus*
	Nonionellina labradorica			

Tab. 6.6. Core 21-03. Main benthic foraminiferal species.

Secondary Benthic foraminiferal species (<5%)				
Calcareous perforate	*Astrononion gallowayi*	*Biasterigerina planorbis*	*Bolivina* spp.	*Bolivina earlandi*
	Bolivina spathulata	*Buccella* spp.	*Cibicides refulgens*	*Discorbis villardeboanus*
	Fissurina spp.	*Globobulimina auriculata*	*Globobulimina arctica*	*Globocassidulina subglobosa*
	Hoeglundina elegans	*Nonionella iridea*	*Patellina corrugata*	*Pullenia bulloides*
	Pullenia osloensis	*Robertinoides charlottensis*	*Rosalina* spp.	*Trifarina angulosa*
	Trifarina carinata	*Trifarina fluens*		
Calcareous imperforate	*Quinqueloculina seminula*			
Agglutinated	*Adercotryma glomerata*	*Labrospira crassimargo*	*Quinqueloculina agglutinata*	Reophax scorpiurus

Tab. 6.7. Core 21-03. Secondary benthic foraminiferal species.

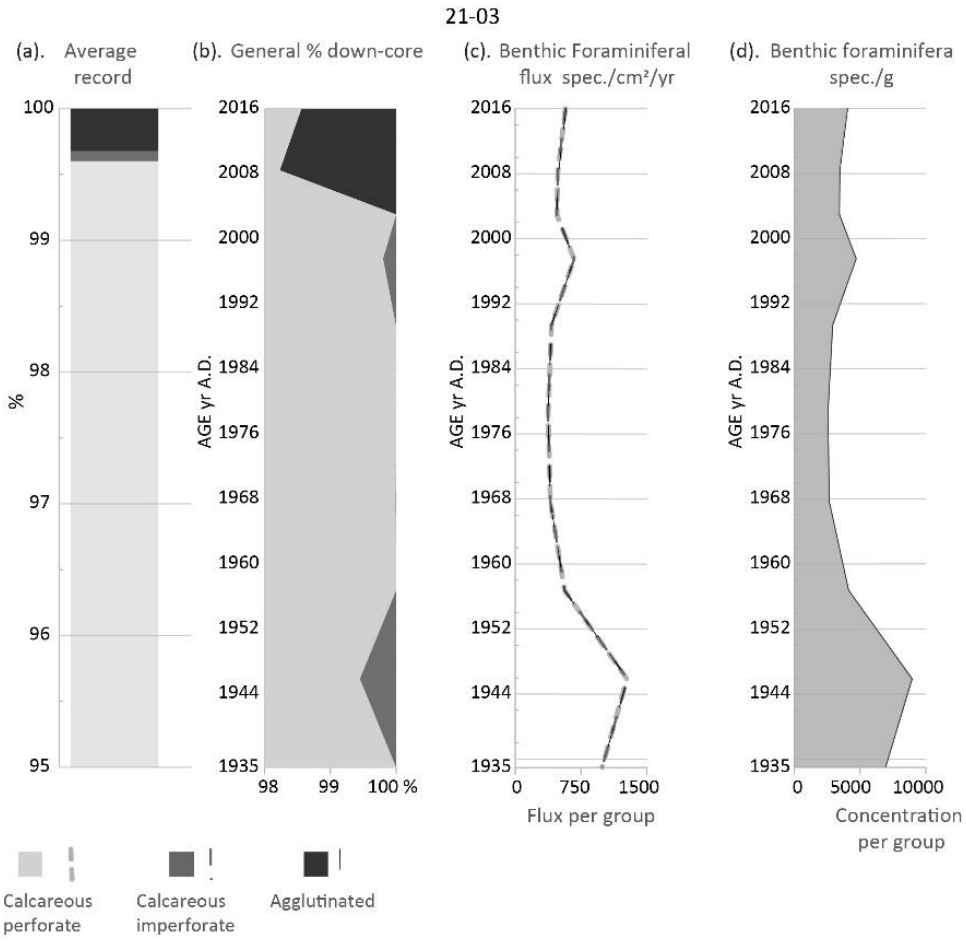


Fig. 6.13 Core 21-03. (a). General average percentage per group in the entire record. (b). General relative abundance per group down-core. (c). Benthic foraminiferal flux. (d). Benthic foraminifera concentration per gram of dry sediment (note that the concentration of the calcareous imperforate and agglutinated groups is less than 1 spec./g). The x-axes are different.

The foraminiferal flux and the foraminiferal concentration show a similar trend, increasing between 1935 and 1946 A.D. (reaching 1281 spec./cm^2/yr and 8964 spec/g, respectively). Both decrease from 1946 until 1989 A.D. (minimum of 402 spec./cm^2/yr and 2664 spec./g respectively), a last peak is shown at 1998 A.D. (671 spec./cm^2/yr and 4709 spec./g). A general decrease is recorded until 2016 A.D. (Fig. 6.13).

Diversity indexes and cluster analysis

The taxa (S) ranges from 20 until 29. Dominance (D) shows low values, with a minimum of 0.09 between 2014 and 2016 A.D. The Shannon index (H) shows values between 2.3 and 2.4, reaching 2.6 between 2008 and 2016 A.D. (Fig. 6.14).

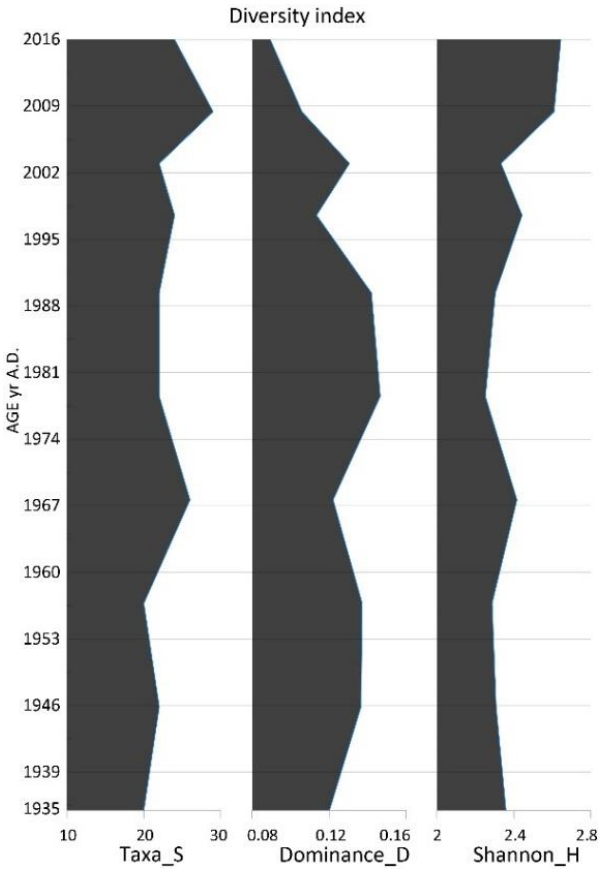


Fig. 6.14. Core 21-03. Diversity indexes. The x-axes are different.

The classical hierarchical Q-mode cluster analysis shows two main clusters (Fig. 6.15), Cluster A corresponds to samples with a high abundance of *C. lobatulus* and Cluster B with a high abundance of *C. laevigata.*

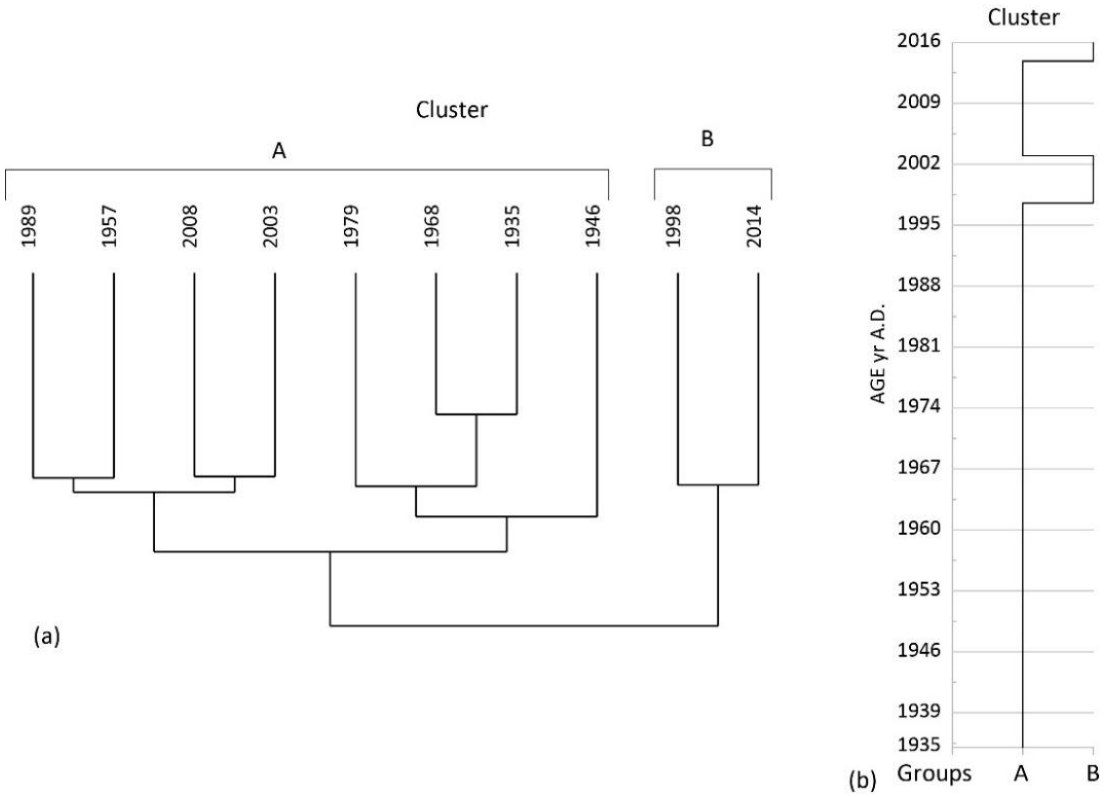


Fig. 6.15. Core 21-03. Q-mode cluster analysis (a). Dendrogram groups. (b). Cluster groups by age distribution down-core.

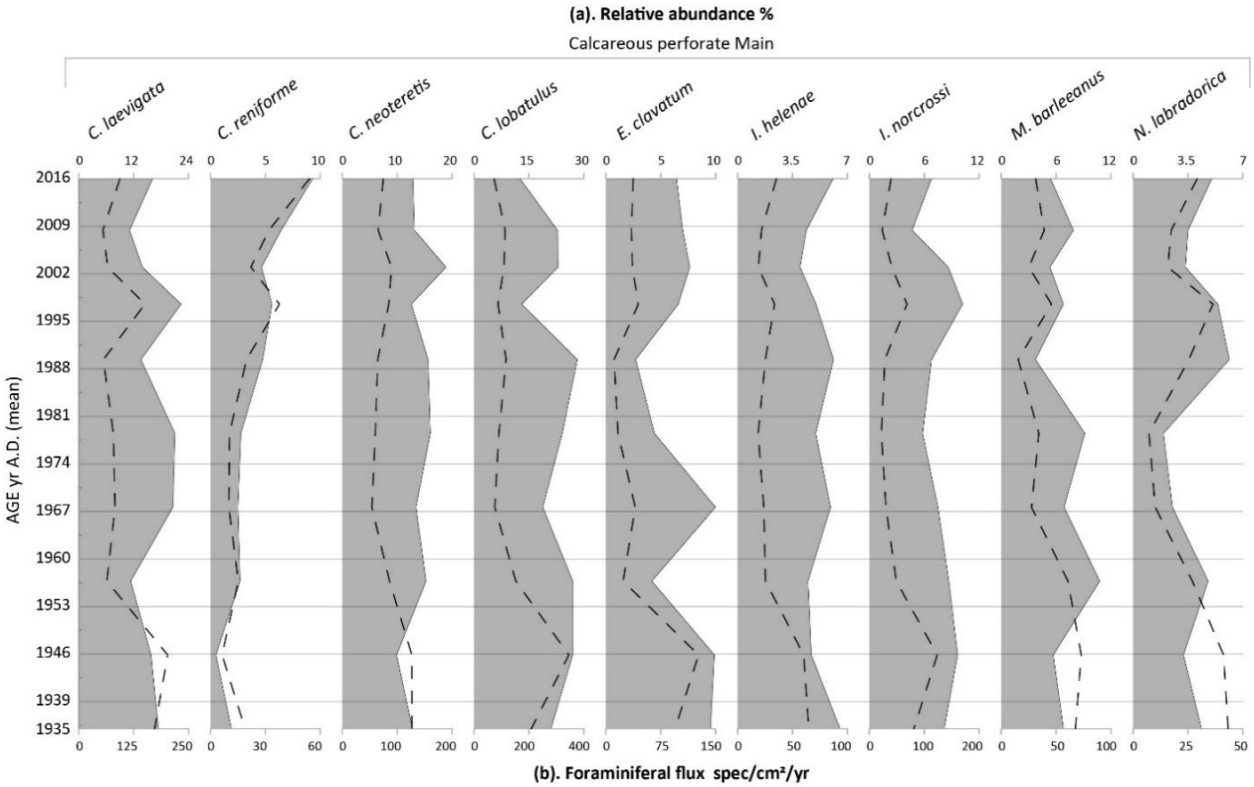


Fig. 6.16. Core 21-03. Benthic foraminifera: (a). Relative abundance (grey) and (b). Foraminiferal flux (black dashed line) of the main species. The x-axes are different.

The secondary species are present with less than 5% in the record (Fig. 6.17).

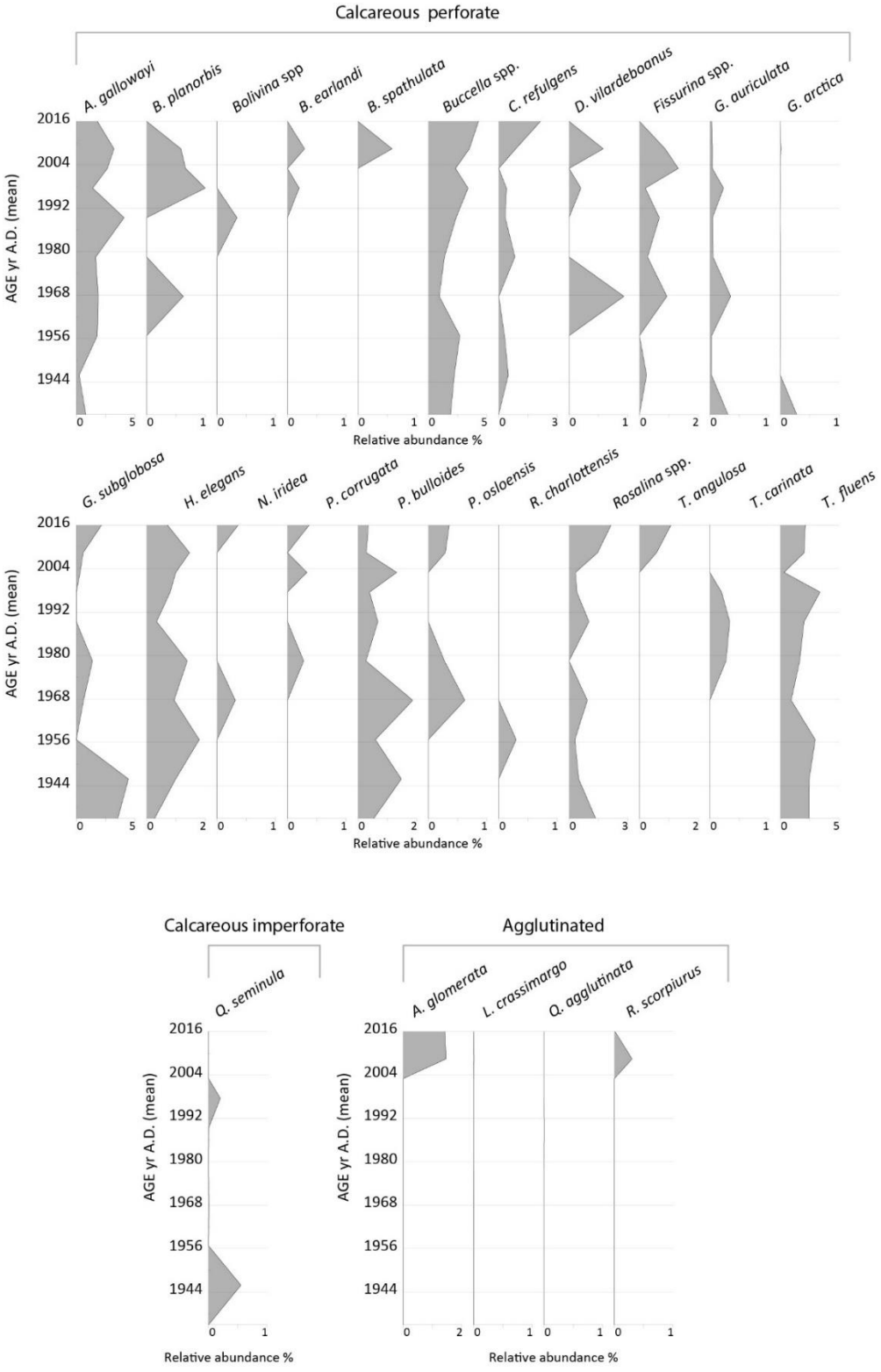


Fig. 6.17. Core 21-03. Secondary species of the station 21-03

d. Station 07-3

Station 07-3 is the shallowest station located outside the trough at the northernmost area; the sedimentary record started at 1908 A.D. with 24 cm bsf (Fig. 6.1, Tab. 6.1., and see chapter 2 for details about the multi-core).

General foraminiferal trend

At station 07-3, a total of 59 species are identified. The calcareous perforate group (42 species of which 14 are main species) occurs with 97% of the total assemblage (Tab. 6.8 and 6.9, Fig. 6.21). The calcareous imperforate group (7 species) with 1.5% of the total assemblage, and the agglutinated group (10 species) with less than 1% of the total assemblage (Fig. 6.18).

Main Benthic foraminiferal species (>5%)				
Calcareous perforate	*Astrononion gallowayi*	*Buccella* spp.	*Cassidulina laevigata*	*Cassidulina neoteretis*
	Cassidulina reniforme	*Cibicides refulgens*	*Cibicidoides lobatulus*	*Discorbis villardeboanus*
	Elphidium clavatum	*Globocassidulina subglobosa*	*Islandiella norcrossi*	*Nonionellina labradorica*
	Patellina corrugata	*Rosalina* spp.		

Tab. 6.8. Core 07-3. Main benthic foraminiferal species.

Secondary Benthic foraminiferal species (<5%)				
Calcareous perforate	*Biasterigina planorbis*	*Bolivina earlandi*	*Bolivinellina pseudopunctata*	*Dentalina inortata*
	Elphidium albiumbilicatum	*Eponides* spp.	*Fissurina* spp.	*Globobulimina auriculata*
	Globobulimina arctica	*Haynesina germanica*	*Haynesina orbiculare*	*Hoeglundina elegans*
	Islandiella helenae	*Lagena* spp.	*Lenticulina* spp.	*Melonis barleeanus*
	Nonionella auricula	*Nonionella iridea*	*Oolina* spp.	*Pullenia bulloides*
	Pullenia osloensis	*Robertinoides normani*	*Robertinoides pumilum*	*Stainforthia fusiformis*
	Stainforthia loeblichi	*Trifarina angulosa*	*Trifarina fluens*	*Trifarina arctica*
Calcareous imperforate	*Cornuspira foliacea*	*Pyrgo oblonga*	*Pyrgo subglobulus*	*Quinqueloculina sclerotica*
	Quinqueloculina stalkeri	*Triloculina tricarinata*		
Agglutinated	*Adercotryma glomerata*	*Astrorhiza* spp.	*Eggerelloides scaber*	*Hormosina pilulifera*
	Labrospira crassimargo	*Lagenammina difflugiformis*	*Quinqueloculina agglutinata*	*Rhabdammina* spp.
	Saccammina sphaerica	*Testulosiphon indivisus*		

Tab. 6.9. Core 07-3. Secondary benthic foraminiferal species.

Down-core the calcareous perforate group is mainly present with more than 96%, with a diminution on top arriving until 90% at 2016 A.D. The calcareous imperforate group is present with a maximum of 2% and the agglutinated group reaches 8% at 2016 A.D.

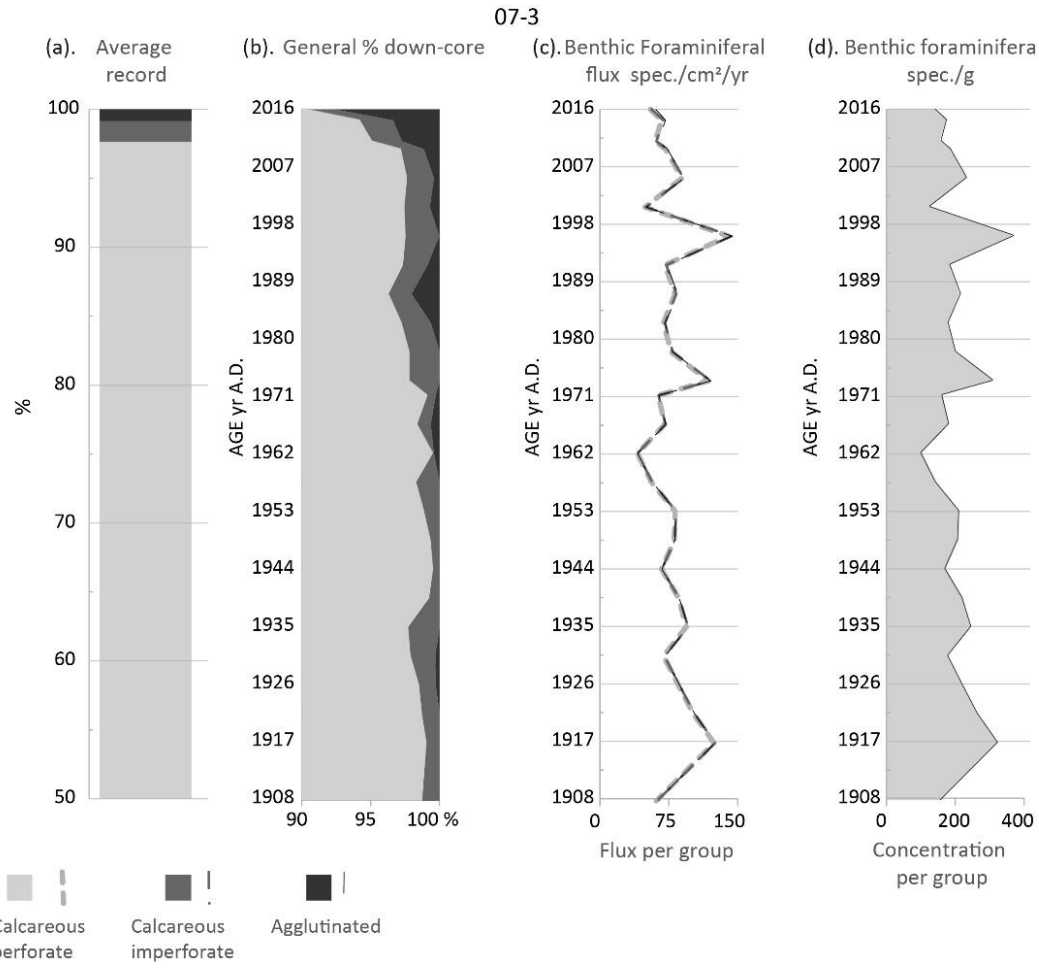


Fig. 6.18. Core 07-3. (a). General average percentage per group in the entire record. (b). General relative abundance per group down-core. (c). Benthic foraminiferal flux. (d). Benthic foraminifera concentration per gram of dry sediment (note that the concentration of the calcareous imperforate and agglutinated groups is less than 1 spec./g). The x-axes are different.

The flux and the concentration show a similar trend, with a general increase from 1908 to 1921 A.D. (reached 125 spec./cm^2/yr and 331 spec./g, respectively). A shifting trend is shown from 1921 until 1973 A.D. (reached a maximum of 96 spec./cm^2/yr and 319 spec./g) and from 1973 until 2016 A.D., a constant increase is shown (Fig. 6.18).

Diversity indexes and cluster analysis

The taxa (S) shows an increasing trend, with an increment on top, from 2014 A.D. surpassed 30 taxa reached 38 at 2016 A.D. The Dominance (D) and Shannon (H) index show an opposite trend. In general, D decreases, with a maximum of 0.15 at 1953 A.D. (Fig. 6.19). The minimum values of D are shown between 2014 and 2016 A.D., with 0.08. The Shannon index (H) shows a general increase, ranging between 2.4 and 2.9 (Fig. 6.19).

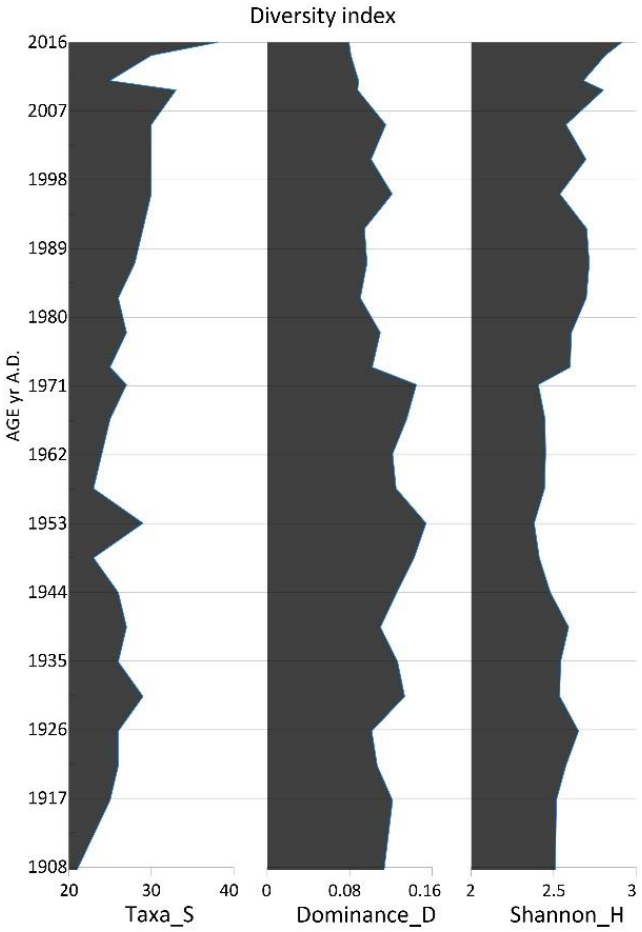


Fig. 6.19. Core 07-3. Diversity indexes. The x-axes are different.

The first Q-mode cluster analysis performed shows an outlier D, corresponding to 1971 A.D. indicating an abundance of *Rosalina* spp. A second cluster analysis is performed without the outlier, resulting in three clusters: Cluster A corresponds to samples with an abundance of *E. clavatum*, Cluster B corresponds to samples with the dominance of *C. reniforme*, and Cluster C corresponds to samples with an abundance of *A. gallowayi* (Fig. 6.20).

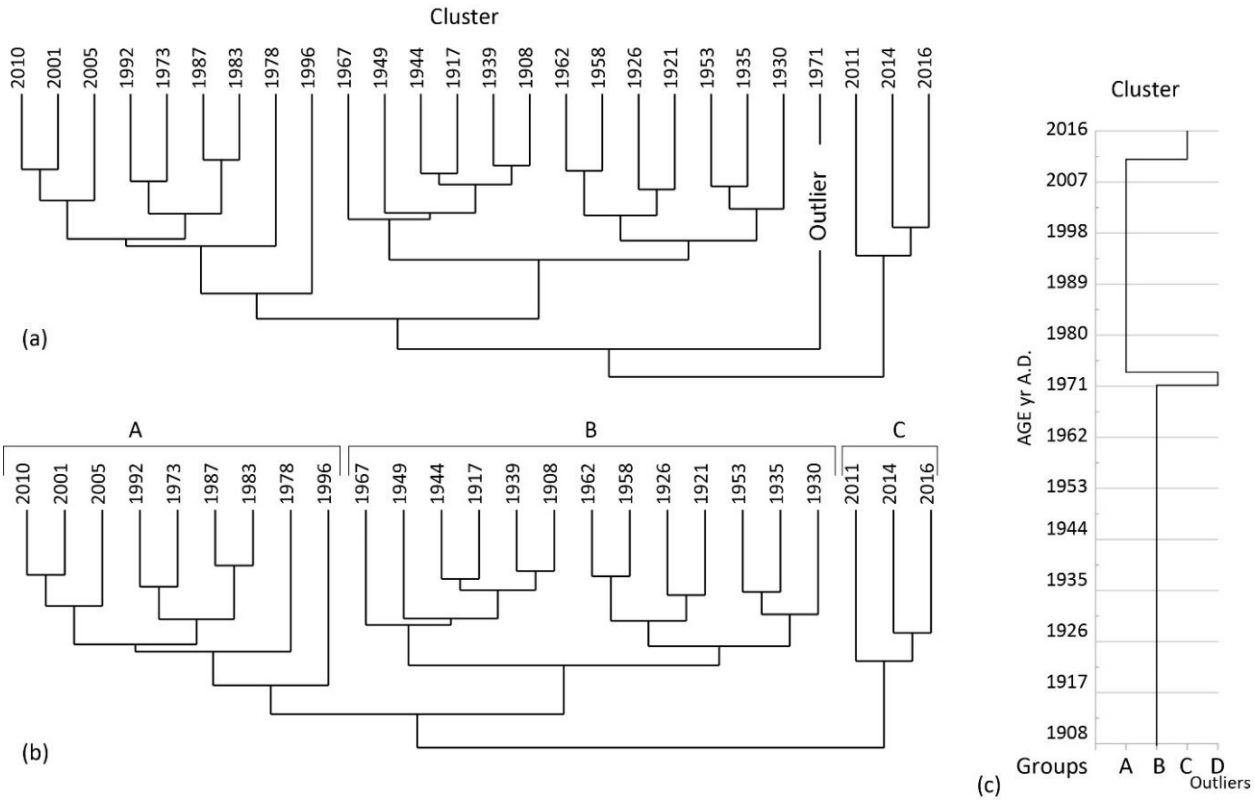


Fig. 6.20. Core 07-3. Q-mode cluster analysis (a). Dendrogram groups with outliers. (b). Dendrogram groups without outliers. (c). Cluster groups by age distribution down-core.

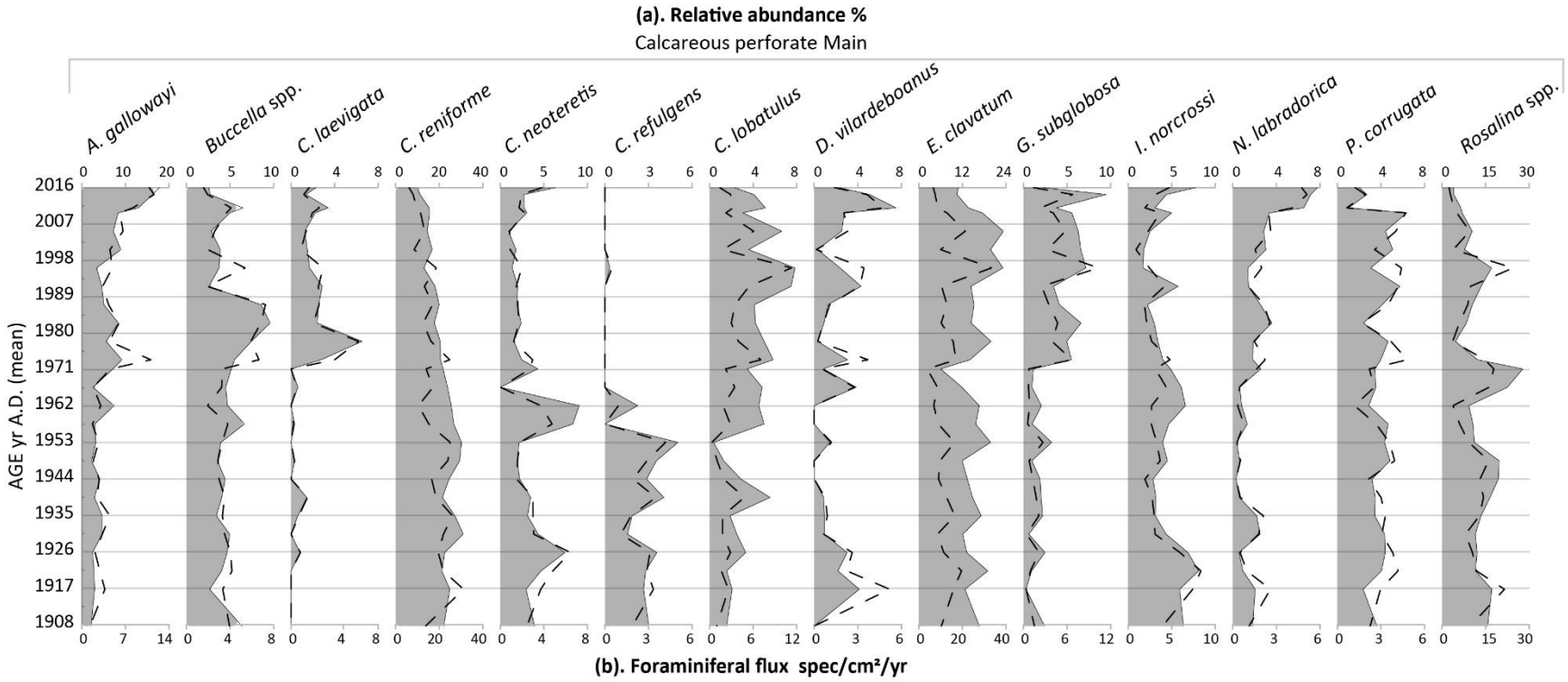


Fig. 6.21. Core 07-3. Benthic foraminifera: (a). Relative abundance (grey) and (b). Foraminiferal flux (black dashed line) of the main species. The x-axes are different.

The secondary species are present in less than 5% in the record (Fig. 6.22).

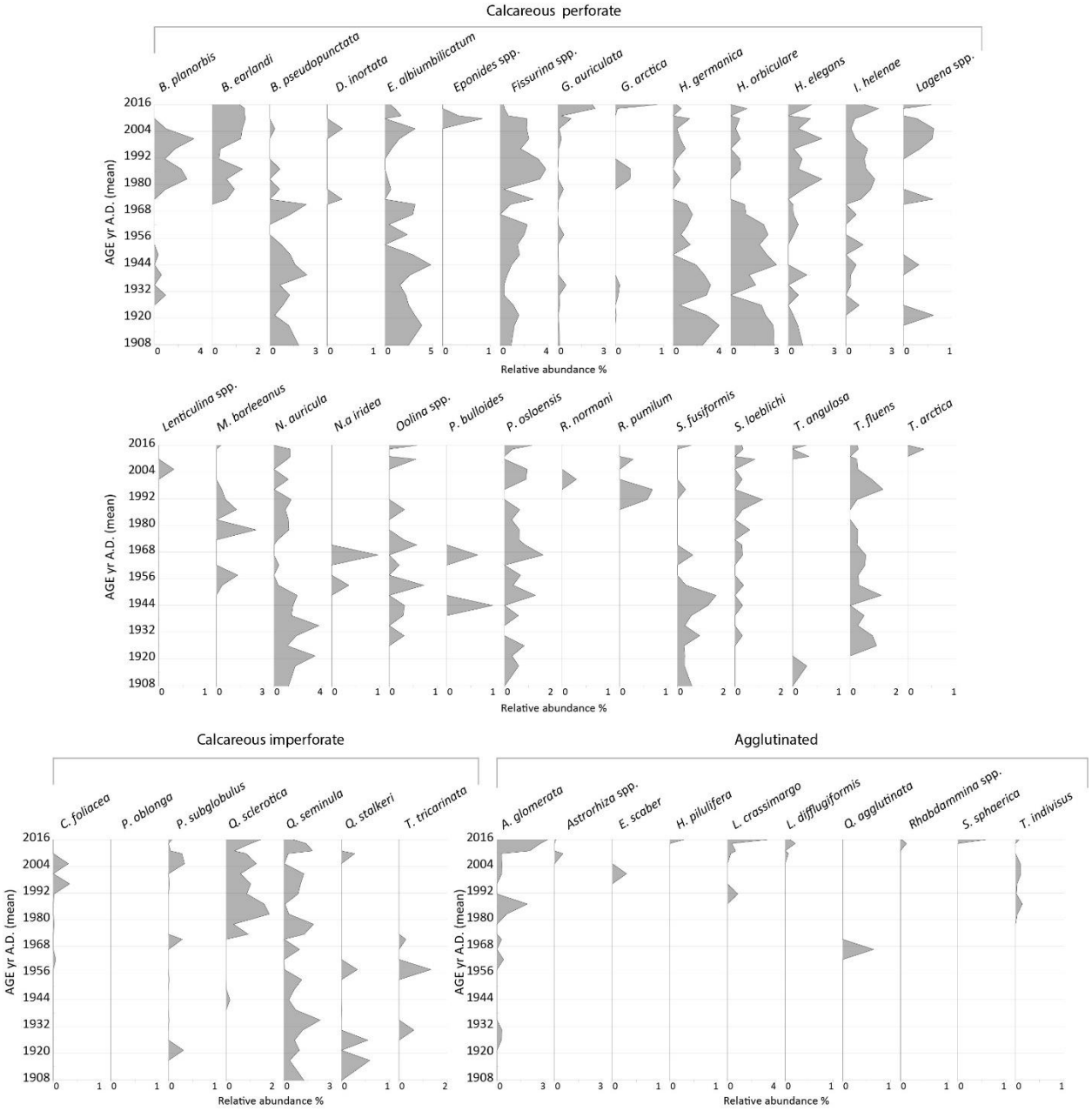


Fig. 6.22. Core 07-3. Secondary species.

6.3.4. Benthic foraminiferal pattern along the Kveithola Trough

On the base of the results of the classical cluster analyses (Figs. 6.10, 6.15, 6.20 and 6.23) and the age model (Tab. 6.1.). The benthic foraminiferal pattern in the Kveithola Trough are described considering two of the main climatic anomalies of the last two millennia, the Little Ice Age (LIA) between 1660 to 1890 A.D. and the Modern period from 1890 A.D. until the present (eg. Lamb, 1977).

LIA Period 1660 to 1890 A.D.

The LIA period is recorded only in stations 02-2 and 21-05.

In the core 02-2, the main species are *C. neoteretis* and *C. lobatulus*, reaching 44% at 1791 A.D. and 32% at 1676 A.D., respectively. *Melonis barleeanus* shows a high relative percentage during this period, reaching 13% at 1682 A.D. During the 1700s, *C. reniforme* and *E. clavatum* reached more than 15%. At *ca.* 1850 A.D., *C lobatulus* decreases, but continues presently with more than 10%. *Cassidulina reniforme, E. clavatum* and *M. barleeanus* show a decrease on top, while *C. laevigata* shows an increase on top reaching 12%at 1889 A.D. (Fig. 6.6). In general, the foraminiferal flux is low during this period and shows a general increase from 1743 A.D. (Fig. 6.6). The species *I. norcrossi, N. labradorica*, *N. iridea*, *T. angulosa, C. refulgens* and *C. laevigata* show shifting record reaching more than 5% (Fig. 6.6).

During the LIA in the middle core 21-05 the dominant species are *C. laevigata, C. neoteretis* and *C. lobatulus,* with maxima of 23%, 21% 19%, respectively. *Cassidulina reniforme* and *C. refulgens* reach more than 10%, showing a peak at 1813 A.D, (with 14% and 12% respectively) (Fig. 6.11). *Elphidium clavatum, I. norcrossi, M. barleeanus* and *N. labradorica* reach more than 5% between 1827 and 1848 A.D. *Globocassidulina subglobosa* is abundant at the bottom, reaching 7% at 1792 A.D. and increases again at the end of the LIA (*ca.* 1890A.D.) (Fig. 6.11). The foraminiferal flux shows a general decrease for all the main species (Fig. 6.8).

Modern Period 1890 to 2016

During the Modern Period, in the core 02-2 the species *C. neoteretis* and *C. lobatulus* remain as the predominant species, with more than 10% and reaching more than 20%. *Astrononion gallowayi, C. reniforme* and *C. laevigata* increase, reaching their maxima between *ca.* 1960 and 1990 A.D. (Fig. 6.6). *Buccella* spp., *E. clavatum, M. barleeanus, T. angulosa*, *T. carinata* and *T. fluens* show a shifting record

surpassing 5% and reaching the maxima after 1960s. The foraminiferal flux increase, showing a high flux between 1904 and 2016 A.D. (Fig. 6.3).

In the core 21-05, the species mainly present during the entire period are *C. laevigata* and *C. lobatulus* reaching more than 20%. *C. neoteretis* continue also as main species with more than 10%, except at 1893 A.D., when it shows a decrease arriving until less than 5%. *Astrononion gallowayi, C. reniforme, I. norcrossi, E. clavatum, I. helenae, M. barleeanus* and *N. labradorica* show a shifting record, increasing from *ca.* 1950 A.D. *Cibicides refulgens* and *G subglobosa* are present with more than 5% until *ca.* 1900 A.D. From *ca.* 2005 until 2016 A.D., the species *C. laevigata, C. reniforme, I. helenae, G. subglobosa* and *M. barleeanus* decreased. The foraminiferal flux remains constant during this period, increasing between 1964 to 2009 A.D., and decreasing between 2014 and 2016 A.D. (Fig. 6.8).

The bottom of the core 21-03, (close to the core 21-05), is dated at 1935 A.D. Three main species during the entire record are *C. laevigata*, *C. neoteretis* and *C. lobatulus,* ranging between 10 to 25% (Fig. 6.16). *Elphidium clavatum, I. helenae*, *I. norcrossi, M. barleeanus* and *N. labradorica* show a shifting record, with maximum values after *ca.* 1975 (except for *M. barleeanus* that reached the minimum at 1989 A.D.). Between 2014 and 2016 A.D., *C. reniforme* reaches the maximum with 9% (Fig. 6.16). The foraminiferal flux is fluctuating during the entire record (Fig. 6.16).

The northern core 07-3 started the record at 1908 A.D., and is characterised by the predominance of the species *C. reniforme, E. clavatum* and *Rosalina* spp. with more than 10%. *Cibicides. refulgens, C. neoteretis* and *I. norcrossi* are abundant from 1908 to *ca.* 1965 A.D. (more than 5%), then decreasing until 2016 A.D. *Cibicidoides lobatulus* and *P. corrugata* are present with a maximum of 5%, while the species *Buccella* spp., *C. laevigata, D. villardeboanus, I. norcrossi* and *N. labradorica*, barely surpassed 5%. The species *A. gallowayi* and *G. subglobosa* become abundant from *ca.* 1998 A.D. reaching 18% and 10% respectively (Fig. 6.21). The foraminiferal flux is fluctuating, showing a decrease until 1971 A.D., with a peak of most of the species at 1996 A.D. and a general increase at 2016 A.D. (Fig. 6.21).

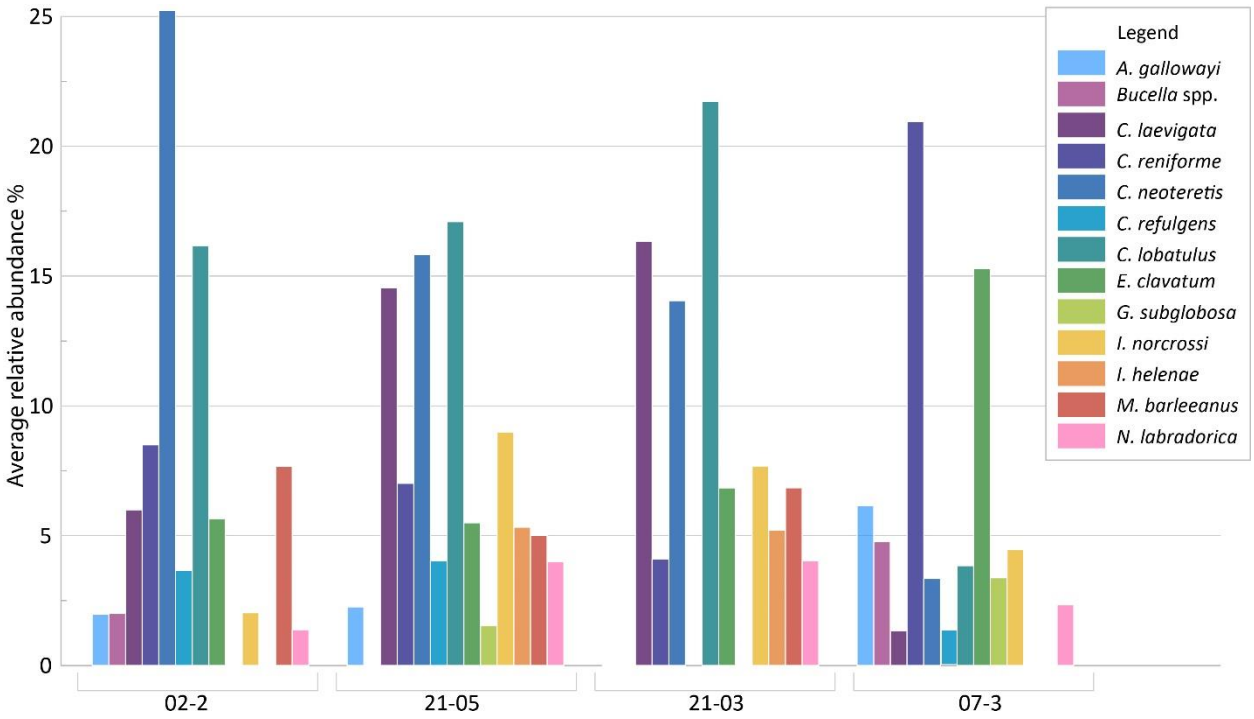


Fig. 6.23. Distribution of the average relative abundance of the main species at each station throughout Kveithola Trough From outer to inner continental shelf.

6.4. Discussion

The AW influx is one of the main environmental factors to be considered in the Barents Sea (Dijkstra et al., 2017b), as it is the main heat distributor in the area (Dickson et al., 2000; Goosse and Holland, 2005; Loeng and Drinkwater, 2007). Furthermore, the AW influx provides an important food source for the foraminiferal because it enhances the primary productivity due to the high quality and quantity of nutrients (Dijkstra et al., 2017b).

Two-time intervals characterised by different benthic foraminiferal assemblages can be distinguished in the sedimentary record of the Kveithola Trough area (Tab. 6.11; Fig. 6.28):

a. LIA 1660 to 1890 A.D.

During the LIA, the Kveithola Trough is characterised by cold conditions registered both in the outermost station 02-2 and in the inner station 21-05. The low foraminiferal flux suggested unfavourable conditions for the foraminifera, that might be related with the presence of seasonal sea ice. Similar environmental conditions are also indicated by Dijkstra et al., (2017b) in Bjørnøyrenna, and reported by Wilson et al. (2011), in the near Barents Sea (Fig. 6.28).

At station 02-2 (frontal area of Kveithola Trough), the cold-bottom water conditions are predominant, indicated by the abundance of the cold ArW-related *C. reniforme* and *Buccella* spp. (Fig. 6.24; Tab. 6.10). From *ca.* 1820 A.D., the input of meltwater gradually reduced, as indicated by the decreasing percentage of *E. clavatum,* allowing the increase of the warm water input, indicated by the increasing percentage of warm water-related species *A. gallowayi* and *C. laevigata*.

The changes in the food supply are probably related to the arriving of the cold bottom currents, shown by the food supply indicators *N. labradorica, I. norcrossi, T. fluens,* and by the bottom currents indicator *T. angulosa*, while a decreasing salinity is recorded by the decreasing percentage of *C. reniforme* in the station 02-2 (Fig. 6.24; Tab. 6.10). These fluctuating conditions in the food supply increased from *ca.*1820 A.D. linked to the strong seasonal productivity, related to warmer conditions. Wilson et al. (2011) and Dijkstra et al. (2017 b) reported similar conditions in areas close to the Kveithola Trough, indicating the end of the LIA. The energy of the bottom currents are testified by the input of coarse sediment and by the abundance of *C. lobatulus* and *C. refulgens* (Fig. 6.24; Tab. 6.10).

The interaction between the different water masses become stronger during the end of the LIA from *ca*. 1820 to 1890 A.D. At station 02-2, between *ca.* 1820 and 1848 A.D., the reduction of the influence of meltwater and cold-water, favouring the increase of the warm-water influx, is indicated by *A. gallowayi* and *C. laevigata*, and the decrease of *E. clavatum* and *N. labradorica* (Fig. 6.24; Tab. 6.10). From *ca.* 1848 A.D., the increasing benthic foraminiferal fluxes of cold indicators *Buccella* spp. and *E. clavatum* suggests the proximity to the Polar front, associated with high productivity (Fig. 6.24; Tab. 6.10). At station 21-05, the cold bottom water conditions are predominant, as testified by the presence of cold-water species *C. reniforme* and *E. clavatum* (Fig. 6.24; Tab. 6.10). The food supply is generally low during this period, with brief impulse of nutrient-rich water confirms by the peaks of the phytodetritivorous species *N. labradorica* and the increase of the food supply indicators *I. norcrossi* and *I. helenae*. The end of the LIA is characterised by fluctuating conditions, with influx of cold ArW and meltwater, suggested by the abundance of *E. clavatum* (Fig. 6.25; Tab. 6.10), alternated by the increasing warm AW influx, testified by the rise of the cooled AW *C. neoteretis,* warm and saline species *C. laevigata* and *A. gallowayi* (Fig. 6.25; Tab. 6.10). The increase of the food supply is possibly related to the warmer conditions and Polar front influence and by the consequent increase in productivity (Dijkstra et al., 2017 b), also reported in the outer station 02-2 (Fig. 6.25; Tab. 6.10).

b. Modern period 1890 to 2016 A.D.

The beginning of the modern period is characterised by warmer temperature and the migration of the Polar front to northern position. At station 02-2, from 1890 until 1901 A.D., the raise in the foraminiferal flux and the number of taxa, reflect warmer conditions, also indicated by the raise of *C. laevigata* and *A. gallowayi*. However, the cold-water influence continues, as shown by the abundance of *C. reniforme* (Fig. 6.24; Tab. 6.10). The food supply is constant, with a peak at 1988 A.D. indicated by *I. norcrossi* that could be relate to the input of cold and saline water shown by the abundance of *C. reniforme* (Fig. 6.24; Tab. 6.10). The increase in flux and abundance of *A. gallowayi*, *C. laevigata* and *C. neoteretis* indicate a further increase of the AW influence and a stronger increase of the temperature, from *ca.* 2000 A.D. (Fig. 6.24; Tab. 6.10).

In station 21-05, the warmer conditions are shown by the increase of *A. gallowayi* and the abundance of *C. laevigata* (Fig. 6.25; Tab. 6.10), also associated with the decrease of the meltwater influx shown by the diminution of *E. clavatum* and the fluctuating record of the cold-water indicator *C. reniforme*. These cold species recorded a decrease between 1960 and 2005 A.D., and then increased during the last part of the

record indicating input of cold water between 2005 and 2016 A.D. These cold conditions together with the increasing record of the AW from the 2000 A.D., suggest unstable conditions in this area with the strong interaction between cold and warm water (Fig. 6.25; Tab. 6.10), also indicated by the increase of AW related species *A. gallowayi*, *C. laevigata* and *C. neoteretis* (Fig. 6.25; Tab. 6.10). The increasing food supply is shown by *I. norcrossi* and *I. helenae* and the presence of *N. labradorica* especially from *ca.* 1960 A.D., coinciding with the increasing warmer conditions. The energy of the bottom currents is constant, with minor fluctuations during this period, shown by the arrival of coarse sedimentats and high abundance of *C. lobatulus* (Fig. 6.25; Tab. 6.10).

In the innermost area, at the station 21-03, the record starts at 1935 A.D., and is characterised by the predominance of AW influence as shown by the abundance of *C. laevigata* and *C. neoteretis,* in agreement with the conditions in the other stations. The continuing interaction between warm and cold-water masses, is indicated by the presence of the AW influence *M. barleeanus* and the glaciomarine *C. reniforme*, indicating changes in the salinity. The high energy of the sea bottom, is associated with the presence of *C. lobatulus*, linked with the speed of the bottom currents (Lantzsch et al., 2017; Dijktra et al., 2017b) and the constant input of coarse sediment (Fig. 6.26; Tab. 6.10). The input of cold-meltwater, indicated by the presence of *E. clavatum*, probably favours the seasonal food supply, testified by the nutrient indicators *I. helenae*, *I. norcrossi* and *N. labradorica* (Fig. 6.26; Tab. 6.10). These food indicator species show an increase from the late 1970s until 2005 A.D., together with the abundance of the saline and warm-water indicator *C. laevigata* (Fig. 6.26; Tab. 6.10). The high fluxes of *C. laevigata* and *C. reniforme* from the end of 1980s indicate warmer conditions, related to the presence of AW (Fig. 6.26; Tab. 6.10).

At the shallowest and north most station 07-3, the cold conditions are prevalent, with the dominance of the cold and saline indicator *C. reniforme*, the glaciomarine and meltwater related *E. clavatum*, and the cold seasonal sea ice associated *Buccella* spp. The input of warm-water is low during the beginning of the record (1908 A.D.), compared to in-trough sites, shown by the slight abundance of AW species *A. gallowayi, C. laevigata* and *C. neoteretis* (Fig. 6.27; Tab. 6.10), these species show a general increase from *ca.* 1950 A.D. The food supply is constant, shown by the abundance of *I. norcrossi*, *N. labradorica* and *P. corrugata* (Fig. 6.27; Tab. 6.10). An increase in the energy of the bottom currents is recorded by the presence of *C. lobatulus*, which registered a peak at 1939 A.D., related to the sand input documented at the same age (Fig. 6.27; Tab. 6.10).

From 1971 A.D., at station 07-3, the benthic foraminiferal assemblages show an increase of the interaction between cold and warm conditions similar to the situation recorded in the trough, indicated by the increasing of the AW species *A. gallowayi* and *C. laevigata*. The cold-water input continued, testified by the influence of the ArW and the proximity of the Polar front (Loeng, 1991, Loeng et al., 1997), suggested in our record by the presence of the glaciomarine and cold meltwater species *E. clavatum*, and from 1970 A.D., by the abundance of *Buccella* spp (Fig. 6.27; Tab. 6.10). The food supply also reflects this unstable environment, showing a low organic input indicated by the presence of the detritivorous species *G. subglobosa*. The velocity of the bottom currents tends to increase as shown by the abundance of *C. lobatulus* and as indicated by Dijkstra et al. (2017b) in the southern area of the Barents Sea.

From the 2010 A.D., in the northern station 07-03, the increase of the warmer conditions are shown by the rise of the AW indicators *A. gallowayi*, *C. laevigata* and *C. neoteretis* (Fig. 6.27; Tab. 6.10). The reducing influence of the sea ice incoming close to Kveithola Trough is show by the decrease in the sea ice indicators *C. reniforme*, *Buccella* spp. and *E. clavatum* (Fig. 6.27; Tab. 6.10). The presence of high food requirements species, like *N. labradorica*, *I norcrossi*, *P. corrugata* and the low organic content related *G. subglobosa,* indicate the different source, quantity and quality of the food entrance to this area (Fig. 6.28; Tab. 6.10). The low abundance of *M. barleeanus* suggests that the main source of food supply is fresh phytodetritus, confirmed by the presence of *N. labradorica*. Dijkstra et al. (2017b), in the area of Bjørnøyrenna, report similar conditions related to the vicinity of the Polar front.

In summary, the Modern period can be divided into two intervals. The first one from *ca.* 1890 to 1975 A.D., with the interaction between warm and cold-water masses, which mark the end of the LIA and the beginning of warming conditions. The increasing abundance of AW species, foraminiferal fluxes and food supply suggests meltwater at north and warmer conditions at south, producing the input and increase of the primary productivity (Fig. 6.28). A second interval, from 1975 to 2016 A.D., marked by the greater inflow of AW, warmer conditions and food supply, is associated with the increase of the foraminiferal fluxes of the species related with the AW conditions. Wilson et al. (2011) also documented these warmer conditions in the Barents Sea over the last 100 years, that improved the preservation potential due to the increased warmer water and reduction of corrosive cold water (Tab. 6.11; Fig. 6.28). This increase in the bottom temperature is greater in the outer station 02- 2 and in the inner stations 21-05 and 21-03, and is lower in the north most station 07-3 (Tab. 6.11; Fig. 6.28 and 6.23).

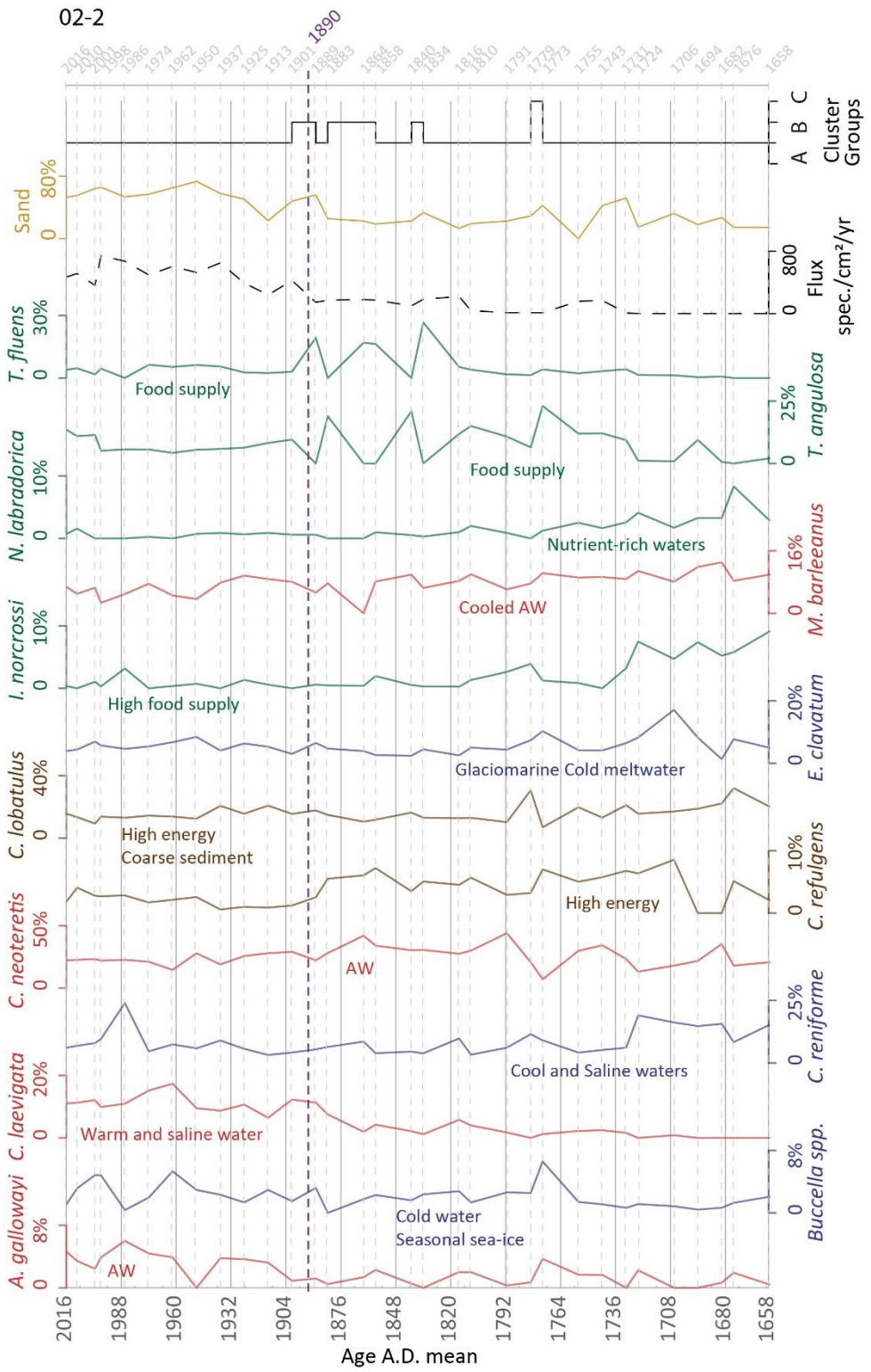


Fig. 6.24. Key proxy correlation at station 02-2 presenting: Cluster division of benthic foraminifera. Sand content. Benthic foraminiferal flux. Relative abundance of the main benthic foraminiferal species. The x-axes are different.

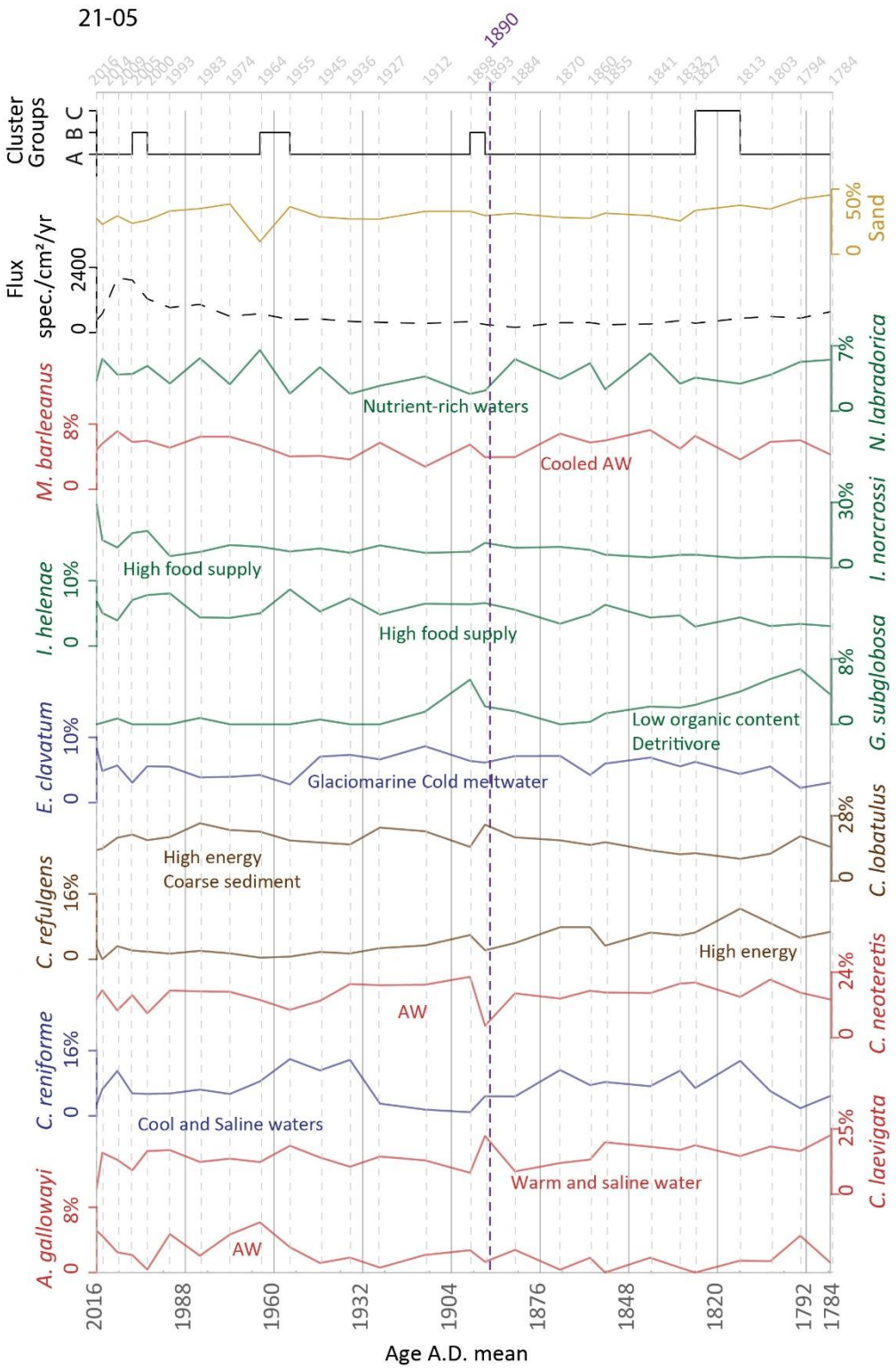


Fig. 6.25. Key proxy correlation at station 21-05 presenting: Cluster division of benthic foraminifera. Sand content. Benthic foraminiferal flux. Relative abundance of the main benthic foraminiferal species. The x-axes are different.

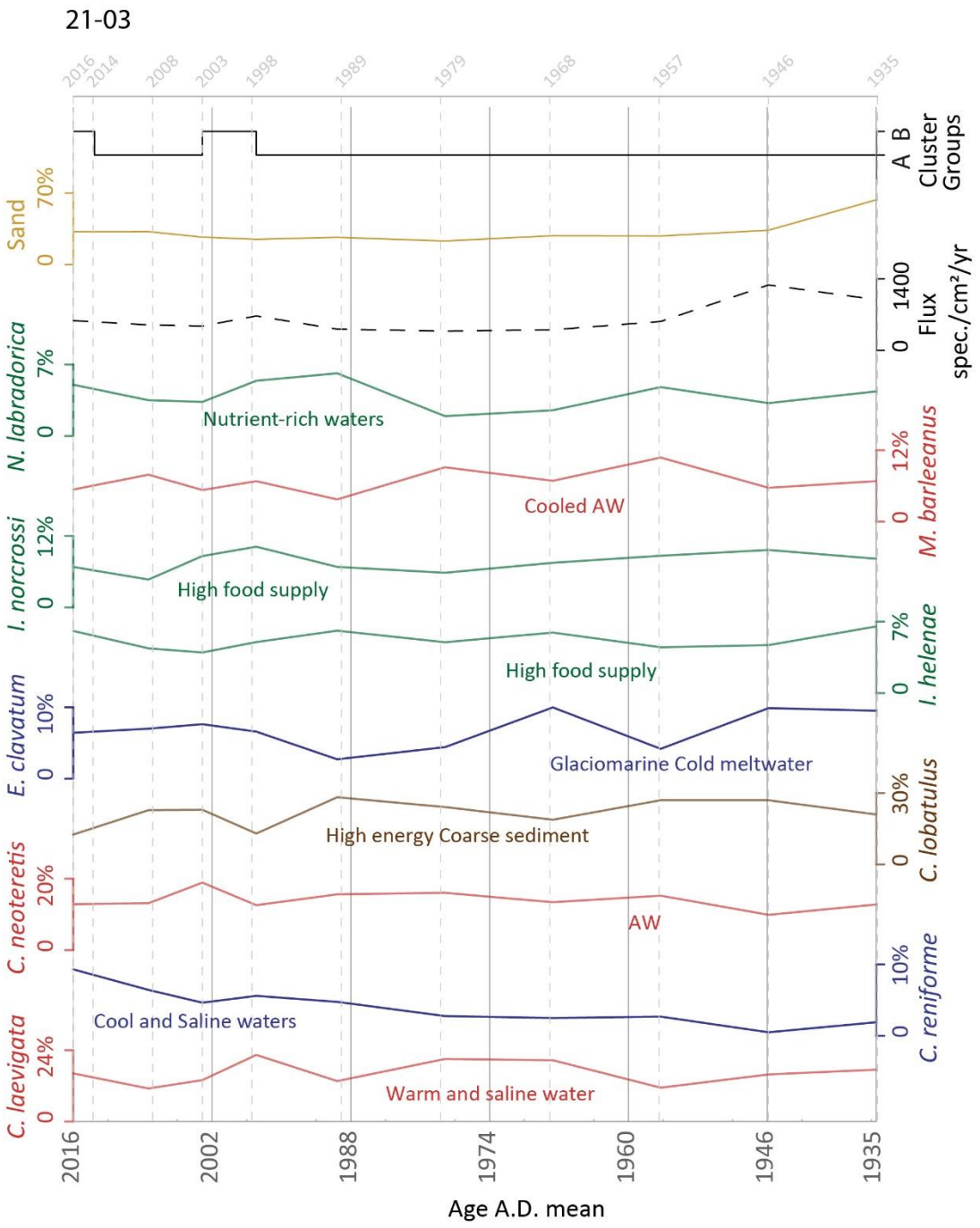


Fig. 6.26. Key proxy correlation in the station 21-03 presenting: Cluster division of benthic foraminifera. Sand content. Benthic foraminiferal flux. Relative abundance of the main benthic foraminiferal species. The x-axes are different.

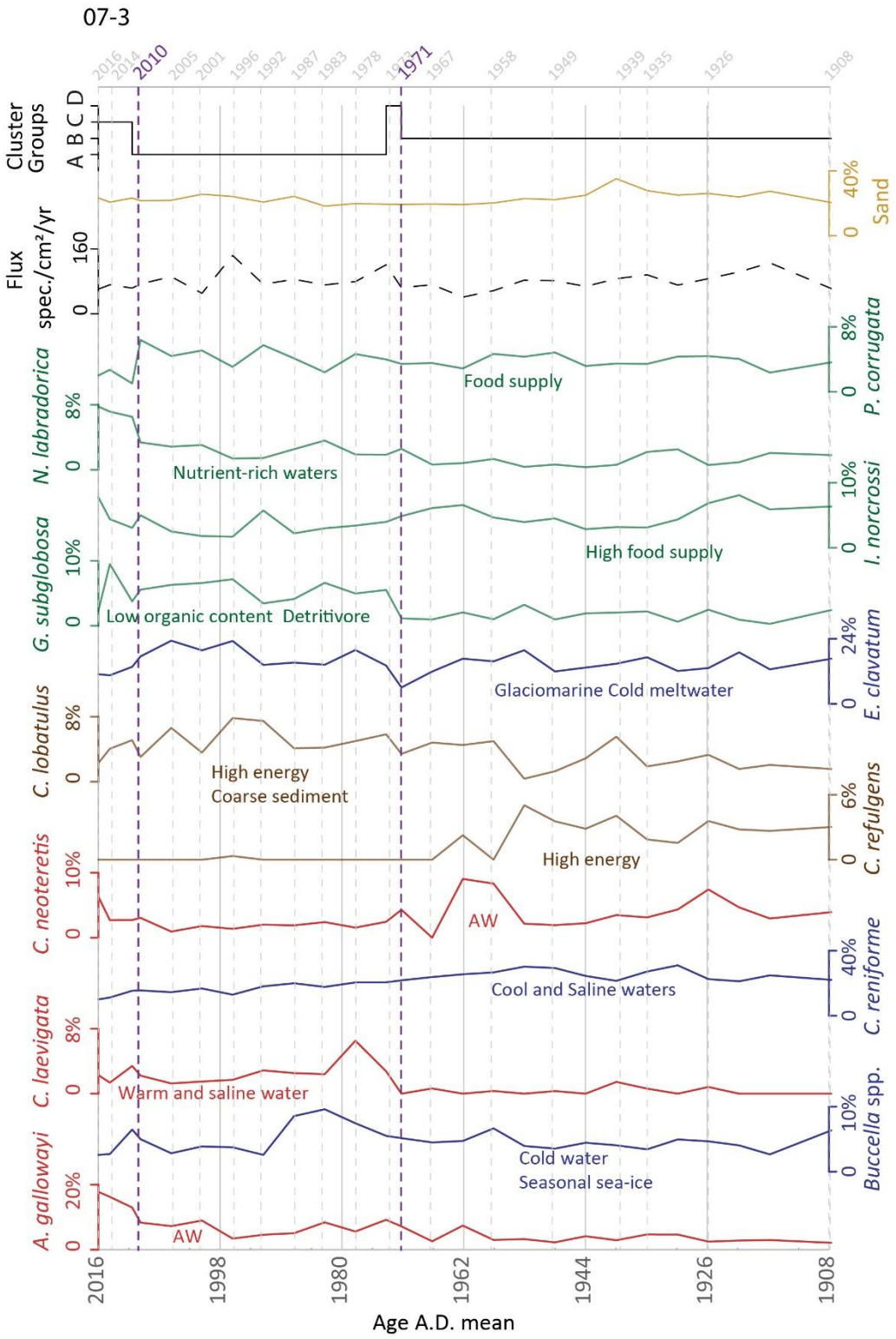


Fig. 6.27. Key proxy correlation in the station 07-3 presenting: Cluster division of benthic foraminifera. Sand content. Benthic foraminiferal flux. Relative abundance of the main benthic foraminiferal species. The x-axes are different.

Main species	Environmental conditions	References
Astrononion gallowayi	Temperature tolerant, warm and saline water, epifaunal. Elevated current activity and coarse sediment.	Polyak et al., 2002; Saher et al., 2009; Saher et al., 2012.
***Buccella* spp.**	Cold water, seasonal ice cover, sandy and shallow areas.	Steinsund et al., 1994; Hald and Korsun, 1997; Saher et al., 2009; Saher et al., 2012.
Cassidulina laevigata	Warm and saline water.	Sejrup et al., 2004; Saher et al., 2009; Steinsund, 1994; Dijkstra et al., 2017b.
Cassidulina reniforme	Cold and salty water, related to glaciomarine environments	Korsun and Hald, 1998; Hald and Korsun, 1997; Murray, 2006; Saher et al., 2009; Saher et al., 2012; Dijkstra et al., 2017b.
Cassidulina neoteretis	Cooled Atlantic water, seasonal ice-free conditions. High seasonal productivity.	Saher et al., 2009; Seidenkrantz, 1995; Dijkstra et al., 2017b.
Cibicidoides lobatulus ***Cibicides refulgens***	Temperature tolerant, sandy sediments, epifaunal, high energy environments.	Steinsund et al., 1994; Hald and Steinsund, 1996; Wollenburg and Mackensen, 1998; Murray, 2006; Saher et al., 2009; Saher et al., 2012.
Elphidium clavatum	Cold bottom water, low salinity, high turbidity.	Steinsund et al., 1994; Sejrup et al., 2004; Murray, 2006; Saher et al., 2009; Saher et al., 2012; Dijkstra et al., 2017b.
Globocassidulina subglobosa	Cold–temperate water, muddy sediments, low organic content, infaunal, detritivore.	Murray, 2006.
***Islandiella* spp.**	Mud-silt sediments, infaunal, free, detritivore, high food supply. High and stable bottom salinities.	Steinsund et al., 1994; Korsun and Hald, 1998; Polyak et al., 2002; Murray, 2006; Saher et al., 2009; Saher et al., 2012; Dijkstra et al., 2017b.
Melonis barleeanus	Arctic-Boreal species. Related to cooled Atlantic Water and degraded organic matter, tolerates dysoxia, maximum abundance under oxic conditions, infaunal, detritivore, mud-silt sediment.	Steinsund et al., 1994; Murray, 2006; Saher et al., 2009; Saher et al., 2012; Dijkstra et al., 2017b.
Nonionella iridea	Phytodetritus species, infaunal	Murray, 2006.
Nonionellina labradorica	Cold water, seasonal sea ice cover, high food supply.	Sejrup et al., 2004; Murray, 2006; Saher et al., 2009; Saher et al., 2012.
Patellina corrugata	Food availability, epifaunal, clinging or attached.	Murray, 2006
Trifarina angulosa	Temperature tolerant; sand-gravel sediments, epifaunal, influence of bottom currents.	Steinsund et al., 1994; Murray, 2006; Saher et al., 2009.
Trifarina fluens	Close to the Polar front. High seasonal biological productivity.	Steinsund et al., 1994; Polyak et al., 2002;

Tab. 6.10. Main ecology indicators

Period	02-2	21-05	21-03	07-3
LIA 1660 to 1890 A.D.	Predominant cold conditions. The cold AW represented the main influence of AW.	Predominant cold conditions, ending with unstable period with peaks of cold and warm water.	No record	No record
Modern Period 1890 to 2016 A.D.	From 1890 to 1975 A.D., interaction between dominant cold conditions with the warm water. From 1975 until 2016 A.D., increased and dominance of the warm water input, and increasing food supply.	Continuing unstable conditions until *ca.* 1940 A.D. Increasing cold and saline bottom water in the period 1940-1960. From the 1960s, increased interaction between cold and warm water, higher input of food supply and stronger bottom current.	Interaction of cold and warm water, with the dominance of AW influence, and the interaction of the cold and high energy bottom currents.	Between1890 to 1975 A.D., predominance of cold conditions, and beginning of the interaction between cold and warm water, with high organic content related to the Polar front influence.From 1975 A.D., cold bottom water with increase of AW influx (amplified from 2010 A.D.). Fluctuating meltwater influx. High phytodetritus input.

Tab. 6.11. Summarised descriptions and interpretations at each core station in Kveithola Trough, using the three main regional intervals.

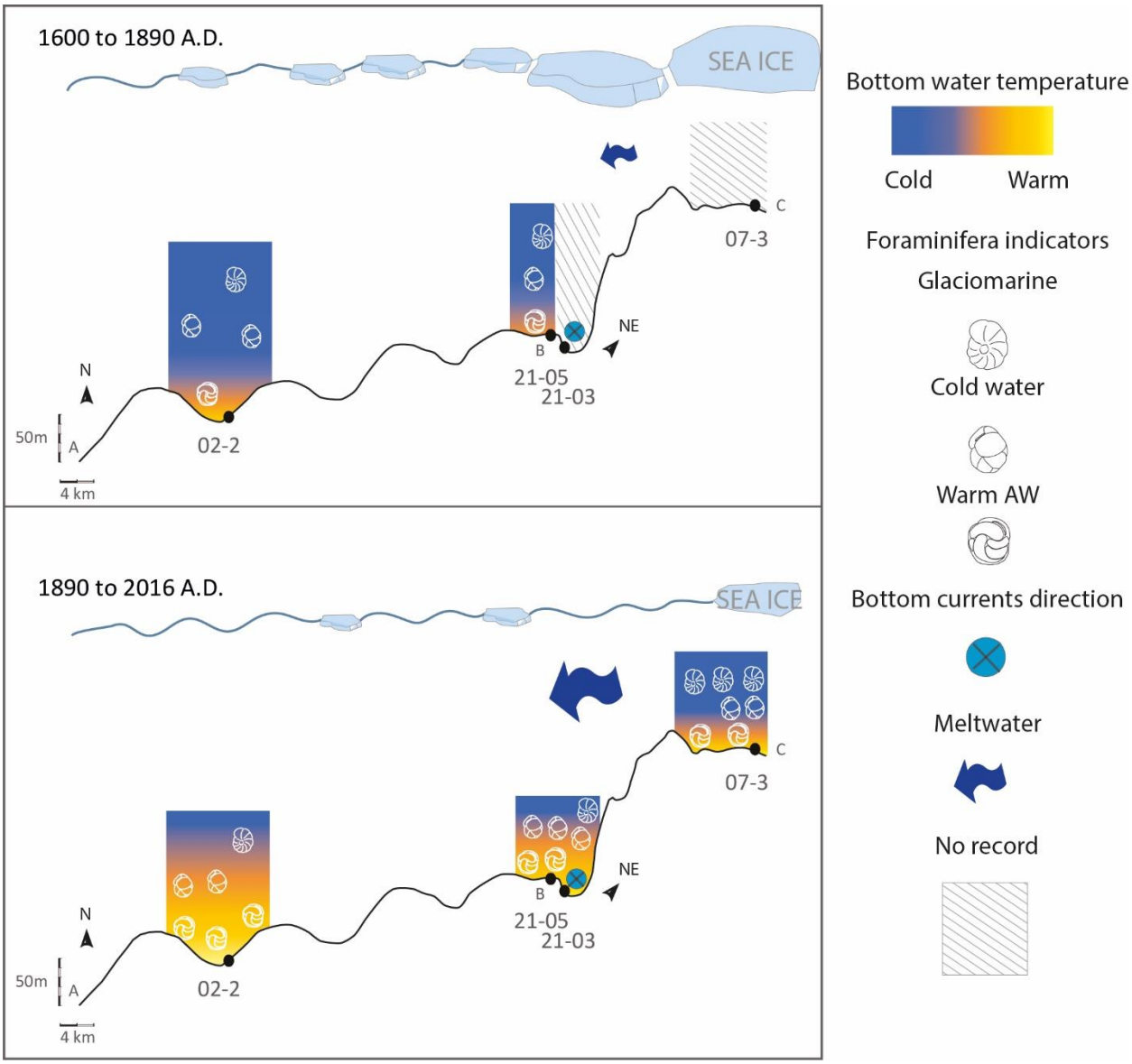


Fig. 6.28. Palaeoenvironmental reconstruction of the record from Kveithola Trough from *ca.* 1660 to 2016 A.D. indicating the two main environmental scenarios.

6.5. Conclusions

This study focused on four multi-cores collected along Kveithola Trough; from the outer station 02-2, corresponding with *ca.* 350 years of sedimentary record (1658-2016 A.D.), two inner stations 21-05 with *ca.* 230 yr (1784-2016 A.D.), and 21-03 with *ca.* 80 yr (1935-2016 A.D.), and the shallower station 07-3, with *ca.* 110 yr (1908-2016 A.D.). This temporal range recorded the period from LIA to Modern Period, and recorded the AW influx into the Barents Sea. Each site reacted differently to these warming conditions, depending on the geographical position, influence of the main water masses, and proximity to the Polar front. The manuscript is divided in three steps: the temporal evolution at each station, the oceanographic response of the Kveithola Trough system and the comparison with other areas of the Barents Sea.

In general, the AW indicators *A. gallowayi, C. neoteretis* and *C. laevigata*, and the cold ArW indicators *Buccella* spp., *C. reniforme* and *E. clavatum* mainly composed the foraminiferal assemblages.

The period from 1660 to 1890 A.D., corresponds to the LIA record (stations 02-2 and 21-05), indicating general cold conditions with AW influence principally in the outer station. At the end of the LIA and at the beginning of the Modern Period, a high interaction among the warm AW, the cold ArW and the bottom currents occurred. The Modern Period is divided into two intervals. The first, from 1890 to 1975 A.D., showed a phase of strong interaction between the cold and warm water masses, with brief warming periods and interrupting cold events. The second from 1975 to 2016 A.D., represents a phase with the greater influx of AW and increasing heat influx into the Barents Sea. Although, the warming of the water masses associated with the inflow of AW into the Barents Sea and the neighbouring areas is also documented by other Authors (e.g. Ingvaldsen et al., 2002; Bengtsson et al., 2004; Willson, 2011; Dijkstra et al., 2015-2017b), it is important to provide further studies to understand the local and the regional response to the ongoing climate changes.

II. The last decades in the Kveithola Trough: taphonomic processes to explain the bias between living (CTG-stained) and dead foraminiferal assemblages

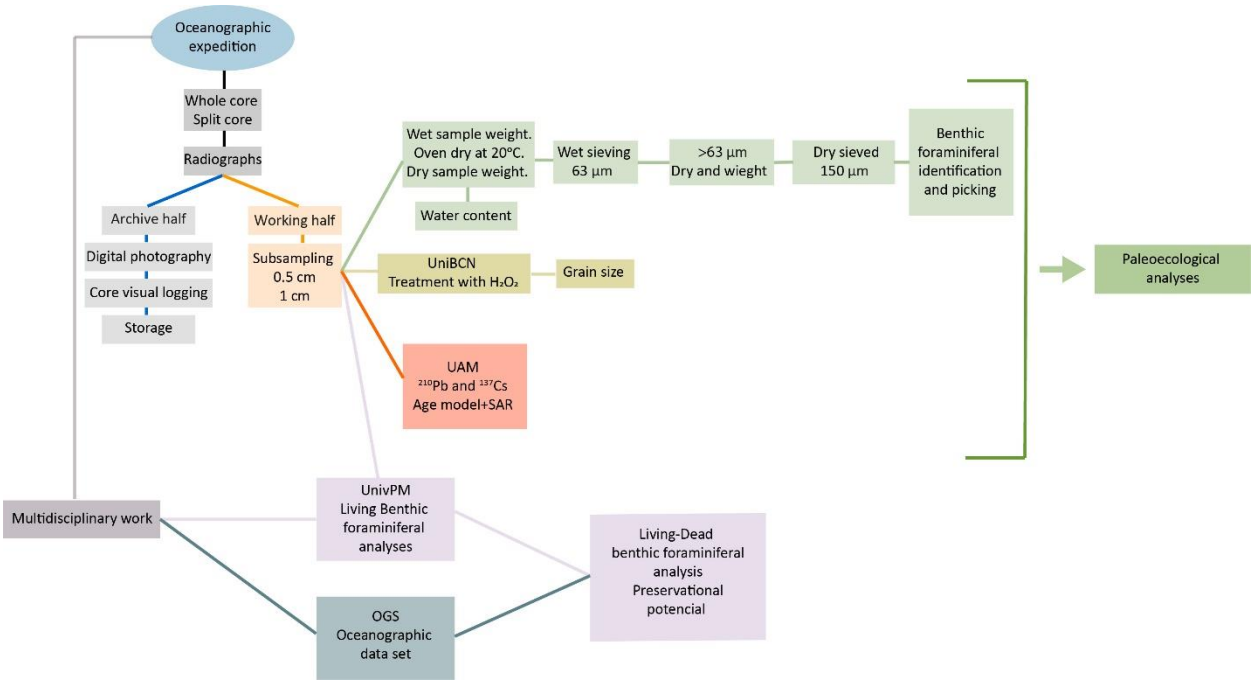
Kveithola Trough corresponds to a complex geomorphological environment located at the sea ice limit and influenced by the interaction of different water masses (Atlantic and Arctic waters) (Fig. 6.1). (Aagaard, 1989; Loeng, 1991; Vinje and Kvambekk, 1991; Loeng et al., 1997; Orvik and Niiler, 2002; Maslowski et al., 2004; Smedsrud et al., 2013). This gives it certain ecological characteristics, such as the high productivity that has increased with the advance of Atlantification in the area (Dijkstra et al., 2017b).

Some of these paleoclimatic studies have been based on benthic foraminifera records from the Barents Sea (Green, 1960; Hald and Korsun, 1997; Sarnthein et al., 2003; Ślubowska-Woldengen et al, 2007; Saher et al., 2009; Groot et al., 2014; Dijkstra et al., 2017a; Dijkstra et al., 2017b). Benthic foraminifera are important (paleo-) ecological indicators due to their wide diffusion in the oceans, and their good potential preservation in the fossil record. In fact, the distribution of the foraminiferal living assemblages (lateral and depth variation) in the Barents Sea, is strongly related to physical, chemical and geographical characteristics of the area (Dijkstra et al., 2017a), the sedimentation, the seasonality (Ivanova et al., 2008 and reference therein), and conditioned by the Atlantic Water and Polar front influence (Dijkstra et al., 2015; 2017a; 2017b). Studies that compare the living and dead benthic foraminiferal assemblages point to some preservation issues (transport, bioturbation, dissolution and/or broken test), which may bias the interpretation of the fossil record (e.g., Hald and Korsun, 1997; Wollenburg and Mackensen, 1998; Dijkstra et al., 2017a; Dijkstra et al., 2017b).

Based on this premise, the objective of this study is three folded: 1) to discuss for the first time the distribution of living foraminiferal assemblages in the Kveithola Trough and their relation to the local oceanographic processes; 2) to evaluate the taphonomic processes that bias the ecological interpretation in a high-latitude environment; and 3) to reconstruct environmental variations of the last decades on the basis of the dead foraminiferal assemblages. To reach these objectives we have analysed oceanographic, geomorphological, and sedimentological data, as potential drivers of the living and dead foraminiferal assemblages.

6.6. Material and methodology

The workflow 6.2 shows the scheme of the materials and methods followed for this chapter. Three cores collected in Kveithola Trough, are studied for radiogenic, grain size, biological, oceanographic and micropaleontological analyses. For this study, we use three stations 02-2, 21-05 and 07-3; called 02, 21 and 07 respectively. The Tab. 6.12 summarises the information about the first 10 cm of the multicores samples used for this study.



Workflow 6.2. Summary scheme of the materials and methods used for the multi-cores from Kveithola Trough. For more details, see chapter 2. Materials and methodology

Station	Coordinates	Water depth (m)	Mean grain size (phi)	Chl-a (µg/g)	BAC (mg/g)	Algal fraction of bpc%	Lipid (mg/g)	CHO (mg/g)
02	74° 51.49' N, 16° 05.84' E	376	4	0.27	2.52	10.45	0.49	2.34
21	74° 52.40' N; 17° 21.60' E	306	5	1.24	6.23	17.27	1.27	7.00
07	4° 59.69' N; 17° 59.72' E	159	6	4.13	5.97	34.13	1.72	7.02

Tab. 6.12. Location and water depth of the multi-cores, and average values (0-10 cm bsf) of physical and biochemical characteristics. Chl-a= Chlorophyll-a, BAC= bioavailable carbon, and algal fraction of BPC, Lipid and CHO= carbohydrates (from Caridi et al., 2019).Results

6.7. Results

6.7.1. Water masses properties and ocean current variability

Based on thermohaline properties, we distinguished the two main water masses in the Kveithola Basin in June 2016: the warmer and saltier AW with θ > 4.50 °C and SAL > 35.10 and the colder and fresher water originating from the Barents Sea and the northern shelves with θ < 4.00 °C and SAL < 35.00. Moreover, lower DO values are associated prevalently with the AW and higher values with the shelf waters. The horizontal and vertical distribution of the physical and biogeochemical properties is investigated along four S-N oriented sections, two of which went through (or close to) the stations where the sediment samples are collected and hence are presented here (Fig. 6.29).

In general, θ and SAL are higher in the upper layer with values from 4.00 to 6.95 °C, and from 34.80 to 35.15, respectively (Fig. 6.29). Below 200 m depth, instead, and especially in the northernmost part of the study area we found a core of cold (<4.00°C), fresh (minimum *ca.* 34.90), oxygenated and turbid water. The distribution of the thermohaline properties reveal a well stratifies water column (according to the potential density anomaly, not shown). A marked horizontal variability is also found in the upper layer, probably associate with strong mesoscale variability. The outermost S-N transect (S1) is characterised by a major presence of AW than the inner transect S3 in its southernmost part. There, θ and SAL highest values are measured in the upper layer and between 50 m and 200 m depth, respectively. Along the transect S3, passing near station 21 and above station 07, the frontal separation between AW and shelf waters became sharper and the latter extended from the surface down to the bottom in the northern part of the section. The near-bottom distributions of θ and SAL reveal the presence of relatively higher values (4.30–5.00 °C and 35.03–35.10) in the southern deep part of the study region than in the northern part (Fig. 6.30). The concentrations of DO (ranging from 4 to 7 ml/l in the whole area), instead, are higher in the north-eastern part of Kveithola, where turbidity data also reveal a large presence of suspended particles (BT values <88%) in near-bottom waters. This water mass distribution indicates that at the time of the cruise, shelf-waters from the Barents Sea are clearly confined in the north-eastern (inner) part of the study area.

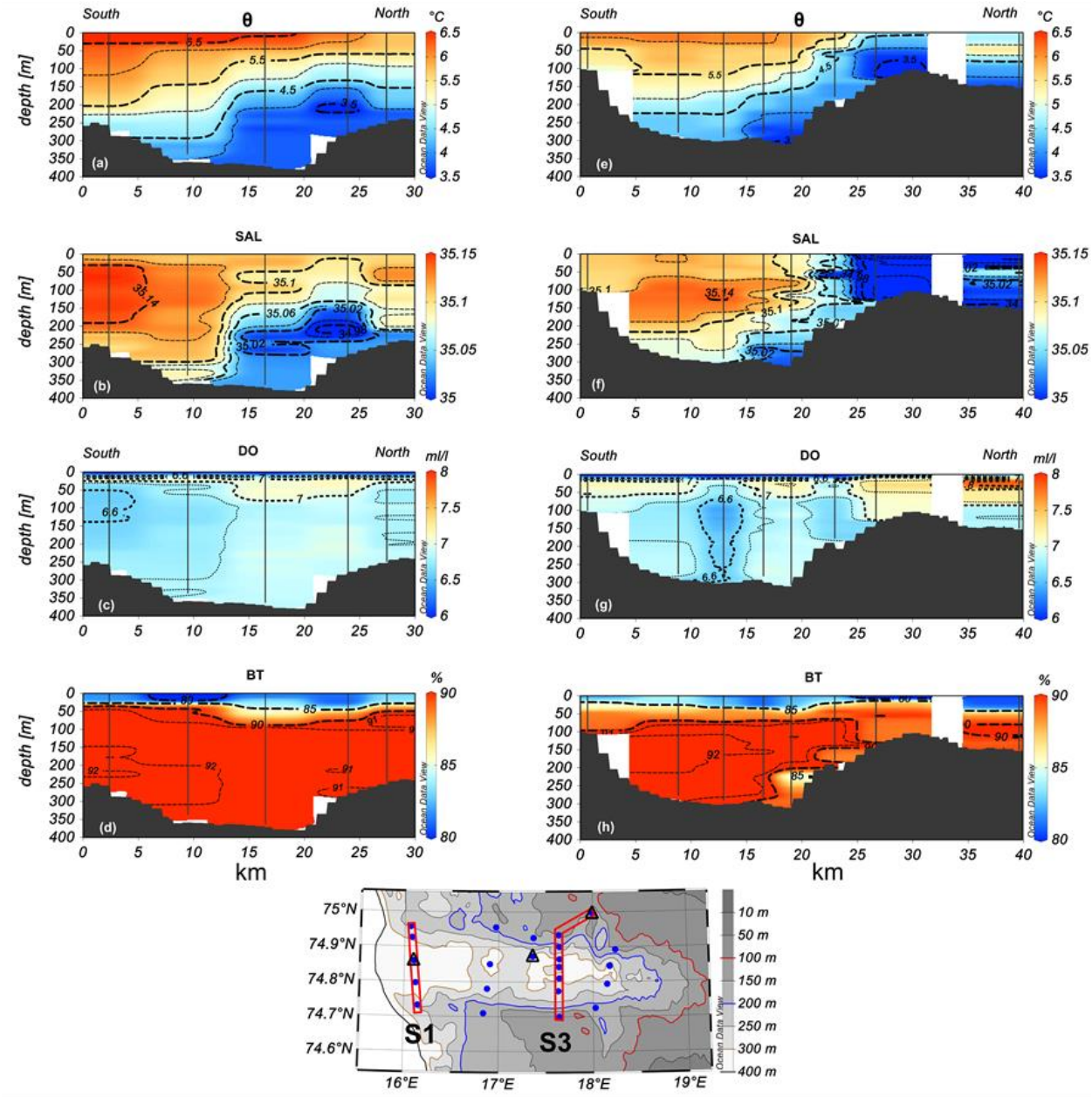


Fig. 6.29. Vertical distribution of θ (°C), salinity (SAL), DO (ml/l), and Beam Transmission (BT, %) along south- north sections S1 (a, b, c, d) and S3 (e, f, g, h). The blue dots in the sections S1 and S3 indicate all the measurement stations along Kveithola Trough, while triangles indicate the MUC stations.

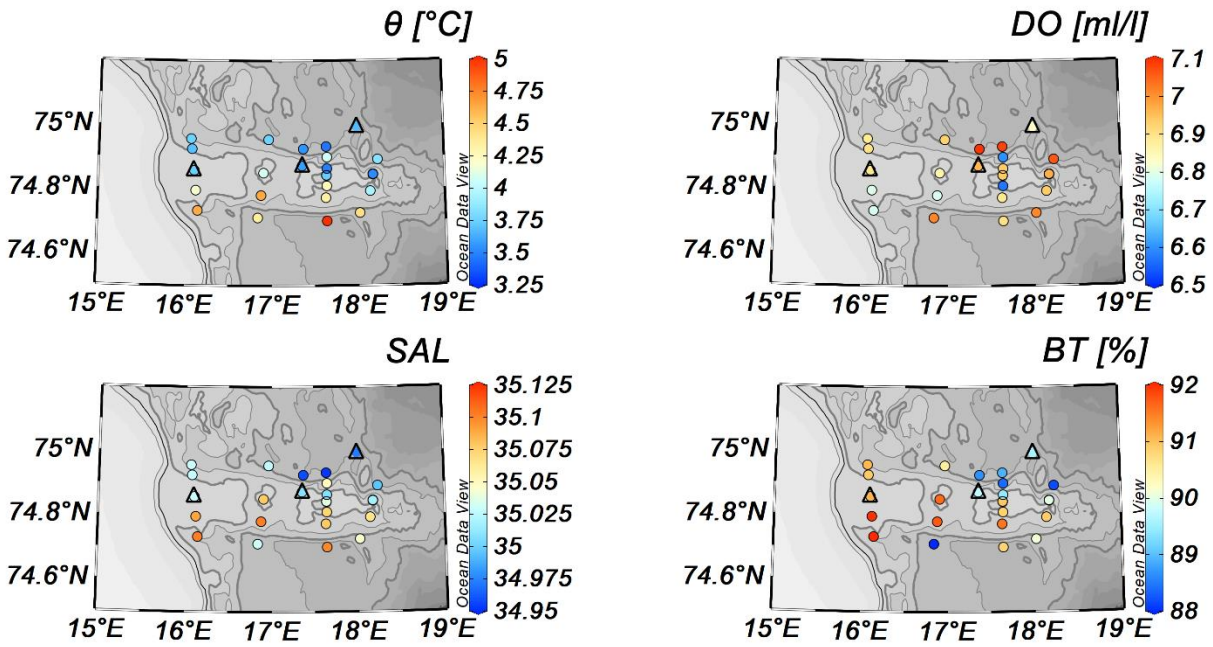


Fig. 6.30. Near bottom values of θ (°C), SAL, DO (ml l-1), and Beam Transmission (BT, %) from the CTD data. The triangles are the MUC stations used in this work.

The current speed measured through most of the water column along the ship's route (Fig. 6.31a) varied between nearly 0 and 0.4 m/s (Fig. 6.31b) showing a large horizontal and vertical variability. Highest values are record between 150 and 200 m depth near the western border of the Kveithola Trough. Current speeds are low and not exceeding 0.09 m/s in the deepest part of the water column reachable by the vmADCP signal and in particular at the three stations 02, 07, and 21 (where sediment cores are collected), while high values are found over areas with the shallower depths within Kveithola. Also, the directions of the current flow are highly variable in the area. By grouping the flow direction into four intervals centred at the four cardinal points (0° or 360° is N, 90° is E, 180° is S, and 270° is W) the data recorded within Kveithola Trough show clear flow inversions along the ship's route, with an almost regular alternation of a prevalent southward or northward flow, approximately every 12 hours (Fig. 6.31c), therefore attributable partially to the tidal influence.

The large spatio-temporal variability of the water masses (Figs. 6.29 and 6.30) and of the local currents (Fig. 6.31) reveal the presence of highly dynamic small-scale oceanic features possibly driven/influence by strong semidiurnal tidal oscillations and bathymetric constraints.

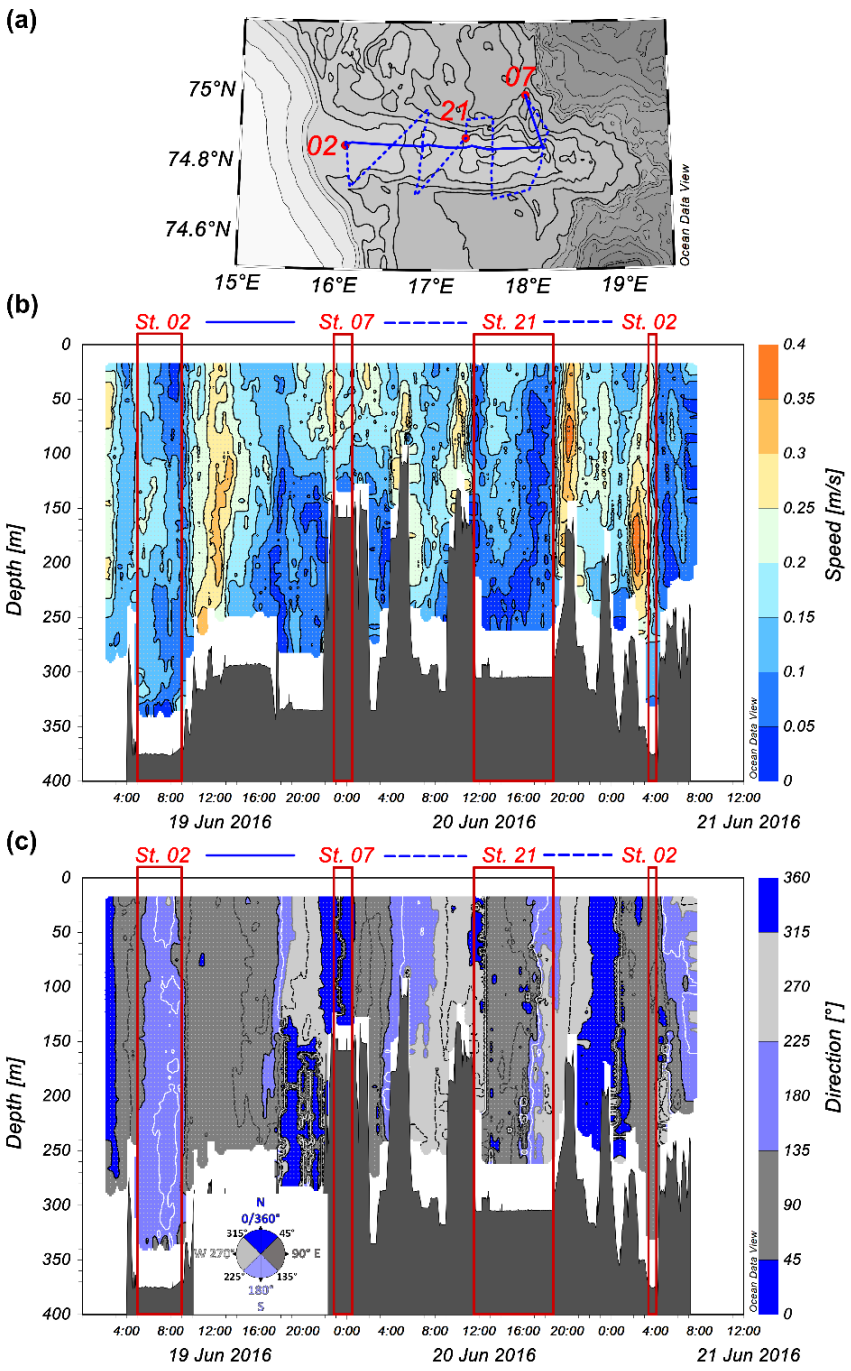


Fig. 6.31. Horizontal flow from the vmADCP in the Kveithola Trough: (a) the location of the three MUC stations (02, 07, and 21) and track of the route (blue solid line: from St. 02 to St. 07, blue dashed line: from St. 07 towards Sts. 21 and 02), time-depth diagram of (b) speed and (c) direction. The direction is grouped into intervals of 90° centred at the four cardinal points (0°/360° indicates a northward current, 90° eastward, 180° southward and 270° westward current). Red rectangles evidence the speed and direction measured during the permanence at each of the three stations. Station 02 is surveyed at the beginning and at the end of the cruise. The sea bottom topography is measured by a ship's echosounder.

6.7.2. Sea ice extension

The maximum seasonal sea ice extent in the Barents Sea usually occurs between March and April. Winter 2016 is characterised by the lowest sea ice extent during the last 40 years (www.mosj.no) as evidence by the satellite images (Fig. 6.32), which show that the sea ice is also scarcely present in the Storfjorden (the southernmost fjord of the Svalbard Archipelago). In recent years, this area of the Arctic has often been characterised by the absence of ice during the winter period (e.g., Peng et al., 2018). One has to go back to winter 2013 to find sea ice throughout the north-western basin of the Barents Sea, even near the Kveithola Trough (Fig. 6.32), while the last above-average value for the period 1979-2019 is recorded in 1998 and 2003.

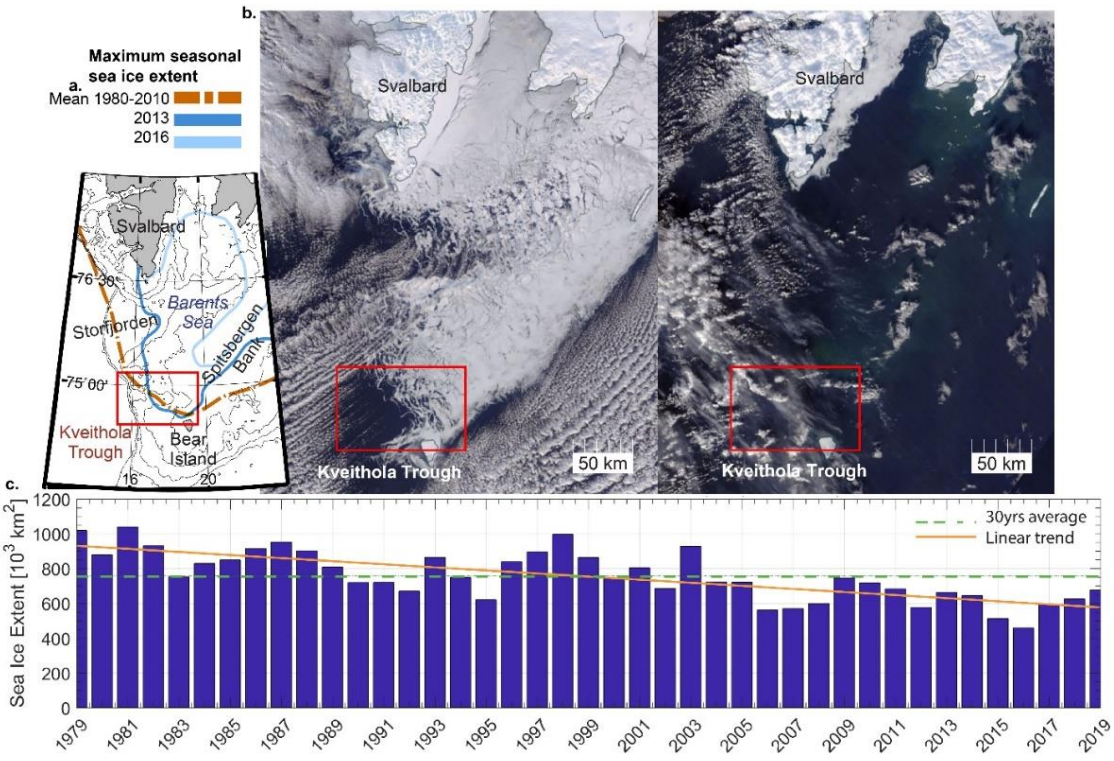


Fig. 6.32. (a). Map of the Barents Sea showing the average maximum seasonal sea ice extent during 1980-2010 (orange dashed line), in 2013 (dark-blue line), and in 2016 (light-blue line) (Faust et al., 2020; NSIDC, https://nsidc.org/) (see Fig 6.1). (b). Satellite images (Terra/Modis, true-colour corrected reflectance) taken on the 8 March 2013 (on the left) and 12 March 2016 (on the right) showing the maximum seasonal sea ice extent in the north-western Barents Sea (the Svalbard Archipelago and the Storfjorden are visible in the northern part of the images). (c). Time series of the mean monthly sea-ice extent in April in the Barents Sea, the month that normally has the largest sea-ice coverage in the area (data source www.mosj.no) for the period 1979 - 2019. The 30 years average value and the linear trend throughout the period are also indicated.

6.7.3. Sedimentation rate (SR)

Activity-depth profiles of excess ^{210}Pb show a quasi-exponential downcore decline, with only small fluctuations. In order to calculate a mean sedimentation rate for each core, the Constant Flux-Constant Sedimentation model (Robbins, 1978) is use, and a best-fit linear regression is apply to the core region with more regularly decreasing activity, thus discarding data from the surface mixed layer or from subsurface peaks.

Station 02, located in the Trough mouth, and is characterise by the lowest average SR (on avg. 0.082 cm/yr). Stations 21 and 07 have higher sedimentation rates (0.092 and 0.22 cm/yr, respectively). ^{137}Cs activities are very low, often below the detection limit. However, at station 07, the Chernobyl peak of 1986 is recognizable, substantially confirming the SR based on the ^{210}Pb profile. The obtained values of SR are comparable with literature values reported for the Barents Sea (e.g., Zaborska et al., 2008). Based on calculated SRs, the analysed sedimentary intervals span different time-periods for the three stations (about 115 years, 81 years and 43 years for cores 02, 21 and 07, respectively).

6.7.4. General faunal distribution and diversity indexes

In the sediment fraction ≥150 µm, we identify 23 CTG-living foraminiferal species (19 calcareous species and 4 agglutinated species). In general, the living foraminiferal assemblages are mainly compose by *ca.* 70-80% of calcareous taxa and 18-26% of agglutinated taxa (Fig. 6.33; Tab. 6.13). The highest number of living foraminiferal individuals are present at station 07 with 149 individuals; the station with more diverse taxa is station 02 with 15 species. The highest concentration of living foraminifera is found in the first 2- 3 cm bsf. The maximum concentration is register at station 07 with 5 spec./g at 2 cm bsf (in this station the living foraminifera also arrive until the maximum depth of 9 cm bsf). The dominance value (D) increase in-depth, indicating the predominance of a few or only one species; the station 02 show high diversity into the living assemblage with a total D value of 0.1 (Tab. 6.13). Shannon (H) values decrease on depth arriving until 0 where only one taxon is present.

In the dead foraminiferal assemblages (fraction ≥150 µm), 68 benthic foraminiferal species (50 calcareous and 18 agglutinated) are identify. The distribution of the dead foraminiferal assemblage in the topmost 10 cm of sediment show a dominance of the calcareous species, which constitute more than 95% in all the stations. The agglutinated group is present with a maximum of 2% at station 07. In general, *ca.* 300 individuals are identified and counted from each sample. The number of taxa (S) range between 36

(station 21) and 49 (station 02). The concentration surpasses 100 spec./g, of which the major contributor is the calcareous group (see supplementary material ST. 1). For all the stations, D values are relatively low (0.1 to 0.2 max.), that indicate the equal presence of all the species into the assemblage; these values are agree with the high H values that indicate many taxa with a few individuals into the assemblage. The calcareous benthic foraminifera are present in the entire record in all the stations, while the agglutinated group compared sporadically down-core (see supplementary material ST 1 and 2).



Fig. 6.33. Cumulative abundance (%) for foraminiferal test of different composition in the living and dead assemblage at each station: calcareous (calcareous perforate), miliolids (calcareous imperforate) and agglutinated. Note that the vertical axis starts at 50%.

Station	Core depth (cm) bsf	Living foraminiferal assemblages					Dead foraminiferal assemblages				
		N	S	spec./g	D	H	N	S	spec./g	D	H
02	0-0.5	25	8	3	0.2	1.9	403	29	3094	0.1	2.3
	0.5-1	15	8	2	0.2	1.9	337	30	3280	0.1	2.5
	1-1.5	2	2	0.2	0.5	0.7	302	28	2262	0.1	2.5
	1.5-2	4	2	0.4	0.5	0.7	342	27	4661	0.1	2.4
	2-3	3	2	0.2	0.6	0.6	313	26	4977	0.1	2.5
	3-4	-	-	-	-	-	420	26	3313	0.1	2.4
	4-5	2	2	0.1	0.5	0.7	315	29	4161	0.1	2.6
	5-6	-	-	-	-	-	286	27	3272	0.1	2.4
	6-7	2	2	0.1	0.5	0.7	368	25	4187	0.1	2.5
	7-8	-	-	-	-	-	310	21	2477	0.1	2.4
	8-9	-	-	-	-	-	363	23	1509	0.2	2.2
	9-10	-	-	-	-	-	325	22	2424	0.2	2.1
0-10 (total)		**52**	**15**	**0.3**	**0.1**	**2.4**	**4084**	**49**	**3357**	**0.1**	**2.5**
21	0-0.5	7	3	1	0.6	0.8	302	25	4069	0.1	2.7
	0.5-1	29	6	4	0.4	1.2	373	29	3478	0.1	2.6
	1-1.5	10	3	1	0.7	0.6	351	22	3431	0.1	2.3
	1.5-2	6	3	1	0.4	1.0	585	24	4709	0.1	2.5
	2-3	-	-	-	-	-	339	23	2921	0.1	2.3
	3-4	1	1	0.1	1.0	0.0	418	22	2556	0.1	2.3
	4-5	-	-	-	-	-	386	26	2664	0.1	2.4
	5-6	-	-	-	-	-	425	20	4135	0.1	2.3
	6-7	-	-	-	-	-	524	22	8960	0.1	2.3
	7-8	-	-	-	-	-	567	20	6998	0.1	2.4
0-8 (total)		**53**	**8**	**0.5**	**0.4**	**1.3**	**4270**	**36**	**4944**	**0.1**	**2.4**
07	0-0.5	22	9	2	0.2	2.0	377	38	160	0.1	2.9
	0.5-1	11	3	1	0.5	0.9	303	29	184	0.1	2.8
	1-1.5	11	3	1	0.4	0.9	296	26	165	0.1	2.8
	1.5-2	43	5	5	0.5	0.8	376	32	191	0.1	2.8
	2-3	28	4	2	0.4	1.1	318	30	232	0.1	2.6
	3-4	17	3	1	0.7	0.6	340	30	130	0.1	2.7
	4-5	6	3	0.3	0.4	1.0	247	29	302	0.1	2.7
	5-6	5	3	0.3	0.4	1.1	355	29	192	0.1	2.7
	6-7	4	2	0.2	0.6	0.6	322	28	222	0.1	2.8
	7-8	3	1	0.2	1.0	0.0	334	25	187	0.1	2.7
	8-9	1	1	0.1	1.0	0.0	321	27	205	0.1	2.6
	9-10	-	-	-	-	-	339	25	318	0.1	2.6
0-10 (total)		**149**	**12**	**0.85**	**0.3**	**1.6**	**3928**	**48**	**214**	**0.1**	**2.8**

Tab. 6.13: Foraminiferal concentrations and diversity data for each core in the fraction ≥150 µm. Number of counted specimens (N), number of species (S), number of foraminiferal specimens per gram of sediment (spec./g), Dominance (D) and Shannon index (H). The total values are also indicated. (See supplementary material ST. 1 and ST. 2 for the separate values for the calcareous and agglutinated groups).

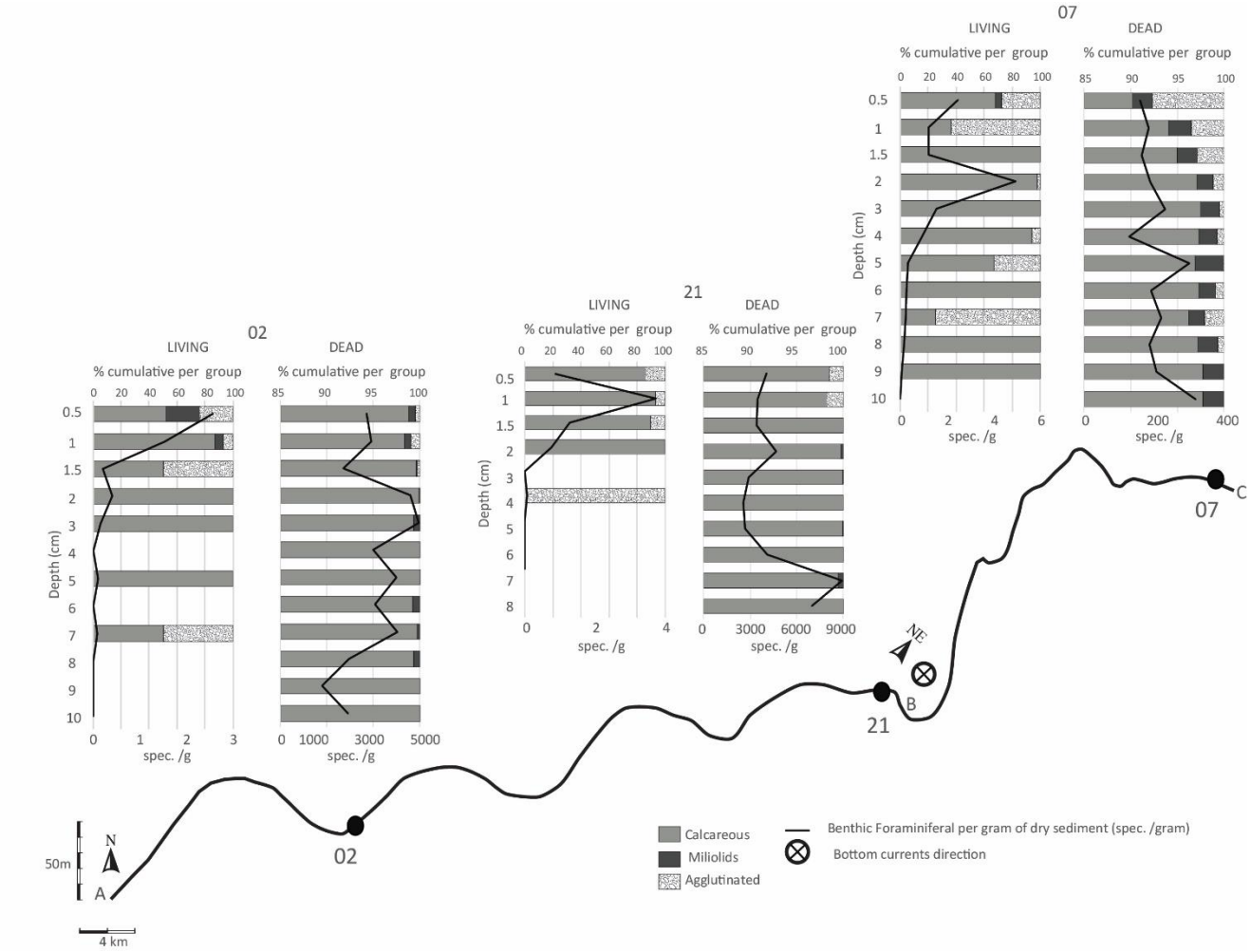


Fig. 6.34. Downcore living and dead foraminiferal concentrations, and distribution of calcareous (calcareous perforate), miliolids (calcareous imperforate), and agglutinated foraminifera shown along the bathymetric profile of Kveithola Trough. The location of the profile and the way points (A, B, C) are shown in Fig. 6.1. The black dots on the profile are the core locations. Note that the horizontal axis starts at 85% for the dead foraminifera.

6.7.5. Main foraminiferal species

The main living and dead foraminiferal species are shown in Fig. 6.35. The agglutinated foraminifera shows high percentages (*ca.* 20-25%; Fig. 6.33) in the living foraminiferal assemblages. In all the stations, they are mainly represented by *Reophax* spp. including *Reophax scorpiurus* and *Reophax fusiformis*. In the dead foraminiferal assemblages, the agglutinated species occur with less than 2%, and only in stations 02 and 07. The main agglutinated taxon is *Reophax* spp., and only few specimens are well preserved whereas numerous specimens are partially or totally broken (Fig. 6.33; Plate 2).

The main calcareous living foraminiferal species include *Cassidulina neoteretis*, *Cibicidoides lobatulus*, *Globobulimina auriculata*, *Islandiella* spp., *Melonis barleeanus*, *Nonionella iridea*, *Nonionellina labradorica*, *Pullenia bulloide*s and *Trifarina angulosa* (Fig. 6.35 and 6.36; Plate 1). The distribution of the living species in the sediment cores reflects the microhabitat of every species (Fig. 6.36). In our study, *T. angulosa* and *P. bulloides* exhibit an epifaunal microhabitat. Few individuals of *P. bulloides* and *C. lobatulus* are also found at 6-7 cm bsf (or deeper), probably transported by the bioturbation process. *C. neoteretis*, *Melonis barleeanus*, *N. labradorica, N. iridea* and *Islandiella* spp. show an infaunal habitat. *Globobulimina auriculata* is present in the first centimetres of sediment at station 21 and deeper at station 07.

The main dead foraminiferal species include only calcareous species as *Astrononion gallowayi*, *Buccella* spp., *Cassidulina laevigata*, *Cassidulina reniforme*, *C. neoteretis*, *C. lobatulus*, *Elphidium clavatum*, *Globocassidulina subglobosa*, *Islandiella* spp. (*I. islandica* + *I. norcrossi*), *M. barleeanus*, *N. labradorica*, Rotaliida spp. and *T. angulosa* (Fig. 6.35 and 6.36; Plate 1).

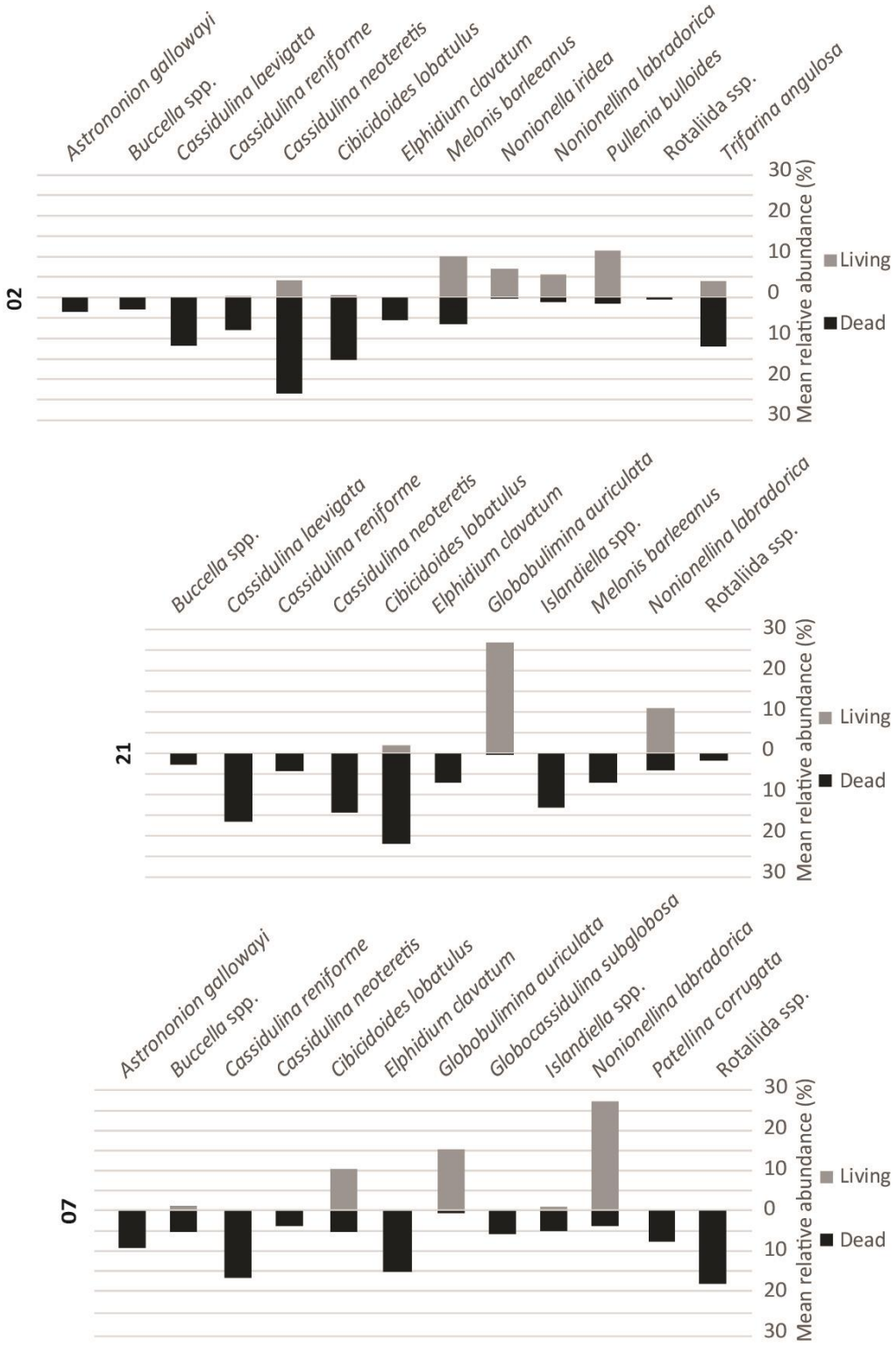


Fig. 6.35. Mean relative abundance of the main living and dead foraminiferal species, within the upper 0-10 cm of the studied cores.

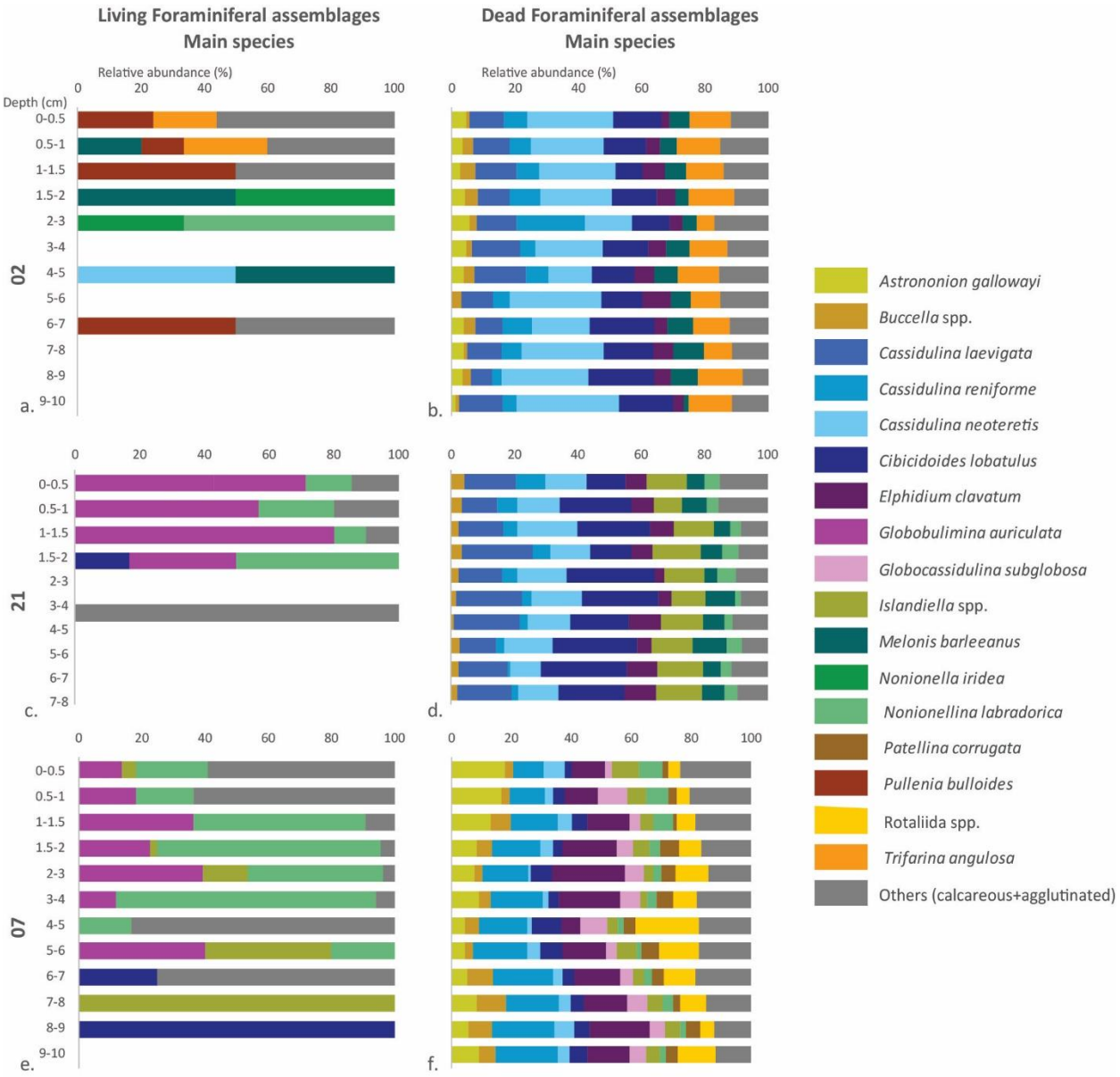


Fig. 6.36. Down core relative abundance of the main living and dead foraminiferal species.

The L/(L+D) ratios are calculated for the main living and dead foraminiferal species (Tab. 6.14). The species *N. iridea* and *N. labradorica* are main contributors to the living foraminiferal assemblage at the three stations, whereas, for the dead foraminiferal assemblage, the abundance of the species varies throughout the trough. At station 02, the living species *M. barleeanus, N. iridea*, *N. labradorica* and *P. bulloides* are present as a part of the main contributors, although in the dead assemblage the species with major presence are *C. reniforme*, *C. neoteretis*, *C. lobatulus* and *T. angulosa*. At station 21, the species

G. auriculata, *N. iridea*, *N. labradorica* represent more abundance in the living assemblage. In the dead assemblage at the station 21, the more abundant species are *C. lobatulus* and *P. bulloides*. At station 07, the more abundant living species are *C. lobatulus*, *G. auriculata*, *N. iridea* and *N. labradorica*, while in the dead assemblage *Buccella* spp. and *M. barleeanus*.

%	02			21			07		
Main Species	LIVING	DEAD	L/(L+D)	LIVING	DEAD	L/(L+D)	LIVING	DEAD	L/(L+D)
Astrononion gallowayi	0	3.31	0	0	1.95	0	0	9.21	0
***Buccella* spp.**	0	2.76	0	0	2.50	0	1.14	5.24	0.18
Cassidulina laevigata	0	11.59	0	0	16.33	0	0	1.27	0
***Cassidulina* reniforme**	0.33	7.76	0.04	0	4.11	0	0	16.62	0
Cassidulina neoteretis	4.17	23.31	0.15	0	14.04	0	0	3.81	0
Cibicidoides lobatulus	0.56	14.89	0.04	1.85	21.72	0.08	10.42	5.18	0.67
Elphidium clavatum	0	5.30	0	0	6.92	0	0	15.24	0
Globobulimina auriculata	0	0.03	0	27.00	0.20	0.99	15.16	0.67	0.96
Globocassidulina subglobosa	0	0.42	0	0	1.30	0	0	5.73	0
***Islandiella* spp.**	0	0.58	0	0	12.89	0	0.38	4.97	0.07
Melonis barleeanus	10.00	6.32	0.61	0	6.84	0	0	0.43	0
Nonionella iridea	6.94	0.04	0.99	0.74	0	1.00	0.38	0	1.00
Nonionellina labradorica	5.56	0.85	0.87	10.85	4.00	0.73	27.32	3.71	0.88
Patellina corrugata	0	0.18	0	0	0.10	0	0	3.93	0
Pullenia bulloides	11.44	1.32	0.90	0.70	4.02	0.15	0	0.47	0
Rotaliida spp.	0	0.14	0	0	0.84	0	0	9.32	0
Trifarina angulosa	3.89	11.85	0.25	0	0.17	0	0	0.08	0

Tab. 6.14: Relative abundance of the main foraminiferal species in the living and dead assemblages, and the relative contribution of the main living species (L/(L+D). The black boxes show the higher relative contribution of the living fauna, 0.4 to 1.00; the grey boxes show the higher relative contribution of the dead fauna 0.01 to 0.39; main species present only in the dead or living assemblages are also listed. Note that species with value 0 are not present in the living or dead assemblage; *N. iridea* and *P. bulloides* represent main species only at the station 02 in the living assemblage, however, their values in other stations are shown.

6.8. Discussion

6.8.1. Modern situation: Link between the living foraminiferal assemblages and the water masses distribution.

In the Barents Sea, the large annual and interannual variations of organic matter, temperature, salinity and oxygen fluxes, strongly condition and favour the proliferation of the benthic foraminiferal fauna and favour the bloom of certain species during the year (e.g. Ivanova et al., 2008; Dijkstra et al., 2015; 2017a; 2017b). The distribution of foraminiferal fauna sampled in 2016 along the Kveithola transect revealed a strong variability in the seabed conditions, water column characteristics, and trophic status along the trough and on the shelf.

The outer trough, station 02, is dominated by the presence of living detritivore and infaunal calcareous species as *P. bulloides* and *M. barleeanus*, which together with a relatively large quantity of organic matter with low nutritional quality (low bioavailable carbon value, Tab. 6.12) indicate oligotrophic conditions or at least organic matter derived by limited fast food sedimentation to the seafloor in relation to seasonal algal blooms (Sakshaug and Slagstad, 1992; Wassmann et al., 1994). According to the oceanographic conditions at the moment of the sediment sampling, this station is strongly dominate by Atlantic water throughout the water column, which is consistent with the presence of *M. barleeanus*, which thrives within relatively warm Atlantic water (Tab. 6.15). The moderate faunal density and diversity (Tab. 6.13) are positively influence by water masses conditions, whereas the faunal vertical distribution, limited to 6- 7 cm bsf (Figs. 6.34 and 6.36), indicates that the environment is characterise by a relatively large quantity of organic matter with lower nutritional quality as indicated by the presence of low bioavailable carbon, BAC value (Tab. 6.12).

At station 21, in the inner part of the trough, the marine environment is characterise by different oceanographic conditions (larger influence of cold and less salty shelf waters) and intermittent seepage activity, where the preservation of organic matter of low quality (Tab. 6.12) causes the oxygen decreasing within the sediment. Here, the benthic assemblage is dominate by *G. auriculata* and *N. labradorica*, typically associated with organic-rich sediment and dysoxic environments (Corliss, 1991; Koho et al., 2008) (Tab. 6.15). *Nonionellina labradorica* is a deep infaunal species that feeds mainly on the buried organic matter (Corliss, 1991). *Globobulimina* genus usually lives in meso-eutrophic settings, deep in the sediments within or below the oxic-redox interface (Fontanier et al., 2002; Licari et al., 2003; Murray, 2006; Koho et al., 2008). These two taxa may become very abundant if rich sources of food are available,

acting also as indicators of highly productive conditions (e.g., Jernas et al., 2018). Due to the intermittent seepage activity observed in the area (Lucchi et al., 2016; Bazzaro et al., 2020) and the presence of dysoxic indicators, we suppose the existence of a strong oxygen gradient at the water-sediment interface. As a matter of fact, *Nonionellina* and *Globobulimina* taxa are not considered seeps endemic specimens, nevertheless, they belong to genera that can respire nitrate instead of oxygen so they could survive in this stressed environment where sulphurs are commonly present (Rathburn et al., 2003; Levin, 2005). This stressed environment also justifies the low faunal density and diversity (Tab. 6.13) and the vertical distribution limited to the first 4 cm, where infaunal species migrate to escape from unfavourable living conditions (Figs. 6.29, 6.30 and 6.36). The oceanographic data, instead hint at a highly dynamic water column characterised by a large spatio-temporal variability of the thermohaline properties as well as of the local currents, suggesting highly oxygenated bottom water. This strong dynamic environment influences sediment deposition and re-suspension, making the seabed an unstable and highly variable environment prone to stressing factors.

Station 07 is locate in the north-eastern part of the study area mainly dominated by cold (<5°C) and relatively low saline (<35) bottom shelf waters. The low salinity water mass allows to discard the hypothesis of the presence of brine-enriched bottom waters produce during the winter season; they are rather associated with ice melting water or, more generally, to shelf water masses circulating in the shallower Barents Sea (Fig. 6.1 and 6.30). During spring, sunlight increases and the seasonal sea ice melts enhancing primary productivity (Sakshaug and Slagstad, 1992). These environmental conditions can explain the accumulation of organic matter driving the proliferation of abundant foraminiferal fauna, dominated by *Nonionella* spp. and *G. auricula*. The vertical distribution of benthic fauna down to 9 cm bsf (Tab. 6.12) can be relate with the more oxygenated bottom waters, which favour the oxygen penetration into the sediments. In fact, Caridi et al. (2019) report for the same station, high macrofaunal bioturbation activity that can favour both the oxygen penetration and the mobility of the foraminifera in the first centimetres of the sediment (Fohrmann et al., 1998; Loubere et al., 2011; Włodarska-Kowalczuk et al., 2013; Duros et al., 2014; Murray, 2006).

The results of the CTG living foraminiferal assemblages confirm the observations made on the living macrofauna of the Kveithola Trough. In that the spatial segregation of the living benthic fauna appears related to the environmental conditions, controlled by the hydrodynamic environment, the primary production and the nutrients influx (Caridi et al., 2019).

6.8.2. Preservation and taphonomic processes

The dead assemblages contain a record of several years of deposition of the foraminiferal test therefore reflecting an ensemble of assemblages associated to seasonal/inter annual succeeding conditions (e.g., one centimetre can contain information about multi-years or decades). Hence, a dead foraminiferal record corresponds to an average of the environmental changes occurred during a specific time interval in a specific area, which gives us an idea of the dynamics of the foraminifera association in function of these changes (Goineau et al., 2015). The living foraminiferal fauna registers a specific moment, which together with the oceanographic, sedimentological and chemical data (among others) acquired at the same time, help us to improve the understanding of the environmental significance of the species that live under certain environmental conditions. Therefore, the living foraminiferal assemblages give a snapshot of the environmental conditions at the time of field sampling, whereas the dead foraminiferal assemblage gives indication on the average of changes occurred during a period of time.

The benthic foraminiferal thanatocoenosis are frequently damaged during the taphonomic processes. Consequently, the dead foraminiferal assemblage can appear different from the living foraminiferal assemblages leading to associate them to different environmental conditions (Murray and Alve, 1999). However, the taphonomic processes are not the only ones to represent a key role in the difference between living and dead assemblages. As a matter of fact, we must take into consideration the seasonality and the variable oceanographic characteristics of the Kveithola Trough. As mentioned above, in our study the living fauna gave a snapshot of the environmental conditions existing during summer (June) 2016, while the dead foraminiferal record indicates the changes occurred in a larger temporal lapse therefore, giving an average of the events occurring throughout seasons over several years.

In our stations, the main difference between living and dead assemblages is the preservation of the agglutinated group (Figs. 6.33 and 6.34). The occurrence of agglutinated foraminifera is partially or totally subordinated to that of calcareous species in both the living and dead assemblages due to major preservational problems (Fig. 6.33). Agglutinated foraminifera have a poor preservation potential due to the mechanical disaggregation, test compaction and degradation of the organic cement that binds together the agglutinated grains (Schröder, 1988; Murray, 2006). Furthermore, also the calcareous or iron compounds of agglutinates cement may dissolve or oxidize (De Stigter et al., 1999; Duros et al., 2014; Dessandier et al., 2018). Our results show an increase of broken agglutinated test below the first centimetres of sediments (Fig. 6.33), and the disappearance of the agglutinated taxa deeper in the

sediment (Fig. 6.34), both in oxygenated and dysoxic environments. Some studies (e.g., Schröder, 1988; De Stigter et al., 1999) have already noted this taphonomic process in different oceanographic contexts, the authors calculate the loss of the dead agglutinated taxa of about 20% compared to the living species. Agglutinated broken tests do not allow the identification of the specimens at the species level and in some cases preclude their recognition even at the genus level (Plate 2). The degree of damage of a test or the definition of a percentage of broken agglutinated tests is difficult to quantify. Further, it is not possible to recognise one individual test by the number of broken pieces found in a sample (De Stigter et al., 1999). Therefore, it is difficult to establish a preservation level division like that defined by Schröder (1988) for agglutinated tests, because *Reophax* spp. is the only agglutinated genus that could be identified in the dead assemblages. In fact, Schröder (1988) classifies most of the *Reophax* species with low preservation potential due to their cemented wall. However, even the amount of *Reophax* spp. is low, and occurs mainly as broken tests preventing the classification at a species level. Due to their high degree of disintegration, any attempt of estimating its abundance can lead to large errors (Plate 2).

The calcareous foraminiferal tests suffer different mechanisms that can lead to their partial or total destruction (Murray, 2006). The dissolution affects especially the delicate and/or aragonitic calcareous tests. Species with delicate tests, such as *G. auriculata* (Ellis and Messina, 1940-1978), occurred with high percentage in the living foraminiferal assemblages (Tab. 6.14; Fig. 6.35 and 6.36), but in the dead foraminiferal assemblages, its percentage is considerably low and many individuals are broken (Tab. 6.14; Figs. 6.35 and 6.36; Plate 2). In this study, we have also frequently observed specimens of *Nonionellina labradorica* and *Nonionella iridea* having a broken ultimate chamber (Tab. 6.14; Figs. 6.35 and 6.36, Plate 2). The calcareous species also showed marks of predation like different boring patterns, holes and cavities that may be produced by phototrophic (cyanobacteria, chlorophyta) and heterotrophic (fungi) organisms (Cherchi et al., 2012) (Plate 2). In all these cases, the species are classified as far as possible especially in the cases when the fragment included the proloculus and/or the aperture zone, for which a correct classification could be made.

Post-mortem bioturbation and reworking of the sediments may also have caused fragmentation, corrosion and disintegration of the foraminiferal tests (Schröder, 1988; De Stigter et al., 1999; Loubere et al., 2011; Duros et al., 2014; Dessandier et al., 2018). These processes intensified with the increase of the amount of macrofauna, as described in Caridi et al. (2019) that is particularly evident at station 07. Bioturbation would facilitate the decrease or even the disappearance of some taxa from the dead foraminiferal record, especially for those specimens having delicate tests that are weaker or not well

cemented (Tab. 6.14; Figs. 6.33 and 6.35). This is the case of the group defined as Rotaliida spp., which includes species occurring with a preferential breaking in the ventral part, not allowing for a correct identification of the species (Plate 2).

In general, as a large amount of material is found in good condition, particularly that of the main ecological indicators, we are confident on the good quality and suitability of the used foraminiferal record for paleoenvironmental reconstructions. We can exclude bias associated with bottom currents sediment reworking. Indeed, the oceanographic data indicate current velocities at the studied stations below 0.1 m/s at 50 m above seafloor (Fig. 6.31), thought to decrease considerably approaching the sea bed due to sea bottom frictional effect. According to the diagram of McCave (1984) that relates bottom current velocity and sediment transport/deposition on the basis of their grain size, the bottom currents in the studied sites could not be stronger than 0.06-0.07 m/s. and an unlikely bottom current velocity greater than 0.2 m/s would be necessary to remobilise the sediment fraction of 150 μm. Such high bottom currents velocities would be more appropriate for the active northern moat crossing longitudinally the Kveithola Trough (Fig. 6.1) rather than the studied sites. The comparison between the percentages of living and dead foraminiferal concentration (spec./g, Tab. 6.14), suggests a good preservation of most of the species. Indeed, the dead foraminiferal assemblages include all the living foraminiferal species although occurring with different percentages, remarking the differences between the living foraminifera snapshot and the dead foraminiferal assemblage information of recent environmental characteristics. For these reasons, the preserved benthic foraminiferal association contains a detailed record of the past-faunal information, allowing their use as paleoenvironmental indicators.

The Kveithola Trough represents a unique environment of the Arctic system: its geographical position located at the margin of the Polar Front, with the constant incursion of warm AW into the trough; the presence of strong tidal currents that can deeply modify the oceanographic configuration; the complex, articulated bathymetry with transversal grounding zone wedges located at recessional steps that delimitate environments at different depths; the well-developed depocenters forming the sediment drifts of the inner area with an active moat crossing the northern margin of the trough; and the presence of active hydrocarbon seepages, driving important local modification of the biogeochemical characteristics of the environment. The interaction with the cold-water produces a cooling effect on the AW, this effect increases during the winter favoured by the presence of the sea ice adjacent to the northern shelf area. On another hand, during summer, the high temperatures facilitate the AW remaining warm longer and "trapped" within the channel, leaving a strong pattern of the AW affecting the benthic assemblages.

During the last decades this effect is amplified by the increase in the temperatures and the free sea ice conditions.

6.8.3. Paleoenvironmental variations during the last decades

The sedimentary cores used for this study cover the last *ca.* 50-100 years (see chapter 4.3, SR), during which the composition of the benthic foraminiferal assemblages is almost stable, which suggest relatively steady conditions during the considered time interval.

The outer station (02), corresponds with the last 115 years and is characterised by sandy sediments, which supported the presence of *Buccella* spp. (Tab. 6.12 and 6.15) and suggesting the presence of relatively strong currents, also confirmed by the high dynamic environment indicator *C. lobatulus* (Fig. 6.31; Tab. 6.15). These high-energy conditions provided a constant supply of organic matter and oxygen, which increments the diversity of the assemblage (Tab. 6.13). Furthermore, the alternate presence of the glaciomarine taxa, *C. reniforme*, and the warm water indicators *C. laevigata* and *C. neoteretis*, suggest strong interaction between the warm AW and the shelf waters (cold water influenced by the presence of sea ice) (Fig. 6.36). The influence of the sea ice to the outer area during the last decades can be traceable in the foraminiferal record, for example, at 2-3 cm bsf (*ca.* 1986) the sea-ice influence is higher than the recent years (Fig. 6.32) indicated by an increase of *C. reniforme* and by the sea-ice data (Fig. 6.32).

During the last *ca.* 81 years, the inner trough station (21), recorded relatively stable environmental conditions. The presence of *Islandiella* spp. and *N. labradorica* indicate a higher trophic level. Mesotrophic to eutrophic conditions could be related to an important accumulation of organic matter likely supported by the presence of strong bottom currents, confirmed by the occurrence of high-energy environment indicator *C. lobatulus* (Tab. 6.13 and. 6.15; Fig. 6.36). The increment in the abundance of *Islandiella* spp., compared to station 02, indicates an increase of nutrients influx, probably related to an augmented influence of the marginal sea ice zone (Fig. 6.32). The foraminiferal assemblage also contains *C. laevigata*, *C. neoteretis* and *C. reniforme*, similar to station 02, reflecting comparable water masses conditions, with the constant interaction between the warm (AW) and the cold (shelf origin) water masses.

The record of the shelf area (station 07), which covered about the last 43 years, is characterised by fresher and colder waters, in accordance with its northernmost position, and therefore, the greater influence of the Arctic water origin. The colder conditions are confirm by the predominance of cold-water indicators, like species *E. clavatum* and *C. reniforme* (Tab. 6.15). The decrease of warm water influence or food supply

related species *Islandiella* spp., *N. labradorica* and *Melonis barleeanus* possibly indicate both the low influence of warm AW and the reduction in the quantity or quality of nutrients availability (Fig. 6.35; Tab. 6.15). However, the increasing presence of *A. gallowayi* on top of the record indicates the interplay between warm and cold-water conditions.

Previous studies have shown how dead benthic foraminiferal assemblages have changed within the last two centuries in the SW and the central Barents Sea, reflecting a warming trend of the Atlantic water also there (Wilson et al., 2011; Saher et al., 2012; Dijkstra et al., 2017a). However, these progressively warming conditions are not observed in our record from Kveithola Trough due to the extent of the record (maximum *ca.* 100 years), comprising the already advancing warm period. Besides, Kveithola Trough has morphological features making it a protected system as hinted by the oceanographic data collected during the cruise and confirmed by the geographical distribution of the dead foraminiferal assemblages, which indicates the strong interaction between cold water (Arctic origin waters) and warm water (AW). This distribution shows the dominance of the AW in the trough, while in the shelf area the strong influence of the sea ice and cold water (ArW origin). Notwithstanding, these spatial differences, in the first 10 cm at each station, do not suggest big changes during the last 100 years. Fig. 6.36 shows how these assemblages changed in depth at each station, where slight changes in the relative abundance of some species indicate the variations related to the arrival of the seasonal sea ice or the increase of the interaction between cold and warm water.

Main species	Environmental conditions	References
Astrononion gallowayi	Temperature tolerant, warm and saline water, epifaunal	Saher et al., 2009; Saher et al., 2012.
***Buccella* spp.**	Cold water, seasonal ice cover, sandy and shallow areas	Steinsund, 1994; Hald and Korsun, 1997; Saher et al., 2009; Saher et al., 2012.
Cassidulina laevigata	Warm and saline water	Sejrup et al., 2004; Saher et al., 2009; Steinsund, 1994; Dijikstra et al., 2017b.
Cassidulina reniforme	Cold marine water, glaciomarine environments.	Hald and Korsun, 1997; Korsun and Hald, 1998; Murray, 2006; Saher et al., 2009; Saher et al., 2012; Dijikstra et al., 2017b.
Cassidulina neoteretis	Relative warm water, cooled Atlantic Water, prefers fresh phytodetritus.	Saher et al., 2009; Seidenkrantz, 1995; Dijikstra et al., 2017b.
Cibicidoides lobatulus	Temperature tolerant, epifaunal, high energy environments, sandy sediments	Steisund, 1994; Hald and Steisund, 1996; Wollenburg and Mackensen, 1998; Murray, 2006; Saher et al., 2009; Saher et al., 2012.
Elphidium clavatum	Cold bottom water, tolerates less than marine salinity	Steinsund, 1994; Sejrup et al., 2004; Murray, 2006; Saher et al., 2009; Saher et al., 2012; Dijkstra et al., 2017b.
Globobulimina auriculata	Infaunal, facultative anaerobe, tolerates dysoxia, detritivore, muddy sediments	Gooday et al., 2001; Murray, 2006; Murray and Alve, 2016.
Globocassidulina subglobosa	Cold–temperate water, low organic content, infaunal, detritivore, muddy sediments	Murray, 2006.
***Islandiella* spp.**	Mud-silt sediments, infaunal, free, detritivore, high food supply	Steinsund, 1994; Murray, 2006; Saher et al., 2009; Saher et al., 2012; Dijkstra et al., 2017b.
Melonis barleeanus	Arctic-Boreal species. Related to cooled Atlantic Water and degraded organic matter, tolerates dysoxia, maximum abundance under oxic conditions, infaunal, detritivore,mud-silt sediment	Steinsund, 1994; Murray, 2006; Saher et al., 2009; Saher et al., 2012; Dijkstra et al., 2017b.
Nonionella iridea	Phytodetritus species, infaunal	Murray, 2006.
Nonionellina labradorica	Cold water, seasonal sea ice cover, high food supply	Sejrup et al., 2004; Murray, 2006; Saher et al., 2009; Saher et al., 2012.
Patellina corrugata	Food availability, epifaunal, clinging or attached	Murray, 2006
Pullenia bulloides	Temperature tolerant, infaunal, detritivore, muddy sediment	Murray, 2006; Saher et al., 2009.
Trifarina angulosa	Temperature tolerant, epifaunal, influence of bottom currents, sand-gravel sediments	Steinsund, 1994; Murray, 2006; Saher et al., 2009.

Tab. 6.15. Ecological characteristics of the main living and dead species.

6.9. Conclusions

Geological and oceanographic data collected during the Eurofleets 2- BURSTER cruise in 2016 reveal the highly dynamic environment of the Kveithola Trough, characterised by significant spatial variability of thermohaline properties, currents and sea bottom conditions, and strong interactions of Arctic and Atlantic water masses. These factors, together with its morphology, create unique conditions in this environment, which differentiate it from the rest of the Barents Sea.

The ecological evidence, obtained from the CTG living foraminiferal records, gave us detailed information about the environmental conditions in the Kveithola Trough during the 2016 summer season. In particular, in the outer station (02), the living foraminiferal assemblages are dominated by the AW related species, *M. barleeanus* and the tolerant temperature species, *P. bulloides.* The inner station (21) is dominated by the high food supply indicator *N. labradorica,* and by the dysoxia species, *G. auriculata* related to the presence of methane seepage. In the shelf station (07), the dominant species are by *G. auriculata*, *N. labradorica* and the high-dynamic environmental indicator, *C. lobatulus*. The dominance of AW species in the outer shelf and the presence of eutrophic species in the inner part of the trough are in accordance with the summer conditions of the sampling period, that correspond to free sea ice environment and , to the enhance flux of the organic matter to the seafloor due to seasonal high primary productivity.

The taphonomical processes affect the preservation of the foraminiferal test, especially the agglutinated foraminifera, increasing the possibility of bias in the paleoenvironmental interpretation when using these taxa as part of the main species. We evaluated as good the preservation of most of the calcareous species that can be successfully used as paleoenvironmental indicators.

The dead foraminiferal assemblages show no significant changes during the last ca. 100 years. At station 02, the dead foraminiferal assemblages indicate the influence of the warm AW by *C. laevigata* and *C. neoteretis* and by strong hydrodynamic conditions indicated by *C. lobatulus* and *T. angulosa*. These conditions agree to the geographical position of station 02, where the main entrance of the AW in Kveithola Trough occurs. Throughout the sedimentological record at station 21, showing changes in the salinity by the increase of *C. laevigata* (salty water), and a decrease in *C. neoteretis* (stable salinity), high energy environment with a constant food supply, by *C. lobatulus*, and *Islandiella* spp., associated with the increasing interaction with the cold-shelf water masses and AW respecting station 02. The dominant

species at station 07 are the cold-water indicators *C. reniforme* and *E. clavatum*, according to the northern position of this station.

In contrast, other studies from surrounding areas of the Barents Sea indicate a larger and progressively increasing influence of the Atlantic water during almost the last 200 years. The main changes are shown as slight increases or decreases in the relative percentages of some species; it possibly related to the intensity and duration of the warm or cold seasonal periods, the interaction of the water masses and the geographical and geomorphological characteristics of Kveithola Trough. We believe that the local articulated morphological features isolated and protected the Kveithola environmental system from external influences responsible for the changes recorded in the rest of the Barents Sea.

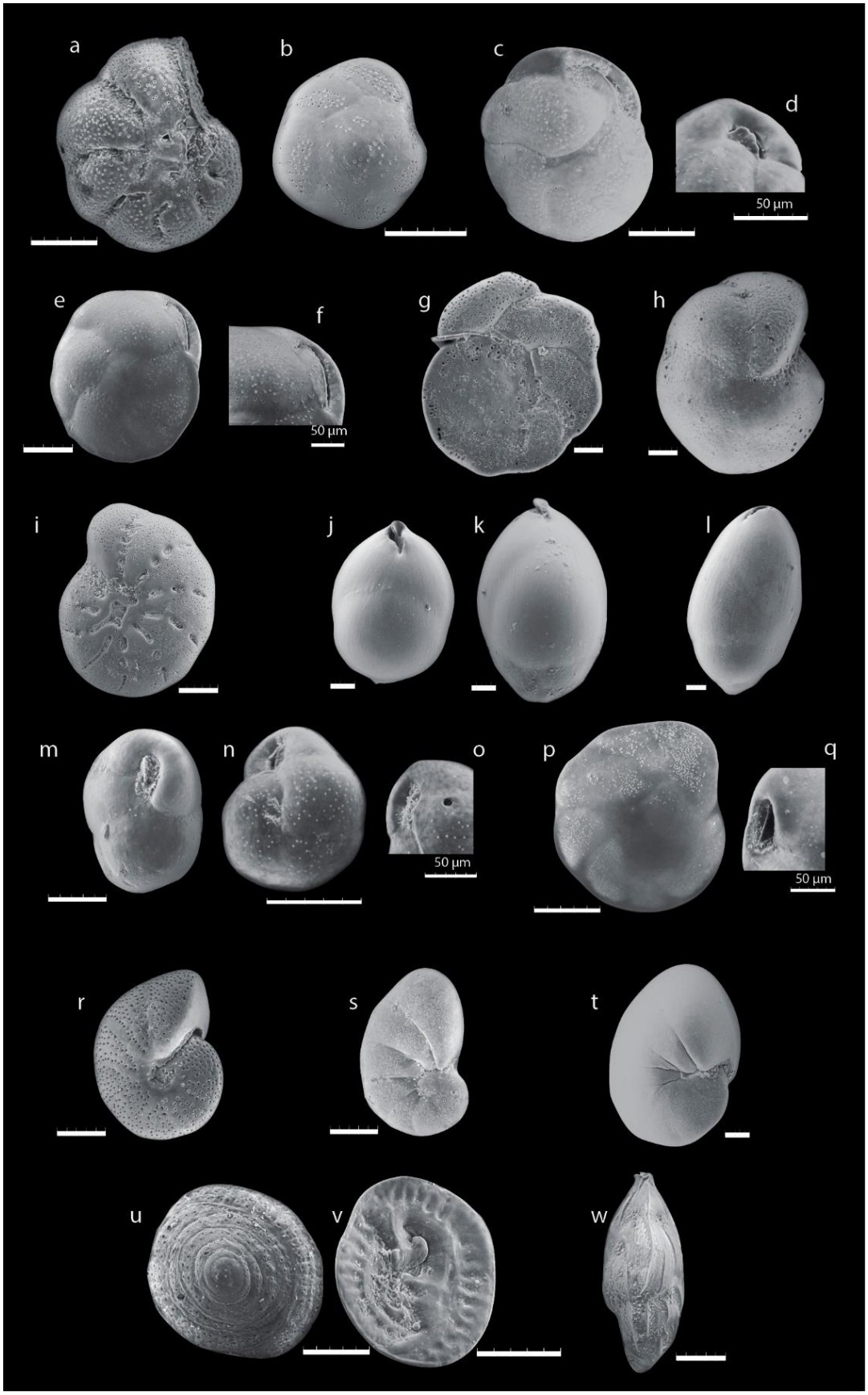

a
b
c
d
50 µm
e
f
50 µm
g
h
i
j
k
l
m
n
o
50 µm
p
q
50 µm
r
s
t
u
v
w

Plate 1: Some of the main calcareous dead foraminiferal species: (a) *Astrononion gallowayi*; (b) *Buccella* spp.; (c) *Cassidulina reniforme*, (d) *C. reniforme* zoom of the aperture; (e) *Cassidulina neoteretis*, (f) *C. neoteretis* zoom of the aperture; (g-h) *Cibicidoides lobatulus*; (i) *Elphidium clavatum*; (j- k- l) *Globobulimina auriculata;* (m-n) *Globocassidulina subglobosa;* (o) *G. subglobosa* zoom of the aperture; (p-q) *Islandiella* spp.; (r) *Melonis barleeanus*; (s) *Nonionella iridea*; (t) *Nonionellina labradorica*; (u) *Patellina corrugata*; and (w) *Trifarina angulosa.* Scale-bar 100 µm, except for the different measure indicated above the scale-bar.

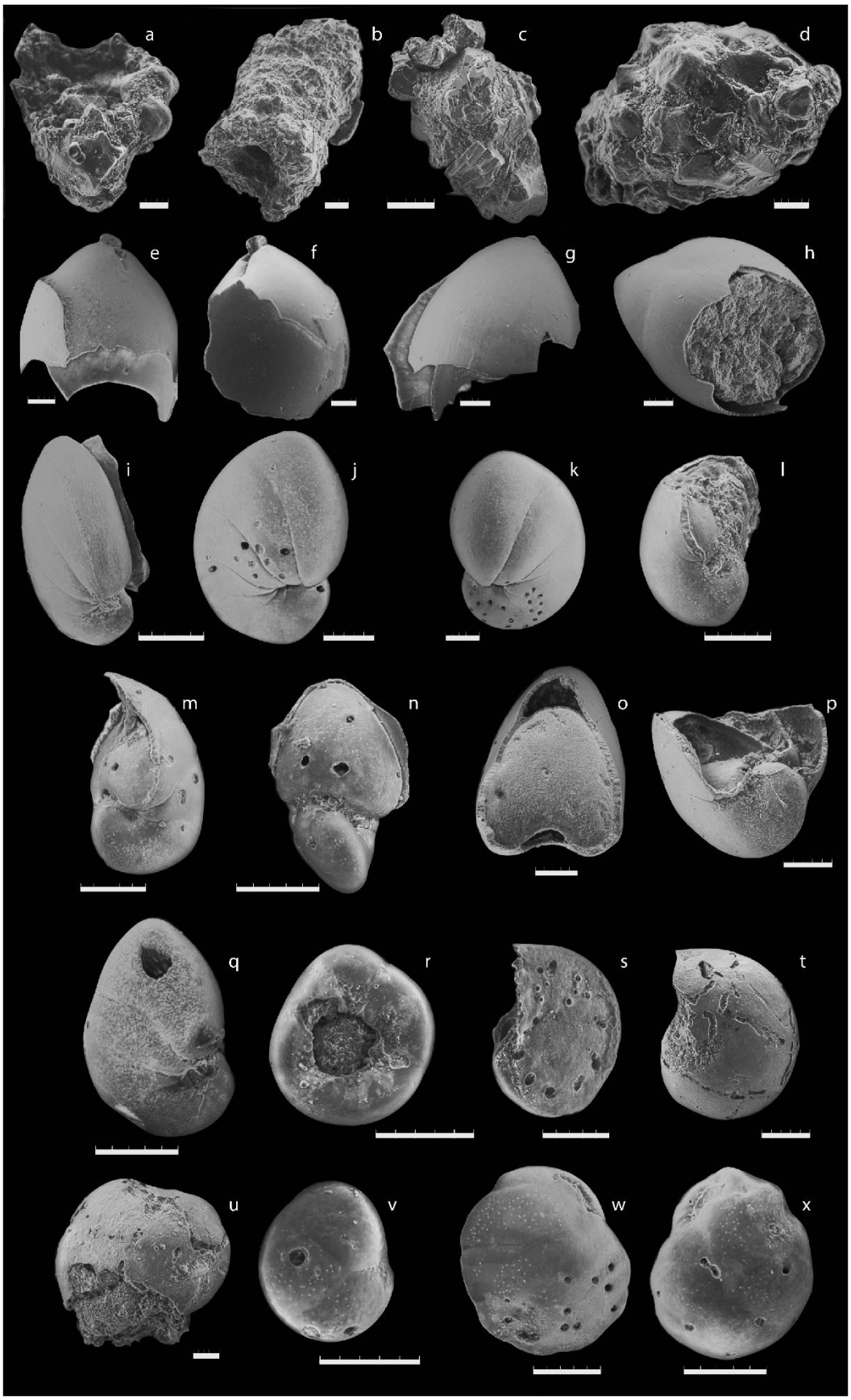

a
b
c
d
e
f
g
h
i
j
k
l
m
n
o
p
q
r
s
t
u
v
w
x

Plate 2: Dead foraminiferal species with taphonomic processes evidences: (a-d) Fragments of agglutinated foraminifera; (e-h) Fragments of *G. auriculata*; (i-q) *N. iridea* and *N. labradorica*: (i) broken test, (j-k) holes (marks predation?), (l-m-n) last chamber broken: (l) partially filled with sediment and (m-n) with holes (predation or post mortem activity?), (o) last chamber separate of the rest of the test, (p) total breakage of the last chambers, (q) last chamber broken (mechanically?); (r) Rotaliida indet. ventral broken; (s- t) *C. lobatulus*: (marks predation?): (s) holes, (t) cavities; (u) *Cassidulina* spp. with marks, broken and partially filled; (v) *C. reniforme* holes (marks predation?); and (w-x) *C. neoteretis* holes (marks predation?). Scale-bar 100 µm.

6.10. References

Aagaard, K. 1989. A synthesis of the Arctic Ocean circulation. Le Conseil. Rapp. P. V. Reun. Cons. Int. Explor. Mer. 188, 11 – 22.

Aagaard, K., Darnall, C., Greisman, P. 1973. Year-long current measurements in the Greenland-Spitsbergen passage. Deep Sea Research. 20 (8), 743-746.

Aagaard, K., Coachman, L. K., Carmack, E. 1981. On the halocline of the Arctic Ocean. Deep Sea Research. Part A 286, 529-545.

Aagaard, K., Swift, J. H., Carmack, E. C. 1985. Thermohaline circulation in the Arctic Mediterranean seas. Journal of Geophysic Research Oceans 90C3, 4833-4846.

Årthun, M., Eldevik, T., Smedsrud, L. H., Skagseth, Ø., Ingvaldsen, R. B. 2012. Quantifying the influence of Atlantic heat on Barents Sea ice variability and retreat. Journal of Climate, 25(13), 4736-4743.

Bazzaro, M., Ogrinc, N., Relitti, F., Lucchi, R.G., Giani, M., Adami, G., Pavoni, E., De Vittor, C., 2020. Geochemical signatures of intense episodic anaerobic oxidation of methane in near-surface sediments of a recently discovered cold seep (Kveithola trough, NW Barents Sea). Marine Geology, 425, 106189.

Bengtsson, L., Semenov, V. A., Johannessen, O. M. 2004. The early twentieth-century warming in the Arctic—A possible mechanism. Journal of Climate, 17(20), 4045-4057.

Bjarnadóttir, L. R., Rüther, D. C., Winsborrow, M. C., Andreassen, K. 2013. Grounding-line dynamics during the last deglaciation of Kveithola, W Barents Sea, as revealed by seabed geomorphology and shallow seismic stratigraphy. Boreas, 42(1), 84-107.

Caridi, F., Sabbatini, A., Morigi, C., Dell'Anno, A., Negri, A., Lucchi, R.G. 2019. Patterns and environmental drivers of diversity and community composition of macrofauna in the Kveithola Trough NW Barents Sea. Journal of Sea Research. 153, 101780.

Cherchi, A., Buosi, C., Zuddas, P., De Giudici, G.B. 2012. Bioerosion by microbial euendoliths in benthic foraminifera from heavy metal-polluted coastal environments of Portovesme south-western Sardinia, Italy. Biogeosciences 9, 4607–4620.

Comiso, J.C., Hall, D.K. 2014. Climate trends in the Arctic as observed from space. Wiley Interdisciplinary Reviews: Climate Change 53, 389-409.

Corliss, B.H. 1991. Morphology and microhabitat preferences of benthic foraminifera from the northwest Atlantic Ocean. Marine Micropaleontology 173-4, 195-236.

De Stigter, H.C., Van der Zwaan, G.J., Langone, L. 1999. Differential rates of benthic foraminiferal test production in surface and subsurface sediment habitats in the southern Adriatic Sea. Palaeogeography. Palaeoclimatology and Palaeoecology. 1491-4, 67-88.

Dessandier, P.A., Bonnin, J., Kim, J.H., Racine, C. 2018. Comparison of living and dead benthic foraminifera on the Portuguese margin: Understanding the taphonomical processes. Marine. Micropaleontology. 140, 1-16.

Dickson, R.R., Osborn, T.J., Hurrell, J.W., Meincke, J., Blindheim, J., Adlandsvik, B., Vinje, T., Alekseev, G. and Maslowski, W. 2000. The Arctic ocean response to the North Atlantic oscillation. Journal of Climate, 13(15). 2671-2696.

Dijkstra, N., Junttila, J., Aagaard-Sørensen, S. 2017a. Environmental baselines and reconstruction of Atlantic Water inflow in Bjørnøyrenna, SW Barents Sea, since 1800 CE. Marine Environmental Research 132, 117-131.

Dijkstra, N., Junttila, J., Skirbekk, K., Carroll, J., Husum, K., Hald, M. 2017b. Benthic foraminifera as bio-indicators of chemical and physical stressors in Hammerfest harbor Northern Norway. Marine pollution bulletin, 1141, 384-396.

Dowdeswell, J.A., Fugelli, E.M.G. 2012. The seismic architecture and geometry of grounding-zone wedges formed at the marine margins of past ice sheets. GSA Bulletin 12411-12, 1750-1761.

Duros, P., Jorissen, F.J., Cesbron, F., Zaragosi, S., Schmidt, S., Metzger, E., Fontanier, C. 2014. Benthic foraminiferal thanatocoenoses from the Cap-Ferret Canyon area NE Atlantic: a complex interplay between hydro-sedimentary and biological processes. Deep Sea Research. Part II 104, 145-163.

Ellis, B.E., Messina, A.R. 1940–1978. Catalogue of Foraminifera. Micropaleontology Press, Am. Museum of Natural History, New York.

Faust, J.C., Tessin, A., Fisher, B.J., Zindorf, M., Papadaki, S., Hendry, K.R., Doyle, K.A. and Maerz, C. 2020. Millennial scale persistence of organic carbon bound to iron in Arctic marine sediments. Nature Communications.

Fohrmann, H., Backhaus, J.O., Blaume, F., Rumohr, J. 1998. Sediments in bottom-arrested gravity plumes: Numerical case studies. J. Phys. Ocean. 2811, 2250-2274.

Fontanier, C., Jorissen, F.J., Licari, L., Alexandre, A., Anschutz, P., Carbonel, P. 2002. Live benthic foraminiferal faunas from the Bay of Biscay: faunal density, composition, and microhabitats. Deep Sea Res. I 494, 751-785.

Goineau, A., Fontanier, C., Mojtahid, M., Fanget, A. S., Bassetti, M. A., Berné, S., Jorissen, F., 2015. Live–dead comparison of benthic foraminiferal faunas from the Rhône prodelta (Gulf of Lions, NW Mediterranean): Development of a proxy for palaeoenvironmental reconstructions. Marine Micropaleontology, 119, 17-33.

Gooday, A. J., Hughes, J. A., Levin, L. A. 2001. The foraminiferan macrofauna from three North Carolina (USA) slope sites with contrasting carbon flux: a comparison with the metazoan macrofauna. Deep Sea Research Part I: Oceanographic Research Papers, 48(7), 1709-1739.

Goosse, H., & Holland, M. M. 2005. Mechanisms of decadal arctic climate variability in the community climate system model, version 2 (CCSM2). Journal of climate, 18(17), 3552-3570.

Green, K.E. 1960. Ecology of some Arctic foraminifera. Micropaleontology 61, 57-78.

Groot, D.E., Aagaard-Sørensen, S., Husum, K. 2014. Reconstruction of Atlantic water variability during the Holocene in the western Barents Sea. Climate of the Past 101, 51-62.

Hald, M., Korsun, S. 1997. Distribution of modern benthic foraminifera from fjords of Svalbard, European Arctic. Journal of Foraminiferal Research. 272, 101-122.

Hald, M., Steinsund, P. I. 1996. Benthic foraminifera and carbonate dissolution in the surface sediments of the Barents and Kara Seas. Berichte zur Polarforschung, 212, 285-307.

Harris, C. L., Plueddemann, A. J., & Gawarkiewicz, G. G. 1998. Water mass distribution and polar front structure in the western Barents Sea. Journal of Geophysical Research: Oceans, 103(C2), 2905-2917.

Ingvaldsen, R., Loeng, H., Asplin, L. 2002. Variability in the Atlantic inflow to the Barents Sea based on a one-year time series from moored current meters. Continental Shelf Research, 22(3), 505-519.

Jernas, P., Klitgaard-Kristensen, D., Husum, K., Koç, N., Tverberg, V., Loubere, P., Prins, M., Dijkstra, N., Gluchowska, M. 2018. Annual changes in Arctic fjord environment and modern benthic foraminiferal fauna: Evidence from Kongsfjorden, Svalbard. Global and Planetary Change 163, 119-140.

Koenigk, T., Mikolajewicz, U., Jungclaus, J.H., Kroll, A. 2009. Sea ice in the Barents Sea: seasonal to interannual variability and climate feedbacks in a global coupled model. Climate dynamics 327-8, 1119-1138.

Koho, K.A., García, R.D., De Stigter, H.C., Epping, E., Koning, E., Kouwenhoven, T.J., Van der Zwaan, G.J. 2008. Sedimentary labile organic carbon and pore water redox control on species distribution of benthic foraminifera: A case study from Lisbon–Setúbal Canyon southern Portugal. Progress in Ocean. 791, 55-82.

Korsun, S., Hald, M. 1998. Modern benthic foraminifera off Novaya Zemlya tidewater glaciers, Russian Arctic. Arctic and Alpine Research, 30(1), 61-77.

Lamb, H.H. 1977. Climate, present, past and future. London: Methuen & Co.

Lantzsch, H., Hanebuth, T.J., Horry, J., Grave, M., Rebesco, M., Schwenk, T. 2017. Deglacial to Holocene history of ice-sheet retreat and bottom current strength on the western Barents Sea shelf. Quaternary. Science Reviews. 173, 40-57.

Levin, L.A. 2005. Ecology of cold seep sediments: Interactions of fauna with flow, chemistry and microbes. Oceanography and Marine Biology. 43, 1-46.

Licari, L.N., Schumacher, S., Wenzhofer, F., Zabel, M., Mackensen, A., 2003. Communities and microhabitats of living benthic foraminifera from the tropical east Atlantic: impact of different productivity regimes. Journal of Foraminiferal Research. 331, 10-31.

Loeng, H. 1991. Features of the physical oceanographic conditions of the Barents Sea. Polar Res. 101, 5-18.

Loeng, H., Ozhigin, V., Ådlandsvik, B. 1997. Water fluxes through the Barents Sea. ICES Journal of Marine Science. 543, 310-317.

Loeng, H., Drinkwater, K. 2007. An overview of the ecosystems of the Barents and Norwegian Seas and their response to climate variability. Deep Sea Research Part II: Topical Studies in Oceanography, 54(23-26), 2478-2500.

Loubere, P., Jacobsen, B., Kristensen, D.K., Husum, K., Jernas, P., Richaud, M. 2011. The structure of benthic environments and the paleochemical record of foraminifera. Deep Sea Research. I 585, 535-545.

Lucchi, R.G., Bazzaro, M., Biebow, N., Carbonara, K., Caridi, F., De Vittor, C., Dominiczak, A., Gamboa Sojo, V.M., Graziani, S., Kovacevic, V., Krueger, M., Le Gall, C., Mazzini, A., Morigi, C., Musco, M.E., Povea, P., Relitti, F., Ruggiero, L., Rui, L., Sabbatini, A., Sánchez Guillamón, O., Tagliaferro, M., Topchiy, M., Wiberg, D., Zoch, D., with the collaboration of the scientific party of the Italian PNRA project DEFROST: Bensi, M., Deponte, D., Langone, L., Laterza, R. 2016. BURSTER - Bottom Currents in a Stagnant Environment, EUROFLEETS-2 Cruise Summary Report. 106 DOI: 10.13140/RG.2.2.24223.36004.

Maslowski, W., Marble, D., Walczowski, W., Schauer, U., Clement, J.L., Semtner, A.J. 2004. On climatological mass, heat, and SAL transports through the Barents Sea and Fram Strait from a pan-Arctic coupled ice-ocean model simulation, Journal of Geophysics Research, 109, C03032, doi:10.1029/2001JC001039.

Mau, S., Römer, M., Torres, M.E., Bussmann, I., Pape, T., Damm, E., Geprägs, P., Wintersteller, P., Hsu, C.W., Loher, M., Bohrmann, G., 2017. Widespread methane seepage along the continental margin off Svalbard-from Bjørnøya to Kongsfjorden. Scientific reports, 7(1), 1-13.

McCave, I. N., 1984. Erosion, transport and deposition of fine-grained marine sediments. Geological Society, London, Special Publications, 15(1), 35-69.

Murray, J.W. 2006. Ecology and applications of benthic foraminifera. Cambridge University Press, UK.

Murray, J. W., Alve, E. 2016. Benthic foraminiferal biogeography in NW European fjords: A baseline for assessing future change. Estuarine, Coastal and Shelf Science, 181, 218-230.

Orvik, K.A., Niiler, P. 2002. Major pathways of Atlantic water in the northern North Atlantic and Nordic Seas toward Arctic. Geophysics Research. Letters 2919, 2-1.

Peng, G., Steele, M., Bliss, A.C., Meier, W.N., Dickinson, S. 2018. Temporal Means and Variability of Arctic Sea Ice Melt and Freeze Season Climate Indicators Using a Satellite Climate Data Record, Remote Sens. 2018, 10, 1328

Pittauerová, D. 2013. Gamma spectrometry for chronology of recent sediments. PhD thesis, Bremen University, 213.

Polyak, L., Korsun, S., Febo, L. A., Stanovoy, V., Khusid, T., Hald, M., Paulsen, B.E., Lubinski, D. J. 2002. Benthic foraminiferal assemblages from the southern Kara Sea, a river-influenced Arctic marine environment. The Journal of Foraminiferal Research, 32(3), 252-273

Rasmussen, T.L., Thomsen, E. 2017. Ecology of deep-sea benthic foraminifera in the North Atlantic during the last glaciation: Food or temperature control. Palaeogeog. Palaeoclimat. Palaeoecol. 472, 15-32.

Rathburn, A.E., Pérez, M.E., Martin, J.B., Day, S.A., Mahn, C., Gieskes, J., J., Ziebis, W., Williams, D., Bahls, A., 2003. Relationships between the distribution and stable isotopic composition of living benthic foraminifera and cold methane seep biogeochemistry in Monterey Bay, California. Geochem. Geophys. Geosyst. 412.

Rebesco, M., Liu, Y., Camerlenghi, A., Winsborrow, M., Laberg, J.S., Caburlotto, A., Diviacco, P., Accettella, D., Sauli, C., Wardell, N., Tomini, I. 2011. Deglaciation of the western margin of the Barents Sea Ice Sheet—A swath bathymetric and sub-bottom seismic study from the Kveithola Trough. Marine Geology. 2791-4, 141-147.

Rebesco, M., Özmaral, A., Urgeles, R., Accettella, D., Lucchi, R.G., Rüther, D., Winsborrow, M., Llopart, J., Caburlotto, A., Lantzsch, H., Hanebuth, T.J. 2016. Evolution of a high-latitude sediment drift inside a glacially-carved trough based on high-resolution seismic stratigraphy Kveithola, NW Barents Sea. Quaternary Science Review. 147, 178-193.

Ritchie, J.C., McHenry, J.R. 1990. Application of radioactive fallout cesium-137 for measuring soil erosion and sediment accumulation rates and patterns: A review. J. Env. Quality 192, 215-233.

Robbins, J.A., Edgington, D.N., 1975. Determination of recent sedimentation rates in Lake Michigan using Pb-210 and Cs-137. Geochim. et Cosmochim. Acta, 393, 285-304.

Rüther, D.C., Bjarnadóttir, L.R., Junttila, J., Husum, K., Rasmussen, T.L., Lucchi, R.G., Andreassen, K. 2012. Pattern and timing of the northwestern Barents Sea Ice Sheet deglaciation and indications of episodic Holocene deposition. Boreas 413, 494-512.

Saher, M.H., Kristensen, D.K., Hald, M., Korsun, S., Jørgensen, L.L. 2009. Benthic foraminifera assemblages in the Central Barents Sea: an evaluation of combining live and total fauna studies in tracking environmental change. Norwegian Journal of Geology. 89, 149-161

Saher, M., Kristensen, D.K., Hald, M., Pavlova, O., Jørgensen, L.L. 2012. Changes in distribution of calcareous benthic foraminifera in the central Barents Sea between the periods 1965–1992 and 2005–2006. Global and Planetary Change 98, 81-96.

Sakshaug, E., Slagstad, D. 1992 Sea ice and wind: Effects on primary productivity in the Barents Sea. Atmosphere-Ocean 30, 579-591.

Sarnthein, M., Van Kreveld, S., Erlenkeuser, H., Grootes, P.M., Kucera, M., Pflaumann, U., Schulz, M. 2003. Centennial-to-millennial-scale periodicities of Holocene climate and sediment injections off the western Barents shelf, 75° N. Boreas 323, 447-461.

Schiermeier, Q. 2012. Ice loss shifts Arctic cycles: record shrinkage confounds models and portends atmospheric and ecological change. Nature, 489(7415), 185-187.

Schlitzer, R. 2018. Ocean Data View, https://odv.awi.de.

Schröder, C.J. 1988. Subsurface preservation of agglutinated foraminifera in the northwest Atlantic Ocean. Abhandlungen der geologischen Bundesanstalt 41, 325-336.

Seidenkrantz, M. S. 1995. Cassidulina teretis Tappan and Cassidulina neoteretis new species (Foraminifera): stratigraphic markers for deep sea and outer shelf areas. Journal of Micropalaeontology, 14(2), 145-157.

Sejrup, H. P., Birks, H. J. B., Kristensen, D. K., Madsen, H. 2004. Benthonic foraminiferal distributions and quantitative transfer functions for the northwest European continental margin. Marine Micropaleontology, 53(1-2), 197-226.

Ślubowska-Woldengen, M., Rasmussen, T.L., Koç, N., Klitgaard-Kristensen, D., Nilsen, F., Solheim, A. 2007. Advection of Atlantic Water to the western and northern Svalbard shelf since 17,500 cal yr BP. Quaternary Science Review 263-4, 463-478.

Smedsrud, L.H., Esau, I., Ingvaldsen, R.B., Eldevik, T., Haugan, P.M., Li, C., Lien, V.S., Olsen, A., Omar, A.M., Otterå, O.H., Risebrobakken, B. 2013. The role of the Barents Sea in the Arctic climate system. Review of Geophysics 513, 415-449.

Smith, W.O., Sakshaug, E. 1990 Polar phytoplankton, in: Smith, W.O. Ed., Polar oceanography, Part B: Chemistry, Biology and Geology. Academic Press, New York, 447-525.

Steinsund, P. I., Polyak, L., Hald, M., Mikhailov, V., Korsun, S. 1994. Distribution of calcareous benthic foraminifera in recent sediments of the Barents and Kara Sea. Benthic Foraminifera in Surface Sediments of the Barents and Kara Seas: Modern and Late Quaternary Application. Ph. D. Thesis, Department of Geology, Institute of Biology and Geology, University of Tromsø, Norway.

Vinje, T., Kvambekk, Å.S. 1991. Barents Sea drift ice characteristics. Polar Res. 101, 59-68.

Wassmann, P., Martinez, R., Vernet, M., 1994. Respiration and biochemical composition of sedimenting organic matter during summer in the Barents Sea. Continental shelf research, 14(1), 79-90.

Wilson, L.J., Hald, M., Godtliebsen, F. 2011. Foraminiferal faunal evidence of twentieth-century Barents Sea warming. The Holocene 214, 527-537.

Włodarska-Kowalczuk, M., Pawłowska, J., Zajączkowski, M. 2013. Do foraminifera mirror diversity and distribution patterns of macrobenthic fauna in an Arctic glacial fjord? Marine Micropaleontology 103, 30-39.

Wollenburg, J. E., Mackensen, A. 1998. Living benthic foraminifers from the central Arctic Ocean: faunal composition, standing stock and diversity. Marine Micropaleontology. 343-4, 153-185.

Yang, X. Y., Wang, G., Keenlyside, N. 2020. The Arctic sea ice extent change connected to Pacific decadal variability. Cryosphere 14, 693–708.

Zaborska, A., Carroll, J., Papucci, C., Torricelli, L., Carroll, M. L., Walkusz-Miotk, J., Pempkowiak, J. 2008. Recent sediment accumulation rates for the Western margin of the Barents Sea. Deep Sea Research. II 5520-21, 2352-2360.

7. General considerations and concluding remarks.

During this work, three areas located along the Fram Strait and the north-western Barents Sea were analysed, each one located in diverse geographical and oceanographical settings. These sites are located along the main zone of the incoming Atlantic Water into the Arctic area, therefore, recording the complex interaction between the cold Arctic Water (ArW) and the warmer, saline Atlantic Water (AW). This study allowed us to reconstruct the Holocene hydrographic changes, with special focus to the last centuries, to improve our knowledge of the centennial and decadal climatic regime and trace the AW impact into the Arctic area.

I. Holocene record

The long core recovered from the contourite depocenter of the Bellsund Drift, located at the eastern side of Fram Strait (western Svalbard margin), corresponding to an expanded Holocene sequence (more than 5 m thick, with a mean sedimentation rate of 0.06 cm/yr), represents an ideal record to study the recent climate history. The Holocene record of the Bellsund Drift showed a general progressive increase of the water temperature. The incoming of the warm AW and the decreasing extension of sea ice, which retreat by melting, produce cold superficial water masses facilitating the increase incoming of the AW into the entire water column. In detail, during the end of the Upper Pleistocene, the water masses are generally cold and the IRD input indicates the presence of sea ice. The Early Holocene is characterised by an increase of warmer conditions, showing a rise in the flux of benthic and planktic foraminifera. A shift from warm to colder conditions occurred during the Mid Holocene, affecting the oceanic productivity. The Late Holocene showed the prevalence of surface cold-water masses related to the ice melting, determined by the increase of AW heat inflow to the Arctic.

II. Little Ice Age and Modern Period, the last *ca.* 350 years

Short cores (box core and multicores) from three different settings in the Arctic region are collected and analysed, with the aim of highlighting in more detail, the oceanographic variations of the last centuries.

The climatic evolution recorded by the Bellsund drift box corer refers to the Modern Period (MP), starting at 1890 A.D. This record outlined the progressively preponderant inflow of the AW initially affecting only the bottom environment and progressively extending to the whole water mass column including superficial water masses.

The Krossfjorden multicore (located at the western margin of Svalbard), a tidewater glacier fjord, recorded the last *ca.* 60 years, from 1956 to 2007 A.D., and the main changes are outlined by the shift between the cold Arctic species *C. reniforme* and *E. clavatum*, indicating periods with the increase of the ice-cover, and periods of increase of the open-water conditions. The environmental sea-bottom evolution during this period, recorded a clear increase of sea ice-free conditions, favouring the primary production in this site. On the other hand, the increment of temperature in this area is not directly associated with the AW inflow in the fjord, as revealed by the benthic foraminiferal association mainly dominated by Arctic species.

Four multicores are studies from the Kveithola Trough, a glacial system located in the NW Barents Sea. The sedimentary record documented the environmental conditions of the last *ca.* 350 years, which corresponds to the Little Ice Age (LIA) and to the Modern Period (MP). During the LIA, the sedimentary sequences recorded the maximum sea ice extent till the western margin of the Barents Sea, followed by a progressively retreat due to an increasing inflow of the AW, producing warmer sea-bottom conditions. During the MP, the sites located in the trough and the one located in the outer-northern area showed different environmental evolution, suggesting a predominant cold ArW influence in the north-eastern area of the glacial trough, and warmer water (AW) influencing the western and southern areas. The absence of sea ice and the general increase in temperature is the clear signature of a constantly strong influence of the warm AW into this area.

Bottom and surface water temperatures, in the studied area, experienced multiyear and decadal oscillations linked to warm and cold periods during the last *ca.* 350 years. These changes indicate that the oceanographic conditions are related to the interaction between the polar superficial cold-water and the warmer deeper AW. The foraminiferal assemblages indicate increasing temperatures, despite the

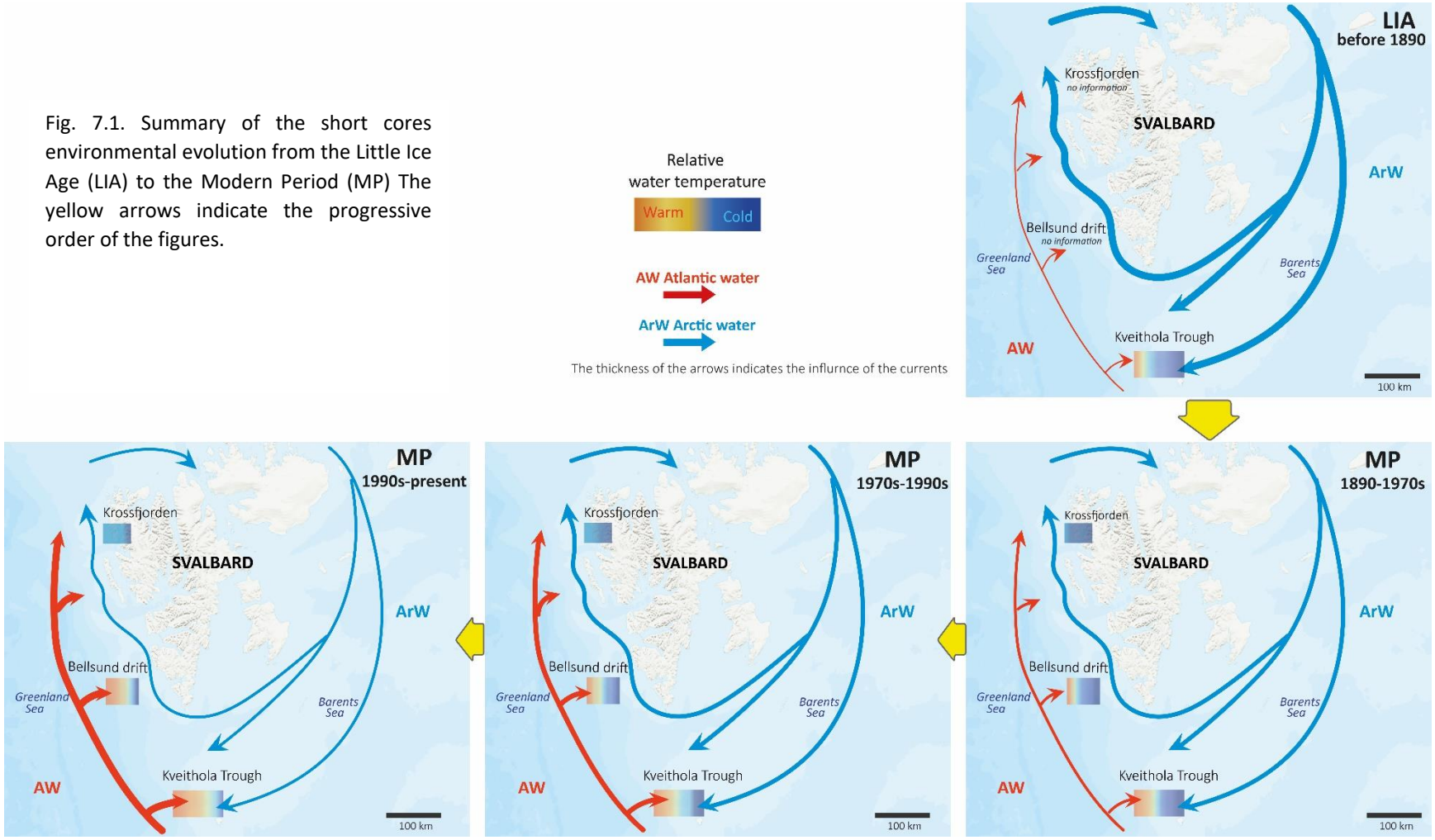
dominance of Arctic species. Warming in the Arctic region is not only a response to the increasing influx of AW, but it is related to a chain of events that can also interfere to this process (CO_2 increase, atmosphere-ocean interaction, intensification of the albedo effect, etc.), triggering stronger heat conditions in the Polar system.

Arctic climatic trend

Several studies indicate that Holocene climatic changes in the Arctic are of higher amplitude than in subpolar areas. Those changes ranged from warm periods with strong seasonality in the early Holocene, to cooler periods with weaker seasonal contrast in the mid-late Holocene (Kaufman et al., 2004). The reconstruction of the paleoenvironmental conditions confirms the global warming trend, reflected in the increasing temperature in the Arctic area, from the Holocene and amplified after the LIA and during MP and in the recent *ca.* 350 years, in agreement with what is now widely recognised for polar areas.

The detailed record of the last ca. 350 years shows at least, four general events (Fig. 7.1). The first event corresponds with the LIA (before 1890 A.D.), characterised by cold conditions, recorded in the Kveithola Trough area (Fig. 7.1). The MP corresponds with an increase of the temperature in the Arctic record, and in general can be divided in three periods. From 1890 to 1970 A.D., the interaction between cold and warm water masses is indicated by the proliferation of the species indicators of warm water conditions (Fig. 7.1). From *ca.* 1970 until 1990 A.D., increasing warmer conditions are recorded, interrupted by multiyear episodes of colder conditions, probably related with the colder winter seasons mainly at the end of the 1980s and beginning of the 1990s (Fig. 7.1). From the 1990s until present, the foraminiferal record indicates an increase of the warm water species. This trend is also recorded by the satellite monitoring, indicating records of warmer temperatures during the last two decades (Fig. 7.1). The benthic and planktic foraminiferal records show an increment in the inflow of AW into the Arctic region (Kveithola Trough and Bellsund drift), that it is traceable by the interaction between cold and warm water indicators. In the Krossfjorden, instead, the warming trend is not directly linked to the enhanced influx of AW but it reflects a complex interaction of other factors, such as atmospheric circulation and sea-ice distribution.

Fig. 7.1. Summary of the short cores environmental evolution from the Little Ice Age (LIA) to the Modern Period (MP) The yellow arrows indicate the progressive order of the figures.



Proxies and multidisciplinary work

Changes in environmental conditions provides information about the magnitude of natural climate and environmental variability, both resulting from external climate drivers and internally generated climate variability at timescales relevant for the Holocene (Borzenkova et al., 2015). The use of the foraminiferal record made possible to trace the oceanographic changes, both in the bottom and water column. The palaeo-bio-geographical patterns of benthic and planktic foraminifera are therefore necessary in palaeoceanography (Murray, 2006), together with sedimentological information, can give a solid interpretation about the past climate change. The use of foraminifera on recent Arctic glaciomarine sediments provides insights into the environmental significance of taxa improving our understanding of the palaeoenvironmental significance of fossil faunas (Korsun et al., 1995).

This work mirror the importance of improving the singular proxies, to understand better the evolution of climatic changes and the interconnections in different environments (land, water, ice, and atmosphere). Understand the driving variability and climate change over centennial timescales, and estimate the extent to which future climate could deviate from the present global trend is proposed for further multidisciplinary and multiproxy studies, including the atmospheric-oceanic interaction as another factor to take into consideration in the climatic equation. Changes at regional scales including deviations from the global average, it can be substantial and should be incorporated in regional policy on adaptation to climate change (Borzenkova et al., 2015; IPCC, 2019). The application of multidisciplinary studies can allow us to understand the pattern of the indisputable increase in global temperature, and how we can preserve the equilibrium of our planet.

7.1. References

Borzenkova I., Zorita, E., Borisova, O., Kalniņa, L., Kisielienė, D., Koff, T., Kunznetsov, D., Lemdahl, G., Sapelko, T., Stančikaitė, M., Subetto, D. 2015. Climate Change During the Holocene (Past 12,000 Years). In: The BACC II Author Team (eds) Second Assessment of Climate Change for the Baltic Sea Basin. Regional Climate Studies. Springer, Cham DOI https://doi.org/10.1007/978-3-319-16006-1_2

IPCC, 2019: IPCC Special Report on the Ocean and Cryosphere in a Changing Climate [H.-O. Pörtner, D.C. Roberts, V. Masson-Delmotte, P. Zhai, M. Tignor, E. Poloczanska, K. Mintenbeck, A. Alegría, M. Nicolai, A. Okem, J. Petzold, B. Rama, N.M. Weyer (eds.)]. In press.

Kaufman, D. S., Ager, T. A., Anderson, N. J., Anderson, P. M., Andrews, J. T., Bartlein, P. J., Brubaker, L.B., Coats, L.L., Cwynar, L.C., Duvall, M.L., Dyke, A. S. 2004. Holocene thermal maximum in the western Arctic (0–180 W). Quaternary Science Reviews, 23(5-6), 529-560.

Korsun, S. A., Pogodina, I. A., Forman, S. L., Lubinski, D. J. 1995. Recent foraminifera in glaciomarine sediments from three arctic fjords of Novaja Zemlja and Svalbard. Polar Research, 14(1), 15-32.

Murray, J. W. 2006. Ecology and applications of benthic foraminifera. Cambridge University Press.

8. Supplementary material

Micropaleontological analysis

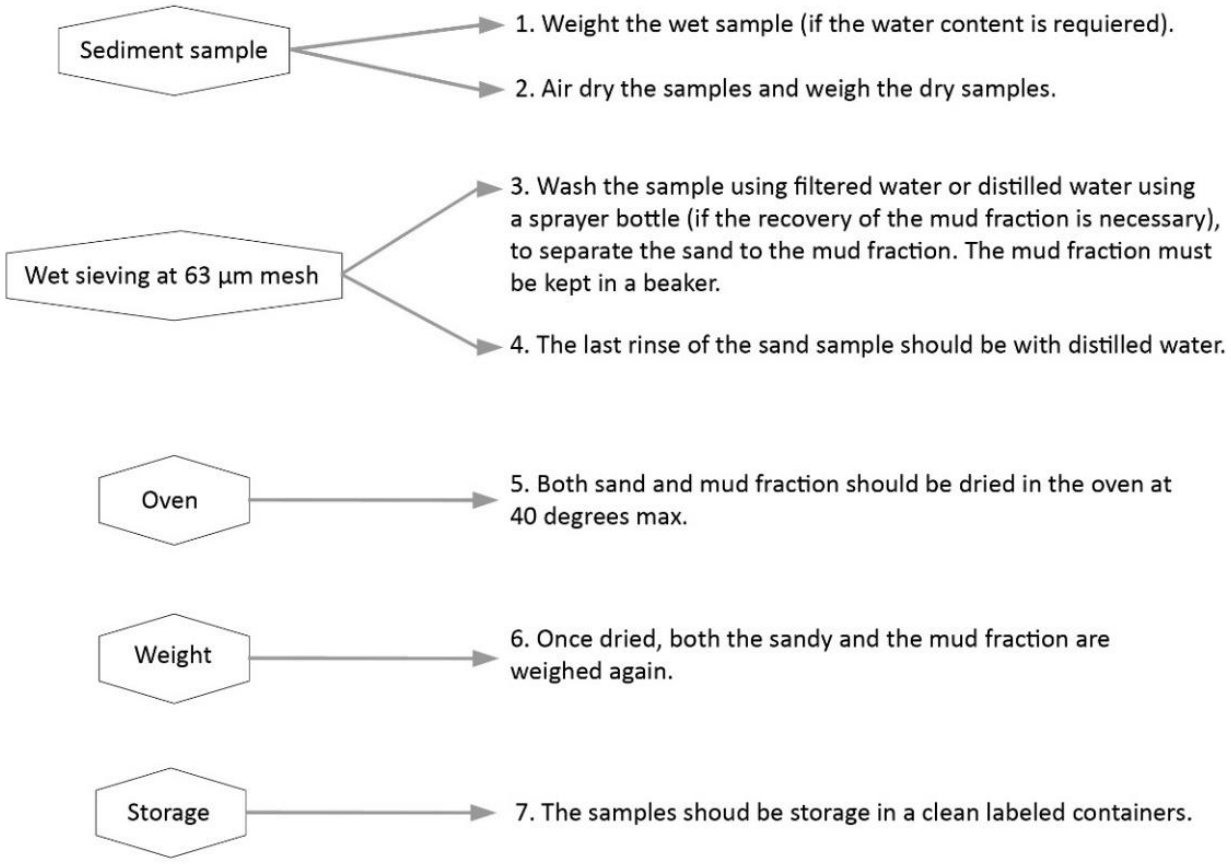
Samples prepared at University of Pisa (UniPi), and workflow of the preparation of the sediment samples.

Sample		**Number of samples**
Calypso piston core	GS191-01PC	293
Box-corer	GS191-02BC	42
Multi-corer	02-2	32
	21-03	10
	21-05	27
	07-3	35

Tab. ST1. Samples prepared at UniPi

Preparation of the sediment samples for micropaleontological analysis

Objective: disgregate the sediment and separate the sand (>63 µm) and the mud fraction (<63µm).



Information obtained by the end of the process
Total wet sample weight, Total dry sediment weight, Weight of the >63µm fraction and Weight of the <63µm

Workflow S1. Preparation of the sediment samples for micropaleontological analysis and XRD analysis (the XRD analysis are in charge of OGS-Trieste).

Plates

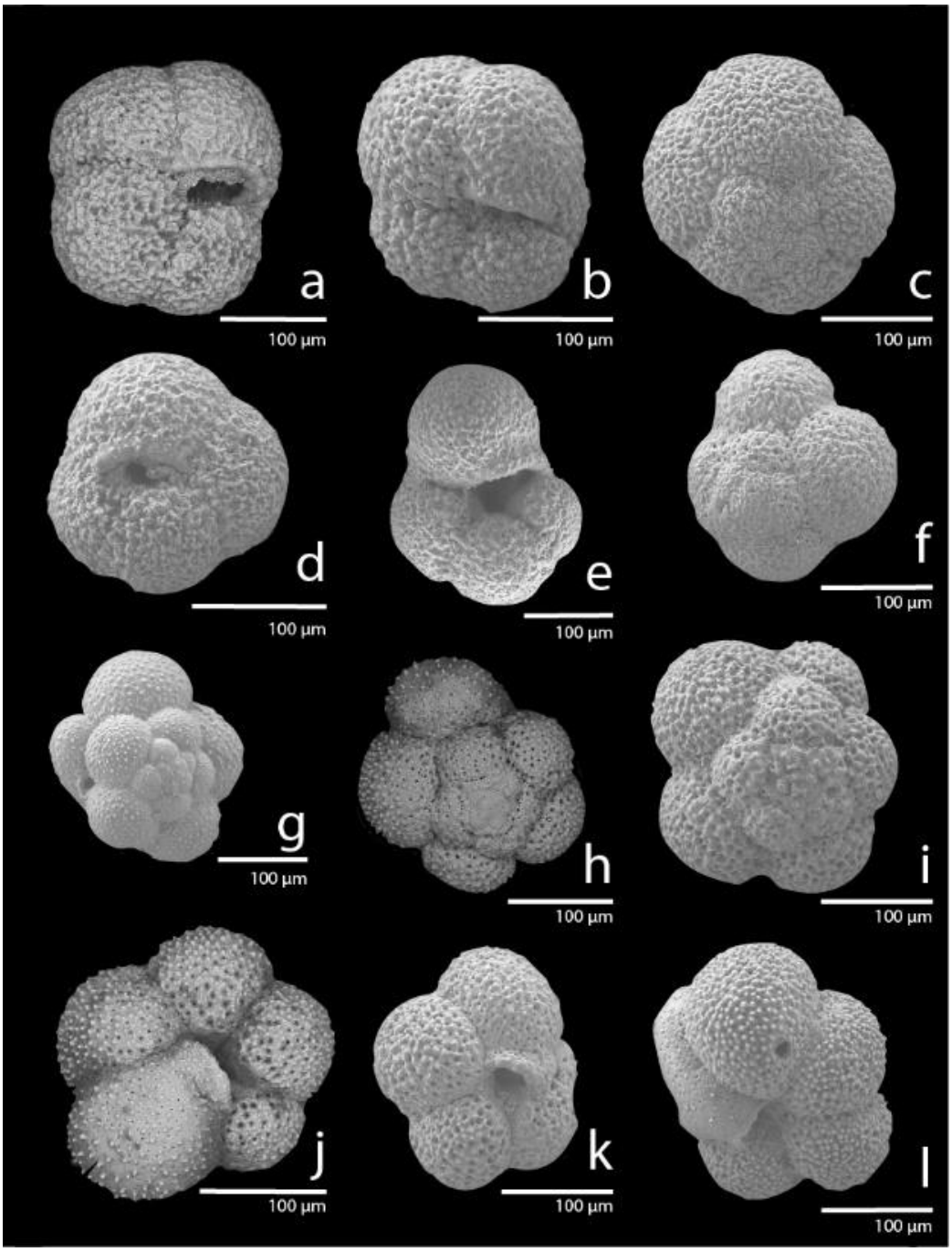


Plate. S1. Planktonic foraminiferal species. SEM pictures. (a-b-c) *Neogloboquadrina pachyderma*; (d) *Neogloboquadrina incompta*; (e- f). *Globigerina bulloides*. (g-h-i-j-k-l). *Turborotalita quinqueloba*; all the specimens are from the box-corer GS191-02BC.



Plate. S2. Planktonic foraminiferal species. Stereomicroscope pictures. (a-b) *Neogloboquadrina pachyderma*; (c- d- e). *Globigerina bulloides*. (f-g-h-i). *Turborotalita quinqueloba*; all the specimens are from the box-corer GS191- 02BC.

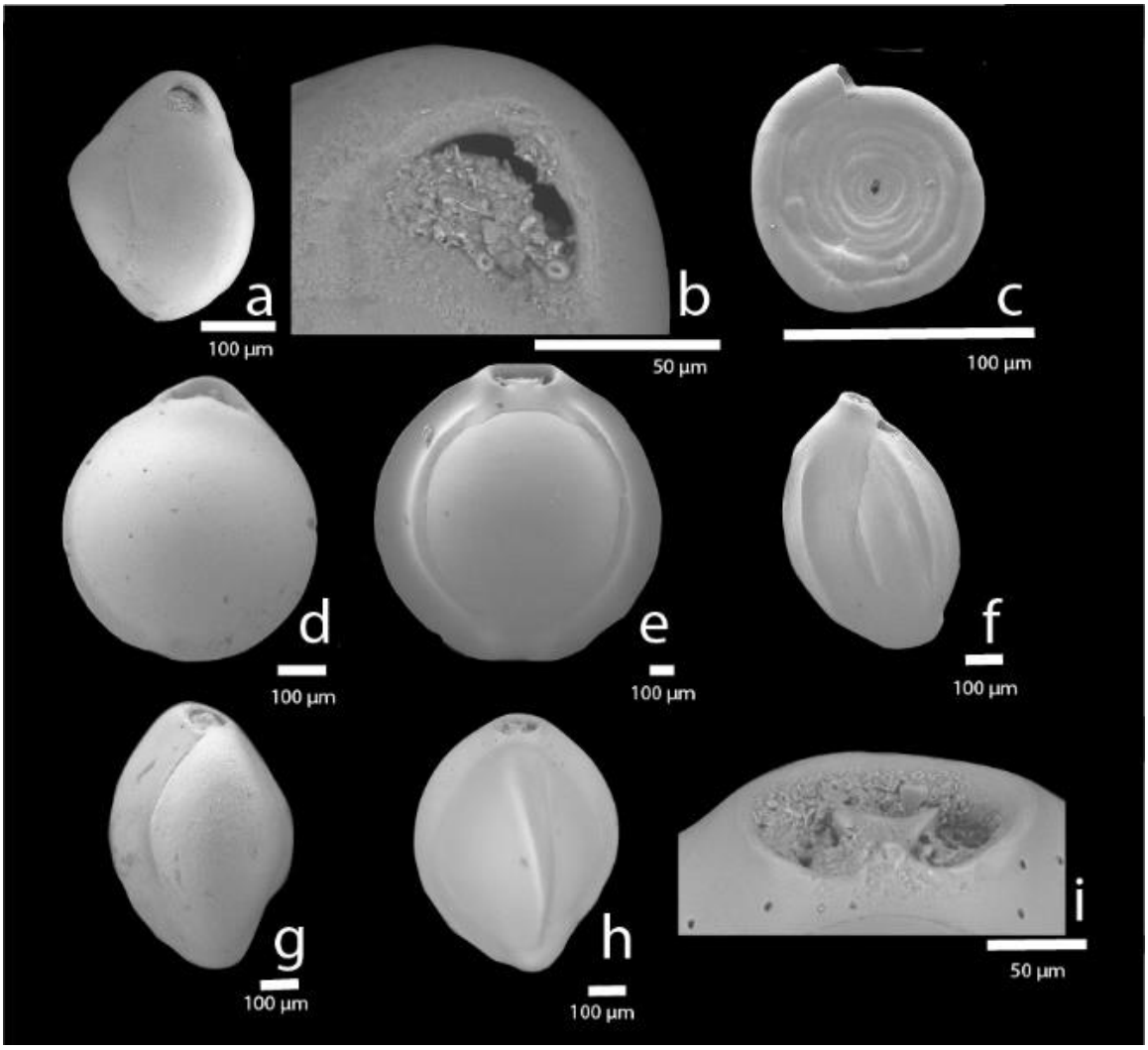


Plate. S3. Calcareous imperforate benthic foraminifera SEM pictures (a). *Miliolinella* cf. *enoplostoma*; (b). Zoom of the aperture of the *Miliolinella* cf. *enoplostoma;* (c) *Cornuspira* spp.; (d-e) *Pyrgo* spp.; (f). *Quinqueloculina annectens*; (g). *Triloculina rotunda*; (h). *Triloculina tricarinata;* (i). Zoom of the aperture of the *Triloculina tricarinata.* All the specimens are from the *Calypso* piston core GS191-01 PC.

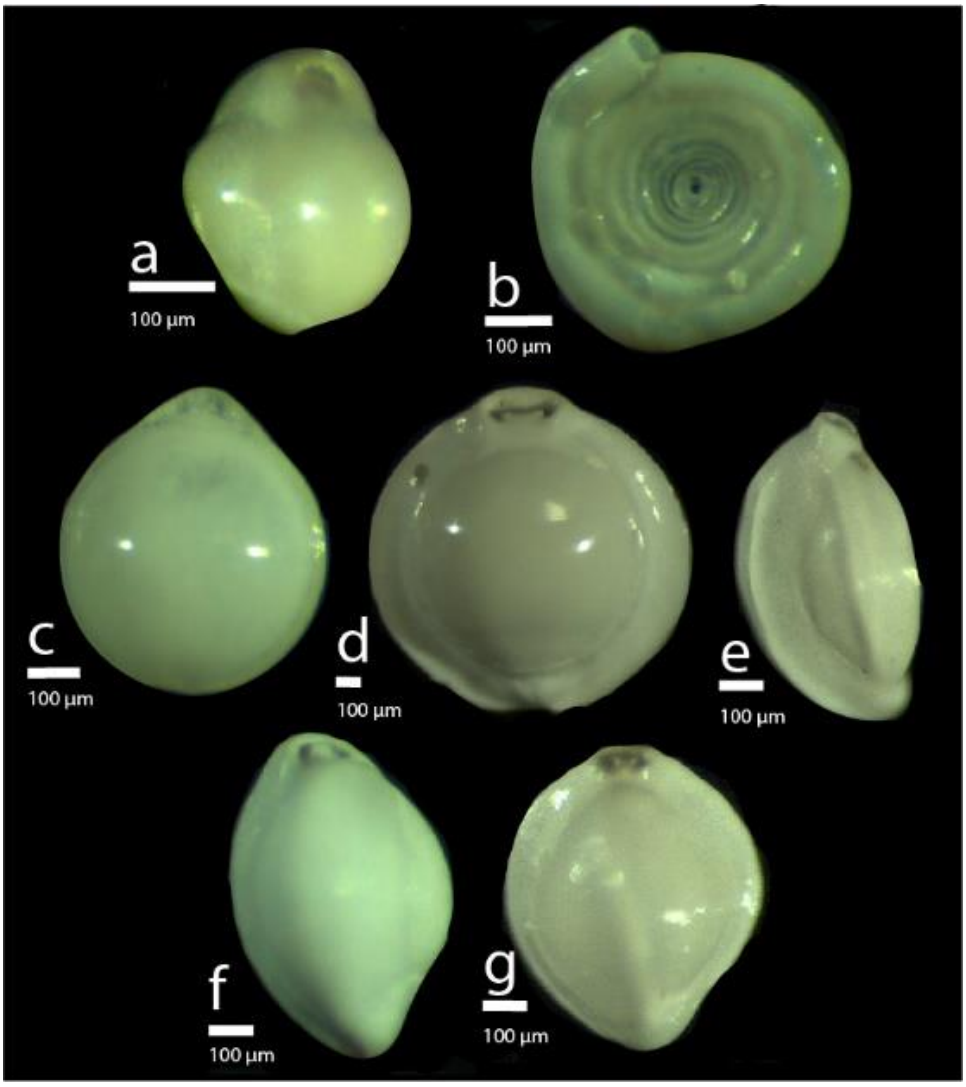


Plate. S4. Calcareous imperforate benthic foraminifera. Stereomicroscope pictures (a). *Miliolinella* cf. *enoplostoma*; (b) *Cornuspira* spp.; (c-d) *Pyrgo* spp.; (e). *Quinqueloculina annectens*; (f). *Triloculina rotunda*; (g). *Triloculina tricarinata.* All the specimens are from the *Calypso* piston core GS191-01 PC.

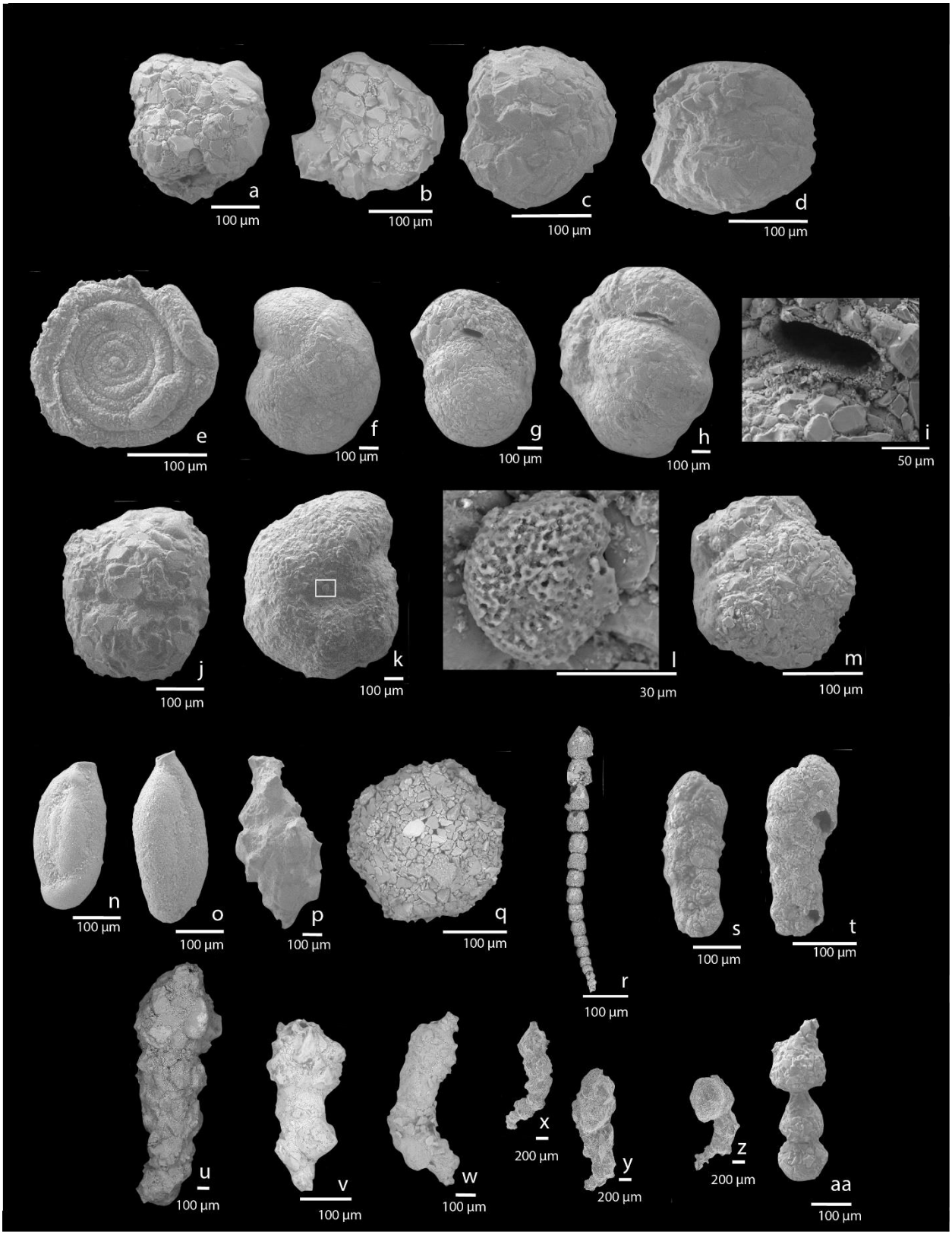

a
100 µm
b
100 µm
c
100 µm
d
100 µm
e
100 µm
f
100 µm
g
100 µm
h
100 µm
i
50 µm
j
100 µm
k
100 µm
l
30 µm
m
100 µm
n
100 µm
o
100 µm
p
100 µm
q
100 µm
r
100 µm
s
100 µm
t
100 µm
u
100 µm
v
100 µm
w
100 µm
x
200 µm
y
200 µm
z
200 µm
aa
100 µm

Plate. S5. Agglutinated benthic foraminifera SEM pictures. (a-b). *Adercotryma* cf. *glomeratum*; (c- d). *Adercotryma glomeratum*; (e). *Ammodiscus minimus*; (f-g-h). *Labrospira crassimargo*; (i). Zoom of the aperture of the *Labrospira crassimargo*; (j). *Recurvoides trochamminiforme*; (k). *Labrospira subglobosa*; (l). Zoom of the white square on the *Labrospira subglobosa*; (m). *Trochammina globigeriniformis*; (n- o). *Quinqueloculina agglutinans*; (p). *Reophax micacea*; (q). *Psammosphaera fusca*; (r). *Reophax catenatus*; (s- t). *Spiroplectammina biformis*; (u-v-w-x-y-z-aa). *Reophax* spp. From *Calypso* piston core GS191-01PC (a-b-j-k-l- m-q-v-w-y); from the box-corer GS191-02BC (e-f-g-h-i-u-x-z-aa); from the multi-core NP16-Kr1 MC (c-d-n-o-p-s-t); from the multicore 21-03 (r).

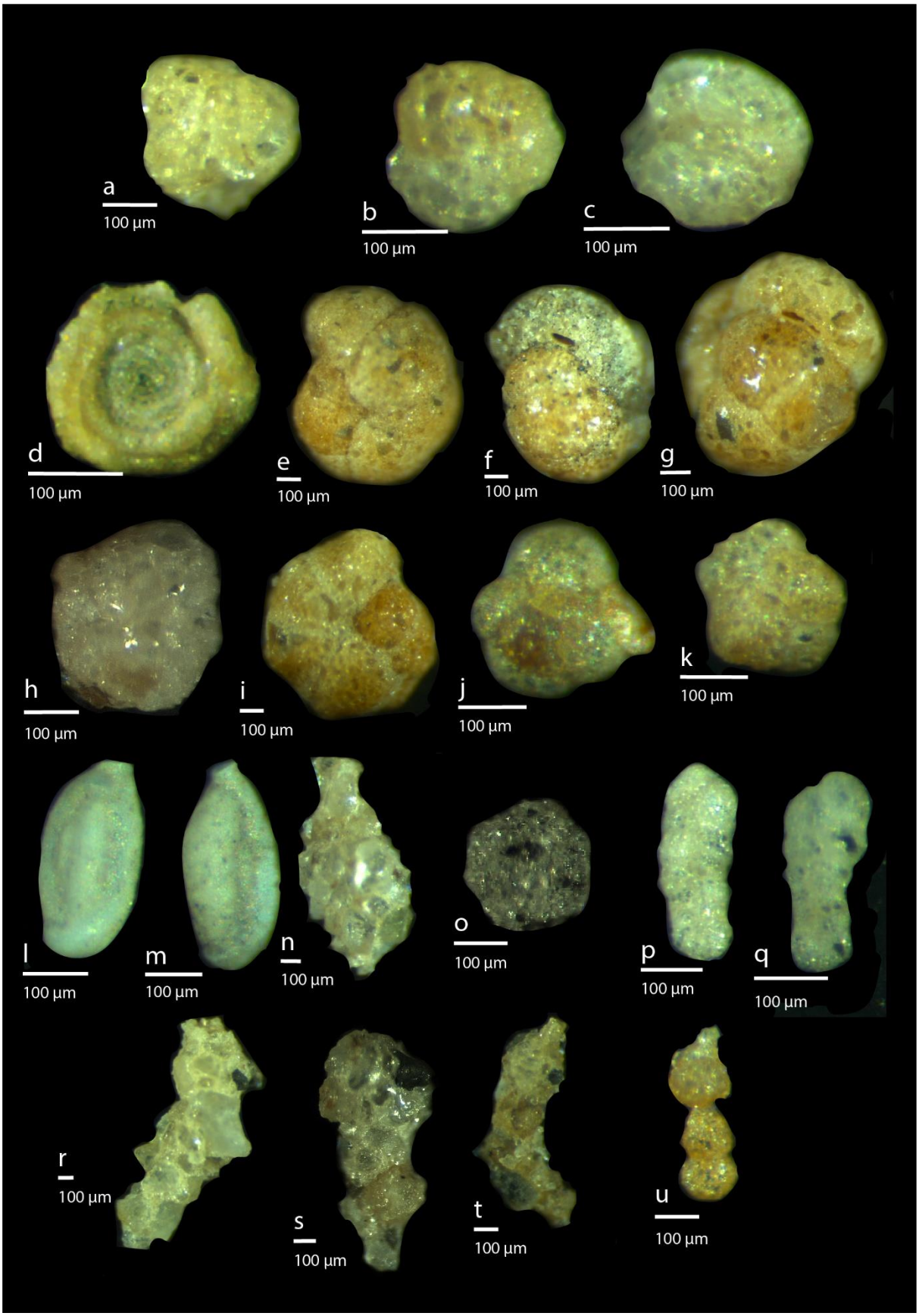

a
100 µm
b
100 µm
c
100 µm
d
100 µm
e
100 µm
f
100 µm
g
100 µm
h
100 µm
i
100 µm
j
100 µm
k
100 µm
l
100 µm
m
100 µm
n
100 µm
o
100 µm
p
100 µm
q
100 µm
r
100 µm
s
100 µm
t
100 µm
u
100 µm

Plate. S6. Agglutinated benthic foraminifera. Stereomicroscope pictures. (a). Adercotryma cf. glomeratum; (b- c). Adercotryma glomeratum; (d). Ammodiscus minimus; (e-f-g). Labrospira crassimargo; (h) Recurvoides trochamminiforme; (i). Labrospira subglobosa; (j-k). Trochammina globigeriniformis; (l- m). Quinqueloculina agglutinans; (n). Reophax micacea; (o). Psammosphaera fusca; (p- q) Spiroplectammina biformis; (r-s-t-u). Reophax spp. From Calypso piston core GS191-01PC (a-h-i-j-k-o-s-t); from the box-corer GS191-02BC (d-e-f-g-r-u); from the multi-core NP16- Kr1 MC (b-c-l-m-n-p-q).

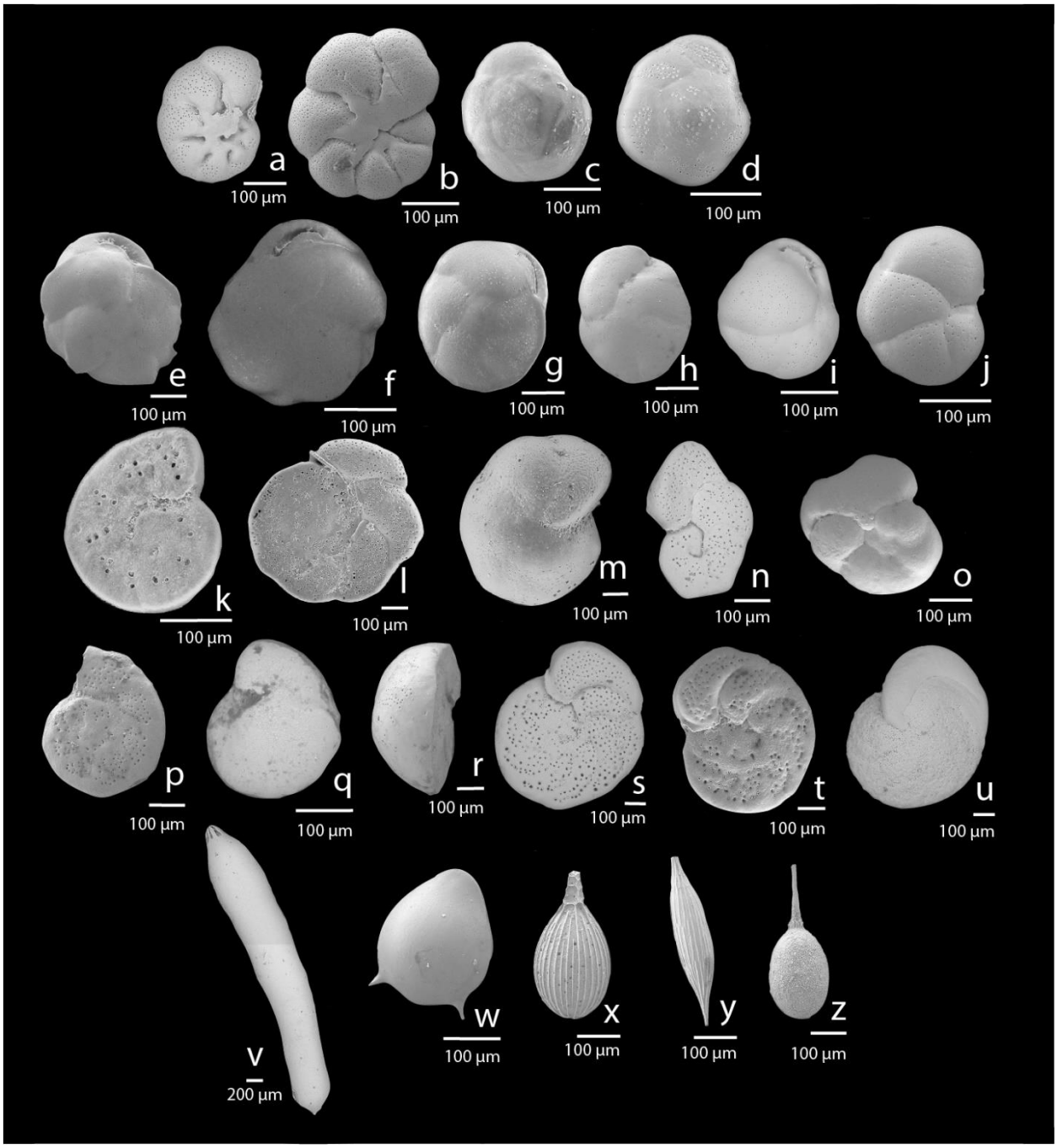


Plate S.7. Calcareous perforate benthic foraminifera SEM pictures (a-b). *Astrononion gallowayi*; (c- d). *Buccella* spp.; (e-f). *Cassidulina laevigata* (g- h). *Cassidulina neoteretis*; (i-j). *Cassidulina reniforme*; (k- l- m- n- o). *Cibicidoides lobatulus*; (p- q- r). *Cibicides refulgens*; (s-t-u). *Cibicidoides wuellerstorfi*; (v). *Dentalina* spp.; (w). *Fissurina* spp.; (x- y- z). *Lagena* spp**.** From the *Calypso* piston core GS191-01PC (a-b-i-j-h-n-o-s-t-u-v-w-x-y-z); from the box-corer GS191-02BC (f-e); from the multi core 02-2 (k-l); from the multi-core 21-03 (c); from the multi-core 07-3 (d-g-p-q-r-m).

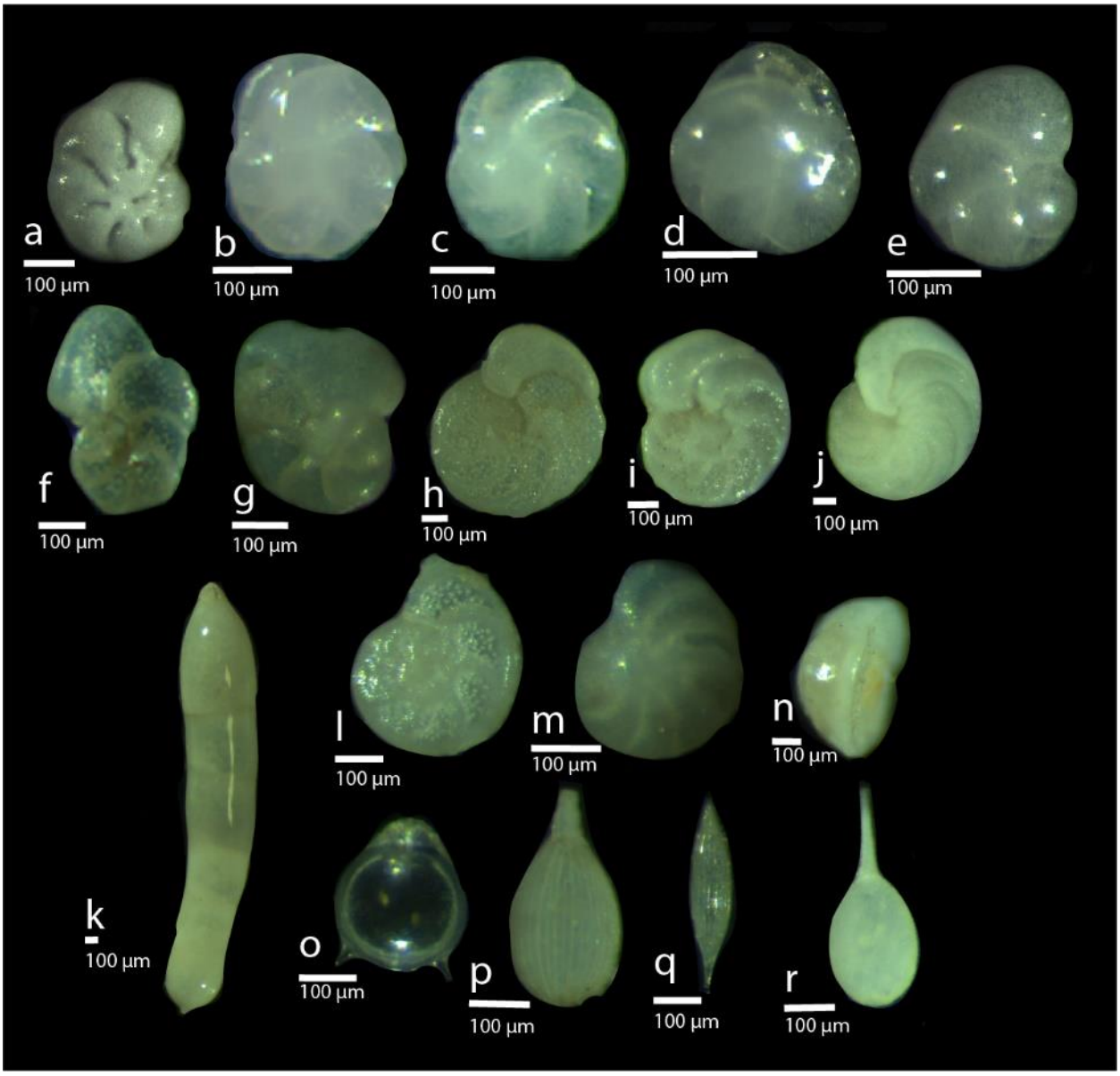


Plate S.8. Calcareous perforate benthic foraminifera. Stereomicroscope pictures (a). *Astrononion gallowayi*; (b). *Cassidulina laevigata;* (c). *Cassidulina neoteretis*; (d-e). *Cassidulina reniforme*; (f-g). *Cibicidoides lobatulus*; (h- i- j) *Cibicidoides wuellerstorfi;* (k). *Dentalina* spp.; (l-m-n) *Cibicides refulgens*; (o). *Fissurina* spp.; (p- q- r). *Lagena* spp**.** From the *Calypso* piston core GS191-01PC (a-c-d-e-f-g-h-i-j-k-o-p-q-r); from the box-corer GS191-02BC (b); from the multi-core 07-3 (l-m-n).

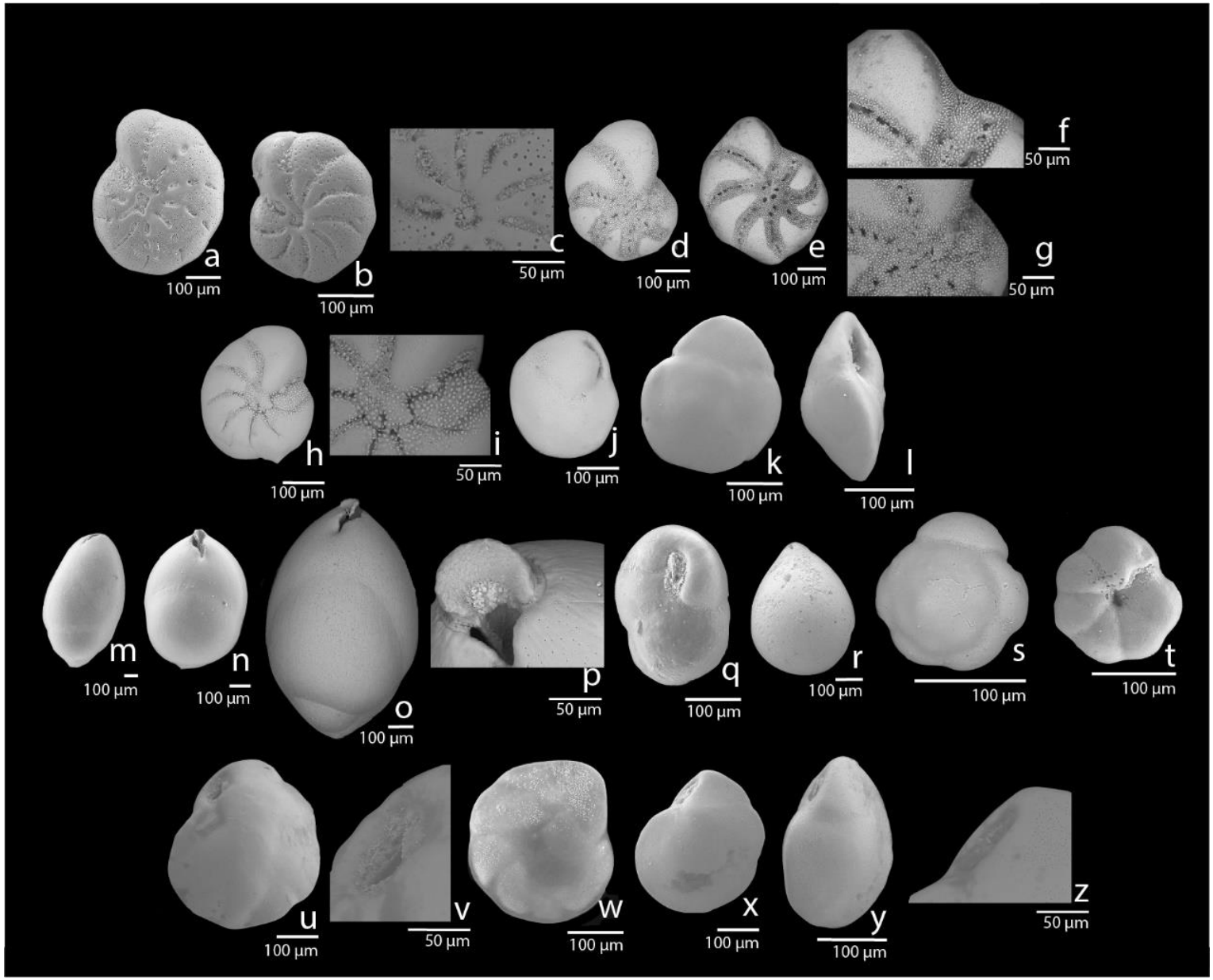

a
100 µm
b
100 µm
c
50 µm
d
100 µm
e
100 µm
f
50 µm
g
50 µm
h
100 µm
i
50 µm
j
100 µm
k
100 µm
l
100 µm
m
100 µm
n
100 µm
o
100 µm
p
50 µm
q
100 µm
r
100 µm
s
100 µm
t
100 µm
u
100 µm
v
50 µm
w
100 µm
x
100 µm
y
100 µm
z
50 µm

Plate. S9. Calcareous perforate benthic foraminifera SEM pictures. (a-b). *Elphidium clavatum*; (c). Zoom umbilical area of *Elphidium clavatum*; (d-e). *Elphidium hallandense*; (f-g). Zoom of the umbilical area and aperture of *Elphidium hallandense*; (h). *Haynesina orbiculare*; (i). Zoom of the umbilical area of *Haynesina orbiculare*; (j- k- l). *Epistominella exigua*; (m). *Globobulimina arctica*; (n- o). *Globobulimina auriculata*; (p). Zoom of the aperture of the *Globobulimina auriculata*; (q). *Globocassidulina subglobosa*; (r). *Globulina landesi*; (s-t). *Ioanella tumidula*; (u). *Islandiella helenae*; (v). Zoom of the aperture of the *Islandiella helenae*; (w-x-y). *Islandiella norcrossi*; (z). Zoom of the aperture of the *Islandiella norcrossi*. From the multi-core 21-03 (a-m-n); from the multi-core 07-3 (o-p-q-w); from the *Calypso* piston core GS191-01PC (d-g-j-k-l-h-i-r-s-t); from the box-corer GS191-02BC (e-f); from the multi-core NP16-Kr1 MC (b-c-u-v-x-y-z).

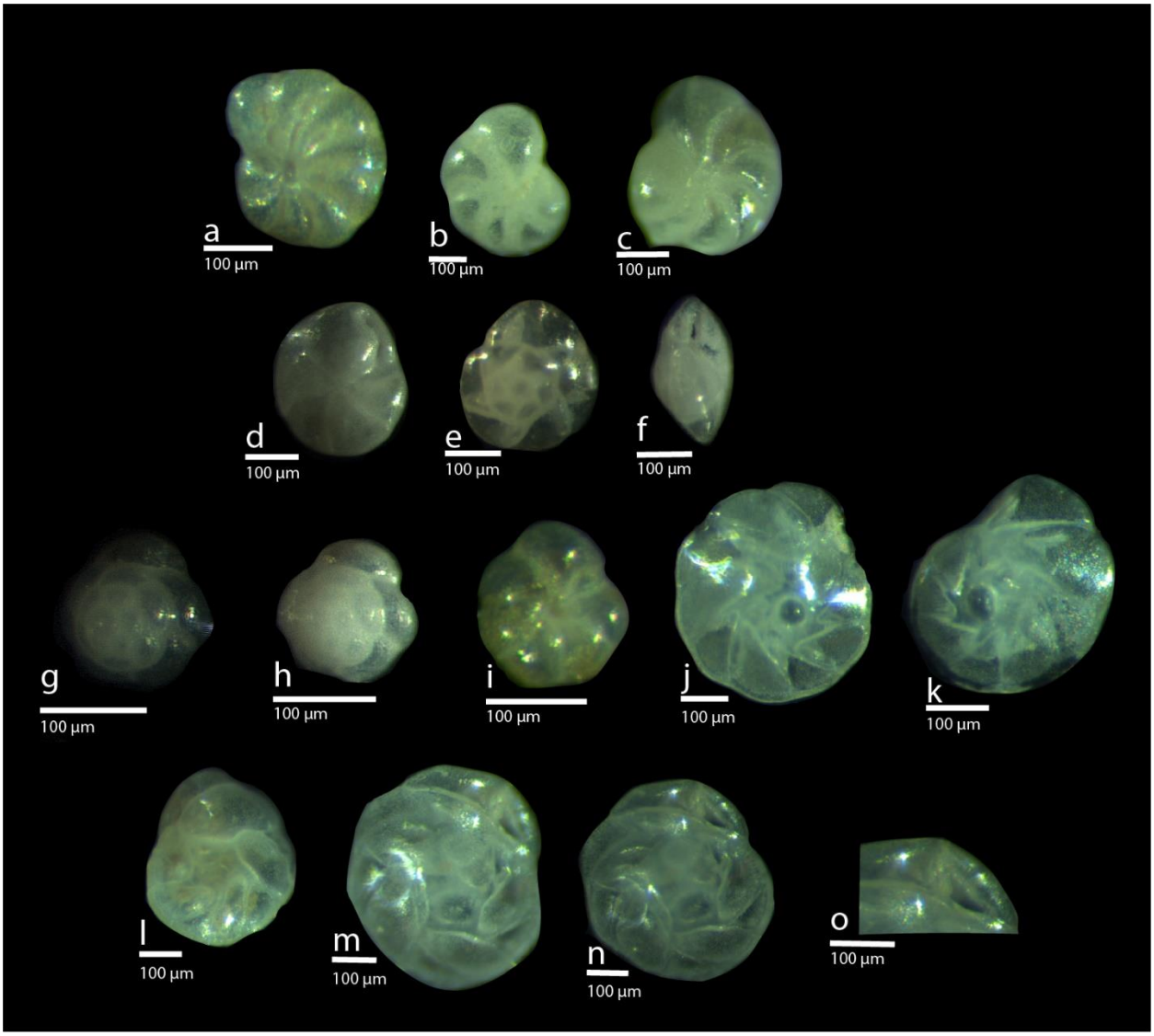


Plate. S10. Calcareous perforate benthic foraminifera. Stereomicroscope pictures. (a). *Elphidium clavatum*; (b). *Elphidium hallandense*; (c). *Haynesina orbiculare*; (d-e-f). *Epistominella exigua*; (g-h-i). *Ioanella tumidula*; (j- k). *Islandiella norcrossi*; (l-m-n-o). *Islandiella helenae*. From the multi-core 21-03 (); from the multi-core 07-3 (j); from the *Calypso* piston core GS191-01PC (b-c-d-e-f-g-h-i); from the box-corer GS191-02BC (e-f); from the multi-core NP16-Kr1 MC (a-k-l-m-n-o).

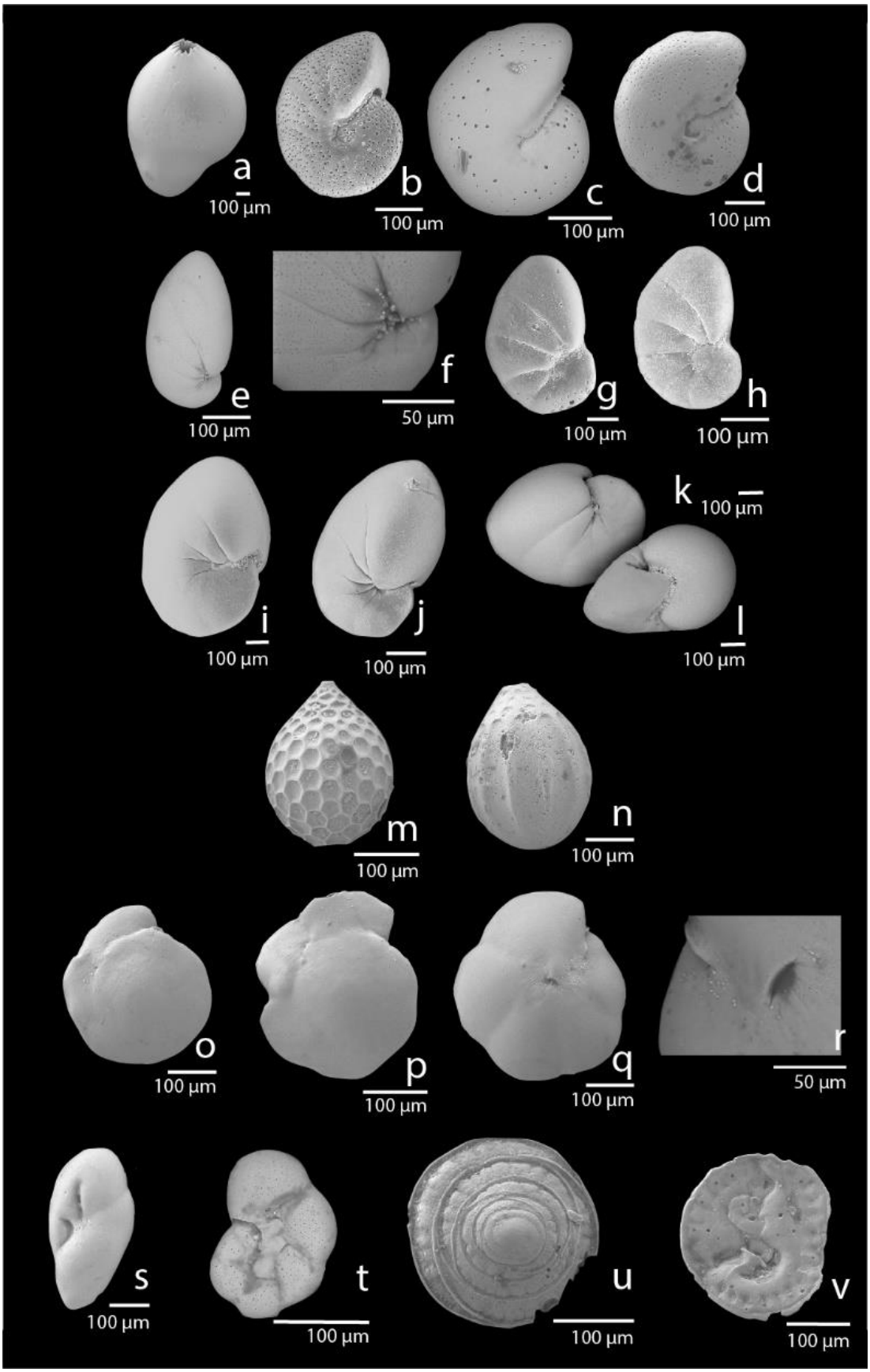

a
100 µm
b
100 µm
c
100 µm
d
100 µm
e
100 µm
f
50 µm
g
100 µm
h
100 µm
i
100 µm
j
100 µm
k
100 µm
l
100 µm
m
100 µm
n
100 µm
o
100 µm
p
100 µm
q
100 µm
r
50 µm
s
100 µm
t
100 µm
u
100 µm
v
100 µm

Plate. S11. Calcareous perforate benthic foraminifera SEM pictures. (a). *Marginulina obesa*; (b- c- d). *Melonis barleeanus*; (e). *Nonionella auricula*; (f). Zoom of the umbilical zone of the *Nonionella auricula*; (g- h). *Nonionella iridea*; (i-j-k-l). *Nonionellina labradorica*; (m-n). *Oolina* spp.; (o- p- q). *Oridorsalis tener*; (r). Zoom of the aperture of the *Oridorsalis tener*; (s). *Robertinoides charlottensis*; (t). *Valvulineria minuta*; (u - v). *Patellina corrugata*. From the Calypso piston core GS191-01PC (a-c-d-e-f-m-n-o-p-q-r-s-t-u-v); from the multi-core 21-03 (b-g); from the multi-core 07-3 (h-j-k-l); from the multi-core 21-05 (i).

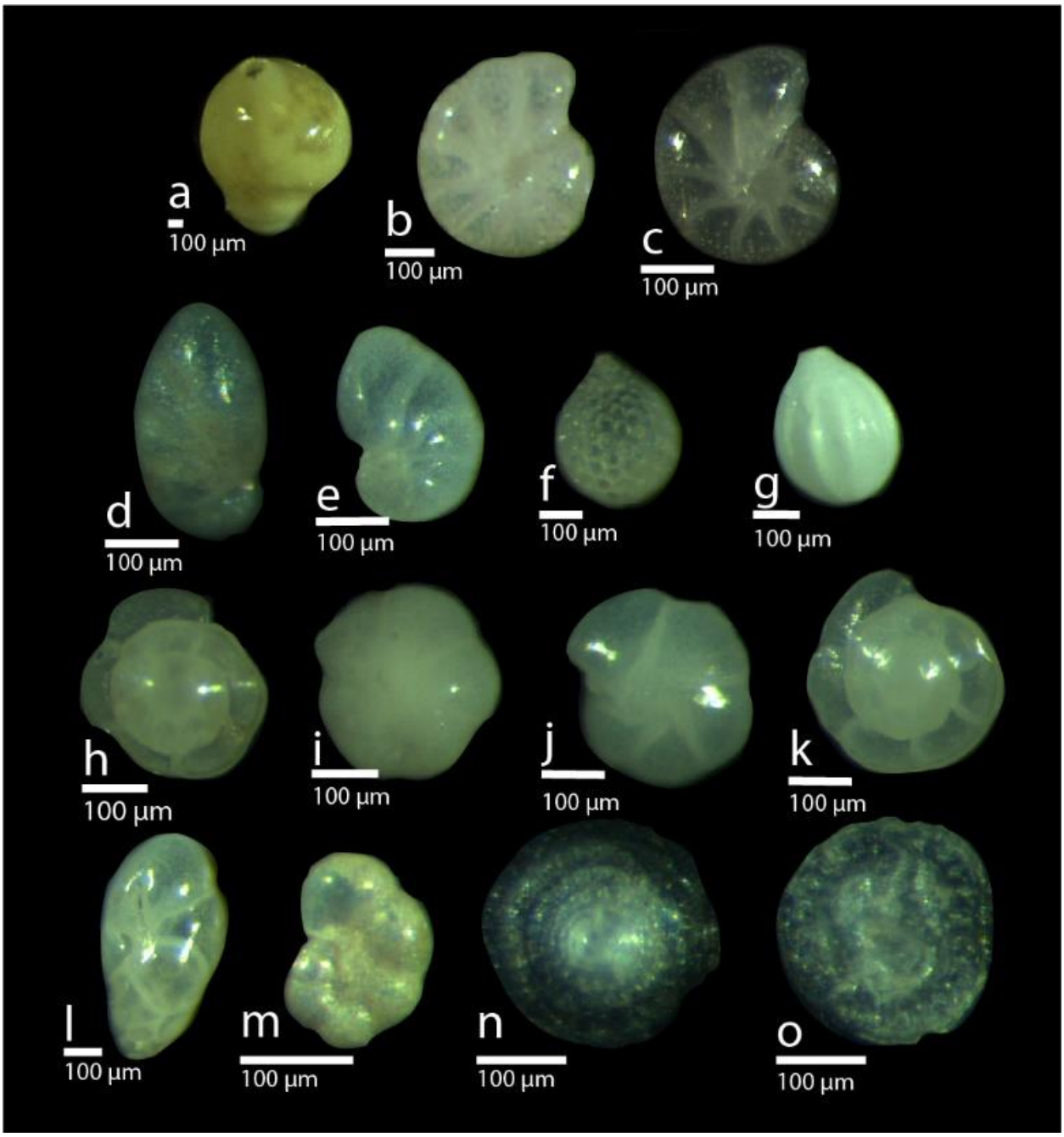


Plate. S12. Calcareous perforate benthic foraminifera. Stereomicroscope pictures. (a). *Marginulina obesa*; (b- c). *Melonis barleeanus*; (d). *Nonionella auricula*; (e). *Nonionella iridea*; (f-g). *Oolina* spp.; (o- p- q). *Oridorsalis tener*; (r). Zoom of the aperture of the *Oridorsalis tener*; (s). *Robertinoides charlottensis*; (t). *Valvulineria minuta*; (u-v). *Patellina corrugata*. From the Calypso piston core GS191-01PC (a-b-c-d-f-g-h-i-j-k-l-m-n-o); from the multi-core 21-03 (e).

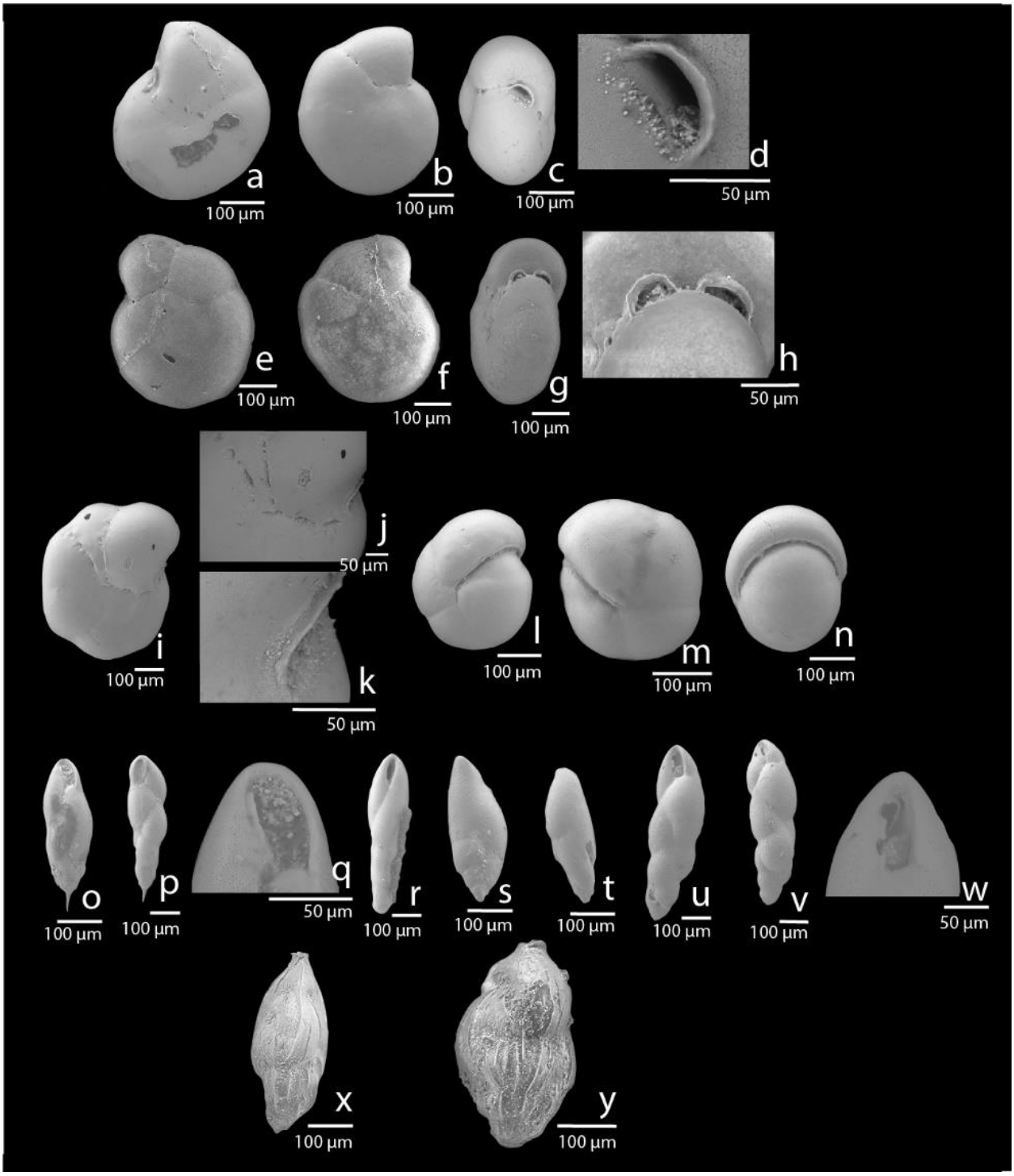

a
100 µm
b
100 µm
c
100 µm
d
50 µm
e
100 µm
f
100 µm
g
100 µm
h
50 µm
i
100 µm
j
50 µm
k
50 µm
l
100 µm
m
100 µm
n
100 µm
o
100 µm
p
100 µm
q
50 µm
r
100 µm
s
100 µm
t
100 µm
u
100 µm
v
100 µm
w
50 µm
x
100 µm
y
100 µm

Plate. S13. Calcareous perforate benthic foraminifera SEM pictures. (a-b-c-e-f-g). *Parrelloides* cf. *healdi*; (d- h). Zoom of the aperture of *Parrelloides* cf. *healdi*; (i). *Pullenia* cf. *catalinaensis*; (j-k). Zoom of the aperture of *Pullenia* cf. *catalinaensis*. (l). *Pullenia bulloides*; (m-n). *Pullenia osloensis*; (o- p). *Stainforthia concava*; (q). Zoom of aperture of *Stainforthia concava*; (r). *Stainforthia feylingi*; (s- t). *Stainforthia fusiformis*; (u-v). *Stainforthia loeblichi*; (w). Zoom of aperture *Stainforthia loeblichi*; (x). *Trifarina angulosa*. (y). *Trifarina fluens*. From the *Calypso* piston core GS191-01PC (a-b-c-d-i-j-k-l-r); from the box corer GS191-02BC (e-f-g-m-n); from the multi-corer NP16-Kr1 MC (o-p-q-s-t-u-v-w).

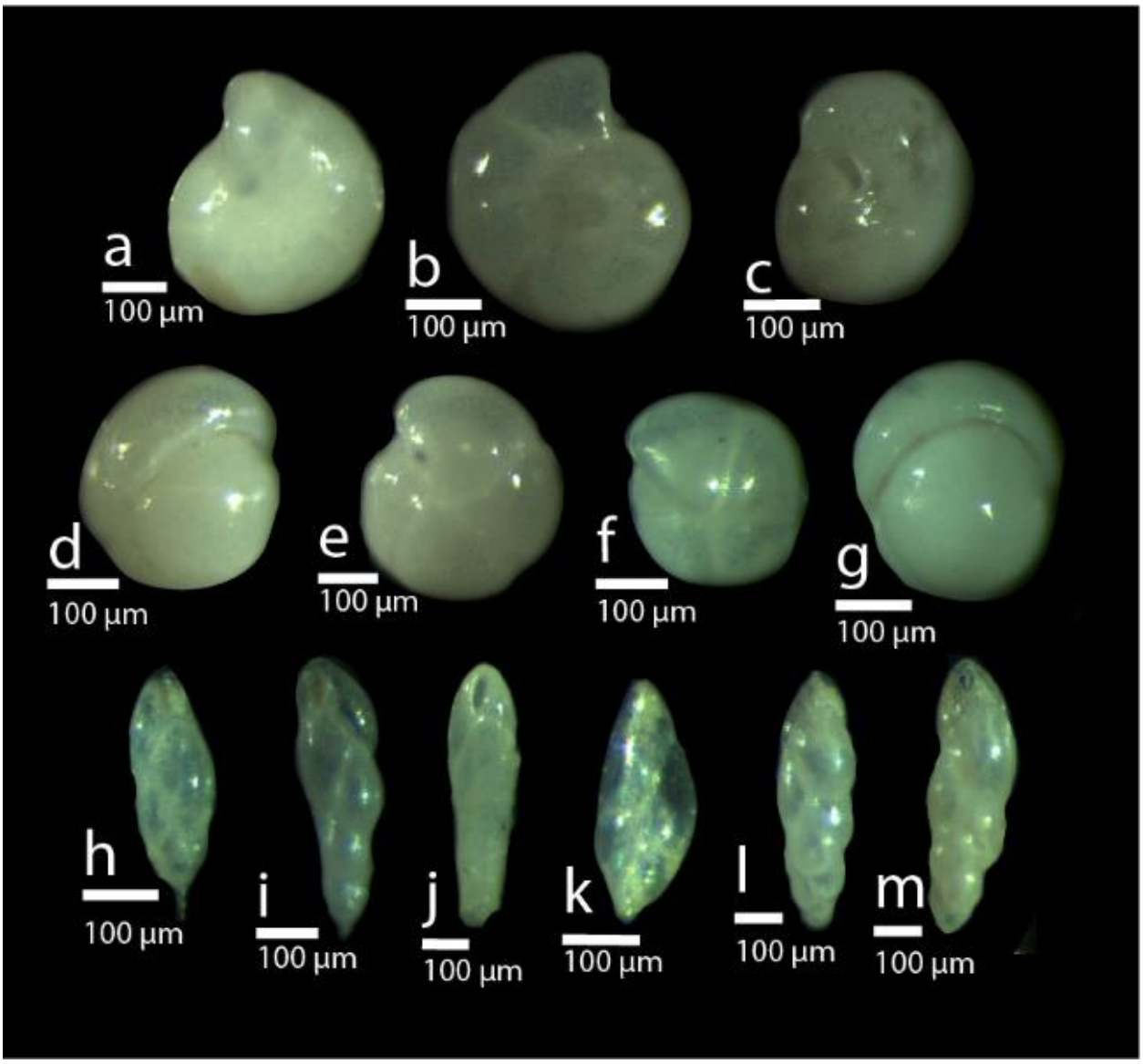


Plate. S14. Calcareous perforate benthic foraminifera. Stereomicroscope pictures. (a-b-c). *Parrelloides* cf. *healdi*; (d- e). *Pullenia bulloides*; (f-g). *Pullenia osloensis*; (h-i). *Stainforthia concava*; (q). Zoom of aperture of *Stainforthia concava*; (j). *Stainforthia feylingi*; (k). *Stainforthia fusiformis*; (l-m). *Stainforthia loeblichi*. From the *Calypso* piston core GS191-01PC (a-b-c-d-j); from the box corer GS191-02BC (e-f-g); from the multi-corer NP16-Kr1 MC (k-l-m).

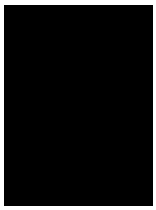
Core	Core depth (cm)	Living foraminiferal assemblages					Dead foraminiferal assemblages				
		N	S	spec./gr	D	H	N	S	spec./gr	D	H
02	0-0.5	19	6	2	0.2	1.5	300	22	3079	0.1	2.3
	0.5-1	14	7	1	0.2	1.8	312	22	3247	0.1	2.5
	1-1.5	1	1	0.1	1.0	0.0	285	25	2253	0.1	2.5
	1.5-2	4	2	0.4	0.5	0.7	332	23	4660	0.1	2.4
	2-3	3	2	0.2	0.6	0.6	312	25	4977	0.1	2.5
	3-4	-	-	-	-	-	420	26	3313	0.1	2.4
	4-5	2	2	0.1	0.5	0.7	314	28	4161	0.1	2.6
	5-6	-	-	-	-	-	286	27	3272	0.1	2.4
	6-7	1	1	0.1	1.0	0.0	368	25	4187	0.1	2.5
	7-8	-	-	-	-	-	310	21	2477	0.1	2.4
	8-9	-	-	-	-	-	363	23	1509	0.2	2.2
	9-10	-	-	-	-	-	325	22	2424	0.2	2.1
	0-10 (total)	**43**	**13**	**0.2**	**0.1**	**2.2**	**3927**	**39**	**3354**	**0.1**	**2.5**
21	0-0.5	6	2	1	0.7	0.5	297	23	4010	0.1	2.6
	0.5-1	28	5	3	0.4	1.1	362	26	3416	0.1	2.6
	1-1.5	9	2	1	0.8	0.3	351	22	3431	0.1	2.3
	1.5-2	6	3	1	0.4	1.0	585	24	4709	0.1	2.5
	2-3	-	-	-	-	-	338	22	2921	0.1	2.3
	3-4	-	-	-	-	-	418	22	2556	0.1	2.3
	4-5	-	-	-	-	-	384	25	2664	0.1	2.4
	5-6	-	-	-	-	-	424	19	4135	0.1	2.3
	6-7	-	-	-	-	-	521	21	8960	0.1	2.3
	7-8	-	-	-	-	-	566	19	6998	0.1	2.4
	0-8 (total)	**48**	**6**	**0.4**	**0.5**	**1.0**	**4246**	**32**	**4940**	**0.1**	**2.4**
07	0-0.5	16	7	1.80	0.2	1.8	340	30	148	0.1	2.8
	0.5-1	4	2	0.45	0.5	0.7	286	25	177	0.1	2.7
	1-1.5	11	3	1.24	0.4	0.9	288	24	160	0.1	2.7
	1.5-2	42	4	4.83	0.6	0.8	357	28	189	0.1	2.8
	2-3	28	4	1.57	0.4	1.1	312	28	231	0.1	2.6
	3-4	16	2	0.90	0.8	0.4	334	27	129	0.1	2.7
	4-5	4	2	0.22	0.6	0.6	244	28	302	0.1	2.7
	5-6	5	3	0.28	0.4	1.1	351	27	191	0.1	2.7
	6-7	1	1	0.06	1.0	0.0	309	26	217	0.1	2.7
	7-8	3	1	0.17	1.0	0.0	330	23	186	0.1	2.7
	8-9	1	1	0.06	1.0	0.0	321	27	205	0.1	2.6
	9-10	-	-	-	-	-	339	25	318	0.1	2.6
	0-10 (total)	**130**	**10**	**0.74**	**0.4**	**1.4**	**3811**	**39**	**212**	**0.1**	**2.8**

Tab. ST2. Calcareous foraminiferal concentrations and diversity data for each core in the fraction ≥150 µm. Number of counted specimens (N), number of species (S), number of foraminiferal specimens per gram of sediment (spec./g), Dominance index (D) and Shannon index (H). The total values referred to 0 - 10 cm are also indicated.

Core	Core depth (cm)	Living foraminiferal assemblages					Dead foraminiferal assemblages				
		N	S	spec./gr	D	H	N	S	spec./gr	D	H
2	0-0.5	6	2	0.6	0.56	0.64	103	7	15	0.6	0.8
	0.5-1	1	1	0.1	1.00	0.00	25	8	33	0.3	1.3
	1-1.5	1	1	0.1	1.00	0.00	17	3	9	0.8	0.4
	1.5-2	-	-	-	-	-	10	4	1	0.3	1.2
	2-3	-	-	-	-	-	1	1	0.03	1.0	0.0
	3-4	-	-	-	-	-	-	-	-	-	-
	4-5	-	-	-	-	-	1	1	0.03	1.0	0.0
	5-6	-	-	-	-	-	-	-	-	-	-
	6-7	1	1	0.1	1.00	0.00	-	-	-	-	-
	7-8	-	-	-	-	-	-	-	-	-	-
	8-9	-	-	-	-	-	-	-	-	-	-
	9-10	-	-	-	-	-	-	-	-	-	-
	0-10 (total)	**9**	**2**	**0.1**	**0.65**	**0.53**	**157**	**10**	**3**	**0.3**	**1.4**
21	0-0.5	1	1	0.1	1.0	0.0	5	2	59	1.0	0.0
	0.5-1	2	1	0.2	1.0	0.0	11	3	62	0.7	0.5
	1-1.5	1	1	0.1	1.0	0.0	-	-	-	-	-
	1.5-2	-	-	-	-	-	-	-	-	-	-
	2-3	-	-	-	-	-	1	1	0.08	1.0	0.0
	3-4	1	1	0.1	1.0	0.0	-	-	-	-	-
	4-5	-	-	-	-	-	2	1	0.1	1.0	0.0
	5-6	-	-	-	-	-	1	1	0.05	1.0	0.0
	6-7	-	-	-	-	-	3	1	0.1	1.0	0.0
	7-8	-	-	-	-	-	1	1	0.04	1.0	0.0
	0-8 (total)	**5**	**2**	**0.04**	**0.6749**	**0.5063**	**24**	**4**	**5**	**0.7**	**0.5**
7	0-0.5	6	2	0.67	0.7	0.4	37	8	12	0.4	1.2
	0.5-1	7	1	0.79	1.0	0.0	17	4	6	0.7	0.7
	1-1.5	-	-	-	-	-	8	2	5	0.6	0.6
	1.5-2	1	1	0.11	1.0	0.0	19	4	2	0.3	1.2
	2-3	-	-	-	-	-	6	2	1	0.6	0.5
	3-4	1	1	0.06	1.0	0.0	6	3	1	0.4	1.0
	4-5	2	1	0.11	1.0	0.0	3	1	0.1	1.0	0.0
	5-6	-	-	-	-	-	4	2	2	1.0	0.1
	6-7	3	1	0.17	1.0	0.0	13	2	5	0.9	0.2
	7-8	-	-	-	-	-	4	2	1	0.9	0.2
	8-9	-	-	-	-	-	-	-	-	-	-
	9-10	-	-	-	-	-	-	-	-	-	-
	0-10 (total)	**19**	**2**	**0.11**	**0.9**	**0.2**	**117**	**9**	**2**	**0.4**	**1.2**

Tab. ST3. Agglutinated foraminiferal concentrations and diversity data for each core in the fraction ≥150 µm. Number of counted specimens (N). number of species (S). number of foraminiferal specimens per gram of sediment (spec./g). Dominance index (D) and Shannon index (H). The total values referred to 0 - 10 cm are also indicated.

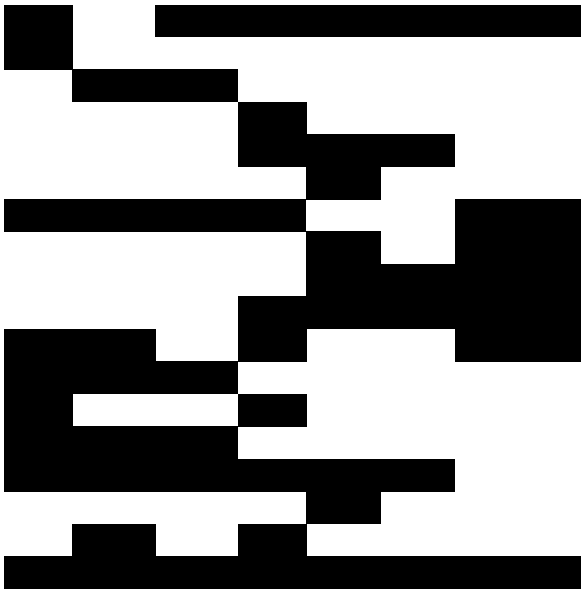
Foraminiferal counting sheets

	List of planktonic foraminifera		Site present PREPARED 01PC 02BC
Planktonic	***Neogloboquadrina pachyderma***	(Ehrenberg, 1861)	
	Neogloboquadrina incompta	(Cifelli, 1961)	
	Globigerina bulloides	d'Orbigny, 1826	
	Turborotalita quinqueloba	(Natland, 1938)	
	Globigerinita glutinata	(Egger, 1893)	
	Globigerinita uvula	(Ehrenberg, 1861)	

Calcareous perforate

List of benthic foraminifera		Site present							
			BURSTER			PREPARED		NP16 Kr1	
		02-2	21-05	21-03	07-3	01PC	02BC	MC	
Alabaminella weddellensis	(Earland, 1936)		■						
Astrononion gallowayi	Loeblich & Tappan, 1953	■	■	■	■	■	■	■	
Biasterigerina planorbis	(d'Orbigny, 1846)			■	■				
***Bolivina* spp.**	d'Orbigny, 1839			■	■				
Bolivinellina pseudopunctata	(Höglund, 1947)	■	■			■	■	■	
***Buccella* spp.**	Andersen, 1952	■	■	■	■	■	■	■	
Cassidulina laevigata	d'Orbigny, 1826	■	■	■	■	■	■	■	
Cassidulina neoteretis	Seidenkrantz, 1995	■	■	■	■	■	■	■	
Cassidulina reniforme	Nørvang, 1945	■	■	■	■	■	■	■	
Cibicides refulgens	Montfort, 1808	■	■	■	■	■	■	■	
Cibicidoides lobatulus	(Walker & Jacob, 1798)	■	■	■	■	■	■	■	
Cibicidoides wuellerstorfi	(Schwager, 1866)					■	■		
***Dentalina* spp.**	Risso, 1826		■		■	■	■	■	
Discorbinella bertheloti	(d'Orbigny, 1839)				■				
Discorbis vilardeboanus	(d'Orbigny, 1839)	■		■	■				
Elphidium clavatum	Cushman, 1930	■	■	■	■	■	■	■	
Elphidium albiumbilicatum	(Weiss, 1954)					■	■	■	
Elphidium hallandense	Brotzen, 1943					■	■	■	
Elphidium macellum	(Fichtel & Moll, 1798)						■		
Epistominella exigua	(Brady, 1884)					■	■	■	
***Eponides* spp.**	Montfort, 1808				■				
***Fissurina* spp.**	Reuss, 1850	■	■	■	■	■	■		
Globobulimina arctica	Höglund, 1947	■	■	■				■	
Globobulimina auriculata	Höglund, 1947	■	■	■				■	
Globocassidulina subglobosa	(Brady, 1881)	■	■	■	■	■		■	
Globulina landesi	(Hanna & Hanna, 1924)					■	■		
***Guttulina* spp.**	d'Orbigny, 1839	■							
Haynesina depressula	(Walker & Jacob, 1798)					■		■	
Haynesina germanica	(Ehrenberg, 1840)					■		■	
Haynesina orbiculare	(Brady, 1881)					■	■	■	
Hoeglundina elegans	(d'Orbigny, 1826)	■	■	■	■	■			
Ioanella tumidula	(Brady, 1884)					■	■		
Islandiella helenae	Feyling-Hanssen & Buzas, 1976	■	■	■	■			■	
Islandiella norcrossi	(Cushman, 1933)	■	■	■	■	■	■	■	
***Lagena* spp.**	Walker & Jacob, 1798	■	■	■	■	■	■	■	
Lagenosolenia lagenoides	(Williamson, 1858)					■			
***Lenticulina* spp.**	Lamarck, 1804	■	■		■	■	■		
Marginulina obesa	Cushman, 1923		■			■	■		
Melonis barleeanus	(Williamson, 1858)	■	■	■	■	■	■	■	
Nonionella auricula	Heron-Allen & Earland, 1930	■	■	■	■	■	■	■	
Nonionella iridea	Heron-Allen & Earland, 1932	■						■	
Nonionella stella	Cushman & Moyer, 1930							■	
Nonionellina labradorica	(Dawson, 1860)	■	■	■	■			■	
Nonionoides turgidus	(Williamson, 1858)	■		■				■	
***Oolina* spp.**	d'Orbigny, 1839	■	■		■	■	■		
Oridorsalis tener	(Brady, 1884)					■	■		
Parrelloides* cf. *healdi	(Stewart and Stewart, 1930)					■	■		
Patellina corrugata	Williamson, 1858	■	■	■	■	■			
Pseudopolymorphina novangliae	(Cushman, 1923)					■	■		
Pullenia bulloides	(d'Orbigny, 1846)	■	■	■		■	■	■	
Pullenia* cf. *catalinaensis	McCulloch, 1977					■	■		
Pullenia elegans	Cushman & Todd, 1943						■		

Pullenia osloensis	Feyling-Hanssen, 1954
Pullenia subcarinata	(d'Orbigny, 1839)
Robertinoides charlottensis	(Cushman, 1925)
Robertinoides normani	(Goës, 1894)
Robertinoides pumilum	Höglund, 1947
Rosalina villardeboana	d'Orbigny, 1839
***Rosalina* spp.**	d'Orbigny, 1826
Stainforthia concava	(Höglund, 1947)
Stainforthia feylingi	Knudsen & Seidenkrantz, 1994
Stainforthia fusiformis	(Williamson, 1858)
Stainforthia loeblichi	(Feyling-Hanssen, 1954)
Trifarina angulosa	(Williamson, 1858)
Trifarina bradyi	Cushman, 1923
Trifarina carinata	(Cushman, 1927)
Trifarina fluens	(Todd in Cushman & McCulloch, 1948)
Valvulineria minuta	(Schubert, 1904)
Turrispirillina arctica	(Cushman, 1933)
Indet.	



Calcareous imperforate

List of benthic foraminifera		Site present						
			BURSTER			PREPARED		NP16 Kr1
		02-2	21-05	21-03	07-3	01PC	02BC	MC
***Cornuspira* spp.**	Schultze, 1854				■	■	■	■
Miliolinella* cf. *enoplostoma	(Reuss, 1851)					■	■	
Miliolina inflata	(d'Orbigny, 1826)							■
Miliolinella subrotunda	(Montagu, 1803)						■	
***Miliolinella* spp.**	Wiesner, 1931					■		
Nodosaria lagenifera	Neugeboren, 1852							■
Pyrgo lucernula	(Schwager, 1866)					■	■	
Pyrgo oblonga	(d'Orbigny, 1839)	■						
Pyrgoella sphaera	(d'Orbigny, 1839)	■						
Pyrgo subglobulus	Parr, 1950		■		■	■	■	■
Pyrgo williamsoni	(Silvestri, 1923)		■			■	■	
Pyrgoella globula	Cushman & White, 1936					■	■	
Pyrgoella sphaera	(d'Orbigny, 1839)					■		
***Pyrgo* spp.**	Defrance, 1824	■	■	■				
Quinqueloculina annectens	(Schlumberger, 1893)					■		
Quinqueloculina arctica	Cushman, 1933						■	
Quinqueloculina sclerotica	Karrer, 1868				■			
Quinqueloculina seminula	(Linnaeus, 1758)	■	■	■	■			
Quinqueloculina stalkeri	Loeblich & Tappan, 1953				■			
***Quinqueloculina* spp.**	d'Orbigny, 1826					■		
Siphonaperta agglutinata	(Cushman, 1917)			■				
Triloculina oblonga	(Montagu, 1803)					■	■	
Triloculina rotunda	d'Orbigny, 1826					■	■	
Triloculina tricarinata	d'Orbigny in Deshayes, 1832	■				■	■	■
Triloculina trigonula	(Lamarck, 1804)		■					

List of benthic foraminifera		Site present						
			BURSTER			PREPARED		NP16 Kr1
		02-2	21-05	21-03	07-3	01PC	02BC	MC
Adercotryma* cf. *glomeratum	(Brady, 1878)					■	■	
Adercotryma glomeratum	(Brady, 1878)			■	■	■	■	■
Ammobaculites agglutinans	(d'Orbigny, 1846)						■	
Ammodiscus minimus	Höglund, 1947						■	
Armorella sphaerica	Heron-Allen & Earland, 1932						■	
***Astrorhiza* spp.**	Sandahl, 1858	■			■			
***Bathysiphon* spp.**	Sars, 1872						■	
Cribrostomoides kosterensis	(Höglund, 1947)							■
Eggerella arctica	Höglund, 1947						■	
Eggerelloides scaber	(Williamson, 1858)	■			■			
Haplophragmoides fragile	Höglund, 1947							■
Haplophragmoides membranaceum	Höglund, 1947							■
***Hyperammina* spp.**	Brady, 1878	■				■	■	
Labrospira crassimargo	(Norman, 1892)			■	■		■	■
Labrospira subglobosa	(Cushman, 1910)						■	
Lagenammina difflugiformis	(Brady, 1879)		■		■		■	
***Lagenammina* spp.**	Rhumbler, 1911							■
Liebusella göesi	Höglund, 1947							■
Psammosiphonella crassatina	(Brady, 1881)	■						
Psammosphaera fusca	Schulze, 1875					■	■	■
***Psammosphaera* spp.**	Schulze, 1875		■					
Quinqueloculina agglutinans	d'Orbigny, 1839		■					■
Quinqueloculina stalkeri	Loeblich & Tappan, 1953							■
Recurvoides contorta	Earland, 1934						■	
Recurvoides trochamminiforme	Höglund, 1947					■	■	■
Reophax catenatus	Höglund, 1947							■
Reophax difflugiformis	Brady, 1879						■	
Reophax guttifer	(Brady, 1881)	■				■	■	
Reophax micaceus	Earland, 1934	■	■			■	■	
Reophax pilulifera	Brady, 1884				■			
Reophax scorpiurus	Montfort, 1808	■		■		■	■	■
Reophax subfusiformis	Earland, 1933	■						■
***Reophax* spp.**	Montfort, 1808	■	■	■	■	■	■	■
***Rhabdammina* spp.**	Sars in Carpenter, 1869	■	■		■	■	■	
***Rhizammina* spp.**	Brady, 1879						■	
Saccammina sphaerica	Brady, 1871				■			
Saccorhiza ramosa	(Brady, 1879)	■						
Spiroplectammina biformis	(Parker & Jones, 1865)					■	■	■
Testulosiphon indivisus	(Brady, 1884)				■			
Textularia earlandi	Parker, 1952							■
Trochammina globigeriniformis	(Parker & Jones, 1865)					■	■	
Trochammina rotaliformis	Heron-Allen & Earland, 1911						■	
Trochammina* cf. *rotaliformis	Heron-Allen & Earland, 1911					■		

Agglutinated

GS191-01PC
Benthic foraminiferal

| Section | Core Depth | | Age yr BP | Sample code | Depth BSF (cm) | Fraction | weight dry sediment | Split | Calcareous peforate: *Astronomion gallowayi* | *Bolivinellina pseudopunctata* | *Buccella* spp. | *Cassidulina laevigata* | *Cassidulina neoteretis* | *Cassidulina reniforme* | *Cibicidoides lobatulus* | *Cibicidoides wuellerstorfi* | *Dentalina* spp. | *Elphidium albumbilicatum* | *Elphidium clavatum* | *Elphidium hallandense* | *Epistominella exigua* | *Fissurina danica* | *Globocassidulina subglobosa* | *Globulina landesi* | *Haynesina depressula* | *Haynesina germanica* | *Haynesina orbiculare* | *Hoeglundina elegans* | *Ioanella tumidula* | *Islandiella norcrassi* | *Lagena* spp | *Lagenosolenia lagenoides* | *Lenticulina cf. angulata* | *Lenticulina gibba* | *Marginulina obesa* | *Melonis barleeanus* | *Nonionella auricula* | *Oolina* spp. | *Oridorsalis tener* | *Parrelloides cf. heaidi* | *Patellina corrugata* | *Pseudopolymorphina novangliae* | *Pullenia bulloides* | *Pullenia cf. catalinaensis* | *Pullenia osloensis* | *Robertinoides pumilum* | *Rosalina villardeboana* | *Stainforthia concava* | *Stainforthia fusiformis* | *Stainforthia feylingi* | *Triforina fluens* | *Valvulineria minuta* | *Indet.* | Total Calcareous perforate | Calcareous imperforate: *Cornuspira* spp. | *Miliolinella* spp. | *Miliolinella cf. enoplostoma* | *Pyrgo lucernula* | *Pyrgo subglobulus* | *Pyrgo williamsoni* | *Pyrgoella globula* | *Pyrgoella sphaera* | *Quinqueloculina annectens* | *Quinqueloculina* spp | *Triloculina oblonga* | *Triloculina rotunda* | *Triloculina tricarinata* | Total Calcareous imperforate | Agglutinated: *Adercotryma cf. glomeratum* | *Adercotryma glomeratum* | *Hyperammina subnodosa* | *Labrospira subglobosa* | *Psammosphaera fusca* | *Recurvoides trochamminiforme* | *Reophax guttifer* | *Reophax micaceus* | *Reophax scorpiurus* | *Rhabdammina scabra* | *Eggerella scabra* | *Trochammina globigeriniformis* | *Trochammina cf. rotaliformis* | Total agglutinated | Total |
|---|---|---

| | | |

GS191-02BC
Benthic foraminiferal

Counting

| AGE | Depth (cm) | Fraction | SAR cm/yr | Density g/cm3 | weight dry sediment | Split | Calcareous perforate | | |

GS191-02BC
Planktonic foraminiferal

Counting

Age mean AD	Depth (cm)	Fraction	SAR cm/yr	Density g/cm3	weight dry sediment	Split	*Neogloboquadrina pachyderma*	*Neogloboquadrina incompta*	*Turborrotalita quinqueloba*	*Globigerina bulloides*	*Globigerinita glutinata*	*Globigerinita uvula*	TOTAL
2014	0-0.5	>150µm	0.1	0.9	1	1	43.0	7.0	110.0	25.0	5.0		190.0
2009	0.5-1	>150µm	0.1	0.9	1.21	1	77.0	14.0	183.0	51.0	12.0	4.0	341.0
2006	1-1.5	>150µm	0.1	0.9	0.7	1	54.0	7.0	132.0	76.0	12.0	5.0	286.0
2003	1.5-2	>150µm	0.1	0.9	1.4	1	97.0	4.0	186.0	119.0	6.0	2.0	414.0
1998	2-3	>150µm	0.1	0.9	1.1	1	84.0	2.0	55.0	62.0	9.0	2.0	214.0
1991	3-4	>150µm	0.1	1.4	1.1	1	213.0	27.0	223.0	42.0	5.0	5.0	515.0
1984	4-5	>150µm	0.1	1.5	0.8	1	35.0	5.0	42.0	62.0	2.0	2.0	148.0
1977	5-6	>150µm	0.1	1.5	1.2	1	29.0	7.0	93.0	108.0	10.0	2.0	249.0
1971	6-7	>150µm	0.1	1.5	1	1	101.0	0.0	98.0	133.0	8.0	4.0	344.0
1964	7-8	>150µm	0.1	1.4	0.7	1	138.0	7.0	166.0	108.0	26.0	9.0	454.0
1957	8-9	>150µm	0.1	1.4	0.7	1	109.0	7.0	194.0	87.0	9.0	1.0	407.0
1950	9-10	>150µm	0.1	1.4	0.6	1	126.0	2.0	110.0	8.0	0.0	3.0	249.0
1944	10-11	>150µm	0.1	1.4	0.6	1	147.0	2.0	311.0	87.0	9.0	1.0	557.0
1937	11-12	>150µm	0.1	1.4	0.8	1	141.0	6.0	131.0	60.0	9.0	2.0	349.0
1930	12-13	>150µm	0.1	1.4	1	0.75	158.0	2.0	72.0	53.0	1.0	0.0	286.0
1923	13-14	>150µm	0.1	1.4	0.7	0.75	169.0	1.0	108.0	60.0	8.0	4.0	350.0
1917	14-15	>150µm	0.1	1.4	0.4	1	173.0	0.0	213.0	30.0	5.0	2.0	423.0
1910	15-16	>150µm	0.1	1.4	1.5	1	91.0	3.0	102.0	47.0	1.0	1.0	245.0
1903	16-17	>150µm	0.1	1.3	0.2	1	87.0	0.0	170.0	45.0	1.0	0.0	303.0
1896	17-18	>150µm	0.1	1.4	0.3	1	114.0	1.0	100.0	40.0	1.0	2.0	258.0
1890	18-19	>150µm	0.1	1.4	0.3	1	65.0	1.0	140.0	58.0	6.0	2.0	272.0

02-2

Benthic foraminiferal

Counting

| Age | Depth (cm) | Fraction | weight wet sediment (g) | weight dry sediment (g) | Split | Calcareous perforate | | |

21-05

Benthic foraminiferal

Counting

| AGE | Depth (cm) | Fraction | weight wet sediment (g) | weight dry sediment | Split | Calcareous perforate | | |

21-03

Benthic foraminiferal

Counting

| AGE | Depth (cm) | Fraction | weight wet sediment (g) | weight dry sediment (g) | Split | Calcareous perforate | | |

07-3

Benthic foraminiferal

Counting

| AGE | Depth (cm) | Fraction | weight wet sediment (g) | weight dry sediment | Split | Calcareous perforate | | |

NP16-Kr1 MC
Benthic foraminiferal

Counting

| Depth (cm) | Age AD (mean) | Fraction | weight dry sediment (g) | Split | Counting Split | Calcareous perforate BF | | |

Acknowledgments

A special thanks to University of Costa Rica for its economic support and for being the engine of social development and for allowing me to go beyond my goals. Thanks to both the University of Florence (administrative headquarter of the PhD course) and the University of Pisa (work headquarter), for receiving me during these years of academic growth.

During these years, I have counted on the support of many people, I have been knowing some of them for many years now; some others have recently arrived in my life; all of them will stay part of it. They are many, and everyone so important and I do not think I can mention all the names because they would be at least two more chapters of the thesis.

First of all, I must thank my tutors, Prof. Caterina Morigi and Prof. Katrine Husum, for their guidance and support, and above all for believing in my work; they are the main artificers of my scientific growth, and because they have led me to know people and places that never in my life I would have even imagined.

Thanks to the director of the Doctorate Course Prof. Lorella Francalanci for her helpfulness and assistance, during these years.

Thanks to the staff of the international affairs office of the UCR, its director Dr. Diana Senior Angulo, its ex director Ing. Leonora de Lemos Medina and the head of the academic mobility section, Wajiha Sasa Marín. Special thanks to a great person, Karol Cordero who has always been available and has always given me support during my “mini-cardiac arrests”.

Thanks to all the amazing scientists, I have met and had the honour to work with. From the OGS the tireless Renata Lucchi for her patience and kindness, her invaluable help, her great enthusiasm and ability to transmit knowledge; the dynamic duo Manuel Bensi and Vedrana Kovacevic; from DiSVA the life-marine duo Anna Sabbatini and Francesca Caridi, and from the ISP-CNR the too much professor Leonardo Langone. To all the people who accompanied me during the fantastic Nordic adventures, to the researchers from the NPI, to the crews of the RV Polarstern, RV Kronprins Haakon and RV Helmer Hanssen, and the respective scientific crews of each research cruises.

Thanks to the teaching and administrative staff of the University of Pisa for their kindness during this years.

Thanks to the teaching and administrative staff of the University of Costa Rica, to all my friends there, for their support during this period.

I am very grateful to my family, for their constant emotional support especially to my mom Leticia and to my dad Carlos, who is not here to see the closure of this, but I know that wherever he is, he always accompanies me. Thanks to Karen and all her family to receive me as a part of them, especially to nonna Cesarina for teaching me to make gnocchi and call me by my artistic name "Viliana", and special to Augusto for all the wine we will not drink, for now (cheers to the sky). Thanks to those who supported me, putting their name at risk, my siblings Marianela and Juan Carlos, my cousin Diana, my colleagues and friends Guaria and Lepolt. Thanks to my friends, both from Costa Rica and Italy, who have always been close to me giving me support and that little push of energy at all times.

I thank everybody for being part of this adventure and being part of my life.

